

Brunel University London

College of Engineering Design and Physical Science

Department of Mechanical and Aerospace Engineering

**Experimental and Numerical Investigation of Air  
Distribution in a Large Air-Conditioned Space Building**

**By**

**Ali Mohammad Alzaid**

Principal Supervisor: Professor Maria Kolokotroni

Supervisor: Professor Hazim Awbi

Thesis submitted in partial fulfillment of the requirement for the degree of  
doctor of philosophy (PhD)

July 2019

London UK

## Abstract

Ventilation of large spaces in buildings differs from spaces with a small volume, because of the additional air that needs treating while the majority of it is above the occupied area. An enclosure is considered to be large when the floor-to-ceiling height is more than 5 meters or the volume of the occupied zone is generally small compared to the entire volume. The thermal comfort and indoor air quality, which have a direct impact on occupants' productivity and health, are crucially influenced by the building layout and volume and the design of the air distribution system. Many studies have been carried out to test these two factors, i.e. thermal comfort and indoor air quality, separately in evaluating the performance of ventilation systems. The Air distribution Index ADI combines the evaluation of thermal comfort and indoor air quality and has been used in spaces with standard floor-to-ceiling height. The aim of this study is to test the Air Distribution Index which combines several parameters, such as overall ventilation effectiveness for removing pollutants and for temperature distribution  $\bar{\varepsilon}_c$ ,  $\bar{\varepsilon}_t$  percentage of dissatisfied PD and predicted percentage of dissatisfied PPD, to assess the performance of ventilation systems in large spaces.

The research involved measurements in an occupied large open plan office (floor-to-ceiling height > 5m), and its occupied zone volume is small compared to the total volume fitted with mixing ventilation MV system to establish its performance characteristics and ability to provide the required conditions for both thermal comfort and air quality. The results from this investigation were used to develop a 3-D CFD model and evaluated it for air temperature, air velocity and CO<sub>2</sub> concentration predictions for this large space.

The 3-D CFD model was used to compare the performance of two different ventilation systems (Impinging jet IJV and mixing) numerically. The comparison was conducted using two different occupancy capacity loads for summer and winter conditions. The IJV system was found to be better in providing a satisfactory indoor environment at all conditions that have been considered as it showed higher ADI values.

Based on these findings, it is concluded that using ADI to assess the effectiveness of different ventilation systems in large enclosures can provide useful information that combines both indoor air quality and thermal comfort. Also, the IJV can be a beneficial air distribution system for use in a large enclosure for achieving thermal comfort and good air quality in the occupied zone and reducing energy consumption.

## **Acknowledgement**

I want to express gratitude and appreciation to my supervisors, Professor Maria Kolokotroni and Professor Hazim Awbi, for their guidance and encouragement throughout my study. Working under their supervision inspired and allowed me to extend my potential.

I am a colonel engineer in the Royal Saudi Air Force (RSAF) at King Faisal Air Academy (KFAA). I would, therefore, like to acknowledge RSAF in general and the KFAA in particular for funding and allowing me the time I needed to complete my PhD degree requirements.

I am thankful to the CSEF at Brunel University London for providing me with the environment and tools to conclude this work. Also, my colleagues Dr Jining Sun, Dr Konstantios Tsamos, Dr Hassan Mroue and Dr Thiago Santos for their support and advice.

Finally, I express special and profound thanks to my father and mother who always pray for my success and wish all the best, my wife, who was patient and never left my side. I dedicate this work to my beautiful kids; Reema, Meshal, Mohammad, and Meshari, all of them, were my best supporters.

## List of Publications

1. Alzaid A, Kolokotroni M, Awbi H (2017), *Experimental and Numerical Investigation of Air Distribution in a Large Space*, 38<sup>th</sup> AIVC International Conference, 13-14 Sep 2017, Nottingham, UK.
2. Alzaid A, Kolokotroni M, Awbi H (2018), *Thermal Comfort Assessment Based on Measurement and Questionnaire Surveys in a Large Mechanically Ventilated Space*, 10th Windsor conference, 12-15 April 2018, Windsor, UK.
3. Alzaid A, Kolokotroni M, Awbi H (2019), *Numerical Modelling of Large Air Conditioned Space: Comparison of Two Ventilation Systems*, 40th AIVC International Conference, 15-16 October 2019, Ghent, Belgium.

# Table of Contents

<b>ABSTRACT</b> .....	<b>I</b>
<b>ACKNOWLEDGEMENT</b> .....	<b>II</b>
<b>LIST OF PUBLICATIONS</b> .....	<b>III</b>
<b>TABLE OF CONTENTS</b> .....	<b>IV</b>
<b>LIST OF FIGURES</b> .....	<b>VII</b>
<b>LIST OF TABLES</b> .....	<b>XI</b>
<b>NOMENCLATURE</b> .....	<b>XII</b>
<b>1 CHAPTER ONE: INTRODUCTION</b> .....	<b>1</b>
1.1 Background .....	1
1.2 Research Aims .....	3
1.3 Research Objectives.....	3
1.4 Structure of Thesis .....	4
<b>2 CHAPTER TWO: LITERATURE REVIEW</b> .....	<b>6</b>
2.1 Introduction .....	6
2.2 Airflow Distribution Strategies Used in Large Spaces .....	6
2.2.1 Introduction.....	6
2.2.2 Displacement Ventilation (DV) .....	7
2.2.3 Mixing Ventilation .....	8
2.2.4 Underfloor Air Distribution System .....	10
2.2.5 Impinging Jet Ventilation .....	11
2.3 Thermal Comfort.....	12
2.3.1 Introduction.....	12
2.3.2 Fanger’s PMV Comfort Model .....	13
2.3.3 Multi-node Thermal Comfort Models .....	16
2.3.4 Adaptive Thermal Comfort Model .....	18
2.4 Indoor Air Quality.....	20
2.4.1 Introduction.....	20
2.4.2 Indoor Air Pollutants .....	20
2.4.3 Ventilation Effectiveness .....	23
2.5 Air Distribution Indices .....	24
2.6 Chapter Summary .....	25
<b>3 CHAPTER THREE: CFD MODELLING</b> .....	<b>26</b>

3.1	Introduction .....	26
3.2	Governing Equations of Fluid Dynamics .....	27
3.2.1	Conservation of Mass.....	27
3.2.2	Conservation of Momentum (Navier-Stokes Equations) .....	28
3.2.3	Conservation of Thermal Energy .....	29
3.2.4	The Concentration of Species.....	29
3.3	Turbulence Models .....	30
3.3.1	Direct Numerical Simulation.....	30
3.3.2	Large-Eddy Simulation .....	30
3.3.3	Reynold Averaged Navier-Stokes Simulation.....	31
3.4	Solution of the Transport Equation .....	33
3.4.1	The Finite Volume Method.....	34
3.4.2	Solution of the Discretisation Equations.....	35
3.5	Boundary Conditions .....	35
3.6	Accuracy of CFD Results .....	37
3.7	Chapter Summary .....	38
<b>4</b>	<b>CHAPTER FOUR: DESCRIPTION OF CASE STUDY BUILDING AND FIELD MEASUREMENTS.....</b>	<b>39</b>
4.1	Introduction .....	39
4.2	Description of Measurement Space and Instruments.....	39
4.2.1	The Building and the Chosen Space .....	39
4.2.2	Environmental Servicing .....	41
4.2.3	Periods of Measurements .....	43
4.2.4	Heat Gains .....	45
4.2.5	Description of the measuring instruments.....	46
4.3	The Measurements Three Phases.....	49
4.3.1	Long-term Measurements Phase .....	49
4.3.2	Spot Detailed Measurements Phase .....	51
4.3.3	Occupant Questionnaire.....	53
4.4	Chapter Summary .....	56
<b>5</b>	<b>CHAPTER FIVE: FIELD MONITORING RESULTS AND DISCUSSION.....</b>	<b>57</b>
5.1	Introduction .....	57
5.2	The Measurements Three Phases' Data and Results.....	57
5.2.1	Data and Results for Long-Term Measurement Phases.....	57
5.2.2	Results for Detailed Spot Measurements Phase .....	68

5.2.3	Occupants Questionnaires Results.....	74
5.3	Chapter Summary .....	77
<b>6</b>	<b>CHAPTER SIX: CFD MODELLING FOR THE CASE STUDY BUILDING.....</b>	<b>79</b>
6.1	Introduction .....	79
6.2	Geometrical Model.....	79
6.3	Numerical Grid.....	81
6.4	Turbulence Modelling and Numerical Aspects .....	81
6.5	Boundary Conditions .....	82
6.6	Grid Independency Study.....	84
6.7	CFD Evaluation with Measurements.....	88
6.8	Predicted Results of Air Temperatures, Air Velocities and CO <sub>2</sub> Concentration.....	93
6.9	Chapter Summary .....	101
<b>7</b>	<b>CHAPTER SEVEN: CFD MODELLING STUDIES OF DIFFERENT AIR DISTRIBUTION SYSTEMS .....</b>	<b>102</b>
7.1	Introduction .....	102
7.2	Test Conditions .....	102
7.2.1	Test Condition Set-up .....	102
7.2.2	Supply Air Flow Rate .....	104
7.2.3	Recirculated Air .....	106
7.3	CFD Results and Discussion .....	108
7.3.1	Full Occupancy Load for Summer Condition (Case F-S).....	108
7.3.2	Full Occupancy Load for Winter Condition (Case F-W).....	115
7.3.3	Half Occupancy Load for Summer Condition (Case H-S).....	123
7.3.4	Half Occupancy Load for Winter Condition (Case H-W) .....	130
7.3.5	Discussion of Results.....	136
7.4	Chapter Summary .....	137
<b>8</b>	<b>CHAPTER EIGHT: CONCLUSIONS AND RECOMMENDATIONS FOR FUTURE WORK .....</b>	<b>138</b>
8.1	Introduction .....	138
8.2	Conclusions .....	139
8.3	Recommendations for Future Work.....	143
	<b>REFERENCES.....</b>	<b>144</b>
	<b>APPENDIX I: THERMAL COMFORT AND INDOOR AIR QUALITY QUESTIONNAIRE .....</b>	<b>154</b>
	<b>APPENDIX II : BOUNDARY CONDITIONS FOR CASE A AND CASE B.....</b>	<b>159</b>

## List of Figures

Figure 2.1 Displacement ventilation system .....	7
Figure 2.2 Contaminant distribution in displacement ventilation system .....	7
Figure 2.3 Contaminant distribution in mixing ventilation system .....	9
Figure 2.4 Underfloor air distribution system .....	10
Figure 2.5 Impinging jet ventilation .....	11
Figure 2.6 Flow regions of an impinging jet .....	11
Figure 2.7 The 7-points thermal sensation scale .....	14
Figure 2.8 Predicted percentage of dissatisfied as a function of PMV .....	15
Figure 3.1 Grid point (P) for a one-dimensional field .....	34
Figure 4.1 Centre of Sustainable Energy Use in Food Chains building .....	40
Figure 4.2 Sketch of the researchers' office at CSEF building. ....	40
Figure 4.3 The researchers' office at CSEF Building .....	41
Figure 4.4 Schematic layout of the researchers' office at CSEF building. ....	42
Figure 4.5 Air Diffuser at CSEF building .....	42
Figure 4.6 Outdoor temperature and relative humidity for the third month. ....	44
Figure 4.7 Outdoor temperature and solar radiation for the third month .....	45
Figure 4.8 TA 465 AirFlow Instrument Air Velocity Meter .....	47
Figure 4.9 HOBO Temp/RH Data Logger .....	47
Figure 4.10 CPS Thermo Anemometer .....	48
Figure 4.11 Telaire 7001 CO <sub>2</sub> Logger .....	48
Figure 4.12 U30-NRC-SYS-C HOBO Weather Station .....	49
Figure 4.13 HOBO Temp/RH data logger attached to the column at three different heights of 0.1, 1.2 and 1.8m .....	50
Figure 4.14 HOBO Temp/RH data logger mounted on the unoccupied zone .....	50
Figure 4.15 Measurements of mean air speed and temperature using a TA465 AirFlow instrument .....	52
Figure 4.16 Measurements of air speed of the diffusers using CPS Thermo Anemometer AM .....	52
Figure 5.1 Temperatures for point C1 at four levels, external and diffuser D1 over nine days. ....	58
Figure 5.2 Temperatures for point C1 at four levels, external and diffuser D1 for one day ....	58
Figure 5.3 Temperatures for point C1 at four levels, external and diffuser D1 for 12 hours ...	59
Figure 5.4 Temperature for points C1, C5, C8 and external over nine days at height 1.2m ....	59
Figure 5.5 Air temperatures for point C1 at five levels, external and diffuser D1 over one month .....	60
Figure 5.6 Air temperatures for point C1 at five levels, external and diffuser D1 for one day. ....	61
Figure 5.7 Air temperatures for point C1 at three level .....	61
Figure 5.8 Relative humidity for C1 at five levels, external and diffuser D1 over one month	62
Figure 5.9 Relative humidity for C1 at five levels, external and diffuser D1 for one day .....	62
Figure 5.10 Relative humidity for five heights at C1 over 12 hours .....	63

Figure 5.11 The mean indoor temperature versus outdoor daily mean temperature for the studied office building during summer 2016. ....	64
Figure 5.12. The mean indoor temperatures versus outdoor daily mean temperature for the studied office building during summer 2017. ....	64
Figure 5.13 The regression lines for different databases.....	66
Figure 5.14 Overlay of the temperature clouds for summer 2016 and summer 2017. ....	66
Figure 5.15 Hourly internal measured temperature during occupant hours (9:00-20:00) weekdays and the thermal comfort temperature with both upper and lower limits.....	68
Figure 5.16 Air speed in six spots at different heights .....	69
Figure 5.17 Air speed in six spots at 1.2 height over five days .....	69
Figure 5.18 Air temperatures in seven spots over five days .....	70
Figure 5.19 Air speed in seven spots at three different times in one day.....	70
Figure 5.20 Temperature in seven spots at three different times in one day.....	71
Figure 5.21 Air speed in seven spots at different heights .....	72
Figure 5.22 Air temperature in seven spots at different heights .....	72
Figure 5.23 The CO <sub>2</sub> concentrations for seven different spots in the office for summer 2018	74
Figure 5.24 Distribution of subjective response to temperature for three days.....	75
Figure 5.25 Distribution of subjective response to humidity for three days.....	76
Figure 5.26 Distribution of subjective response to air movement for three days.....	76
Figure 5.27. Distribution of subjective response to overall comfort for three days .....	77
Figure 6.1 The CFD model of the researchers' office for summer 2016.....	80
Figure 6.2 The CFD model of the researchers' office for summer 2017.....	80
Figure 6.3 The CFD model of the researchers' office for summer 2018.....	81
Figure 6.4 Comparisons between simulation results profiles along with the height of 0.1, 1.2, 1.8 m of the spot (S2) for three mesh densities (a) mean velocity and (b) mean temperature for summer 2016.....	85
Figure 6.5 Mesh configuration in the computational domain for the summer 2016 model. ..	85
Figure 6.6 Comparison between simulation results profiles along the height of 0.1, 1.2, 1.8 m of the spot (S2) for three mesh densities (a) mean velocity and (b) mean temperature for summer 2017. ....	86
Figure 6.7 Mesh configuration in the computational domain for summer 2017 model. ....	86
Figure 6.8 The measured and predicted CO <sub>2</sub> concentration using different numerical grids for summer 2018 model. ....	87
Figure 6.9 Mesh configuration in the computational domain for summer 2018 model .....	87
Figure 6.10 Comparisons between simulation results with measurements along three heights for spot (S1, S4, S5 and S6) (See figure 4.4): (a) mean velocity and (b) mean temperature for summer 2016. ....	89
Figure 6.11 Comparison between simulation results with measurements along three heights for spots (S1, S4, S5, and S6) (See figure 4.4): (a) mean velocity and (b) mean temperature for summer 2017. ....	92
Figure 6.12 Comparison between the predicted and measured CO <sub>2</sub> concentration at the six selected room locations in the occupied zone for summer 2018.....	92
Figure 6.13 Researchers' office plans location.....	93
Figure 6.14 Temperature contour at the local plane (z=6.6m) for summer 2016. ....	94

Figure 6.15 Temperatures contours at different height (a) $y=0.1m$ , (b) $y=1.2m$ and (c) $y=1.8m$ for summer 2016.....	95
Figure 6.16 (a) velocity vectors (b) velocity contour on the lateral plane ( $z=6.6m$ ) for summer 2016 .....	96
Figure 6.17 Temperature contour at the lateral plane ( $z=6.6m$ ) for summer 2017. ....	97
Figure 6.18 Temperature contours at different height (a) $y=0.1m$ , (b) $y=1.2m$ and (c) $y=1.8m$ for summer 2017.....	98
Figure 6.19 (a) velocity vectors (b) velocity contour on the lateral plane ( $z=6.6m$ ) for summer 2017. ....	99
Figure 6.20 Researchers' office plane locations for summer 2018.....	100
Figure 6.21 The CO <sub>2</sub> concentrations on the lateral plane at $z=6.6m$ .....	100
Figure 7.1 CFD Model of the office with full occupancy.....	103
Figure 7.2 CFD model of the office with half occupancy.....	103
Figure 7.3 The Size and locations of the IJV inlet diffusers used in the CFD simulation .....	106
Figure 7.4 Recirculation system of the modelled office for full occupancy. ....	107
Figure 7.5 Recirculation system of the modelled office for half occupancy. ....	107
Figure 7.6 Mesh configuration in the computational domain for the IJV system of Case F-S .....	110
Figure 7.7 Temperature contour plots on a lateral plane located in the middle of the office for Case F-S: (a) MV system at $Z=6.6 m$ and (b) IJV system at $Z=7.2 m$ .....	111
Figure 7.8 Velocity vector plots on a lateral plane located in the middle of the office for Case F-S: (a) MV system at $Z=6.6 m$ and (b) IJV system at $Z=7.2 m$ .....	112
Figure 7.9 Velocity contour plots on a plane located at a height $Y=0.1 m$ for Case F-S: (a) MV system and (b) IJV system. ....	113
Figure 7.10 CO <sub>2</sub> concentrations contours on a lateral plane located in the middle of the office for Case F-S: (a) MV system at $Z=6.6 m$ and (b) IJV system at $Z=7.2m$ .....	114
Figure 7.11 Heat transfer through a plan wall : (a) temperature distribution (b) equivalent thermal circuit.....	116
Figure 7.12 Temperature contour plots on a lateral plane located in the middle of the office for Case F-W: (a) MV systems at $Z=6.6 m$ and (b) IJV system at $Z=7.2 m$ .....	119
Figure 7.13 Velocity vector plots on a lateral plane located in the middle of the office for Case F-W: (a) MV system at $Z=6.6 m$ and (b) IJV system at $Z=7.2 m$ .....	120
Figure 7.14 Velocity contour plots on a plane at a height $y=0.1 m$ for case F-W: (a) MV system and (b) IJV system. ....	121
Figure 7.15 CO <sub>2</sub> concentration contours on a lateral plane located in the middle of the office for Case F-W: (a) MV system at $Z=6.6 m$ and (b) IJV system at $Z=7.2 m$ .....	122
Figure 7.16 Mesh configuration in the computational domain for the IJV system for the Case H-S.....	125
Figure 7.17 Temperature contour plots on a lateral plane located in the middle of the office for Case H-S: (a) MV system at $Z=6.6 m$ and (b) IJV system at $Z=7.2 m$ .....	126
Figure 7.18. Velocity vectors on a lateral plane located in the middle of the office for Case H-S: (a) MV system at $Z=6.6 m$ and (b) IJV system at $Z=7.2 m$ .....	127
Figure 7.19 Velocity contour plots on a plane located at a height $Y=0.1 m$ for Case H-S: (a) MV system and (b) IJV system .....	128

*Figure 7.20 CO<sub>2</sub> concentrations contour on a lateral plane located in the middle of the office for Case H-S: (a) MV system at Z=6.6 m and (b) IJV system at Z=7.2 m. ....129*

*Figure 7.21 Temperature contour plots on a lateral plane located in the middle of the office for Case H-W: (a) MV system at Z=6.6m and (b) IJV system at Z=7.2 m. ....132*

*Figure 7.22 Velocity vector plots on a lateral plane located in the middle of the office for Case H-W: (a) MV system at Z=6.6 m and (b) IJV system at Z=7.2 m. ....133*

*Figure 7.23 Velocity contour plots on a plane at a high Y=0.1 m for Case H-W: (a) MV system and (b) IJV system. ....134*

*Figure 7.24 CO<sub>2</sub> concentration contours on a lateral plane located in the middle of the office for Case H-W: (a) MV system at Z= 6.6 m and (b) IJV system at Z= 7.2 m.....135*

## List of Tables

<i>Table 2.1 Suggested acceptable temperature range for free-running building with an explanation of application.</i>	19
<i>Table 3.1 The k-<math>\epsilon</math> model family.</i>	32
<i>Table 3.2 The k-<math>\omega</math> model family</i>	33
<i>Table 4.1 Outdoor air temperature and relative humidity for each month during the summer season for the years 2016 and 2017.</i>	44
<i>Table 4.2 Total heat gain in the office for one day of summer 2016, summer 2017 and summer 2018</i>	46
<i>Table 4.3 Measuring points for air temperature and relative humidity.</i>	50
<i>Table 4.4 Date and occupants numbers for each spot detailed measurement.</i>	52
<i>Table 4.5 Measuring spots' locations and heights.</i>	53
<i>Table 4.6 Rating scales for subjective evaluation parameters</i>	55
<i>Table 4.7 Indexes to elaborate the questionnaires.</i>	55
<i>Table 5.1 The regression lines equations for different databases</i>	65
<i>Table 5.2 Air speed at diffusers.</i>	71
<i>Table 5.3 Synthesis of measured data for several days during summer 2016 and 2017</i>	73
<i>Table 5.4 Questionnaires numbers, date and analysis: synthesis of main results</i>	75
<i>Table 6.1 Grid densities for summer 2016, 2017 and 2018</i>	81
<i>Table 6.2 The Boundary conditions for CFD models for summer 2016, summer 2017.</i>	83
<i>Table 6.3 Boundary conditions for summer 2018 CFD model.</i>	84
<i>Table 6.4 The average relative percentage error between prediction and measurement across the four measured spots of the air velocity and air temperature with the RNG k-<math>\epsilon</math> and SST k-<math>\omega</math> models.</i>	88
<i>Table 6.5 Model accuracy criteria.</i>	90
<i>Table 7.1 Design assumptions for the calculating of the office cooling load for full and half occupancy</i>	104
<i>Table 7.2 The calculated supply air flow rate for full and half occupancy from HAP</i>	105
<i>Table 7.3 The CFD cases used for the MV and IJV system performance comparison</i>	108
<i>Table 7.4 Boundary conditions of Case F-S for the MV and IJV systems</i>	109
<i>Table 7.5 The predicted ADI for the MV and IJV systems for Case F-S</i>	115
<i>Table 7.6 The values of internal surface temperatures, heat transfer and the thermal resistance for the south wall, ceiling and window</i>	117
<i>Table 7.7 Boundary conditions of Case F-W for the MV and IJV systems.</i>	117
<i>Table 7.8 The predicted ADI for the Case F-W</i>	123
<i>Table 7.9 Boundary conditions of Case H-S for the MV and IJV systems.</i>	124
<i>Table 7.10 The predicted ADI for the MV and IJV systems for Case (H-S).</i>	130
<i>Table 7.11 Boundary conditions for Case H-W for MV and IJV systems.</i>	131
<i>Table 7.12 The predicted ADI for case H-W</i>	136
<i>Table 8.1 The predicted ADI for the four cases</i>	142

## Nomenclature

$A$	Body surface area	$m^2$
$A_{Du}$	Dubois body surface area	$m^2$
$C'$	Deviation from the mean concentration due to turbulence	$ppm$
$C_e$	Concentration of the exhaust	$ppm$
$C_i$	Concentration of the supply air	$ppm$
$C_m$	Mean concentration in the occupied zone	$ppm$
$C_p$	Concentration at a certain point (p) in the indoor space or specific heat capacity	$ppm$ $J/kg.K$
$f_{cl}$	The ratio of clothed body surface area to nude body surface area	
$g_x, g_y, g_z$	Acceleration of gravity in the x, y and z direction	$m/s^2$
$H_e$	Hours of exceedance	hours
$h_c$	Convective heat transfer coefficient	$W/m^2.K$
$h_e$	Evaporative heat transfer coefficient	$W/m^2.K$
$I_{cl,f}$	Whole-body thermal insulation for garments	clo
$I_{clo}$	Thermal insulation	clo
$k$	Turbulence kinetic energy or thermal conductivity	J $W/m.K$
$L$	Distance to nearest wall	m
$M$	Metabolic rate	Kcal/h
$\dot{m}_{in}$	Mass flux flowing into the control volume	kg/s
$N_c$	The air quality number	
$N_t$	The thermal comfort number	
$P_a$	Water vapour pressure in the air	pa
$Q$	Volume flow rate	$m^3/s$
$Q_v$	Ventilation load	W
$q_w$	Wall heat flux	$W/m^2$
$S_c$	The rate of concentration production within the control volume (concentration source term)	
$S_k$	The turbulence generation due to viscous and buoyancy forces (turbulence source term)	
$S_T$	The rate of heat generation within the control volume (Heat source term)	
$t_a, T_a$	Air temperature	$^{\circ}C$
$T_c$	Indoor comfort temperature	$^{\circ}C$
$t_{cl}$	Clothed body surface temperature	$^{\circ}C$
$T_{comp}$	Comfort temperature	$^{\circ}C$
$T_e$	Temperature at the exhaust	$^{\circ}C$
$T_g$	Globe temperature	$^{\circ}C$
$T_i$	Indoor mean temperature or inlet air temperature	$^{\circ}C$
$t_{mrt}$	Mean radiant temperature	$^{\circ}C$
$t_o$	Operative temperature	$^{\circ}C$
$T_{od}$	Daily mean temperature	$^{\circ}C$
$T_o$	Outdoor mean temperature or outlet air temperature	$^{\circ}C$
$\bar{t}_r, \bar{T}_r$	Mean radiant temperature	$^{\circ}C$
$T_{rm}$	Weighted running mean temperature	$^{\circ}C$
$T_{upp}$	Upper limit temperature	$^{\circ}C$
$U, V, W$	Velocity components in the x, y and z directions	m/s
$U$	Local mean velocity	m/s

$U_i, V_i, W_i$	Velocity components of the supply air	m/s
$U_o$	Velocity of the air jet at the opening slot of the MV system	m/s
$v$	Relative velocity between the body and the air	m/s
$V$	Room volume	$m^3$
$\dot{v}$	Ventilation rate	L/s
$W_e$	Daily weighted exceedance	kg
$y^+$	Non-dimensional wall distance	
$y_p$	The distance between the node (p) and the wall surface	m

### Greek Letters

$\alpha$	Under relaxation factor	
$\eta$	External mechanical efficiency	
$\varepsilon$	Kinetic energy dissipation rate	$m^2/s^3$
$\varepsilon_c$	Ventilation effectiveness for contaminant removal	
$\varepsilon_t$	Effectiveness for heat removal	
$\phi$	Scalar quantity such as temperature, concentration, local mean age of air	
$\Gamma$	Diffusion coefficient	$m^2/s$
$\Gamma_t$	The turbulent diffusion coefficient	$m^2/s$
$\mu$	Dynamics viscosity	kg/m.s
$\mu_t$	Turbulence eddy viscosity	kg/m.s
$\omega$	The ratio of $\varepsilon$ over $k$	
$\rho$	Fluid density	$kg/m^3$
$\sigma$	Prandtl number of a fluid or the Stephen-Boltzmann constant	
$\theta$	Effective draught temperature	$^{\circ}C$

### Abbreviations

ADI	Air Distribution Index
ADPI	Air Diffusion Performance Index
ADS	Airflow Distribution Strategy
ASHRAE	American Society of Heating, Refrigeration and Air-Conditioning Engineers
BRE	Building research establishment
CBE	The Centre of the Built Environment at the University of California at Berkeley
CFD	Computational Fluid dynamics
CIBSE	Chartered Institution of Building Services Engineers
CJV	Confluent Jet Ventilation
CO <sub>2</sub>	Carbon Dioxide
DNS	Direct Numerical Simulation
DTS	Dynamic Thermal Sensation
DV	Displacement Ventilation
ET	Effective Temperature
FEM	Finite Element Method
FVM	Finite Volume Method
HVAC	Heating, Ventilation and Air Conditioning
IAQ	Indoor Air Quality
IJV	Impinging Jet Ventilation
ISO	International Organisation for Standardisation
LES	Large Eddy Simulation

LMV	Local Thermal Mean Vote
LTC	Local Thermal Comfort
LTS	Local Thermal Sensation
LR	The Lewis Ratio
LRN k- $\epsilon$	Low Reynolds number k-epsilon
MR	Metabolic Rate
MRT	Mean Radiant Temperature
MV	Mixing Ventilation
NHS	National health service
OTC	Overall Thermal Comfort
OTS	Overall Thermal Sensation
Pe	Peclet number
PMV	Predicted Mean Vote
PPD	Predicted Percentage of Dissatisfied with the thermal environment
Re	Reynolds number of a flow
RH	Relative Humidity
RNG k- $\epsilon$	Renormalisation group k-epsilon
RSM	Reynolds Stress Model
SD	Standard Deviation
SBS	Sick Building Syndrome
SET*	Revised Standard Effective Temperature
SIMPLE	Semi-Implicit Method for Pressure Linked Equations
SST k- $\omega$	Shear Stress Transport k-omega
UFAD	Underfloor Air Distribution systems
UK	United Kingdom
USA	United States of America
VP	Ventilation Parameter, Ventilation performance
WHO	World Health Organisation

# 1 CHAPTER ONE: INTRODUCTION

---

## 1.1 BACKGROUND

Large single cell spaces have become a considerable characteristic of modern buildings. Examples include shopping malls, lecture theatres, airports terminals, gymnasiums and large open plan offices. Because of their large volume such spaces present different challenges in the design of systems to provide thermal comfort and indoor air quality than typical volume spaces. Therefore, recently more emphasis is being placed upon the research related to the indoor environment in these large enclosures.

An enclosure with more than 5 meters floor-to-ceiling height can be considered as a large space (Li *et al.*, 2009), or when the volume of the occupied zone is generally small compared to the entire volume (International Energy Agency IEA, 1998). Ventilation of such spaces needs more careful attention by design engineers than spaces with a small volume, i.e. those with a ceiling height of 3 meters or less. When warm air under the effect of buoyancy rises, a positive temperature gradient between floor and ceiling is formed, known as stratification (Calay, Borresen and Holdø, 2000) and the air flow pattern should be arranged and controlled to ensure an acceptable indoor air quality and thermal comfort in the occupied zone without the need for excessive air flow rates to conserve energy (Heiselberg, Murakami and Roulet, 1998).

A large survey conducted by Huizenga *et al.* (2006) of the indoor environment in an office building showed that the main occupant dissatisfaction was with thermal discomfort. In Chinese offices, similar studies by Geng *et al.* (2017) in offices indicated that the optimal productivity was fulfilled when the occupants felt “neutral” or “slightly cool”, and the rise of thermal satisfaction led to an increase in the productivity. Fanger (2000) also showed that there is a connection between the room air quality and occupants’ productivity. Kukadia and Upton (2019) pointed that improving occupant health can be achieved by creating good indoor air quality. For example, in 2015 the Building Research Establishment BRE found that enhancing the 3.5 million poorly ventilated houses in England would save the National Health

Service NHS £1.4 billion of medical treatment costs in the first-year. Therefore, thermal comfort and air quality of indoor spaces are both essential to the well-being of the occupants. Heating, ventilation and air conditioning systems HVAC are used to supply the spaces with acceptable levels of air temperature, humidity, air velocity and acceptable indoor air quality by removing the contaminants from the spaces. Therefore, implementation of a suitable air distribution system will have a significant impact on the air flow patterns and indoor air quality within the ventilated space.

Furthermore, thermal discomfort can be generated by unwanted heating or cooling of a particular segment of the body. This is known as local discomfort and can be caused by four factors, which are: draught, vertical air temperature differences, radiant temperature asymmetry and cold or warm floors (BSI, 2005). Hence, the types of air distribution can have a considerable effect on the thermal condition around the occupants.

In order to characterise the combined thermal environment and indoor air quality in buildings Awbi and Gan (1993) and Awbi (1998) developed the concept of the Ventilation Parameter VP which was re-named later the Air Distribution Index (Awbi, 2003; T. Karimipanah, Awbi and Moshfegh, 2008). This index is used to assess the thermal comfort, indoor air quality and energy performance of an air distribution system.

In addition, International Energy Agency IEA (2018) suggests that the buildings and buildings construction sectors combined are responsible for 36% of global final energy consumption and nearly 40% of total direct and indirect CO<sub>2</sub> emissions. In the EU, buildings are responsible for approximately 40% of energy consumption and 36% of CO<sub>2</sub> emissions, making them the single largest energy consumer in Europe (Commission, 2018). In the UK, domestic and service sector final energy consumption accounted for 43% of total final energy consumption (Liz, 2018). Of these, space heating and cooling constitute 32-33% of the total building energy use (Ürge-Vorsatz *et al.*, 2015). The increase in the energy demand of existing technologies raises the CO<sub>2</sub> emission, which contributes to climate change and global warming. Therefore, this increases the interest in studying the performance of different ventilation systems.

## 1.2 RESEARCH AIMS

The Air Distribution Index is an important index combining the level of thermal comfort, indoor air quality and consequently energy performance provided by an air distribution system used in typical spaces. The ADI has been studied in typical occupied spaces but not for large enclosures. The aim of this study is, therefore, to apply the ADI for assessing the performance of ventilation systems used in large spaces. The research was carried out in three stages, which are: measurements, simulations and parametric studies with performance comparisons. One promising ventilation system is the impinging jet which provides benefits compared to conventional systems, such as mixing ventilation and displacement ventilation DV. Therefore, the second aim of the study is to examine the performance of impinging jet ventilation system numerically in large spaces and compare it with the mixing ventilation system which is typically used. The literature suggests that there has been only two recent works reported in the literature on evaluating the performance of impinging jet ventilation system in large spaces.

## 1.3 RESEARCH OBJECTIVES

The objectives of this research are given as follows:

### Objective 1:

Monitor an existing large space building with mixing ventilation system and analyse the results to understand the airflow pattern, temperature distribution, thermal comfort and indoor air quality for that space.

### Objective 2:

Investigate the capability of different thermal comfort models in predicting human responses in a large space for different seasons.

### Objective 3:

Develop and evaluate a three dimensional 3-D computational fluid dynamics CFD model for the large space and investigate its capability for prediction the air temperature, air velocity and CO<sub>2</sub> concentration in that space.

#### Objective 4:

Investigate various airflow distribution strategies used in large spaces for providing thermal comfort, indoor air quality and energy consumption. However, more emphasise will be placed on the most promising one which is the impinging jet system.

#### Objective 5:

Compare the performance of two different ventilation systems impinging jet and mixing in providing acceptable indoor environment for a large space. The comparison is to be carried out using two different occupancy capacity loads for summer and winter conditions to investigate the effect of these parameters on the performance of the ventilation systems. The assessment will be performed numerically using the CFD model.

## 1.4 STRUCTURE OF THESIS

This thesis consists of eight chapters, and a brief description of the chapters' content is given below:

Chapter 2 reviews the current state of knowledge in the subject area under consideration to comprehend that the ideas are supporting such studies. A description of different airflow distribution strategies used typically in large spaces is given. Also, well-known thermal models and indoor air pollutants are described in detail. Finally, a comprehensive index which is used to assess ventilation system performance is explained in details.

In chapter 3, background information on CFD techniques is presented. A detailed description of the governing equations of fluid dynamics and the capability of different turbulence models in predicting the airflow patterns and indoor environments are presented. Finally, a description of the solution of the CFD discretisation equations, boundary conditions and accuracy of CFD results are mentioned.

Chapter 4 describes the first stage of the research methodology followed in this work which is a measurement stage. The chosen large space case-study building, measurement periods, heat gains and measurement instruments are explained. The experimental set-up and measurement procedures for air temperatures, air velocity, humidity, CO<sub>2</sub> concentration are

described in detail. Finally, full details of the occupants' questionnaire, which was designed to assess the performance of the mixing ventilation system used in the chosen large space, are presented.

Chapter 5 presents the data and results that are obtained from the measurements. The performance of the thermal comfort models was tested. Finally, the results from the subjective test in the large space building are described.

Chapter 6 describes the second stage of research, which is the CFD modelling and evaluation. The capability of the CFD model in predicting the air temperatures, air velocities and CO<sub>2</sub> concentrations over the large space is tested.

In chapter 7, the last stage of the research work, which is the parametric studies is presented. The performance of two different air distribution systems (mixing and impinging jet) under two different loads for summer and winter is evaluated. The index for ventilation performance assessment, which is Air Distribution Index, is tested. Finally, a comparison between the performances of the two systems in providing an acceptable indoor environment in large spaces is presented.

Chapter 8 summarises the most important findings and concludes the results that have been achieved from this study. Suggestions for future work that might be carried out in the research area is also given.

# 2 CHAPTER TWO: LITERATURE REVIEW

---

## 2.1 INTRODUCTION

An extensive literature review has been carried out on work undertaken by several researchers in the field of indoor thermal environment in large single zone spaces. Section 2.2 presents airflow distribution strategies used typically in large spaces. Two factors must be considered in the design of these ventilation strategies which are thermal conditions and indoor air quality for the occupied zone since they influence the comfort and well-being of the human occupants within these spaces (Awbi, 2003). Thus, sections 2.3 and 2.4 introduce these two factors respectively. Section 2.5 describes a comprehensive index called the air distribution index which is a combination of thermal comfort, indoor air quality and the effectiveness for removing both internal pollution and heat in the space.

## 2.2 AIRFLOW DISTRIBUTION STRATEGIES USED IN LARGE SPACES

### 2.2.1 Introduction

The distribution strategy of fresh air from the supply diffusers into the enclosure has an essential influence on the airflow pattern formed inside the enclosed space. Any air distribution system that enhances a healthy and comfortable environment for occupants, as well as energy efficiency, can be nominated as a good air distribution system (Karimipannah, Awbi and Moshfegh, 2008). In 2017, an extensive literature survey was carried out on studies of HVAC systems' performance in large rooms which found that only three types of room air distribution strategies are used in large rooms. These are displacement ventilation, mixing ventilation and underfloor air distribution systems UFAD (Mateus and Carrilho da Graça, 2017). In addition, a fourth system, impinging jet ventilation which has been evaluated only in two recent studies by Ye *et al.* (2016) and (Ye *et al.*, 2019) when it was used in the ventilation of a large space. It is traditionally used in typical spaces and described as having a promising potential for large spaces.

## 2.2.2 Displacement Ventilation (DV)

This is a type of ventilation which is based on displacing the impure enclosure air with fresh outside air, see Figure 2.1 and Figure 2.2 . The cool air normally supplied at or near the floor with low velocity (normally  $< 0.5$  m/s) creating an upward airflow motion (thermal plumes) as it gets warmer by heating sources in the enclosure. Therefore, vertical gradients of air velocity, temperature and contaminant density will usually be created.

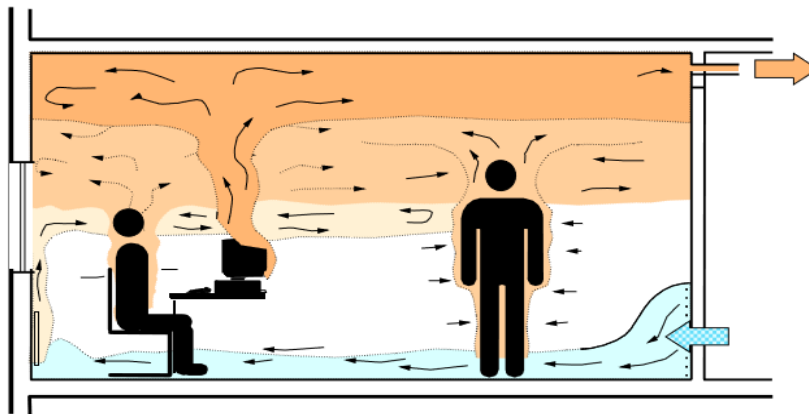


Figure 2.1 Displacement ventilation system (Skistad et al., 2002).

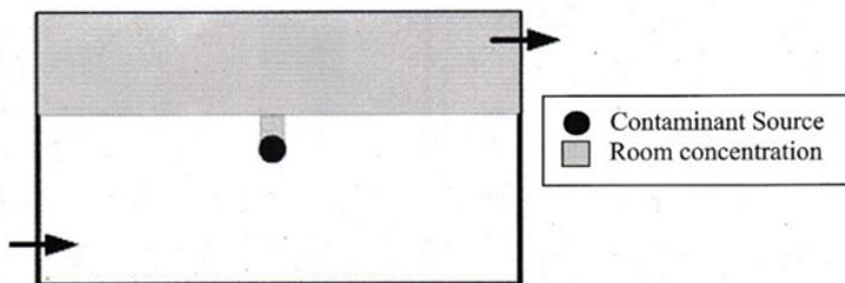


Figure 2.2 Contaminant distribution in displacement ventilation system

Mateus and Carrilho da Graça, (2017) used two large occupied rooms with displacement ventilation systems for performing a set of detailed temperature and CO<sub>2</sub> measurements. These measurements were utilised to estimate the thermal comfort and indoor air quality IAQ performance of these ventilation systems. The results demonstrate that the performance of the displacement ventilation system in both large rooms were adequate in terms of both CO<sub>2</sub> concentration and thermal comfort provision. In addition to this, the measurements of temperature and CO<sub>2</sub> stratification profiles in both rooms showed two different layers: an upper layer occupying a great part of the room volume and contains the heat and pollutant

accumulation and a lower layer with significant temperature and pollutant gradients. The separation between the two layers is known as interface or neutral height  $h_i$  which represents the height where the total plume flow matches the inflow rate.

A displacement ventilation system was used in Gjorik Mountain hall which was a purpose-built sports stadium in Norway. This building was utilised for comparing both long term and transient measurement of the air temperature distribution, airflow rates and energy consumption with predictions from CFD simulation. The results showed a favourable comparison between calculated and measured temperature and velocity fields. However, the result of the computed temperature gradient showed lower values than the measurements (International Energy Agency IEA, 1998).

Ricciardi, Ziletti and Buratti (2016) performed measurements of the DV system performance in a typical eighteen-century Italian theatre with five anders balconies. Their measurements indicated that thermal stratification ranged from 23°C in the parterre (ground floor of the theatre) to 30 °C in the upper order (highest) balconies. The stratification was the main problem in this theatre particularly for the audience in back rows and the balcony areas. Similar measurements were conducted in a theatre in the city of Belgrade by Kavagic et al. (2008). They highlighted two significant issues for displacement ventilation system performance which need to be taken into account. First, space was over-ventilated which may result in the extravagant consumption of energy. The second issue was that the occupants complained of cold discomfort around their feet due to cold draughts.

### 2.2.3 Mixing Ventilation

It is a type of ventilation system where the fresh air is mixed with impure enclosure air to provide a fresh supply of air and reduce the impurity concentrations as shown in Figure 2.3. The air jet is usually supplied in the top parts of the enclosure with velocity (normally > 2.0 m/s) to provide air circulation around the enclosure. The new temperature and contaminant density in the room should be uniform with this method of air supply.

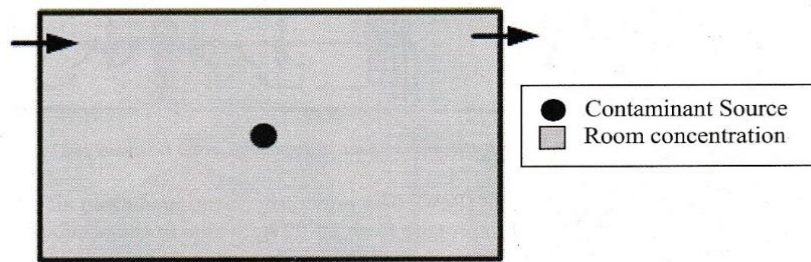


Figure 2.3 Contaminant distribution in mixing ventilation system

Hangan et al. (2001) applied a commercial CFD software to obtain the temperature and velocity distribution for a realistic model of large internal space with complex boundary conditions. These large spaces with mixing ventilation systems were located in the Miami centre of performing arts, USA, and they were two large halls, an opera house and a concert hall. The results obtained demonstrated the power of the CFD software to offer the HVAC designers useful information to optimize the ventilation design for large rooms by testing different airflow distribution strategy ADS in the initial design stage.

A mixing ventilation system was used in a large lecture hall at the University of Putra Malaysia which has been used to carry out measurements of air velocity, air temperature, and relative humidity for one month. The measurements were employed as input parameters for three – dimensional CFD model to study the potential of a new specific insulator which was utilised as an insulating material placed on the lecture hall’s external wall. The study concluded that the CFD simulation results showed that the system is effective in reducing the consumption of the total energy used to cool the hall by 10%. Therefore, CFD was considered to be an appropriate tool to control and identify potential problems and explore the airflow pattern and system performance (Muhielddeen, Adam and Salman, 2015).

The experimentally and numerically investigation by Cheong et al. (2003) in an air- conditional lecture theatre in a Tertiary institution in Singapore showed that the value of the temperature, air velocity and humidity were within the limits recommended by ISO Standard 7730 (BSI, 2005). However, the main issues detected were the presence of recirculation zones which lead to the accumulation of CO<sub>2</sub> in the occupied zone.

## 2.2.4 Underfloor Air Distribution System

In this ventilation type, the conditioned air is supplied from the “bottom up” and not the “top to bottom” as in the overhead type ventilation system. As shown in Figure 2.4, the goal of this system is to provide fresh air immediately to the occupied zone.

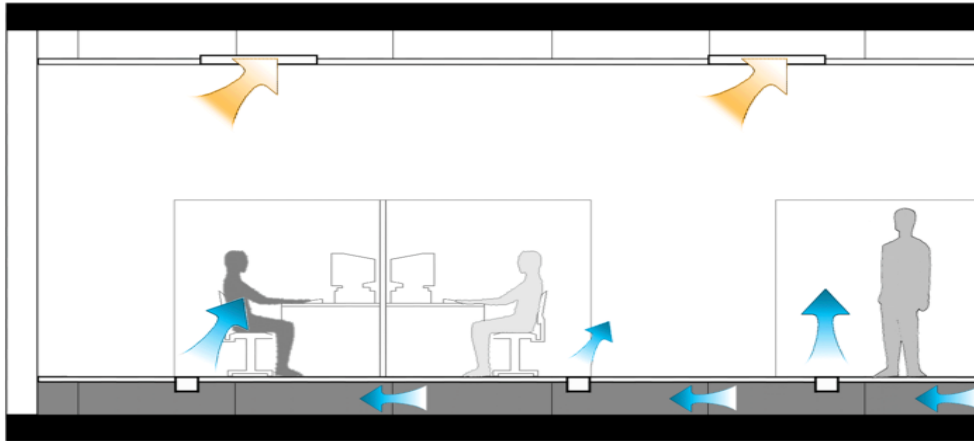


Figure 2.4 Underfloor air distribution system ((Skistad et al., 2002)

Fathollahzadeh et al. (2016) conducted a study using CFD methods to decide what produces a better performance for the underfloor air distribution system in a large place. They found that different locations of the air diffusers, as well as different air supply velocities, were necessary to achieve that target. In spite of discomfort by air drafts which were induced by higher supply air velocity, UFAD was tolerated for the higher difference between room and inflow air temperatures and as a consequence, higher cooling capacity. In the same way, the thermal environment for a large theatre space equipped with an underfloor air distribution system was simulated by using a CFD software. In this system, the air was immediately provided to the bottom of the occupied zone, which generates temperature stratification from the lowest level to the highest level of the zone. The investigation of the UFAD system in a large space showed that the system was capable of producing a smaller vertical variant of the air temperature and more comfortable environment in a dense occupied space.

## 2.2.5 Impinging Jet Ventilation

Karimipناه & Awbi (2002) developed a new ventilation strategy known as impinging jet ventilation. In this type of ventilation, a high momentum air jet discharged downwards onto the floor see Figure 2.5. As the jet impinges onto the floor, it spreads over a considerable area causing the jet momentum to recede but still has enough force reaching long distances in the room. This method makes the air jet able to conquer the buoyancy force created from heat sources resulting into more efficient ventilation in the occupied area compared to a displacement ventilation system (Awbi 2003).

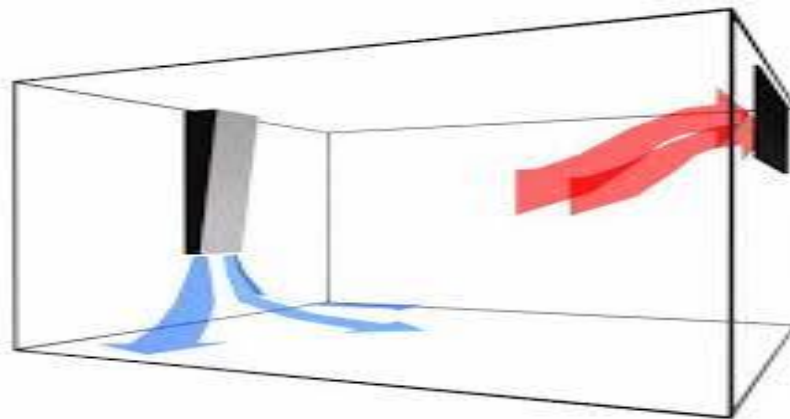


Figure 2.5 Impinging jet ventilation

The flow field of the impinging jet consists of three regions which are the free jet region, the impingement region and the wall jet region, as shown in Figure 2.6 (Chen, Moshfegh and Cehlin, 2012).

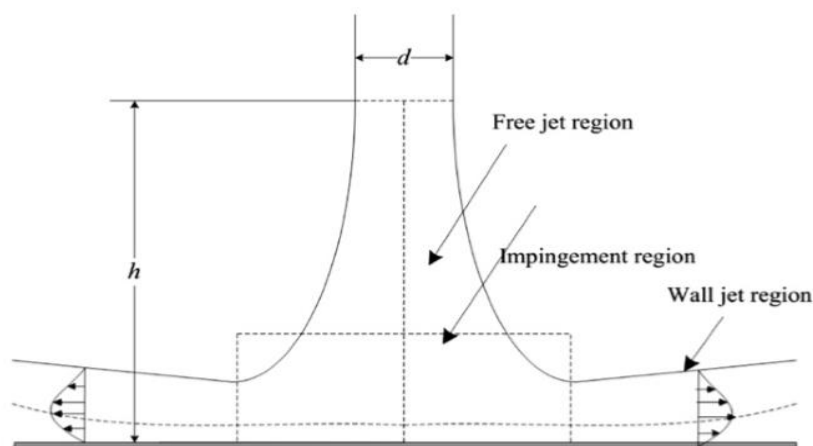


Figure 2.6 Flow regions of an impinging jet (Chen, Moshfegh and Cehlin, 2012)

Only two studies have been carried out to evaluate the ventilation performance of the IJV system in a large space. The first one was conducted numerically by Ye et al. (2016) to study the airflow patterns and the temperature fields of the IJV and MV systems used in heating modes in a large space located in Shanghai. The results show that the IJV system can distribute the warm supply air more easily into the occupied zone than the MV. They also found that the total heating energy consumption for the MV system was higher when compared with the IJV system. The same authors Ye et al. (2019) performed numerically another study as well to predict the distribution of indoor gaseous contaminate concentration using CO<sub>2</sub> for the same large space and ventilation systems. The results revealed that the breathing zone has lower contaminant concentration for the IJV than that for the MV. The results also showed that the IJV has a higher ventilation efficiency and thus more beneficial in supplying good air quality than the MV.

## 2.3 THERMAL COMFORT

### 2.3.1 Introduction

The goal of any ventilation system is to create a suitable microclimate in the ventilated place. In this case, microclimate refers to the thermal environment and air quality. These two factors are essential to the comfort of the occupants of the spaces (Awbi, 2003). The thermal balance can be affected by several factors which are physical activity, clothing resistance and environmental parameters such as air temperature, mean radiant temperature, air humidity and air velocity. To predict the thermal sensation for the body as a whole, the Predicted Mean Vote PMV index can be used for estimating or evaluating the above factors. This model assumes the body to be a single node with regards to its interaction with the local environment. The percentage of the people who are dissatisfied with the thermal environment is measured by Predicted Percentage Dissatisfied PPD index. In addition to that, a person's body is considered as a complicated thermal system in which any parts of the body may react to changes in temperature in different ways. Therefore, multi-node models were introduced to represent the person's body by two or more nodes to deal with inhomogeneous effects in the environment.

Thermal comfort has been defined by the American Society of Heating, Refrigerating and Air-Conditioning Engineers ASHRAE (Standard, 2017) as the condition of mind in which

satisfaction is expressed with the thermal environment. There are six factors affecting thermal comfort: Four physical variables (air temperature, mean radiant temperature, air velocity and relative humidity), and two personal variables (clothing insulation and activity level, i.e. metabolic rate) (Fanger, 1972).

Furthermore, thermal discomfort can be generated by unwanted heating or cooling of one nominated segment of the body. This is known as local discomfort and can be caused by four factors which are draft, vertical air temperature differences, radiant temperature asymmetry and cold or warm floors (BSI, 2005). Moreover, the adaptive model of thermal comfort is also used to estimate comfort conditions. It starts with a behavioural adaptation which is made by people to stay comfortable rather than fully comply with the theory of heat exchange. Such adaptation is a two-way process. The person adapts himself to suit the environmental by such action like changing clothes or posture. He also adapts his thermal environment to suit himself by opening windows or adjusting the heating or cooling provision (Humphreys, Rijal and Nicol, 2013).

The following section describes these three types of thermal comfort models which are Fanger's PMV, Multi-node and adaptive thermal comfort models with specific focus on large spaces.

### 2.3.2 Fanger's PMV Comfort Model

In the 1970s, Fanger's predicted mean vote model was developed from wide climate chamber and laboratory studies carried out on lightly clothed sedentary subjects who were exposed to different thermal environments (Fanger, 1972). According to Fanger (1967), sweat rate and mean skin temperature were the only physiological processes affecting heat balance and were a function of activity level. To derive a linear relationship between sweat rate and activity level, Fanger utilised data from both McNall's study and his study which was conducted by using twenty participators. The two linear relationships that were derived from these studies were substituted into balance equations to generate the comfort equation that can anticipate occupants' conditions for perceiving thermally neutrality.

Furthermore, Fanger (1972) has expanded the comfort equation to be used for non-neutral subjects by using data from 1396 participators. The expanded equation characterised the

thermal comfort as an imbalance between the real heat flow from the body in a specific thermal environment and the heat flow needed for neutral comfort for a specific activity. This equation started to be known as the Predicted Mean Vote index which can be expressed as follows:

$$PMV = \left( 0.352 * e^{\left(-0.42 \frac{M}{A_{Du}}\right)} + 0.032 \right) \times \left\{ \frac{M}{A_{Du}} (1 - \eta) - 0.35 \times \left[ 43 - 0.061 \frac{M}{A_{Du}} (1 - \eta) - p_a \right] - 0.42 \left[ \frac{M}{A_{Du}} (1 - \eta) - 50 \right] - 0.0023 \frac{M}{A_{Du}} (44 - p_a) - 0.0014 \frac{M}{A_{Du}} (34 - t_a) - 3.4 \times 10^{-8} f_{cl} \times [(t_{cl} + 273)^4 - (t_{mrt} + 273)^4 - f_{cl} h_c (t_{cl} - t_a)] \right\} \quad (2.1)$$

where  $A_{Du}$  is Dubois body surface area ( $m^2$ ),  $M$  is the metabolic rate (kcal/h),  $\eta$  is the external mechanical efficiency ( $\eta = W/M$ ,  $W$  is the external mechanical work),  $p_a$  is the water vapour pressure (Pa),  $t_a$  is the air temperature ( $^{\circ}C$ ),  $t_{cl}$  is the clothed body surface temperature ( $^{\circ}C$ ),  $t_{mrt}$  is the mean radiant temperature in relation to a person at a given location ( $^{\circ}C$ ),  $f_{cl}$  is the ratio of clothed body surface area to nude body surface area and  $h_c$  is the convective heat transfer coefficient which is given by:

$$\text{For free convection: } h_c = 2.38(t_{cl} - t_a)^{0.25} \quad (2.2)$$

$$\text{For forced convection: } h_c = 12.1\sqrt{v} \quad (2.3)$$

where  $v$  is the relative velocity between the body and the air ( $m/s$ ).

The PMV index that has been arranged by Fanger is based on the seven-point psychophysical scale as shown in Figure 2.7.

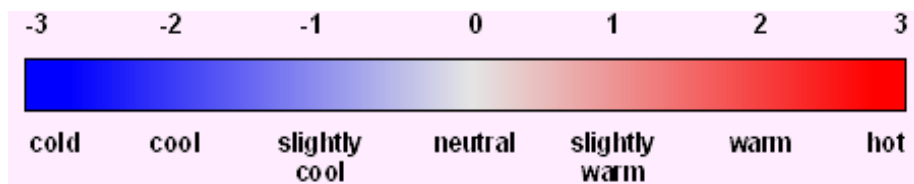


Figure 2.7 The 7-points thermal sensation scale

Fanger correlated the percentage ratio of the people who were dissatisfied with the thermal environment with the predicted mean vote from the experimental data obtainable to him. This developed rational became known as the predicted percentage of dissatisfied which is expressed as (Fanger, 1972):

$$PPD = 100 - 95e^{-\{0.03353(PMV)^4 + 0.2179(PMV)^2\}} \quad (2.4)$$

The PPD value may be calculated using equation (2.4), or for convenience, it may be estimated using Figure 2.8.

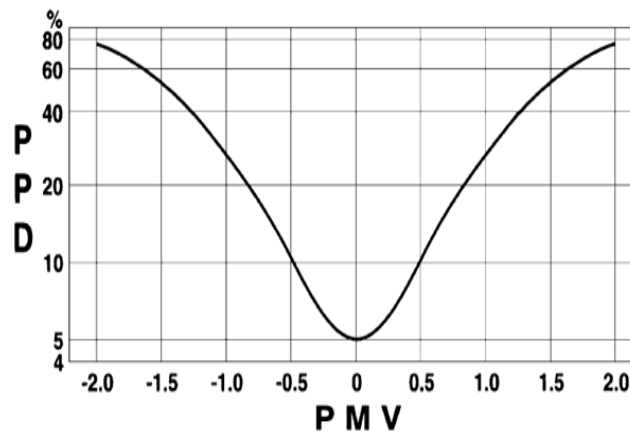


Figure 2.8 Predicted percentage of dissatisfied as a function of PMV

Choeng et al. (2003) evaluated the thermal comfort in a large air-conditioned lecture theatre in a tropical region by using subjective assessment, objective measurement and CFD modelling. The calculated PMV and PPD indices exposed that the occupants felt the theatre to be slightly cool and 20.6% of the people were unsatisfied with the indoor environment. Similarly, the subjective assessment revealed that the people were slightly uncomfortable in the lecture theatre.

To investigate prayers thermal comfort in the state of Kuwait, a field study was performed in six air-conditioned large mosque building by Al-ajmi (2010) during the summer of 2007. The main results of the study showed significant variation in average temperature and as a result thermal discomfort occurred in several mosques. In other words, some were perceived to be within the acceptable range of comfort whereas others were on the slightly cool zone. The reasons behind this variation were probably due to the design and performance of the air distribution strategy. Therefore, there was a need for a further investigation of how thermal comfort was affected by the type of air distribution strategy.

Ricciardi & Buratti (2015) published their work about the assessment of thermal comfort in an ancient Italian theatre by comparing data from a questionnaire to field measurement data. Consequently, they recommended that the PMV questionnaire scale requires to be rescaled resulting in 13 values. In addition to that, they used the neutral comfort temperature method

to evaluate thermal comfort in the same theatre. Their results reveal that the technique is useable to theatres and could be a simple tool for assessing thermal comfort immediately (Ricciardi, Ziletti and Buratti, 2016).

A numerical study by Fathollahzadeh et al. (2016) was conducted in a large and densely occupied space to evaluate the thermal comfort condition of occupants in terms of the PMV and PPD indices and local thermal discomfort indices which are draught and temperature gradient in the vertical direction. This space was ventilated by underflow air distribution system. They found that it was achievable to have a reasonably even distribution of temperature in the occupied zone if the diffusers were located in front of the seats with sufficient air supply momentum. A higher temperature was recorded at a relatively lower position if the diffusers were located under the seats. Moreover, the temperature gradient in the vertical direction was in the acceptable range of ISO 7730 standard particularly that an even distribution of temperature in the occupied zone was accomplished.

### 2.3.3 Multi-node Thermal Comfort Models

The multi-node thermal comfort models are advanced thermal comfort models that are applicable to transient and non-uniform environments while Fanger's PMV models were developed to address steady-state and uniform environments. Almesri & Awbi (2011) pointed out that many mathematical comfort models have been developed in the past forty years to estimate the thermal comfort of occupants in an internal environment. For example, Fanger's PMV model (Fanger, 1970) and the standard effective temperature SET\* (Gagge, Fobelets and Berglund, 1986) were developed to focus on steady-state and uniform environments. Fiala's model (Fiala, 1998) can address transient and uniform environments while Wyon and Ingersoll models (Wyon et al. 1989; Ingersoll et al. 1992) is capable of addressing steady-state and non-uniform environments. A comprehensive model that is capable of solving transient and non-uniform thermal environments is the CBE Center for Built Environment at Berkeley comfort model (Huizenga et al. 2001; Zhang et al. 2005). In addition to this, Fiala and the CBE models are two models which can predict comfort levels that are based on physiological parameters. Fiala's comfort model is a statistical model which predicts the dynamic thermal sensation DTS. Fiala has modified his original model to be able to predict the DTS in stratified environments.

This can be achieved by allocating several environmental parameters at four various levels of the human body: head, trunk, legs and feet.

### The Modified Fiala Comfort Level

According to Almesri & Awbi (2011) a wide range of thermal comfort experiments have been conducted to produce the dynamic thermal sensation DTS model involving a variety of environmental conditions. The dynamic thermal sensation model by Fiala's (Fiala, 1998) considers the link between the skin and body core temperatures in steady-state and dynamic situations. The following formula represents this model:

$$DTS = 3 \tanh \left[ a \Delta T_{sk,m} + \phi + \frac{0.114 \left( \frac{dT_{sk,m}}{dt} \right)^{-1} + 0.137 \left( \frac{dT_{sk,m}}{dt} \right)^{+1} \times \exp(-0.681 \Delta t)}{1 + \phi} \right] \quad (2.5)$$

where  $a = 0.298 \text{ 1/K}$  and  $1.026 \text{ 1/K}$  for  $T_{sk,m} < 0$  and  $\Delta T_{sk,m} > 0$ , respectively,  $\Delta T_{sk,m} = T_{sk,m} - T_{sk,m,set}$ ,  $\Delta T_{hy} = T_{hy} - T_{hy,set}$ .

$$\phi = 6.662 \times \exp\left(\frac{-0.565}{\Delta T_{hy}}\right) \times \exp\left(\frac{-7.634}{5 - \Delta T_{sk,m}}\right) \quad (2.6)$$

### The CBE Comfort Model

According to Almesri & Awbi (2011) the optimum comfort model for the indoor environment should have a prediction capability for both the local and overall thermal sensation as well as thermal comfort in transient and the non-uniform environment. The following formula can express the local thermal sensation LTS:

$$LTS = 4 \left[ \frac{2}{1 + \exp\left(-C_1 \times (T_{sk,local,set}) - K_1 \left( (T_{sk,local} - T_{sk,m}) - (T_{sk,local,set} - T_{sk,m,set}) \right) \right)} - 1 \right] + C_{2i} \frac{dT_{sk,local}}{dt} + C_{3i} \frac{dT_{core}}{dt} \quad (2.7)$$

where  $C_i$  and  $K_i$  are coefficient varying for various body segments.  $C_{2i}$  represents the thermal capacity of the skin while  $C_{3i}$  represents the thermal capacity of the core node. The following formula can calculate the overall thermal sensation OTS:

$$OTS = \frac{\varepsilon Weight_i \times LTS_i}{\varepsilon Weight_i} \quad (2.8)$$

where i indicate different body parts.

$$Weight_i = a \times (LTS_i - LTS_i) \quad (2.9)$$

a is the slope of the linear model, and  $LTS_i$  is the mean of the local thermal sensation.

The local thermal comfort LTC is affected by both local thermal sensation and overall thermal sensation.

$$LTC = f(LTS, OTS) \quad (2.10)$$

The overall thermal comfort OTC can be estimated from two rules which are a function of local thermal comfort.

Rule one: By calculating the average of the two lowest local thermal comforts votes. Rule two: By calculating the average of the two most usual local thermal comfort votes with the two highest local thermal comforts votes. This rule can be used when the second-lowest local thermal comfort vote is  $> (-2.5)$ , and the thermal conditions are transient. Alternatively, rule one can be used if rule two cannot be applied.

### 2.3.4 Adaptive Thermal Comfort Model

The adaptive approach in thermal discomfort can be explained as the reaction of the space occupants to retrieve their comfort. This can be done by changing their activity, clothing or by controlling windows, curtains, fans and mechanical ventilation systems with unconditioned air (BS EN 16798-1, 2019). The adaptive comfort temperature inside a free-running building is the temperature at which most of the space occupants perceive comfort and it is related to the outdoor temperature over the previous days. In other words, it will be higher in warm weather than in cooler weather (CIBSE, 2013).

According to European standard BS EN 16798-1 (2019), the equation which relates the comfort temperature to the outdoor temperature is

$$T_{comp} = 0.33 T_{rm} + 18.8 \quad (2.11)$$

where  $T_{rm}$  is the exponentially weighted running mean of the daily mean outdoor air temperature ( $^{\circ}\text{C}$ ) as the measure of the outdoor temperature and can be calculated by the following equation

$$T_{rm} = (T_{od-1} + 0.8T_{od-2} + 0.6T_{od-3} + 0.5T_{od-4} + 0.4T_{od-5} + 0.3T_{od-6} + 0.2T_{od-7})/3.8 \quad (2.12)$$

where  $T_{od-1}$ ,  $T_{od-2}$ , etc. are the daily mean outdoor air temperatures ( $^{\circ}\text{C}$ ) from yesterday, the day before yesterday and so on.

As indicated in BS EN 16798-1, the comfort temperature in equation (2.11) can be different depending on the type of building, with explanation and suggested acceptable range as shown in Table 2.1 for four building categories.

Table 2.1 Suggested acceptable temperature range for free-running building with an explanation of application (BS EN 16798-1, 2019).

Category	Explanation	Suggested acceptable range (K)
1	High level of expectation only used for spaces occupied by very sensitive and fragile persons	$\pm 2$
2	Normal expectation (for new buildings and renovations)	$\pm 3$
3	A moderate expectation (used for existing buildings)	$\pm 4$
4	Values which are outside the criteria for the above categories (only acceptable for a limited period)	$> 4$

CIBSE overheating task force (2013) proposed three criteria to provide an assessment of building overheats if the indoor space temperature exceeds the acceptable range presented in table 2.1. Any space that fails two out of the three criteria are considered overheated.

1. Criteria one (Hours of exceedance  $H_e$ ): The number of hours that the operative temperature exceeds the upper limit of the acceptable operative temperature by 1K or more i.e.  $\Delta T \geq 1\text{K}$ , during the summer season (1 May to 30 September) not to exceed 3% of the occupied hours.
2. Criteria two (Daily weighted exceedance  $W_e$ ): the weighted exceedance shall be less than or equal to 6 in any one day to avoid overheating.

$$W_e = (h_{e1} \times 1) + (h_{e2} \times 2) + (h_{e3} \times 3) \dots \quad (2.13)$$

where  $h_{e1}$  is the time in hours where  $\Delta T=1$ ,  $h_{e2}$  is the time in hours where  $\Delta T=2$ ,  $h_{e3}$

time in hours where  $\Delta T=3$  and so on.

3. Criteria three (Upper limit temperature  $T_{upp}$ ): The maximum operative temperature shall not exceed 4K above comfort temperature at any time.

## 2.4 INDOOR AIR QUALITY

### 2.4.1 Introduction

Indoor air quality is a significant topic which has a short term impact as well as a long term impact on the occupants' health (Wargocki *et al.*, 2002). People can be affected in three areas when indoor air quality is poor. The first area is comfort such as the smelly and stuffy environment. The second area is serious health effects like burning eyes, conveyance of airborne illness. The third area is delayed health effects which may take many years to appear (Awbi, 2003).

Two main strategies are usually exercised by building designers to provide acceptable IAQ in buildings. In the first place, to improve the quality of indoor air by raising the air ventilation rate, which successively decreases air pollutant concentrations, called 'dilution' ventilation. The second strategy is minimising the pollution source inside and outside the building to reduce the spread of contaminants in the internal air (Al horr *et al.*, 2016).

### 2.4.2 Indoor Air Pollutants

The primary sources of the pollution inside buildings are the occupants' activities, furniture and the materials used in buildings. The internal air is usually polluted by odour, CO<sub>2</sub>, volatile organic compounds including formaldehyde, tobacco smoke, ozone, nitrogen oxides, aerosols and particulate matter (PM) (Awbi, 2003; BS EN 16798-1, 2019; Kukadia and Upton, 2019).

#### **Odour**

Even if, the exposure to odour is not enjoyable, it does not usually have health effects. Odour is always linked with waste, bathroom activities, cooking and occupancy. Body odour is driven out by the people as a consequence of sweat and sebaceous secretion through the skin as well as the digestive system. For a space allocation of 5.7 m<sup>3</sup> per person and to overcome an

ordinary odour intensity, 9.9 L/s and 7.6 L/s per person of outdoor air flow rate are required for adults and child occupancy respectively (Awbi, 2003).

### **Carbon dioxide**

The rate of production of carbon dioxide CO<sub>2</sub> by the human respiratory system is associated with the metabolic rate by the equation (MacIntyre, 1980):

$$G = 4 \times 10^{-5} MA \quad (2.14)$$

where  $G$  is the CO<sub>2</sub> production in (L/s),  $M$  is the metabolic rate in (W/m<sup>2</sup>) and  $A$  is the body surface in (m<sup>2</sup>).

An average sedentary adult produces around 0.005 L/s of CO<sub>2</sub> by the respiratory system. CO<sub>2</sub> is nominated as a perfect indicator of the level of the internal air quality since it cannot be filtered or absorbed like some other contaminants such as tobacco smoke.

The majority of ventilation standards advise that the maximum concentration of CO<sub>2</sub> is 0.5% or 5000 ppm. Nevertheless, several studies generally acknowledged that this limit is excessively high for human comfort and the concentration below 0.1 % or 1000 ppm is desired to avoid headache and discomfort (Awbi, 2003; BS EN ISO-16000-26, 2012; BS EN 16798-1, 2019).

Nowadays, many researchers use CO<sub>2</sub> concentration measurements to assess building ventilation and indoor air quality. These measurements are uncomplicated and competitive compared to other methods like the tracer gas methods (Santamouris et al. 2008; Mahyuddin & Awbi 2010; Gładyszewska-Fiedoruk 2011; Shah & Dufva 2017)

### **Ozone**

Ozone is a molecule with a chemical formula O<sub>3</sub> and can exist naturally in outdoor air. Also, it can be generated indoors by e.g. office machines namely laser printers and photocopies. If it is present in high concentration it might cause chronic effects on humans. A maximum concentration of 100mg/m<sup>3</sup> or 50 p.p.b (part per billion) for 8 hours continues exposure is recommended by both ASHRAE standard 62.1 (American Society of Heating, 2016) and the World Health Organisation WHO (Organization, 2010).

## **Radon**

Radon is a radioactive gas which exists naturally as a result of the decay of radium. The main concern with radon is the perspective for causing lung cancer for occupants of places where very high concentration has been found. In some areas, considerable amounts of radon can go into a building from the soil through cracks in basement walls or slab floors. Pressurization of a space is reducing its levels in that space since its entry rate from soil depends on the pressure differences (McQuiston and Parker, 1982). In UK, remedial action should be taken at radon level of  $200 \text{ Bq. m}^{-3}$  in a building (Denman, Crockett and Groves-Kirkby, 2018).

## **Volatile Organic Compounds VOCs**

Volatile organic compounds are a type of organic chemicals that are often produced in modern indoor environments. They are a consequence of combustion sources, building materials, plants and animals, cleaning agents and solvents. One of the most popular VOCs is Formaldehyde gas which can cause several problems like asthmatic and is potentially classified as a cancer hazard (McQuiston and Parker, 1982). The acceptable concentration is in the range of  $0.3 \text{ mg/m}^3$  for an 8-hour exposure (Kukadia and Upton, 2019).

## **Particulate Matter**

Particulate matter is composed of a mixture of liquid and solid particles suspended in the air such as complex organic chemicals, carbon, ammonium, mineral dust and water. The particulate matter can be generated from transport, construction, combustion and demolition activities. Coarse particulate matter  $PM_{10}$  (up to 10 micrometre in diameter) and fine particulate matter  $PM_{2.5}$  (up to 2.5 micrometre in diameter) are typically measured due to the significance of their size with regards to the human respiratory system (Kukadia and Upton, 2019).

## **Carbon monoxide CO**

It is an odourless and colourless gas generating from incomplete fossil fuels combustion. It can be found in high concentrations in close spaces like car parking buildings or traffic intersections during peak traffic hours. It can reduce the ability of blood delivering oxygen to vital body tissues, and symptoms involve headaches, fatigue and dizziness (Hackley, Feinstein

and Dixon, 2007). The maximum concentration of CO is 10 ppm for an 8-hour exposure (Kukadia and Upton, 2019).

### 2.4.3 Ventilation Effectiveness

There are two values which can be used to define the effectiveness of an air distribution system in removing generated pollutants or heat from the ventilated space. The first one is called ventilation effectiveness for the removal of pollutants  $\varepsilon_c$  and is defined in terms of the concentration and the distribution of pollutants inside the space (Sandberg, 1981). The second one is called ventilation effectiveness for the removal of heat  $\varepsilon_t$  and is defined in terms of the temperature and its distribution within the space (Awbi and Gan, 1993). The local ventilation effectiveness indicate the ability of the ventilation system in providing fresh air to different parts of the room. It can be presented as a local relative effectiveness or as overall relative effectiveness for the entire occupied zone (BS EN 16798-3, 2017).

The local ventilation effectiveness for the removal of pollutants is defined as:

$$\varepsilon_c = \frac{C_e - C_\infty}{C_p - C_\infty} \quad (2.15)$$

And the overall ventilation effectiveness for the removal of pollutants  $\bar{\varepsilon}_c$  is defined as:

$$\bar{\varepsilon}_c = \frac{C_e - C_\infty}{\bar{C} - C_\infty} \quad (2.16)$$

where  $C_e$  is the contaminant concentration of air exhaust (p.p.m),  $C_\infty$  is the contaminant concentration at air supply (p.p.m),  $C_p$  is the contaminant concentration at a point (p.p.m) and  $\bar{C}$  is the contaminant concentration in the occupied zone (p.p.m).

The local ventilation effectiveness for heat removal is defined as:

$$\varepsilon_t = \frac{t_e - t_\infty}{t_p - t_\infty} \quad (2.17)$$

and the overall ventilation effectiveness for heat removal  $\bar{\varepsilon}_t$  is defined as:

$$\bar{\varepsilon}_t = \frac{t_e - t_\infty}{\bar{t} - t_\infty} \quad (2.18)$$

where  $t_e$  is the air temperature at air exhaust ( $^{\circ}\text{C}$ ),  $t_\infty$  is the air temperature of air supply ( $^{\circ}\text{C}$ ),  $t_p$  is the air temperature at a point ( $^{\circ}\text{C}$ ) and  $\bar{t}$  is the mean air temperature in the occupied zone ( $^{\circ}\text{C}$ ).

## 2.5 AIR DISTRIBUTION INDICES

Even though high values of both the overall ventilation effectiveness for the removal of pollutants and for heat removal state a high efficiency of the ventilation system, they do not alone offer a strong indication of the air quality and thermal comfort in the occupied zone (Awbi, 2003). Awbi and Gan (1993) combined  $\bar{\varepsilon}_c$  with Fanger's Percentage of Dissatisfied for air quality and  $\bar{\varepsilon}_t$  with Fangers Predicted Percentage of Dissatisfied to define two new numbers that include the percentage of dissatisfied for air quality and thermal comfort, thus:

$$N_c = \frac{\bar{\varepsilon}_c}{PD} \quad (2.19)$$

$$N_t = \frac{\bar{\varepsilon}_t}{PPD} \quad (2.20)$$

where  $N_c$  is the air distribution number for air quality and  $N_t$  is the air distribution number for thermal comfort.

The expression for PD and PPD are as follow (Fanger 1988; BSI 2007)

$$PD = 395 \times EXP(-1.83\dot{v}^{0.25}) \quad (2.21)$$

$$PPD = 100 - 95 \times EXP - \{0.03353(PMV)^4 + 0.2179(PMV)^2\} \quad (2.22)$$

where  $\dot{v}$  is the outdoor air flow rate (L/s) per standard person and  $PMV$  is the Predicted Mean Vote as defined in ISO 7730 (BSI, 2005)

The two numbers  $N_c$  and  $N_t$  have been combined by (Awbi and Gan, 1993) to produce what they called the Air Distribution Index :

$$ADI = \sqrt{(N_c \times N_t)} \quad (2.23)$$

Achieving a value of  $ADI \geq 10$  by ventilation systems designed for acceptable values of 10% for both PD and PPD can be assumed to be a good air distribution system. However, a large value of ADI would not ensure the existence of a good air distribution system as unwanted local conditions might be still present. Consequently, ADI should be applied along with room temperature distribution and air movement measurements or predictions to evaluate the global and the local conditions particularly the presence of high or low temperature or local draughts regions within the occupied region (Awbi & Gan 1993; Awbi 1998).

Furthermore, various work reported in the literature review have used the Air distribution Index to assess different air distribution system performance namely, (Awbi 2008; Jurelionis & Seduikyte 2008; Karimipanah et al. 2008)

## 2.6 CHAPTER SUMMARY

This chapter presented a literature review covering the background of this study. The literature point out four airflow distribution strategies used in large spaces, which are displacement ventilation, mixing ventilation, under floor air distribution system and impinging jet ventilation. It was identified that only one study reported an evaluation of the performance of using impinging jet ventilation in large spaces for heating mode. Also, three thermal comfort models and indoor air pollutants were described in detail. The chapter was concluded by presenting the air distribution Index, which has been used to characterise ventilation systems in typical spaces but, it has not been studied for large spaces to date.

# 3 CHAPTER THREE: CFD MODELLING

---

## 3.1 INTRODUCTION

During the last two decades, computational fluid dynamics has shined like a new field for predicting the air flow in a ventilated room. The solution of the conservation equations of mass, momentum, energy along with the transport equations for turbulent velocity and its scale in two and three dimensions are the base of these CFD programs.

Awbi (1989) applied computational fluid dynamics to predict the heat transfer and air flow in 2-D enclosures and 3-D flow of a wall jet over surface-mounted obstacles. Logically good results are generated by CFD for the air velocity and the distribution of temperature in an enclosure cooled by a ceiling jet. Also, the heating and cooling prediction for the enclosure and the wall jet flow over an obstacle appear to be physically reasonable and can be used in situations when there were no experimental data available. The use of CFD simulations for room ventilation designs provides countably more qualitative and quantitative information than physical model tests. The reason is that measurement does not usually provide a full description of the flow pattern, particularly for flows at low velocity and turbulence as it is usually the case in ventilated enclosures. However, it is essential that a CFD prediction is evaluated before using it with confidence in different room ventilation studies. Chen (2014) mentioned in her doctoral thesis that as the growth of the computer technology together with the easier use of CFD programs, CFD technique has obtained growing publicity in both research and industry to explore the physics of complex flows and develop equipment and handling strategies. For example, D'Agostino & Congedo (2014) used a three-dimensional CFD model to examine the efficiency of natural ventilation in a historical building in the South of Italy. The CFD results helped them to clarify how natural ventilation can generate several microclimatic conditions and how these different conditions can impact on moisture dynamics and artworks conservation.

The following sections describe the governing equation of fluid dynamics, the turbulence modelling, solution of the transport equation, boundaries of transport equations and accuracy of CFD results. More details regarding the principles and concepts of CFD are mentioned in many text books, e.g. Anderson (1995), Ferziger & Peric (2012), Wesseling

(2009). Additional information related to room airflow and heat transfer is provided in Awbi (2003) and Nielsen *et al.* (2007).

## 3.2 GOVERNING EQUATIONS OF FLUID DYNAMICS

The equations that characterise the fluid flow, heat and concentration distribution within an enclosure are based on the conservation of mass, momentum (Navier-Stokes equations), thermal energy and concentration within the enclosure. These are described in the following sections.

### 3.2.1 Conservation of Mass

Assuming  $U$ ,  $V$  and  $W$  to be the velocity components in  $x$ ,  $y$  and  $z$  directions, respectively,  $\rho$  the fluid density and  $(t)$  the time, then the rate of increase in the fluid mass within the control volume  $dx.dy.dz$  is equal to the net rate of influx of mass to the control volume:

$$\frac{\partial \rho}{\partial t} + \frac{\partial}{\partial x}(\rho U) + \frac{\partial}{\partial y}(\rho V) + \frac{\partial}{\partial z}(\rho W) = 0 \quad (3.1)$$

The equations of velocity are substituted by a time-mean component and a fluctuating component when turbulent flow is considered, i.e.:

$$U = u + u' \quad V = v + v' \quad W = w + w'$$

It has been assumed that the fluctuation  $u'$ ,  $v'$  and  $w'$  occur over a much shorter time interval than  $\partial t$  so  $u \approx U$ ,  $v \approx V$  and  $w \approx W$  during this time interval.

Thus, the conservation of mass equation becomes:

$$\frac{\partial \rho}{\partial t} + \frac{\partial}{\partial x}(\rho u) + \frac{\partial}{\partial y}(\rho v) + \frac{\partial}{\partial z}(\rho w) = 0 \quad (3.2)$$

For steady state and incompressible flow, equation (3.2) becomes:

$$\frac{\partial u}{\partial x} + \frac{\partial v}{\partial y} + \frac{\partial w}{\partial z} = 0 \quad (3.3)$$

### 3.2.2 Conservation of Momentum (Navier-Stokes Equations)

By applying the law of conservation of momentum, i.e. the net change of momentum in the x, y and z directions, the following equations are achieved:

Conservation of U-momentum:

$$\begin{aligned} \frac{\partial}{\partial t}(\rho U) + \frac{\partial}{\partial x}(\rho UU) + \frac{\partial}{\partial y}(\rho UV) + \frac{\partial}{\partial z}(\rho UW) = -\frac{\partial P}{\partial x} + \frac{\partial}{\partial x}\left(\mu \frac{\partial U}{\partial x}\right) + \frac{\partial}{\partial y}\left(\mu \frac{\partial U}{\partial y}\right) + \frac{\partial}{\partial z}\left(\mu \frac{\partial U}{\partial z}\right) + \\ \frac{1}{3} \frac{\partial}{\partial x} \left[ \mu \left( \frac{\partial U}{\partial x} + \frac{\partial V}{\partial y} + \frac{\partial W}{\partial z} \right) \right] + \rho g_x \end{aligned} \quad (3.4)$$

Conservation of V-momentum:

$$\begin{aligned} \frac{\partial}{\partial t}(\rho V) + \frac{\partial}{\partial x}(\rho UV) + \frac{\partial}{\partial y}(\rho VV) + \frac{\partial}{\partial z}(\rho VW) = -\frac{\partial P}{\partial y} + \frac{\partial}{\partial x}\left(\mu \frac{\partial V}{\partial x}\right) + \frac{\partial}{\partial y}\left(\mu \frac{\partial V}{\partial y}\right) + \frac{\partial}{\partial z}\left(\mu \frac{\partial V}{\partial z}\right) + \\ \frac{1}{3} \frac{\partial}{\partial y} \left[ \mu \left( \frac{\partial U}{\partial x} + \frac{\partial V}{\partial y} + \frac{\partial W}{\partial z} \right) \right] + \rho g_y \end{aligned} \quad (3.5)$$

Conservation of W-momentum:

$$\begin{aligned} \frac{\partial}{\partial t}(\rho W) + \frac{\partial}{\partial x}(\rho UW) + \frac{\partial}{\partial y}(\rho VW) + \frac{\partial}{\partial z}(\rho WW) = -\frac{\partial P}{\partial z} + \frac{\partial}{\partial x}\left(\mu \frac{\partial W}{\partial x}\right) + \frac{\partial}{\partial y}\left(\mu \frac{\partial W}{\partial y}\right) + \\ \frac{\partial}{\partial z}\left(\mu \frac{\partial W}{\partial z}\right) + \frac{1}{3} \frac{\partial}{\partial z} \left[ \mu \left( \frac{\partial U}{\partial x} + \frac{\partial V}{\partial y} + \frac{\partial W}{\partial z} \right) \right] + \rho g_z \end{aligned} \quad (3.6)$$

where  $p$  is the static pressure (Pa),  $\mu$  is the dynamic viscosity of the fluid (kg/m.s) and  $\rho g_x$ ,  $\rho g_y$  and  $\rho g_z$  are the body force in the x, y and z directions.

By replacing U, V and W by the time-mean and fluctuating components and using a similar expression for P where  $P = p + p'$  then equation (3.4) to (3.6) become:

$$\begin{aligned} \frac{\partial}{\partial t}(\rho u) + \frac{\partial}{\partial x}(\rho uu) + \frac{\partial}{\partial y}(\rho uv) + \frac{\partial}{\partial z}(\rho uw) = -\frac{\partial P}{\partial x} + \frac{\partial}{\partial x}\left(\mu \frac{\partial u}{\partial x}\right) + \frac{\partial}{\partial y}\left(\mu \frac{\partial u}{\partial y}\right) + \frac{\partial}{\partial z}\left(\mu \frac{\partial u}{\partial z}\right) + \\ \frac{1}{3} \frac{\partial}{\partial x} \left[ \mu \left( \frac{\partial u}{\partial x} + \frac{\partial v}{\partial y} + \frac{\partial w}{\partial z} \right) \right] + \frac{\partial}{\partial x}(-\rho \overline{u'u'}) + \frac{\partial}{\partial y}(-\rho \overline{u'v'}) + \frac{\partial}{\partial z}(-\rho \overline{u'w'}) + \rho g_x \end{aligned} \quad (3.7)$$

$$\begin{aligned} \frac{\partial}{\partial t}(\rho v) + \frac{\partial}{\partial x}(\rho uv) + \frac{\partial}{\partial y}(\rho vv) + \frac{\partial}{\partial z}(\rho vw) = -\frac{\partial P}{\partial y} + \frac{\partial}{\partial x}\left(\mu \frac{\partial v}{\partial x}\right) + \frac{\partial}{\partial y}\left(\mu \frac{\partial v}{\partial y}\right) + \frac{\partial}{\partial z}\left(\mu \frac{\partial v}{\partial z}\right) + \\ \frac{1}{3} \frac{\partial}{\partial y} \left[ \mu \left( \frac{\partial u}{\partial x} + \frac{\partial v}{\partial y} + \frac{\partial w}{\partial z} \right) \right] + \frac{\partial}{\partial x}(-\rho \overline{u'v'}) + \frac{\partial}{\partial y}(-\rho \overline{v'v'}) + \frac{\partial}{\partial z}(-\rho \overline{v'w'}) + \rho g_y \end{aligned} \quad (3.8)$$

$$\begin{aligned} \frac{\partial}{\partial t}(\rho w) + \frac{\partial}{\partial x}(\rho u w) + \frac{\partial}{\partial y}(\rho v w) + \frac{\partial}{\partial z}(\rho w w) &= -\frac{\partial P}{\partial z} + \frac{\partial}{\partial x}\left(\mu \frac{\partial w}{\partial x}\right) + \frac{\partial}{\partial y}\left(\mu \frac{\partial w}{\partial y}\right) + \frac{\partial}{\partial z}\left(\mu \frac{\partial w}{\partial z}\right) + \\ \frac{1}{3} \frac{\partial}{\partial z}\left[\mu\left(\frac{\partial u}{\partial x} + \frac{\partial v}{\partial y} + \frac{\partial w}{\partial z}\right)\right] &+ \frac{\partial}{\partial x}(-\rho \overline{u'w'}) + \frac{\partial}{\partial y}(-\rho \overline{v'w'}) + \frac{\partial}{\partial z}(-\rho \overline{w'w'}) + \rho g_z \end{aligned} \quad (3.9)$$

where  $(-\rho \overline{u'u'})$ ,  $(-\rho \overline{v'v'})$ ,  $(-\rho \overline{w'w'})$ ,  $(-\rho \overline{u'v'})$ ,  $(-\rho \overline{u'w'})$ ,  $(-\rho \overline{v'w'})$  are turbulent Reynolds stresses.

### 3.2.3 Conservation of Thermal Energy

By applying the law of conservation of thermal energy which states that the net increase in internal energy in the control volume equals to the net flow of energy by convection plus the net inflow by thermal mass diffusion, in the control volume  $dx dy dz$ , the following equation is obtained:

$$\begin{aligned} \frac{\partial}{\partial t}(\rho T) + \frac{\partial}{\partial x}(\rho u T) + \frac{\partial}{\partial y}(\rho v T) + \frac{\partial}{\partial z}(\rho w T) \\ = \frac{\partial}{\partial x}\left(\Gamma \frac{\partial T}{\partial x}\right) + \frac{\partial}{\partial y}\left(\Gamma \frac{\partial T}{\partial y}\right) + \frac{\partial}{\partial z}\left(\Gamma \frac{\partial T}{\partial z}\right) + \\ \frac{\partial}{\partial x}(-\rho \overline{u'T'}) + \frac{\partial}{\partial y}(-\rho \overline{v'T'}) + \frac{\partial}{\partial z}(-\rho \overline{w'T'}) + S_T \end{aligned} \quad (3.10)$$

where  $\Gamma$  is the diffusion coefficient ( $m^2/s$ ), and it is given by  $\Gamma = \frac{\mu}{\sigma}$ ,  $\sigma$  = the Prandtl number of fluid and it is given by  $\sigma = \frac{\mu C_p}{k}$ ,  $C_p$  is the specific heat capacity (J.kg/K),  $k$  is the thermal conductivity (W/m.K).

$S_T$  = source term for the rate of thermal energy production.

$(\rho \overline{u'T'})$ ,  $(\rho \overline{v'T'})$ ,  $(-\rho \overline{w'T'})$  = the turbulent heat fluxes.

### 3.2.4 The Concentration of Species

Replacing  $S_T$  in equation (3.10) by  $S_c$ , which is the rate of concentration production, the equation of concentration of species will be obtained as follow:

$$\begin{aligned} \frac{\partial}{\partial t}(\rho c) + \frac{\partial}{\partial x}(\rho u c) + \frac{\partial}{\partial y}(\rho v c) + \frac{\partial}{\partial z}(\rho w c) \\ = \frac{\partial}{\partial x}\left(\Gamma \frac{\partial c}{\partial x}\right) + \frac{\partial}{\partial y}\left(\Gamma \frac{\partial c}{\partial y}\right) + \frac{\partial}{\partial z}\left(\Gamma \frac{\partial c}{\partial z}\right) + \end{aligned} \quad (3.11)$$

$$\frac{\partial}{\partial x}(-\rho\overline{u'c'}) + \frac{\partial}{\partial y}(-\rho\overline{v'c'}) + \frac{\partial}{\partial z}(-\rho\overline{w'c'}) + S_c$$

where  $c$  is the time-mean concentration,  $c'$  is the deviation from the mean and  $(-\rho\overline{u'c'})$ ,  $(-\rho\overline{v'c'})$ ,  $(-\rho\overline{w'c'})$  are the turbulent diffusion fluxes.

### 3.3 TURBULENCE MODELS

The solution of the majority of practical fluid flow problems can be obtained by using several classical turbulence models which are based on the eddy (turbulent) viscosity and the eddy (turbulent) diffusivity concepts. In other words, these concepts were established on the assumption that there is identification between the effects of viscous stresses and Reynolds stresses on the mean flow (Awbi, 2003). In terms of predicting turbulent flow, there are three different turbulence approaches which can deal with the varying elements of flow. They are Direct Numerical Simulation DNS, Large-Eddy Simulation LES and Reynolds Averaged Navier-Stokes simulation RANS (Chen and Srebric, 2011).

#### 3.3.1 Direct Numerical Simulation

The Direct Numerical Simulation predicts a turbulent flow by solving the Navier-Stokes equations directly without approximations. An exact numerical resolution is required to compute all the details of the turbulent flow successfully. According to Zhai et al. (2007), the smallest eddy size for most indoor airflow is about 0.01 to 0.001 m and required grid size to predict the solution for a small office of around  $1 \times 10^{15}$  to  $1 \times 10^{18}$  cells which may take a long computing time to accomplish a solution. Therefore, applying DNS to air flow in an enclosed environment is not practical for design at present.

#### 3.3.2 Large-Eddy Simulation

In LES, the turbulent flow motion is separated into large scale motion and small scale motion. The large scale motion is immediately computed in LES while the small scale motion requires to be modelled since it affects the large scale motion. Appropriate subgrid-scale model should be used for the simulation which is the most crucial part of this approach. LES model solves three dimensional, steady and time-dependent flows where it computes a mean of the time-dependent flow fields to acquire the steady-state solution. Consequently, considerable

computing time is needed which explains why only a small number of indoor space modelling have been carried out to present using LES models (Davidson and Nielsen, 1996; Zhang and Chen, 2000).

### 3.3.3 Reynold Averaged Navier-Stokes Simulation

The RANS approaches is divided into two main groups: eddy-viscosity models and Reynolds Stress models (Zhai *et al.*, 2007).

#### 3.3.3.1 RANS Eddy-Viscosity Models

The Eddy-viscosity models are based on the Boussinesq suggestion in which the Reynolds Stresses could be linked to the mean rate of strain through an eddy viscosity (Awbi, 2003). Depending on the number of transport equations used, the Eddy-Viscosity model is generally classified to the following models (Zhai *et al.*, 2007).

##### Zero-Equation Eddy-Viscosity Models

These models are the simplest eddy viscosity models where they have one algebraic equation for turbulent viscosity and zero additional partial differential equation beyond the Reynolds-averaged equations. Chen & Xu (1998) developed the zero-equation models to model airflows in enclosed environments by using uniform turbulence intensity assumption. They derived an algebraic expression for defining the turbulent viscosity ( $\mu_t$ ):

$$\mu_t = 0.03874 \times U \times L \quad (3.12)$$

where  $U$  is Local mean velocity (m/s) and  $L$  is distance to the nearest wall (m).

Often these models are used for obtaining an initial and quick solution of the flow domain (Nielsen, 1998).

##### One-Equation Eddy-Viscosity Models

Sometimes the turbulence viscosity correlations for zero-equation models may fail due to their physical deficiencies. Consequently, the effects of non-local and flow history on turbulent kinetic energy,  $k$ , is used by one-equation models to calculate eddy viscosity  $\mu_t$  as follows (Zhai *et al.*, 2007):

$$\mu_t = C \times k^{1/2} \times l \quad (3.13)$$

where  $k$  is the turbulent kinetic energy (J) and is obtained by solving a transport equation,  $l$  is the turbulent length scale (m) and  $C$  is constant coefficient.

Several one equation models derive the transport equation for other turbulent variables while most of them are used to solve the transport equations (Baldwin and Barth, 1990).

### Two-Equation Eddy-Viscosity Models

The two-equation eddy-viscosity models solve a second partial differential transport equation in addition to the k-equation. More turbulence physics is represented by a variable  $z$  which is related to the turbulence length scale with the following formula:

$$z = k^\alpha \times l^\beta \quad (3.14)$$

where  $\alpha$  and  $\beta$  are indices the values of which vary from one model to another.

The two-equation models are more sophisticated than the zero and one-equation models since they do not need previous knowledge of turbulence structure.

### **k-ε two-equation eddy-viscosity model**

The k-ε model family is the most prevalent turbulence model which is summarised in Table 3.1.

*Table 3.1 The k-ε model family.*

<b>k-ε model family &amp; developer</b>	<b>General remarks</b>
<b>Standard k-ε by Launder and Spalding (1972)</b>	It is one of the most popular models which provides reasonable results mostly for global flow and temperature patterns. However, it faces difficulty when high buoyancy effect or large temperature gradient exists in a room.
<b>Renormalisation group RNG k-ε model by Yakhot &amp; Orszag (1986)</b>	The model is capable of predicting indoor airflow, temperature and gas concentration distribution in enclosed environments such as a large office area.
<b>Realisable k-ε model by Shih <i>et al.</i> (1995)</b>	This model gives much better results for swirling flows and flows inclosing separations.

## k- $\omega$ two-equations eddy-viscosity model

The k- $\omega$  model family has started to draw more attention in several industrial applications in the last ten years or so. Table 3.2 summarises these models.

Table 3.2 The k- $\omega$  model family

k- $\omega$ model family & developer	General remarks
<b>Standard k-<math>\omega</math> by Wilcox (1988)</b>	This flow model is capable for predicting adverse equilibrium pressure flows, while it has minimal robustness in the wake part and free shear flows (Wilcox, 1988 ; Huang et al. 1992).
<b>Shear stress transport SST k-<math>\omega</math> model by Menter (1994)</b>	The model was developed by combining both standard k- $\omega$ with a standard k- $\epsilon$ models. It is equivalent to a k- $\epsilon$ model in areas far from walls. This model has been used by many studies and has superior performance to both the standard k- $\epsilon$ and RNG k- $\epsilon$ models in general.

### 3.3.3.2 RANS Reynolds Stress Models

The Reynolds Stress Models solve the transport equations for the Reynolds stresses together with an equation for dissipation rate to close the RANS equations. Since the RSM takes into account the effects of anisotropy, it can give a more accurate prediction for complex flow than the one and two-equation models based on isotropic turbulence (Sorensen and Nielsen 2003).

## 3.4 SOLUTION OF THE TRANSPORT EQUATION

The transport equations for conservation of momentum, conservation of thermal energy, conservation of species and the equations for dissipation of turbulence all have the following general form:

$$\begin{aligned} & \frac{\partial}{\partial t}(\rho\phi) + \frac{\partial}{\partial x}(\rho u\phi) + \frac{\partial}{\partial y}(\rho v\phi) + \frac{\partial}{\partial z}(\rho w\phi) \\ & = \frac{\partial}{\partial x}\left(\Gamma\phi\frac{\partial\phi}{\partial x}\right) + \frac{\partial}{\partial y}\left(\Gamma\phi\frac{\partial\phi}{\partial y}\right) + \frac{\partial}{\partial z}\left(\Gamma\phi\frac{\partial\phi}{\partial z}\right) + S_\phi \end{aligned} \quad (3.15)$$

where  $\phi$  is the dependent variable,  $S_\phi$  is the source term that has different expression for different transport equations and  $\Gamma_\phi$  is the diffusion coefficient for scalar variables and it is the effective viscosity for vector variables.

This is the form of the transport equations which can be discretised and solved numerically by one of the conventional methods, such as the finite-difference method FDM, finite-volume method FVM and finite-element method FEM. The finite-volume method is the most popular method in computational fluid dynamics since it is more durable and frugal in computational time. This method will be described in the next section; it is used by most commercially CFD codes.

### 3.4.1 The Finite Volume Method

It is necessary to create a computational grid in which the discrete of the dependent variables  $\phi$ 's are estimated at grid points. In other words, the distribution of  $\phi$  flow domain is discretised and this is defined as discretisation.

To develop the finite volume equation for a grid point  $P$ , which is a point of intersection of grid lines, an integrating the following equations is required:

$$\frac{\partial}{\partial x}(\rho u \phi) = \frac{\partial}{\partial x} \left( \Gamma \phi \frac{\partial \phi}{\partial x} \right) + S_\phi \quad (3.16)$$

which is a one –dimensional transport equation including convection and diffusion terms, or by obtaining it directly from the cell shown in Figure 3.1.

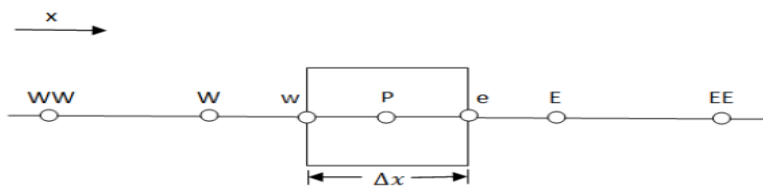


Figure 3.1 Grid point (P) for a one-dimensional field

Different discretisation schemes can be applied to create the discretised equation such as the upwind difference, central difference and hybrid schemes. The central difference is suitable for solving problems that are dominated by diffusion and for uniform grid spacing.

The upwind difference is used when the central scheme does not give a converged solution. This happens when the control volume Reynolds number or Peclet number is high, and an unrealistic solution will be achieved (Patankar, 1980). The Peclet number  $Pe$ , is defined as the ratio of convection flux to diffusion flux and has the following formula:

$$Pe = \frac{F}{D} = \frac{\rho U \Delta X}{\Gamma} \quad (3.17)$$

The hybrid scheme is a combination of both the central and upwind difference schemes and can be used mostly for solving equations that have both convection and diffusion terms. When the control volume Peclet number is  $-2 \leq Pe \leq 2$ , the hybrid scheme is identical to the central difference and to the upwind scheme when  $|Pe| > 2$ . For more details of the finite volume method, see Awbi's textbook (Awbi, 2003).

### 3.4.2 Solution of the Discretisation Equations

The most reasonable approach for solving the discretisation equation and achieving convergence is known as the iterative method. This approach is utilised as the transport equations are non-linear. In deriving the transport equations and their discretised forms, there will be no equation for pressure except that the pressure gradient is added to the source terms. For achieving a converged solution, a proper pressure field has to be used in the momentum equation which allows the velocity components to satisfy continuity. Patankar & Spalding (1983), depicted a procedure to link the velocity to the pressure with a view to fulfilling continuity and is known as the SIMPLE Semi-Implicit Method for Pressure-Linked Equations.

## 3.5 BOUNDARY CONDITIONS

The solution accuracy of the discretization equations will be based on the accuracy of how to specify the quantities physically at the boundary of the flow domain as well as the methods of linking these values to the bulk of the flow. Several types of boundaries are generally used in solving room flow problems as described in the following (Awbi, 2003):

## Wall Boundary

The transport equations for turbulence quantities (i.e.,  $k$  and  $\epsilon$ ) in their standard format cannot be applied to the wall due to the damping effect of the wall. To overcome this problem extra source terms for  $k$  and  $\epsilon$  are added and a highly fine grid close to the surface is defined to make sure that the first points are within the laminar sublayer, which is called “low Reynolds number turbulence modelling”. Many of the low Reynolds number models can describe the effect of damping of the wall, but a high number of grid point will be required.

## Free Boundary

When the boundary pressures are known the free boundary is used in the flow domain like a free stream at the boundary or a sluggish embracing fluid. Air jet diffusing in stagnant surroundings and buoyancy-driven flows are such examples.

## Conditions at Supply Outlets

A designation of the velocity components, fluid temperature, concentration level and turbulence quantities are required at the supply outlet for solving the flow equations. These are generally known or can be calculated from the values of the flow domain.

## Exit Conditions

At the exit, two velocity components are set to zero while the longitudinal exit velocity,  $U_e$  is represented by:

$$U_e = U_o \left( \frac{A_o \rho_o}{A_e \rho_e} \right) \quad (3.18)$$

where  $U_o$  is the supply opening velocity (m/s),  $A_o$  and  $A_e$  are the areas of the supply opening and exit opening respectively ( $m^2$ ),  $\rho_o$  and  $\rho_e$  are the fluid density of the supply opening and exit opening respectively ( $kg/m^3$ ).

## Obstacle Boundaries

When there is a barrier inside the domain, a false source term should be added to the discretization equations for every dependent variable. Therefore, the source and sink terms

coefficients are given hypothetical large values and the wall functions for solid boundaries in the domain may be used for the boundaries of the obstacle too.

### 3.6 ACCURACY OF CFD RESULTS

According to Awbi (2003), there are several factors that affect the accuracy of solving the transport equations and these are mainly the following:

#### **The Discretization Scheme**

Producing non-physical “overshoots” in the solution domain are often due to higher-order solution schemes which may be linked to grid-related errors that are similar to those from the first-order scheme. This kind of errors can be reduced by selecting a finer grid.

#### **The Computational Grid**

Although having a sensible well-constructed grid is a positive approach, there will be common computational errors that may be reduced by increasing the number of grid points.

#### **The Near-wall Boundary Conditions**

When a low Reynolds number turbulence model is used, some small cells should be positioned within the laminar sublayer to utilise the wall functions. Thus, it needs a highly fine grid which is inefficient economically for 3-D flow problems.

#### **The Convergence Criteria**

A residual (error) in an iterative solution is used as an indicator of the change of variables that occur from one iteration to the next. Most of CFD codes use a default convergence criterion which considers that a converged solution is fulfilled when it is reached.

There are always slight differences between measurement and CFD results due to the presence of both experimental and CFD errors. The experimental error is defined as the difference between a measurement and the actual value or between two measured values. Two types of experimental errors are existing, which are systematic errors and random errors. The systematic errors are errors that influence the accuracy of the measurement. The

conventional sources of these errors are faulty calibration of measuring instruments, poorly maintained instruments, or incorrect reading of tools by the user. The random errors are errors that have an impact on the precision of the measurement. The familiar sources of this type of errors are problems estimating quantity on an instrument and the failure to read an instrument which cannot be stopped without replacing the instrument(Taylor, 1997).

On the other hand, there are four sources of errors in CFD which are inappropriate modelling of the underlying physics or material properties of the case, inadequate input at the domain boundaries, non-physical effects created by the numerical method of solution and low or lousy quality resolution computational grids. The experience of the user who generates the grid has a direct influence on its resolution quality, which can have significant effects on the solution accuracy. A sufficient fine grid is required to represent the geometry of the problem being studied and allow the numerical scheme to resolve the physics of the governing equations as well. The geometric quality of the cells such as aspect ratio, skewness, maximum corner angle, etc. might also initiate error in the numerical solution. Thus, to accept the limitations of the CFD algorithms and models, minimising the grid induced error is significant to assure the preferable possible solution (Anderson, Tannehill and Pletcher, 1997).

According to of the America Institute Aeronautics and Astronautics (1998), uncertainty is defined as a potential deficiency in any phase or activity of the modelling process that is due to lack of knowledge. However, the error is defined as a recognisable deficiency in any phase or activity of modelling and simulation that is not due to lack of knowledge.

### **3.7 CHAPTER SUMMARY**

This chapter provided background information on the CFD techniques used in this study. Full description of the governing equations of fluid dynamic and different kinds of turbulence models used to predict the air flow pattern in indoor environments were presented. Furthermore, the solution of the discretization equations, boundary conditions and accuracy of CFD results were mentioned.

# 4 CHAPTER FOUR: DESCRIPTION OF CASE STUDY BUILDING AND FIELD MEASUREMENTS

---

## 4.1 INTRODUCTION

This chapter presents the measurements' stage of the research work which focuses on understanding the air flow, temperature variation and thermal comfort in the large space case-study building. Measurements were carried out in three phases; long-term measurements during the summer of 2016 and 2017, spot detailed measurements for short time periods in the summers of 2016, 2017 and 2018 and occupant questionnaire surveys only in summer 2017. The chapter starts by describing the chosen space with geometrical details, environmental servicing, periods of measurements, heat gains and measurement instruments. Then the following section presents the three evaluation phases; long-term measurements, spot detailed measurements and occupant questionnaire.

## 4.2 DESCRIPTION OF MEASUREMENT SPACE AND INSTRUMENTS

### 4.2.1 The Building and the Chosen Space

The large space chosen for the case study is located in the Centre of Sustainable Energy Use in Food Chains CSEF building at Brunel University London, see photo Figure 4.1. It consists of several offices used by the academic team and a large open plan office used by research staff and students. Also, the CSEF building has a large open plan laboratory with four different size environmental chambers for use by the researchers to perform their experiments and testing. In addition to that, two conference rooms, kitchen and toilets are included in the building.

The large open plan office which is used by the research staff and students was chosen as the case-study for a large space ventilation because its floor-to-ceiling height is 6m and the volume of the occupied zone ( $362m^3$ ) is small compared to the total volume ( $1014m^3$ ). The enclosure has dimensions of 15.5m x14m x 6m (length, width and height) and a floor area of  $201 m^2$  with brick external walls and metal roof which includes two large skylights. Two big rectangle windows are located on the south facing wall of the building with dimensions 3.5m

x 1.1m and 4.2m x 1.1m. There is one door at each end wall of the buildings, see Figure 4.2 and photo in Figure 4.3.



Figure 4.1 Centre of Sustainable Energy Use in Food Chains building

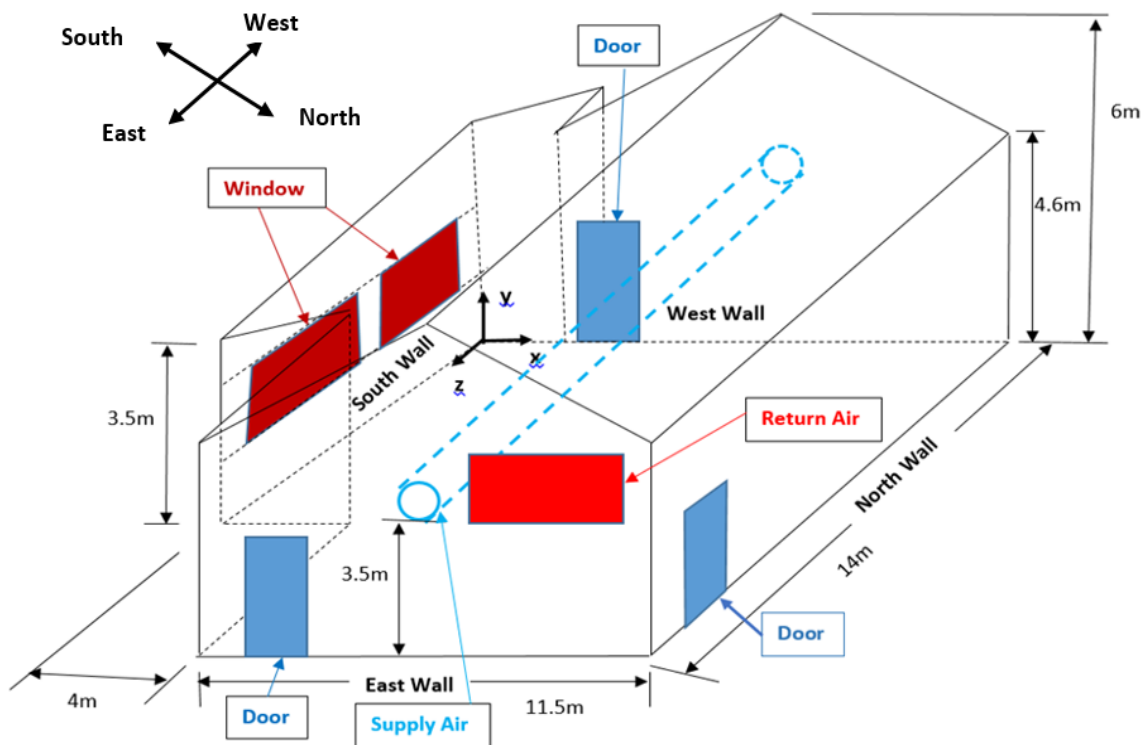


Figure 4.2 Sketch of the researchers' office at CSEF building.



*Figure 4.3 The researchers' office at CSEF Building*

## 4.2.2 Environmental Servicing

The researchers' large open plan office which will be called "researchers' office" in this thesis, has the following environmental servicing systems: heating, lighting and ventilation.

### **Heating**

The researchers' office is provided with a heating system which consists of a gas fired boiler with five radiators attached to the walls to create comfortable conditions for occupants, especially in the winter season.

### **Lighting**

Daylight and an electric lighting system are used in the researchers' office to supply the occupants with their visual needs. The two windows that were mentioned previously and the roof skylights are used for providing daylight. However, there are five rows of suspended Thorlux lights with a height of 3m from the floor covering all the space. These artificial lighting comprising of 46 luminaires each equipped with two 49 W lamps giving a total internal heat gains of  $11.2 \text{ W/m}^2$  for the office.



The space is occupied from 9:00 to 18:00 during weekdays and used for sedentary and moderate active office work inside the occupied zone. The ventilation system starts at 6:00 am and stops at 6:00 pm every day from Monday to Friday, while at the weekend, it starts at 6:00 am and stops at 9:00 am.

### 4.2.3 Periods of Measurements

The measurements were conducted during the summer season for the years 2016 and 2017 with some additional CO<sub>2</sub> concentration measurements in summer 2018. During the summer of 2016, the measurements were carried out over a period of 28 days from 24/8/2016 to 21/9/2016 which can be considered late summer season in London. During this period and according to the weather station mounted on the building (about 3m above the roof), the external average temperature was 18.5°C, the maximum was 28.9°C, the minimum temperature was 11.3°C while solar radiation reached a peak of 740 W/m<sup>2</sup>. On the other hand, the external average relative humidity for the same periods was 80%, the maximum was 100% and the minimum was 39.4%.

For the summer of 2017, the measurements were carried out over a period of three months from 21/6/2017 to 19/9/2017 which is considered as the summer season in London. The first month started from 21/6/2017 to 19/7/2017 while the second and the third months began from 22/7/2017 to 19/8/2017 and from 22/8/2017 to 19/9/2017 respectively. During this period the mean outdoor temperature was 17.3°C, the maximum was 34.7°C, and the minimum temperature was 6.6°C while solar radiation reached 943 W/m<sup>2</sup>. On the other hand, the outdoor air was generally humid with an average relative humidity of 75.6%, the maximum of 99.8% and a minimum of 30.2%. In general, these periods of the year can be considered the hottest months in London. In addition to that, occupant questionnaire surveys were conducted during three days in this summer on 31/8/2017, 5/9/2017 and 11/9/2017.

For the summer of 2018, the measurements were carried out on 25/5/2018. On that day the mean outdoor temperature was 15.5°C, the maximum was 18.5°C, and the minimum temperature was 13.4°C while the outdoor CO<sub>2</sub> concentration was 400 ppm.

Table 4.1 provides the ranges of the variables for each month during the summer season for the years 2016 and 2017.

Table 4.1 Outdoor air temperature and relative humidity for each month during the summer season for the years 2016 and 2017

Months	Outdoor Air Temperature (°C)			Outdoor Relative Humidity (%)		
	Mean	Max.	Min.	Mean	Max.	Min.
24/8/2016 to 21/9/2016	18.5	28.9	11.3	80	100	39.4
21/6/2017 to 19/7/2017	19.5	34.7	11.4	69.3	99.1	30.2
22/7/2017 to 19/8/2017	16.9	24.6	9.3	77.5	99.3	33.2
22/8/2017 to 19/9/2017	15.5	28.5	6.6	80.1	99.8	37.7

Since the occupant questionnaire surveys were conducted in the third month of summer 2017 more measurements details are shown below.

The outdoor air temperature and relative humidity during the third month of summer 2017 from 22/8/2017 to 19/9/2017 are shown in Figure 4.6. It could be observed that the highest measured temperature was on 28/8/2017 afternoon whereas the highest measured relative humidity was on 4/9/2017 at night.

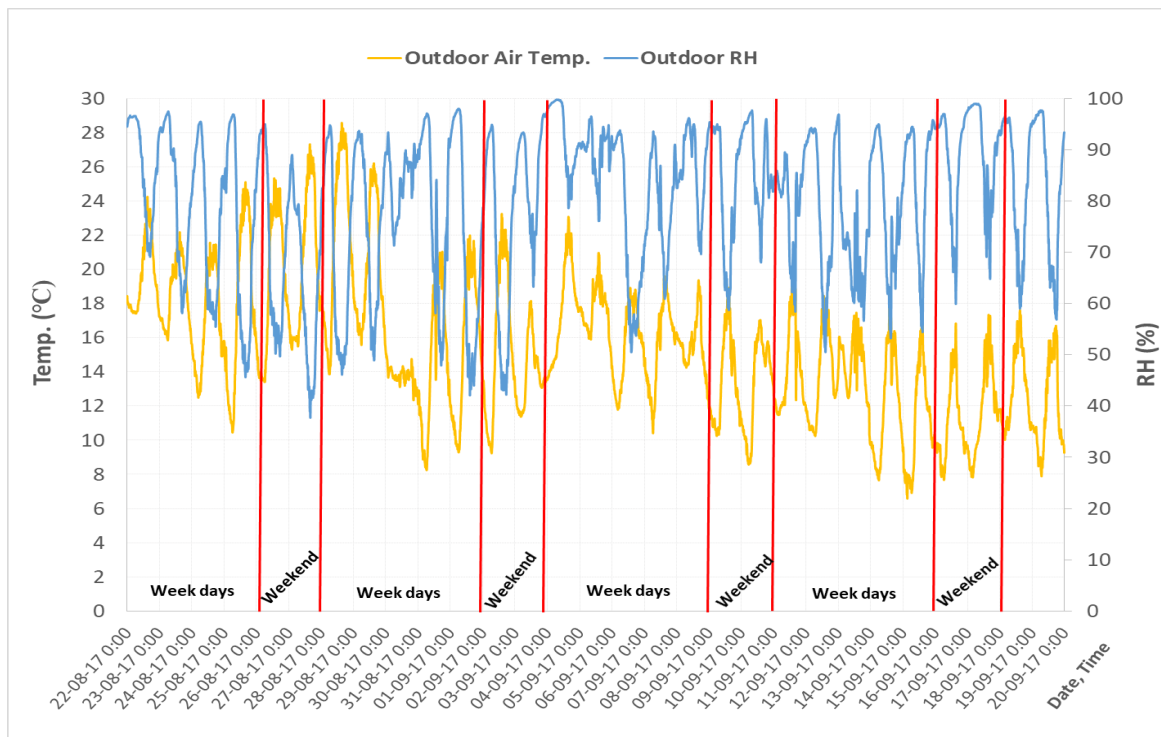


Figure 4.6 Outdoor temperature and relative humidity for the third month.

Figure 4.7 shows the outdoor air temperature with solar radiation during the third month of the measurement period from 22/8/2017 to 19/9/2017. The highest maximum recorded solar

radiation was  $943 \text{ W/m}^2$  on 31/8/2017 at 12:50 while the lowest day was 30/8/2017 with  $163 \text{ W/m}^2$  maximum.

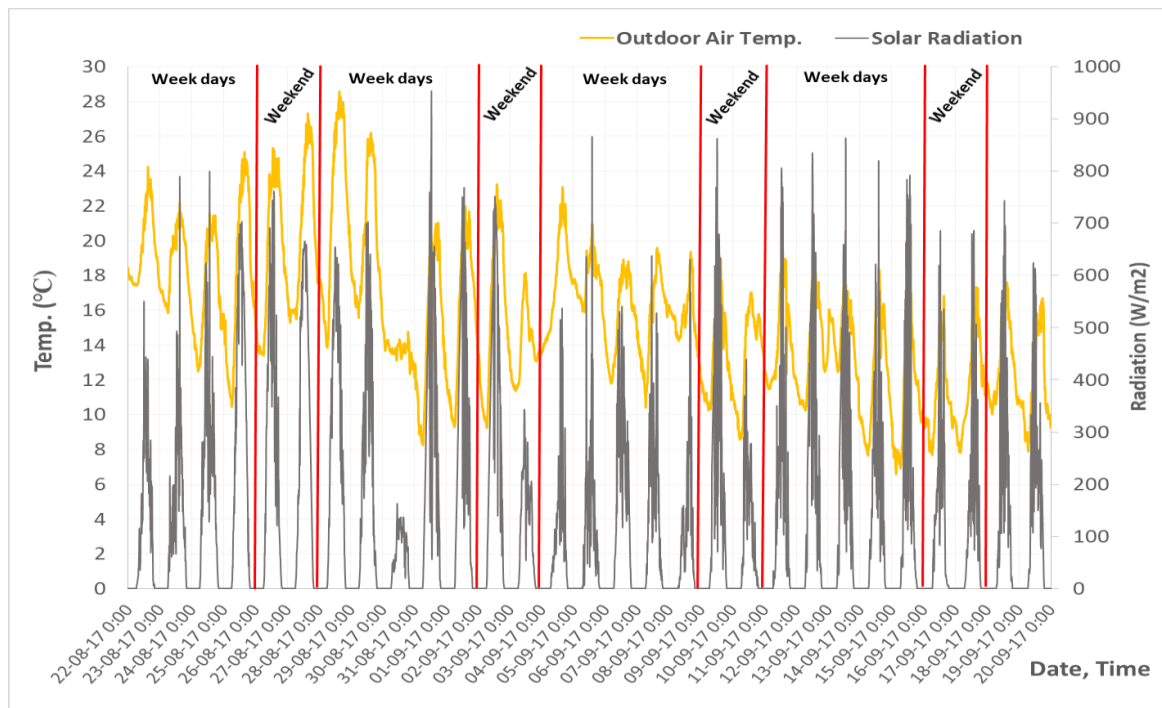


Figure 4.7 Outdoor temperature and solar radiation for the third month

#### 4.2.4 Heat Gains

Heat gains in the office are presented by heat gain through building fabric as sensible gains, solar gains through windows as sensible gains and internal heat gain as sensible and latent gains (Tymkow et al. 2013). Due to conduction heat transfer through solid construction, the heat is transmitted to the researcher's office through one external wall, roof and the two windows. In addition to that, solar radiation passes on through the two windows which have an impact on the office. The building fabric heat gain and the solar heat gain were calculated using HAP 4.9 Hourly Analysis Program which is a microcomputer program developed by Carrier Corporation (Carrier, 2010).

Finally, several heat sources which are placed inside the researcher's office can produce internal heat gains such as occupants (sensible and latent gains) and lighting, personal computers and office equipment (sensible gains). Since the heat gains have a substantial impact on the performance of the ventilation system in the researcher's office at CSEF building and on the thermal comfort as well, Table 4.2 summarised all the values of total heat gains for selected days of summer 2016, summer 2017 and summer 2018.

Table 4.2 Total heat gain in the office for one day of summer 2016, summer 2017 and summer 2018

Heat gain	Summer 2016 7/9/2016 (15:00)			Summer 2017 7/9/2017 (15:00)			Summer 2018 25/5/2018 (15:00)		
	Details	Sensible (W)	Latent (W)	Details	Sensible (W)	Latent (W)	Details	Sensible (W)	Latent (W)
<b>BUILDING FABRIC GAIN</b>									
<b>Roof</b>	209 m <sup>2</sup>	2330	-	209 m <sup>2</sup>	2330	-	209 m <sup>2</sup>	2080	-
<b>External wall</b>	27 m <sup>2</sup>	389	-	27 m <sup>2</sup>	389	-	27 m <sup>2</sup>	202	-
<b>Internal walls</b>	245 m <sup>2</sup>	0	-	245 m <sup>2</sup>	0	-	245 m <sup>2</sup>	0	-
<b>Windows</b>	8 m <sup>2</sup>	112	-	8 m <sup>2</sup>	112	-	8 m <sup>2</sup>	52	-
<b>Floor</b>	201 m <sup>2</sup>	0	-	201 m <sup>2</sup>	0	-	201 m <sup>2</sup>	0	-
<b>SOLAR GAIN</b>									
<b>Windows</b>	8 m <sup>2</sup>	1814	-	8 m <sup>2</sup>	1814	-	8 m <sup>2</sup>	1667	-
<b>INTERNAL GAIN (CIBSE, 2015)</b>									
<b>Occupants</b>	12	900	660	24	1800	1320	14	1050	770
<b>Lighting</b>	46	2254	-	46	2254	-	46	2254	-
<b>Computers</b>	12	2244	-	24	4488	-	14	2618	-
<b>Photocopier</b>	1	400	-	1	400	-	1	400	-
<b>Total</b>		10443	660		13587	1320		10323	770

Therefore the total sensible heat gains for the office were 52.0 W/m<sup>2</sup>, 67.6 W/m<sup>2</sup> and 51.4 W/m<sup>2</sup> for a particular day of summer 2016, summer 2017 and summer 2018 respectively. Also, the total latent heat gains were 3.3 W/m<sup>2</sup>, 6.5 W/m<sup>2</sup> and 3.8 W/m<sup>2</sup> for the same periods.

#### 4.2.5 Description of the measuring instruments

A well-established technique that can register a particular quantity with a given accuracy should be used to measure objective information. This data can be utilised to describe the indoor environment. Some critical parameters like temperature, velocity, relative humidity and CO<sub>2</sub> concentration were measured in this study by using the following apparatus.

### TA 465 AirFlow Instrument Air Velocity Meter

It is a thermal anemometer which can measure velocity, temperature, relative humidity, dew point and heat flow. This instrument has been used in our experiment to measure velocity, temperature and relative humidity simultaneously, see photo in Figure 4.8. Typically, the range of this device for measuring the velocity is from 0 to 50 m/s with an accuracy of  $\pm 3\%$  while from  $-10$  to  $60\text{ }^{\circ}\text{C}$  is the range of temperature with an accuracy of  $\pm 0.3\text{ }^{\circ}\text{C}$ . The relative humidity R.H has a scale from 5 to 95% RH and accuracy of  $\pm 3\%$  RH.



Figure 4.8 TA 465 AirFlow Instrument Air Velocity Meter

### HOBO Temp/RH Data Logger

The HOBO Temp/RH data logger is used in indoor environments to record temperature and relative humidity, see photo in Figure 4.9. The logger operating ranges are from  $-20$  to  $70\text{ }^{\circ}\text{C}$  for temperature and from 0 to 95% RH for relative humidity with  $\pm 3.5\%$  accuracy (HOBO, no date).



Figure 4.9 HOBO Temp/RH Data Logger

### CPS Thermo Anemometer AM50

It is a thermos anemometer which can measure air speed and air temperature. This instrument has been used in our experiment to measure the diffusers' air supply speed, see a photo in Figure 4.10. Typically, the range of this device for measuring the speed is from 0 to 45 m/s with an accuracy of  $\pm 3\%$  while from 0 to 60 °C is the range of temperature with an accuracy of  $\pm 0.8$  °C.



Figure 4.10 CPS Thermo Anemometer

### Telaire 7001 CO<sub>2</sub> Logger

This data logger records Carbon dioxide and temperature data in indoor environments using non-dispersive infrared NDIR technology, see photo in Figure 4.11. Temperature range and accuracy are from 0 to 40°C and  $\pm 0.1$  °C respectively. The CO<sub>2</sub> sensor range is from 0 to 2500 ppm and  $\pm 50$  ppm or 5% of reading which is greater as the accuracy.



Figure 4.11 Telaire 7001 CO<sub>2</sub> Logger

## U30-NRC-SYS-C HOBO Weather Station

This kit supports the following measurements: air temperature, wind speed, wind direction, solar radiation, and relative humidity, see photo in Figure 4.12. The operating ranges are from – 20 to 75 °C for the temperature with  $\pm 0.21$  °C accuracy and from 0 to 100 % RH for relative humidity with  $\pm 3.5\%$  accuracy (HOBO, no date).



*Figure 4.12 U30-NRC-SYS-C HOBO Weather Station*

## 4.3 THE MEASUREMENTS THREE PHASES

### 4.3.1 Long-term Measurements Phase

The air temperature and relative humidity were measured during the summers of 2016 and 2017 using nine HOBO Temp/RH data loggers attached to three columns (C1, C5 and C8) which are located at three different heights of 0.1, 1.2 and 1.8m (between the floor and standing height), see Figure 4.4 and photo in Figure 4.13. Also, eight HOBO Temp/RH data loggers were used to measure the air temperature at the eight diffusers, and four more loggers were mounted at heights of 4m and 5m in two different locations to measure the air temperature and relative humidity in the area above the occupied zone, see Figure 4.14 and Table 4.3.

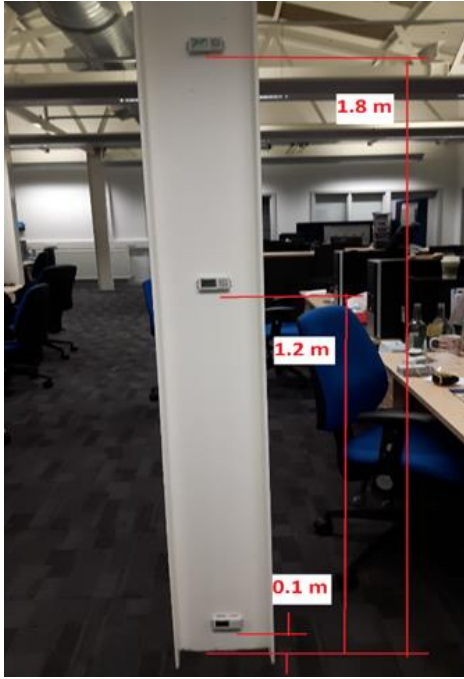


Figure 4.13 HOBO Temp/RH data logger attached to the column at three different heights of 0.1, 1.2 and 1.8m



Figure 4.14 HOBO Temp/RH data logger mounted on the unoccupied zone

Table 4.3 Measuring points for air temperature and relative humidity.

Zone	Point	Logger Name	Location		Height Y (m)	Period	
			X (m)	Z (m)		From	To
Occupied Zone	C1	C11	10.0	12.0	0.1	24/8/2016	21/9/2016
		C12			1.2		
		C13			1.8		
	C5	C51	9.0	6.5	0.1		
		C52			1.2		
		C53			1.8		
	C8	C81	0.2	1.5	0.1		
		C82			1.2		
		C83			1.8		
Unoccupied Zone	D1	D1	10.0	11.5	3.7	21/6/2017	19/9/2017
	D2	D2	9.5	11.5	3.7		
	D3	D3	10.0	9.0	3.7		
	D4	D4	9.5	9.0	3.7		
	D5	D5	10.0	6.5	3.7		
	D6	D6	9.5	6.5	3.7		
	D7	D7	10.0	2.0	3.7		
	D8	D8	9.5	2.0	3.7		
	V1	V1	10.25	12.0	4.0		
	V2	V2	10.5	12.0	5.0		
	V3	V3	10.25	9.5	4.0		
	V4	V4	10.5	9.5	5.0		

The air temperature and relative humidity were recorded based on one-minute interval during the measuring period. The raw data were downloaded from the loggers, and HOBOWare Pro which is the data logging software that was used for launching the data logger, data read out, graphing new data, data analyses and reporting. The accuracy of the air temperature measurement was estimated to be  $\pm 0.21^{\circ}\text{C}$  and  $\pm 3.5\%$  for the relative humidity measurements.

#### 4.3.2 Spot Detailed Measurements Phase

The measurements of air mean speed and air temperature were conducted in the summer of 2016 over five days from 5/9/2016 to 9/9/2016 at three different times of a day (11:00, 13:00 and 15:00). In the summer of 2017, the measurements were performed over three days on 31/8/2017, 5/9/2017 and 11/9/2017 at 13:00. In summer 2018 similar measurements for the mean speed and air temperature were carried out as well as for the  $\text{CO}_2$  concentration on 25/5/2018 at 11:00, see Table 4.4. The environmental parameters were obtained for seven different spots as shown in Figure 4.4, which were chosen to represent typical positions of the occupants. At each spot, measurements of air temperature, air speed, and relative humidity were taken at heights of 0.1m (foot level), 1.2m (head level of a seated individual) and 1.8m (head level of a standing individual) above the floor, see

Table 4.5. These parameters were measured over two minutes with a sampling interval of ten seconds by using a TA465 AirFlow instrument, see photo in Figure 4.15. The accuracy of the air speed measurement is estimated to be  $\pm 0.015$  m/s or  $\pm 3\%$  while the error of measured temperature is estimated to be  $\pm 0.3^{\circ}\text{C}$ . For the  $\text{CO}_2$  concentration, the measurements were taken at height of 1.2m for the same spots. It was measured over four minutes with a sampling interval of thirty seconds by using the Telaire 7001 logger where the accuracy of this logger was  $\pm 5\%$  or  $\pm 50$  ppm. In addition, a CPS Thermo Anemometer AM50 were used to measure the air speed at the eight diffusers for three different days 31/8/2017 at 13:00, 11/9/2017 at 13:00 and 25/5/2018 at 11:00 where the accuracy of this anemometer was  $\pm 3\%$ , see photo in Figure 4.16. The air speed at the eight diffusers was also measured twice in the summer of 2016 by using the TA465 AirFlow instrument on 6/9/2016 and 8/9/2016 at 13:00.



Figure 4.15 Measurements of mean air speed and temperature using a TA465 AirFlow instrument



Figure 4.16 Measurements of air speed of the diffusers using CPS Thermo Anemometer AM

Table 4.4 Date and occupants numbers for each spot detailed measurement.

Date	Time	Number of Occupants	Measured Points at the Three Heights (see Figure 4.4)
<b>5/9/2016</b>	11:00	12	S1,S2,S3,S4,S5,S6,S7
	13:00	3	
	15:00	11	
<b>6/9/2016</b>	11:00	12	
	13:00	2	
	15:00	12	
<b>7/9/2016</b>	11:00	12	
	13:00	1	
	15:00	12	
<b>8/9/2016</b>	11:00	10	
	13:00	2	
	15:00	11	
<b>9/9/2016</b>	11:00	12	
	15:00	12	
<b>31/8/2017</b>	15:00	14	
<b>5/9/2017</b>	15:00	16	
<b>11/9/2017</b>	15:00	20	
<b>25/5/2018</b>	11:00	14	For the CO <sub>2</sub> at one height (1.2m)

Table 4.5 Measuring spots' locations and heights.

Point (See Figure 4.4)	Location		Height Y (m)
	X (m)	Z (m)	
S1	14.5	11.5	0.1
			1.2
			1.8
S2	14.5	10.0	0.1
			1.2
			1.8
S3	13.5	2.4	0.1
			1.2
			1.8
S4	9.75	9.0	0.1
			1.2
			1.8
S5	5.0	11.5	0.1
			1.2
			1.8
S6	1.0	5.0	0.1
			1.2
			1.8
S7	1.0	9.0	0.1
			1.2
			1.8

### 4.3.3 Occupant Questionnaire

Ricciardi et al. (2016) used a questionnaire which complies with ISO 10551, and it was composed of three parts. In the first part, occupant fills his age and gender while the evolution of temperature and air speed, overall thermal comfort and local discomfort feeling are in the second part. In the last part of the questionnaire the interviewed person had to indicate his seat on the theatre's plan. Another investigation by Buratti & Ricciardi (2009) shows that data about subjective comfort sensations were taken into account through questionnaires distributed to the occupants. The questionnaire was amended from the model presented in UNI EN ISO 10551/2002 and combined with extra questions regarding the change of individual microclimatic control in the environment so as to study the human thermal environment interaction behaviour. The questionnaire consisted of three parts which were personal data (age and gender) as part one, whereas part two was judgmental about the tolerability of thermal environment, air movement, and the temperature difference between head and ankle. Part three was about individual microclimatic control and the location inside the room. A recent study by Zhao et al. (2017) conducted a questionnaire survey on the internet to study the thermal sensation and environment control strategy in several climate parts of China. The questionnaire contents include basic information of respondents as the first part of gender, age and current residential location. The second part was to assess the Indoor thermal

condition by voting the thermal, humidity and draught sensations using 7-points index scale. The last part of the questionnaire was about personal behaviour and usage of cooling and refrigeration devices as a strategy to control the environment. According to another study by Cheong & Lau (2003), subjective assessments was one of the approaches used to develop an indoor air quality audit methodology and apply it to a tertiary institutional building in the tropics to verify the status of the indoor air quality . A questionnaire was used and completed by the building's users for this survey. It consisted of several sections, namely, occupants' work and health, environmental conditions, control of the environment by the individual and the office environment cleanliness and odour. All of this was to determine occupants' perception of the indoor air quality.

The research staff who work at the large open-plan office investigated were recruited for this study in summer 2017. The participants consisted of young females and males who have various ethnic origins and nationalities. To comply with the requirements of the Brunel University's Research Ethics Committee, letter of approval was obtained for the proposed study and participant's information sheet was provided to all participants in this experiment, copy of this letter is shown in Appendix I.

The subjective study involved collection of data using questionnaires provided by ISO 10551 (BS EN 15251, 2007) and guided by recent literature (Ricciardi et al. (2016), Zhao et al. (2017)). The questionnaire was developed to assess the thermal environment based on the occupant's thermal sensation vote and air movement in the office. This assessment is based on judgements at the head and foot levels and overall comfort sensation as well as an individual preference for different conditions. ASHRAE's seven points thermal sensation scale (from -3 to +3) was used to evaluate thermal sensations and rate the impressions of comfort due to air movement. This is to collect the quantified thermal sensation of the occupants. A similar seven-points scale is used for the thermal preference vote for direct comparison with the thermal sensation vote. The freshness of air was used to assess the air quality inside the office. The questionnaire also addressed the clothing garments for the participants to obtain the clothing insulation value. In addition to that, the participants had to indicate their location on the office's plan. The rating scales for these parameters are shown in Table 4.6. Besides that, PMV, PPD and several other aspects were considered to elaborate the questionnaires as proposed by Ricciardi et al. (2016), (Ricciardi and Buratti, 2015) and (Buratti and Ricciardi,

2009), see Table 4.7. The subjects were required to make only one choice from the scale for each question. The final version of the survey questionnaire is provided in Appendix A. Both questionnaire distribution and measurements were carried out at 15:00 each day, to allow the participants to adjust to the environmental condition after the lunch break.

Table 4.6 Rating scales for subjective evaluation parameters

Parameters	Rating Scales						
	-3	-2	-1	0	+1	+2	+3
<b>Thermal Sensation TS</b>	Cold	Cool	Slightly cool	Neither hot nor cold	Slightly warm	Warm	Hot
<b>Thermal Preference TP</b>	Much cooler	Cooler	Slightly cooler	Without change	Slightly warmer	Warmer	Much warmer
<b>Air Movement AM</b>	Very still	Still	Slightly still	Acceptable	Slightly draughty	Draughty	Very draughty
<b>Air movement Preference AMP</b>	Much more air movement	More air movement	Slightly more air movement	Without change	Slightly less air movement	Less air movement	Much less air movement
<b>Relative Humidity RH</b>	Very dry	Dry	Slightly dry	Neutral	Slightly humid	Humid	Very humid
<b>Relative Humidity Preference RHP</b>	Much drier	Drier	Slightly drier	Without change	Slightly more humid	More humid	Much more humid
<b>Thermal Comfort TC</b>				Comfortable	Slightly comfortable	Uncomfortable	Very uncomfortable
<b>Air quality AQ</b>	Very fresh	Fresh	Slightly Fresh	Neutral	Slightly stuffy	Stuffy	Very stuffy
<b>Air Quality Preference AQP)</b>				Acceptable	Slightly acceptable	Unacceptable	Very unacceptable

Table 4.7 Indexes to elaborate the questionnaires

Index (%)	Definition	Related Question
<b>Thermal dissatisfaction TDI</b>	Percentage of individuals who vote, uncomfortable, very uncomfortable	What is your thermal comfort?
<b>Thermal preference TPI</b>	Percentage of individuals who vote much cooler, cooler, warmer, much warmer	What would you like to feel?
<b>Unacceptable air movement UAMI</b>	Percentage of individuals who vote very still, still, draughty, very draughty	How would you describe the air movement?

## 4.4 CHAPTER SUMMARY

This chapter focused on outlining the parameters and apparatus used for measurements to understand the air flow and temperature variation in both the occupied and unoccupied zones for the case-study of a large space building CSEF. At the occupied zone, three different heights of 0.1m (ankle level), 1.2m (seating head level) and 1.8m (standing head level) were used to conduct these measurements for prediction the temperature gradients. Several points at different heights in the unoccupied zone were used for forecasting the thermal stratification. The chapter also describes measurements of air speed and direction and CO<sub>2</sub> concentration within the space and also designing the occupants' questionnaire. The next chapter will present the field monitored data and their analysis, and the evaluation of the thermal comfort and indoor air quality for this large space as well as the results from occupants' questionnaire.

# 5 CHAPTER FIVE: FIELD MONITORING RESULTS AND DISCUSSION

---

## 5.1 INTRODUCTION

This chapter presents the data for the three monitoring phases; long-term, detailed spot measurements for short time period and occupant questionnaire surveys which were described in chapter 4. Section 5.2 gives the air temperature, air speed, relative humidity and CO<sub>2</sub> concentration measurements data, analysis and the evaluation of the thermal comfort and indoor air quality for this large space building, CSEF. Section 5.3 discusses the results of these three measurements phases.

## 5.2 THE MEASUREMENTS THREE PHASES' DATA AND RESULTS

### 5.2.1 Data and Results for Long-Term Measurement Phases

#### **For summer 2016**

Figure 5.1 shows the air temperature variation for C1 point (see Figure 4.4) at four levels, external and diffuser D1 for one day. It can be seen that all the six temperature lines fluctuated during the measuring period. There were sharp drops in temperature in each day at 06:00 hour for the interior temperatures due to turning on time for the cooling system. For the period 03-04/09/2016, the temperature readings were nearly the lowest compared with the other days as they were for weekend days. The temperatures reached a peak in 7/9/2016 where both the diffuser and external temperatures were more than 28°C.

There was nearly a 5°C difference between the diffuser and outside temperatures when the cooling system was off, whereas the gap was reduced to approximately 1°C when the cooling system was turned on. Also, the temperature at diffuser outlet rose sharply by 3°C when the system was turned off due to hot air buoyancy force, followed by a moderate decrease in the temperature to match the temperatures at 1.2m, 1.8m and 4.0m, see Figure 5.2.

Figure 5.3 shows the temperature trend for the four heights of 0.1m, 1.2m, 1.8m and 4.0m at column C1 over 12 hours which was the ON period of the cooling system. The temperatures

at 1.2m were precisely the same as the temperatures at 1.8m during that time. However, the temperatures at 4.0m were higher than the temperatures at 0.1, 1.2m and 1.8m from 06:00 to 18:00. There was a study state in all the temperatures from 15:00 to 17:00.

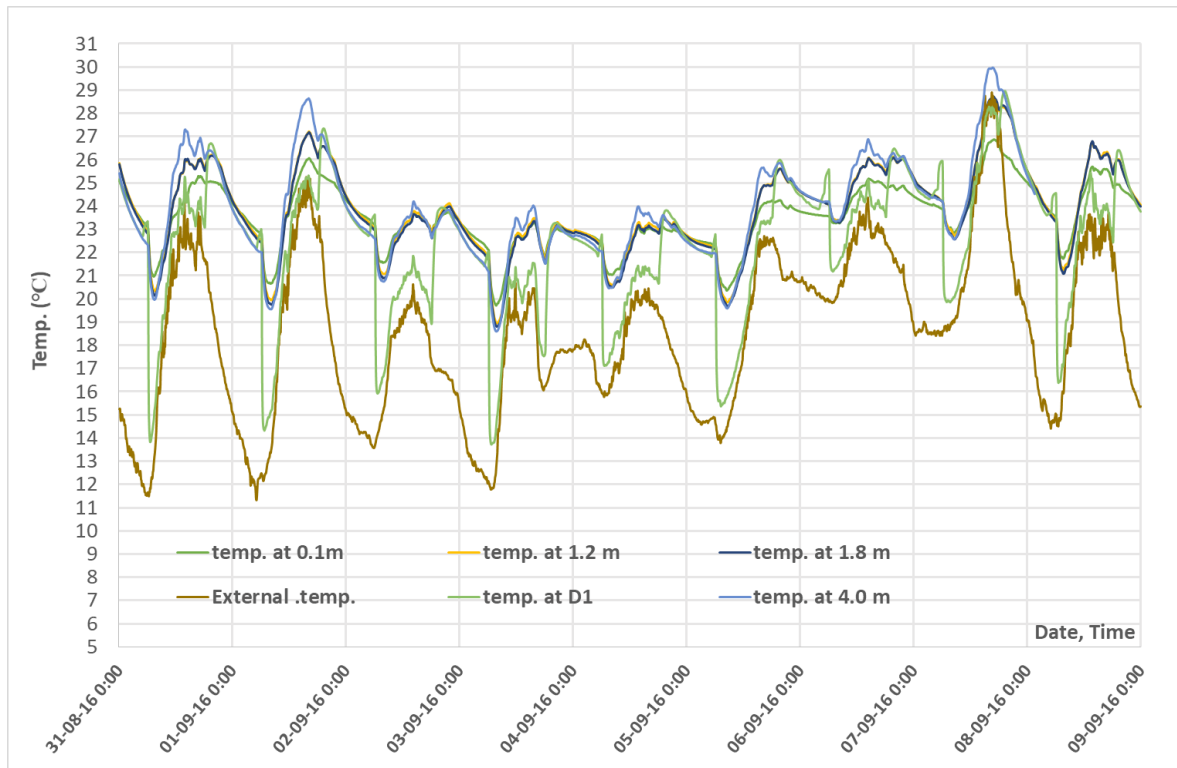


Figure 5.1 Temperatures for point C1 at four levels, external and diffuser D1 over nine days.

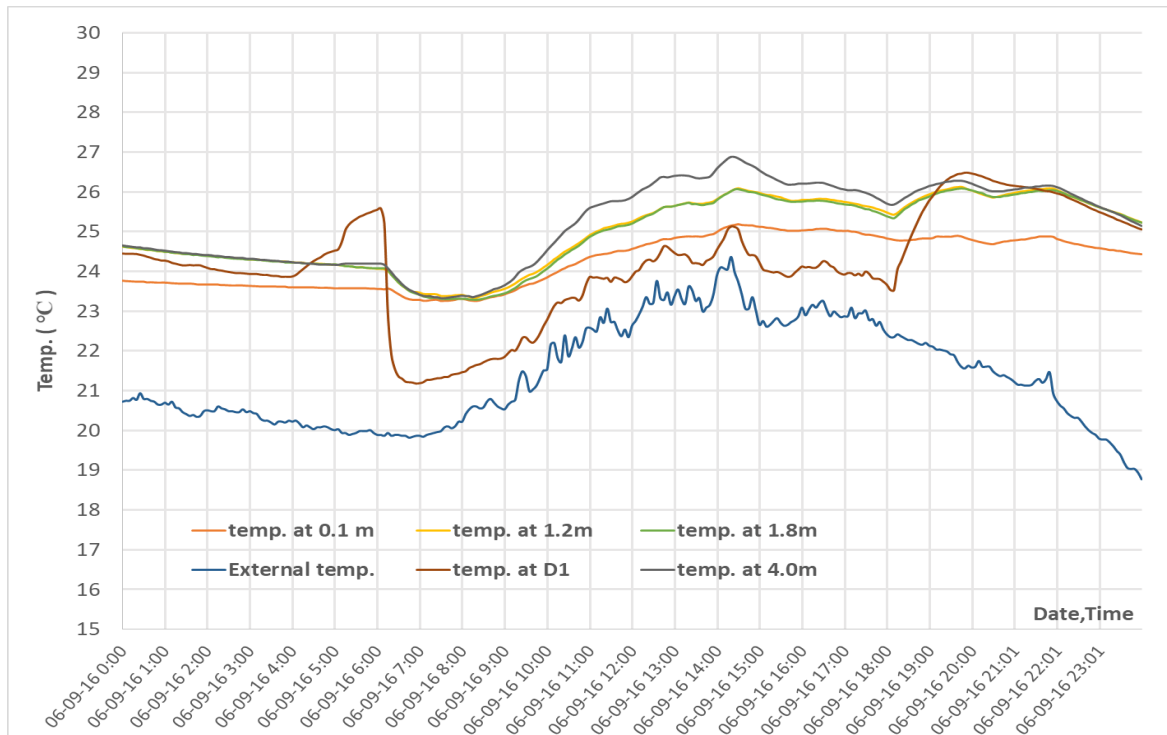


Figure 5.2 Temperatures for point C1 at four levels, external and diffuser D1 for one day

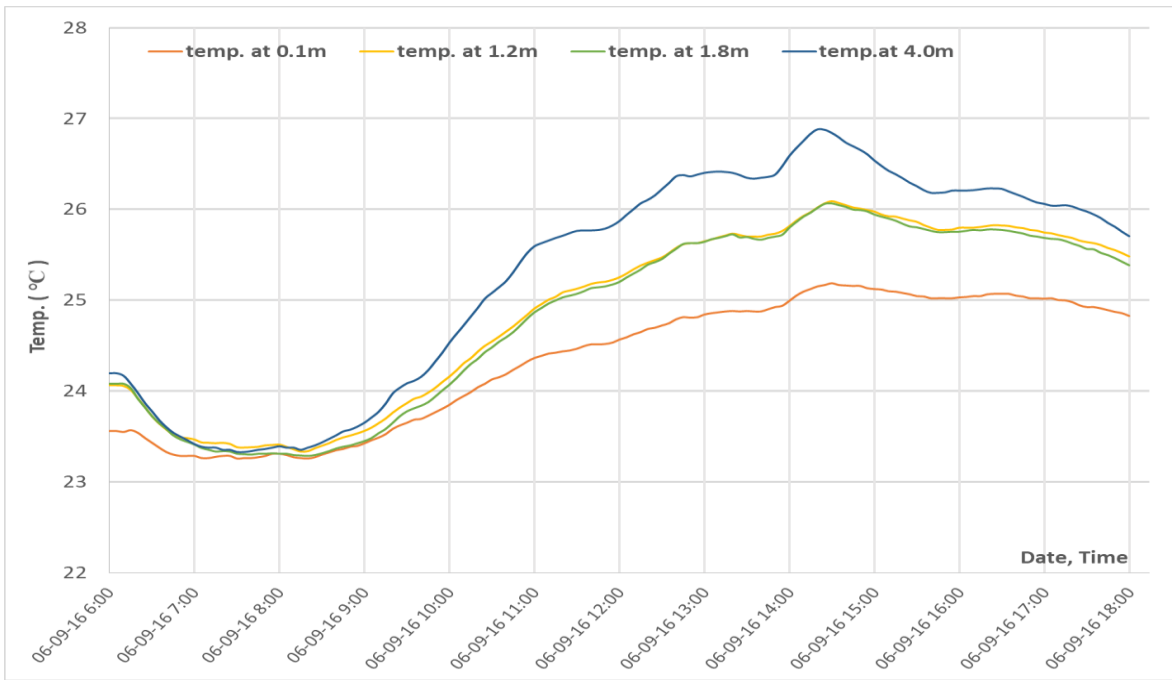


Figure 5.3 Temperatures for point C1 at four levels, external and diffuser D1 for 12 hours

Figure 5.4 shows the air temperature trend for three different locations in the enclosure which were C1, C5 and C8 at 1.2m over 9 days as well as external temperature. The temperature at point C8 was much higher compared to the temperatures at both C1 and C5 because it was very closed to the external wall facing the south side and this can be seen clearly at mid-day of 7/9/2016.

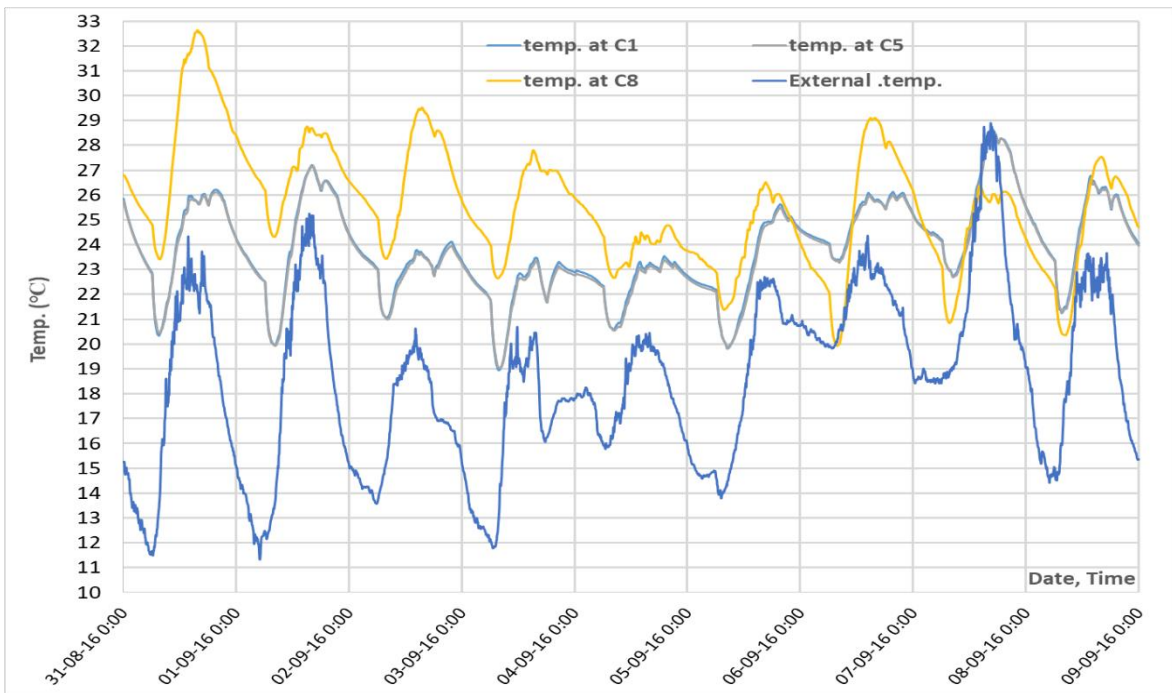


Figure 5.4 Temperature for points C1, C5, C8 and external over nine days at height 1.2m

## For summer 2017

Figure 5.5 and Figure 5.6 show the indoor air temperature for C1 at five levels, external and diffuser D1 temperatures for the last month of measurements from 22/8/2017 to 19/9/2017 and for one of the days which was 6/9/2017. The indoor air temperature lines change from day to day during the measurement month due to the fluctuating of outdoor air temperature, ranging from 6.6°C to 28.5°C and heat loss or gain from the office building. There were slight drops in air temperature on each day at 06:00 for interior temperature lines which were at 0.1, 1.2, 1.8, 4.0 and 5.0m and at D1 due to turning on time the cooling system. On 10/9/2017, temperature readings were nearly the lowest compared with other days as it was a weekend day. The trend line reached a peak in 28/8/2017 where both the diffuser and external air temperatures were more than 28°C. The difference between the mean ambient air temperature and the mean indoor air temperatures was about 4°C for the first ten days then it increased to be about 8°C for the rest of the period. This is because of the heat gain inside the office. As seen from Figure 5.6 the diffuser air temperature was lower than the air temperatures at five heights in the mornings of the 6/9/2017. However, it increased sharply by 7°C in the afternoon while there was no significant rise in the ambient air temperature. This is because the ventilation system was not able to maintain the office with an acceptable air temperature level. As a result, a significant temperature stratification condition was created in the office.

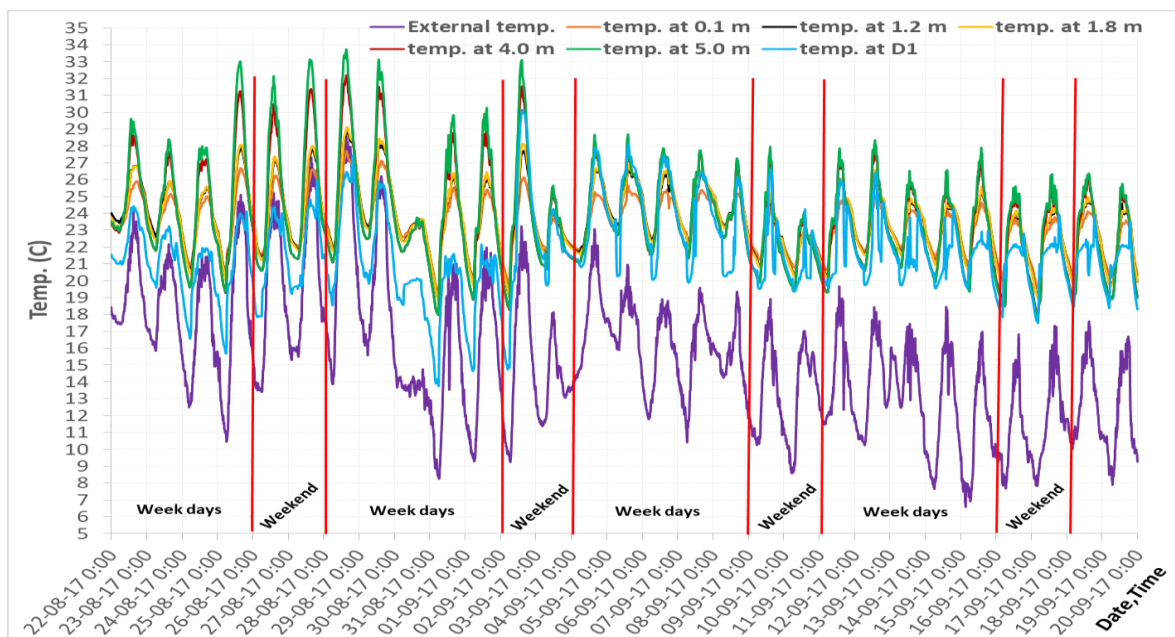


Figure 5.5 Air temperatures for point C1 at five levels, external and diffuser D1 over one month

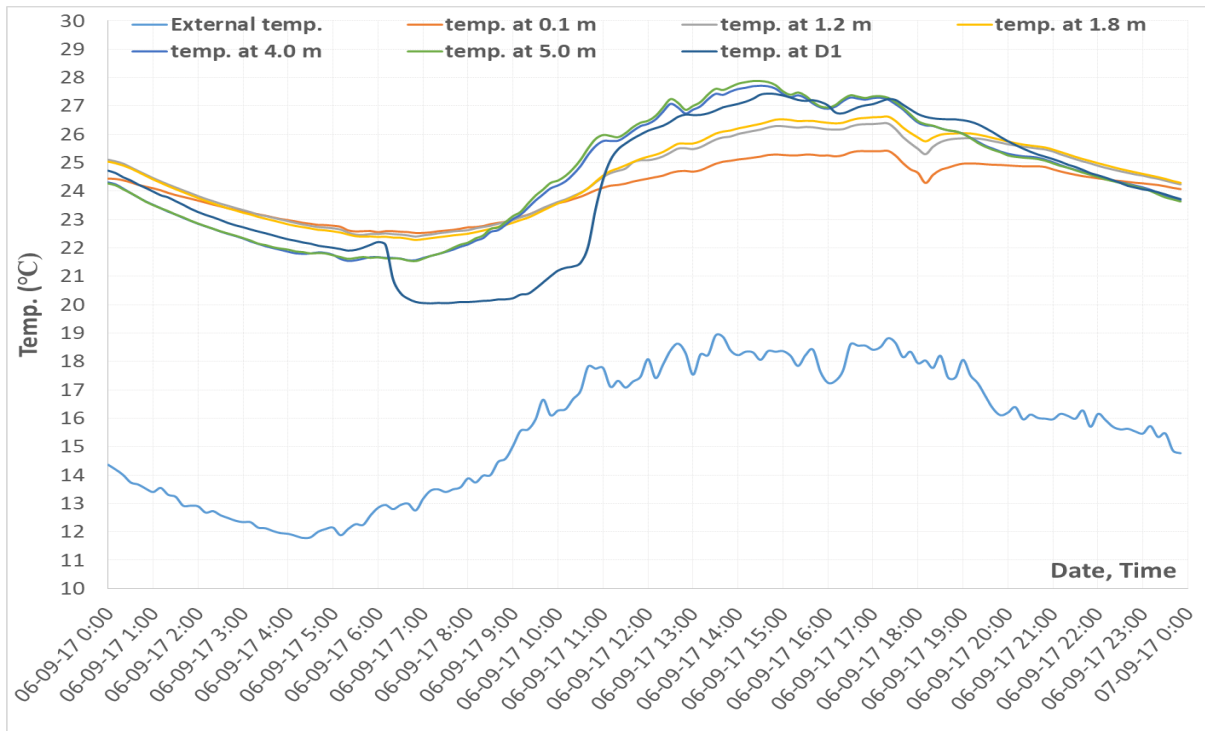


Figure 5.6 Air temperatures for point C1 at five levels, external and diffuser D1 for one day.

Figure 5.7 shows the air temperature trend for the three heights 0.1m, 1.2m, 1.8m, at column C1 over 12 hours which was ON period of the cooling system. The air temperatures at 1.2m were almost precisely the same as the air temperatures at 1.8m at that time. Although, the air temperatures at 1.8m were higher than the air temperatures at 0.1m by 1.5°C from 13:00 to 18:00. A steady state was observed from 15:00 to 16:00 for all the air temperatures levels.

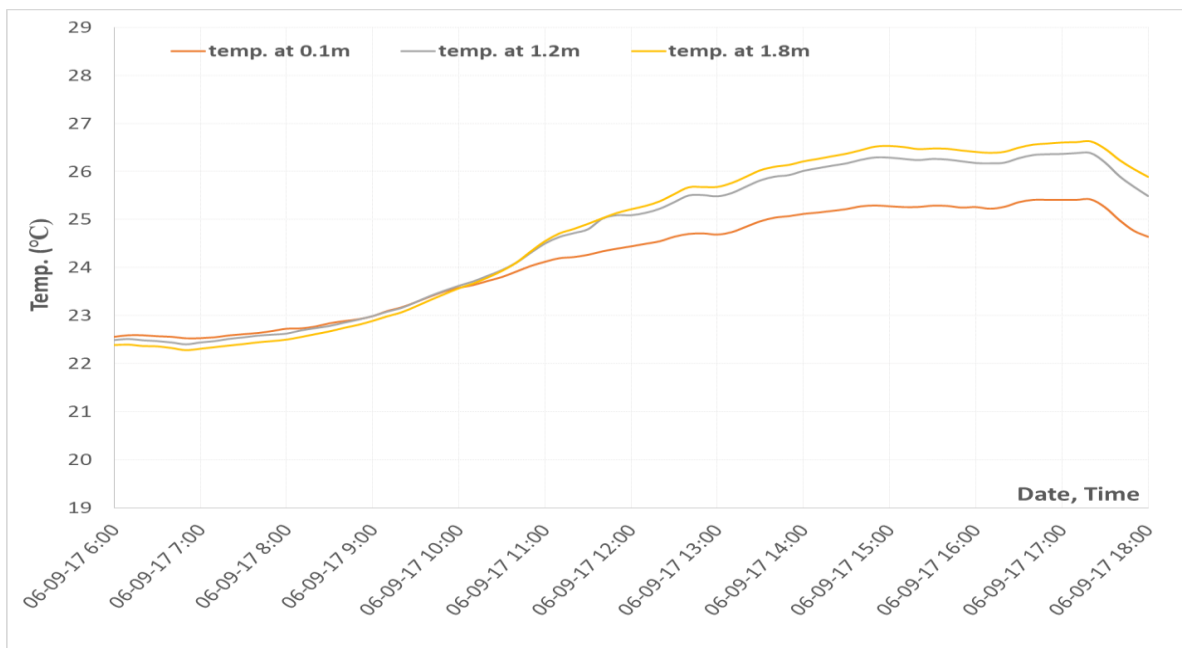


Figure 5.7 Air temperatures for point C1 at three level

Figure 5.8 and Figure 5.9 show the relative humidity for C1 at five levels, external and diffuser D1 R.H. for the last month of our measurements from 22/8/2017 to 19/9/2017 and for one of the days which was 6/9/2017, respectively. A fluctuation of the relative humidity in the office at all levels was assumed to be due to the change in the external relative humidity from day to day during that month. The relative humidity in the office throughout the measurements periods was ranging from 30% to 65% with a mean of 50%. Figure 5.9 shows that there was a small increase in the relative humidity at the supply diffuser on 6/9/2017 from 55% to 60% due to the cooling system turning on time which was at 6:00.

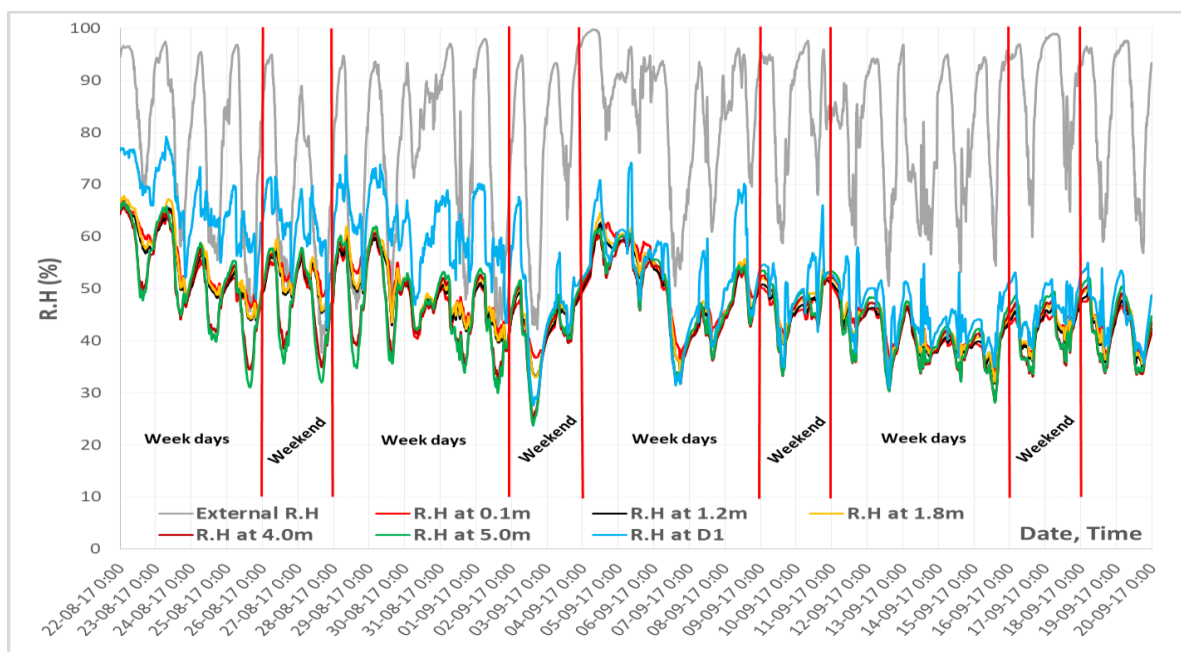


Figure 5.8 Relative humidity for C1 at five levels, external and diffuser D1 over one month

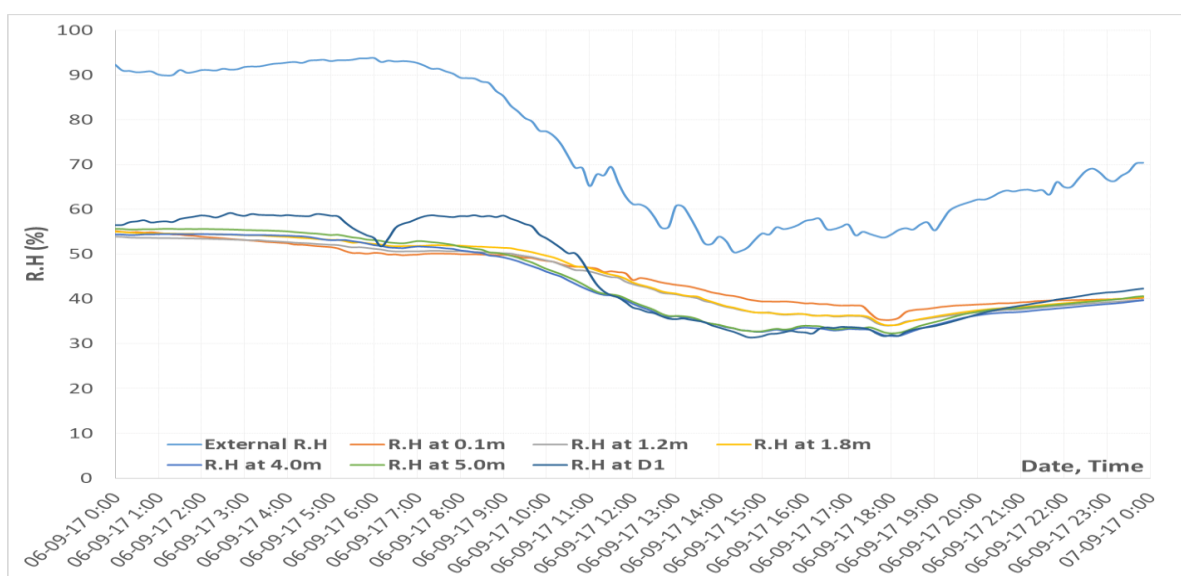


Figure 5.9 Relative humidity for C1 at five levels, external and diffuser D1 for one day.

The relative humidity trend for the five heights at C1 over 12 hours during the ON period of the cooling system is shown in Figure 5.10. The relative humidity at all levels was quite similar from 6:00 to 9:00 but they started to deviate afterwards. Both relative humidities at 4.0m and 5.0m declined to 35% at 15:00 then remained steady until 17:00. At 0.1m the relative humidity was the highest from 11:00 to 18:00 compared to other levels due to the higher air temperature at this low position in the office.

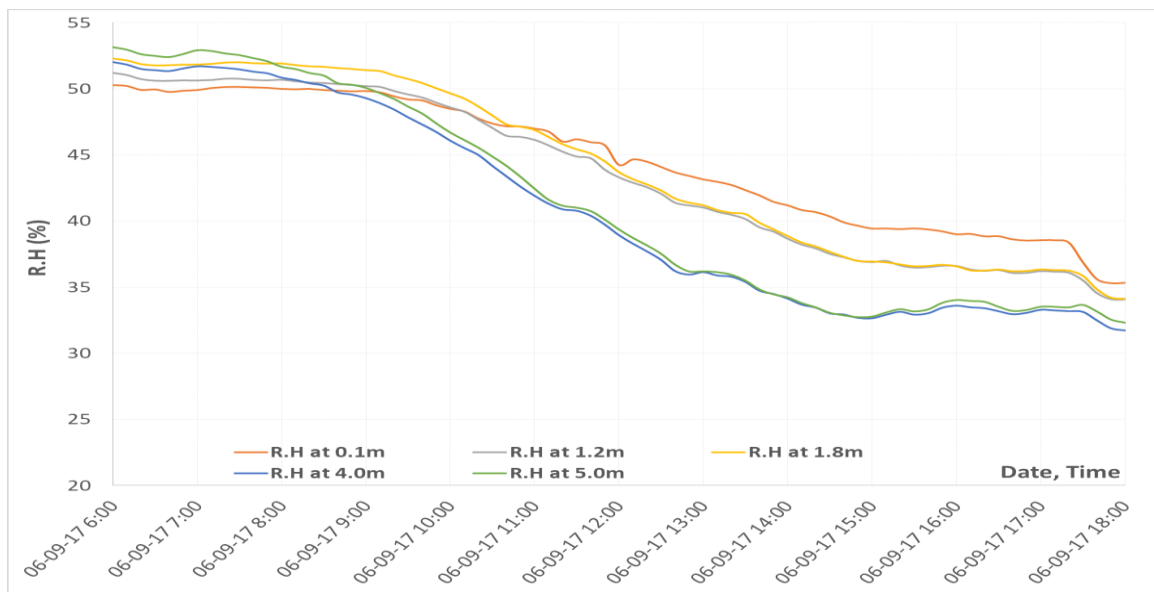


Figure 5.10 Relative humidity for five heights at C1 over 12 hours

### Adaptive thermal comfort for summers 2016 and 2017

CIBSE TM52 (CIBSE, 2013) indicates that the adaptive comfort temperature inside a free-running building is the temperature at which most of the space occupants perceive comfort, and is related to outdoor temperature over several days. In other words, it will be higher in warm weather than in the cooler case. Humphreys et al. (2013) and Nicol et al. (2017) have shown that internal temperatures vary in both free-running FR and mechanically heated or cooled spaces and that there is a correlation with external temperatures. They have termed such graphs as temperature clouds.

Following this approach, the indoor hourly mean temperature in the building studied is plotted against outdoor hourly mean temperature during the summer of 2016. The results are shown in the temperature cloud in Figure 5.11. The regression – line equation is shown in the graph while the width of the 95% interval of indoor operation temperature is 6 K.

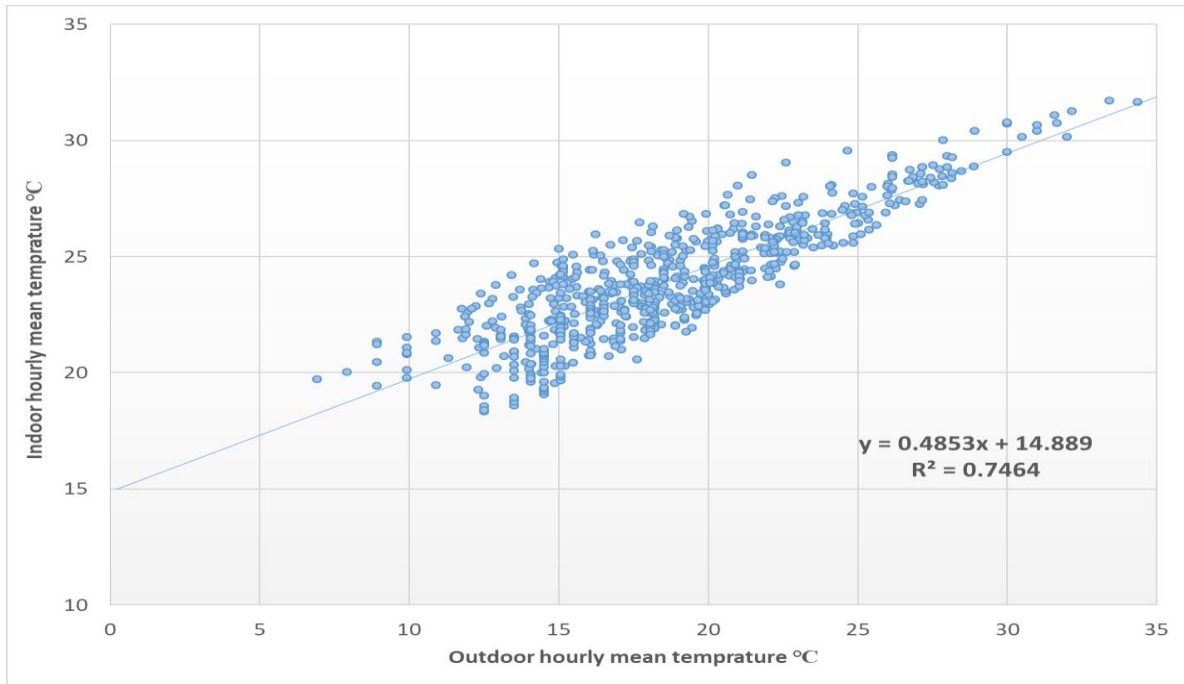


Figure 5.11 The mean indoor temperature versus outdoor daily mean temperature for the studied office building during summer 2016.

In the same way, the indoor temperature is plotted against outdoor mean temperature during the summer of 2017. The results are shown in the temperature cloud in Figure 5.12, together with the regression – line equation. In this case, too, the width of the 95% interval of indoor operation temperature is 6 K.

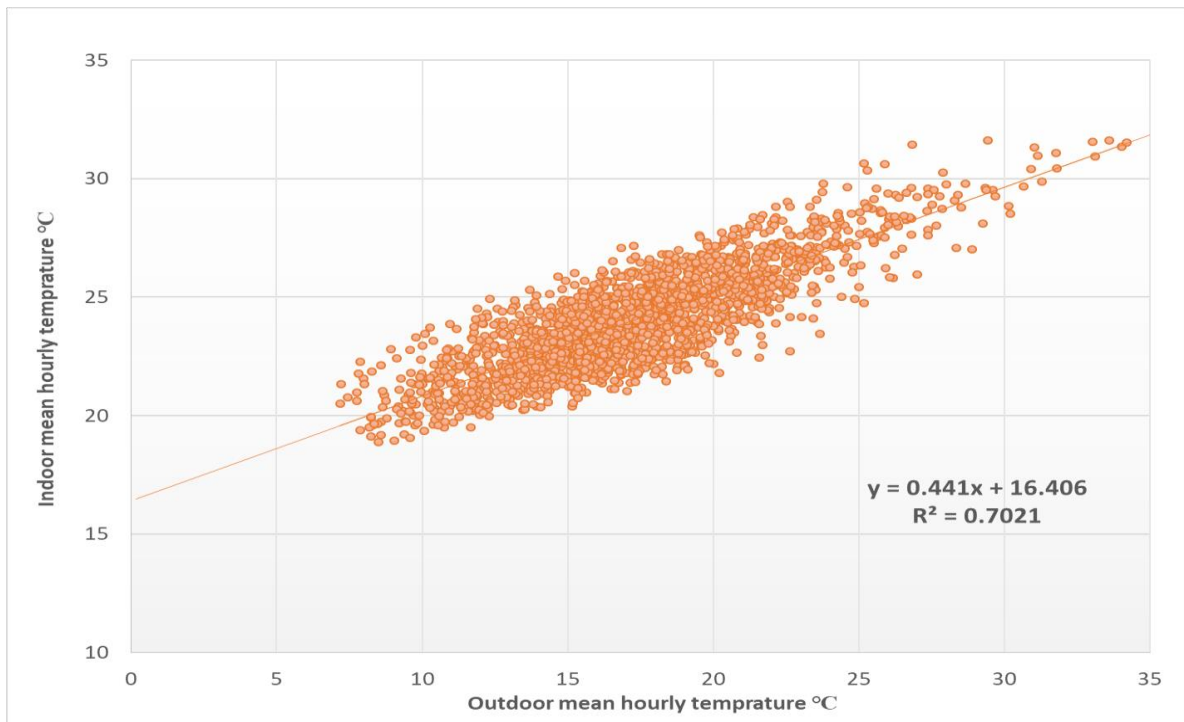


Figure 5.12. The mean indoor temperatures versus outdoor daily mean temperature for the studied office building during summer 2017.

Table 5.1 and Figure 5.13 compare the results from the studied office using the regression lines and equations for the summers of 2016 and 2017; with the adaptive thermal comfort lines and equations for the naturally ventilated building given in the European standard BS EN 16798-1 (2019) and ASHRAE standard 55 (2017). Also shown are the regression line and equation for a database used by Humphreys et al. (2013) for indoor and outdoor temperatures from 700 comfort surveys. This database is called the database of thermal comfort summary statistics DTCCS. Both equations for the office building for the two summers have roughly the same regression coefficients. Such a regression coefficient is characteristic for a free running building (Humphreys, Rijal and Nicol, 2013) while it differs clearly from the gradient of the regression line for the mechanical ventilation building as introduced by Nicol (2017). The findings show that comfort in this office relates to outdoor conditions in the same way as for an FR building and not as a mechanically heated or cooled building.

*Table 5.1 The regression lines equations for different databases*

<b>Database</b>	<b>Adaptive equations</b>	<b>Note</b>	<b>Building ventilation</b>
<b>Office Building (summer 2016)</b>	$T_i = 0.48 T_o + 14.9$	$T_i$ is indoor temperature $T_o$ is outdoor temperature	Mechanical
<b>Office Building (summer 2017)</b>	$T_i = 0.44 T_o + 16.4$	$T_i$ is indoor temperature $T_o$ is outdoor temperature	Mechanical
<b>European standard BS EN 15251</b>	$T_{comf} = 0.33 T_{rm} + 18.8$	$T_{comf}$ is comfort temperature $T_{rm}$ is running daily mean outdoor temperature	Free Running
<b>ANSI/ASHRAE standard 55</b>	$T_{comf} = 0.31 T_{om} + 17.8$	$T_{comf}$ is comfort temperature $T_{om}$ is monthly mean outdoor temperature	Free Running
<b>Humphreys et al. (2013)</b>	$T_n = 0.53 T_o + 13.8$	$T_n$ is indoor temperature $T_o$ is outdoor temperature	Free Running
<b>Nicol (2017)</b>	$T_i = 0.08 T_{od} + 23.0$	$T_i$ is indoor temperature $T_{od}$ is outdoor temperature	Mechanical

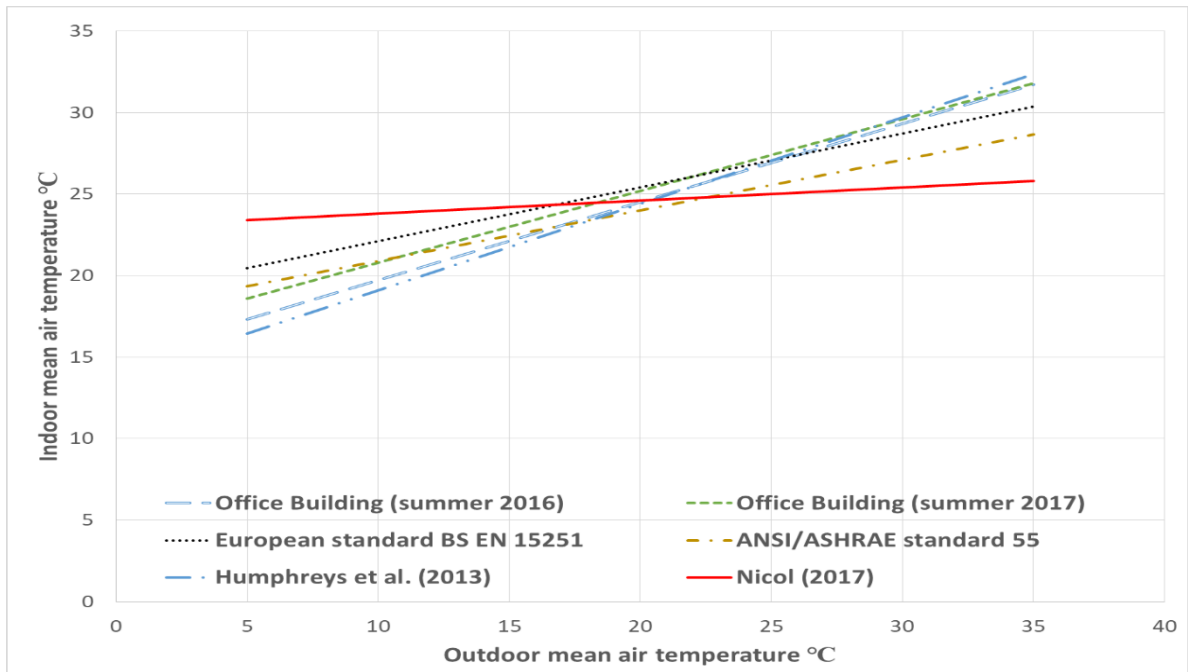


Figure 5.13 The regression lines for different databases

Figure 5.14 overlays the temperature clouds for summer 2016 (Figure 5.11) and summer 2017 (Figure 5.12). The results show that the indoor temperatures start to rise more quickly in summer 2017 than summer 2016 as the outdoor temperature rises. Notably, the two temperature clouds together have a range of indoor temperatures of about (6-8 K) that is somewhat similar to the FR region (Nicol, 2017).

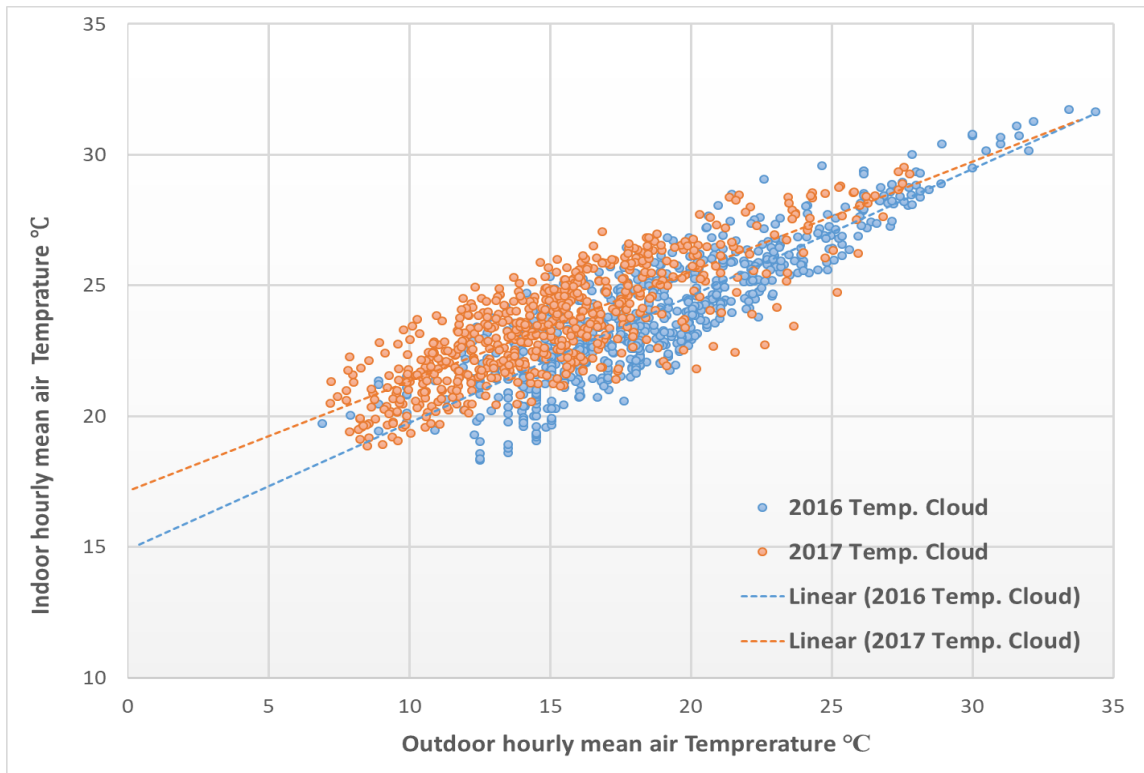


Figure 5.14 Overlay of the temperature clouds for summer 2016 and summer 2017.

Taking into consideration the findings above, we present the long term monitored temperatures for the mechanically ventilated space studied according to European standard BS EN 16798-1 (2019) for FR buildings, using the equation 2.11 which mentioned earlier in section 2.3.4 to relate the comfort temperature to the outdoor temperature as follows:

$$T_{\text{comp}} = 0.33 T_{\text{rm}} + 18.8$$

where  $T_{\text{rm}}$  is the exponentially weighted running mean of the daily mean outdoor air temperature ( $^{\circ}\text{C}$ ) as the measure of the outdoor temperature and can be calculated by the following equation 2.12 .

$$T_{\text{rm}} = (T_{\text{od}-1} + 0.8 T_{\text{od}-2} + 0.6 T_{\text{od}-3} + 0.5 T_{\text{od}-4} + 0.4 T_{\text{od}-5} + 0.3 T_{\text{od}-6} + 0.2 T_{\text{od}-7}) / 3.8$$

where  $T_{\text{od}-1}$ ,  $T_{\text{od}-2}$ , etc. are the daily mean outdoor air temperatures ( $^{\circ}\text{C}$ ) from yesterday, the day before yesterday and so on.

Since the office is located in a renovated building, the suggested category by BS EN 16798-1 is a category II as described earlier in section 2.3.4 where the suggested acceptable temperature range is  $\pm 3$  K.

Figure 5.15 shows the hourly internal air temperatures and the thermal comfort curves during operation hours (9:00 - 20.00) for the monitoring period from 21/6/2017 to 19/9/2017. As the space studied does not include any heated or cooled surfaces, the air temperature can be approximated to the operative temperature. The number of hours ( $H_e$ ) during which  $\Delta T$  is greater or equal to one degree (K) above the upper thermal comfort limit during that period were 44 hours of the 936 occupied hours. Here,  $\Delta T$  can be defined as the difference between the indoor air temperature at any time and the upper thermal comfort temperature. The percentage of these hours was 4.7% which was higher than 3% suggested by BS EN 15251. The highest overheated hours during the measurement periods were reported on Thursday 6/7/2017 with 9 hours, followed by Wednesday 5/7/2017 with 8 hours, and Wednesday 21/6/2017 with 7 hours. The lowest overheated hours during the same period were recorded in 4 different days with 3 hours for each day. In general, the number of days in which the indoor air temperature exceeded the upper thermal comfort limits during the survey months was 9 occurrences.

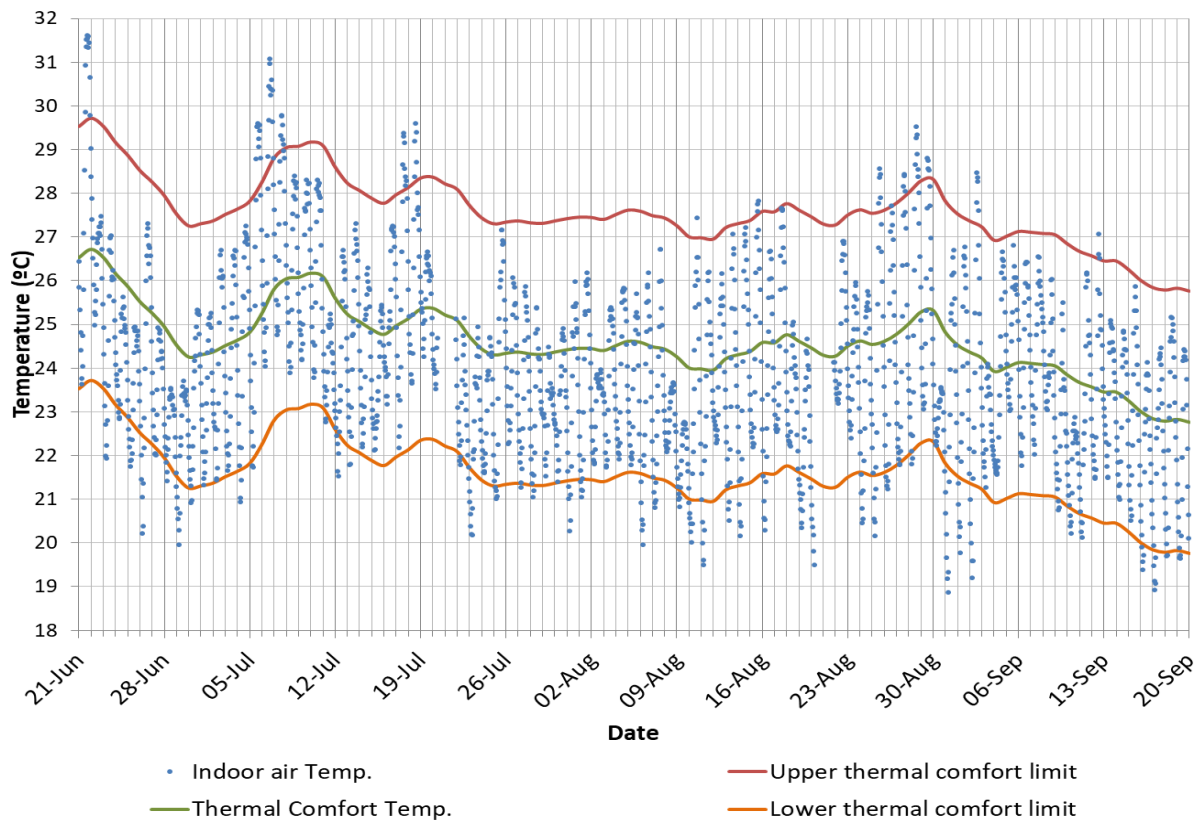


Figure 5.15 Hourly internal measured temperature during occupant hours (9:00-20:00) weekdays and the thermal comfort temperature with both upper and lower limits.

## 5.2.2 Results for Detailed Spot Measurements Phase

### For summer 2016

The measured velocities are presented in Figure 5.16 for six different spots in the enclosure. Air speed at spots 1 and 3 (see Figure 4.4) show a similar trend compared to the other spots because they have the same air flow direction and were located at the same distance from the diffusers. Spot 5 has the maximum speed for both heights 0.1m and 1.2m compared to the others. Both spots 5 and 2 have similar air speed tendency but the air speed curve at spot 6 has a unique shape compare to others. The speed at spot 4 was about 0 m/s for the three levels due to its location as it was under the main duct.

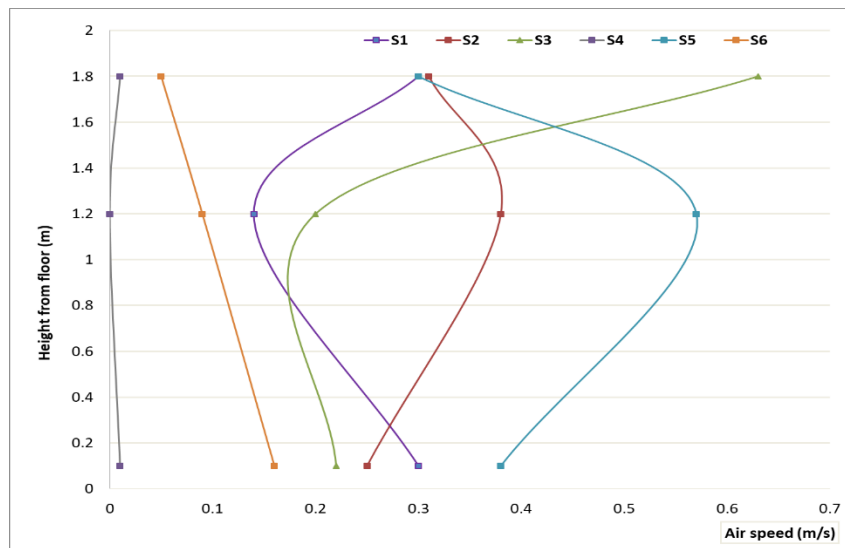


Figure 5.16 Air speed in six spots at different heights

Figure 5.17 shows the air speed for seven spots measured at a height of 1.2m and at 15:00 over five days. The speeds at spots 1, 6 and 7 were within the acceptable range, while it was just above that range at spots 2 and 3. At spot 5, the speeds were twice the recommended speed in the occupied zone which is 0.25 m/s.

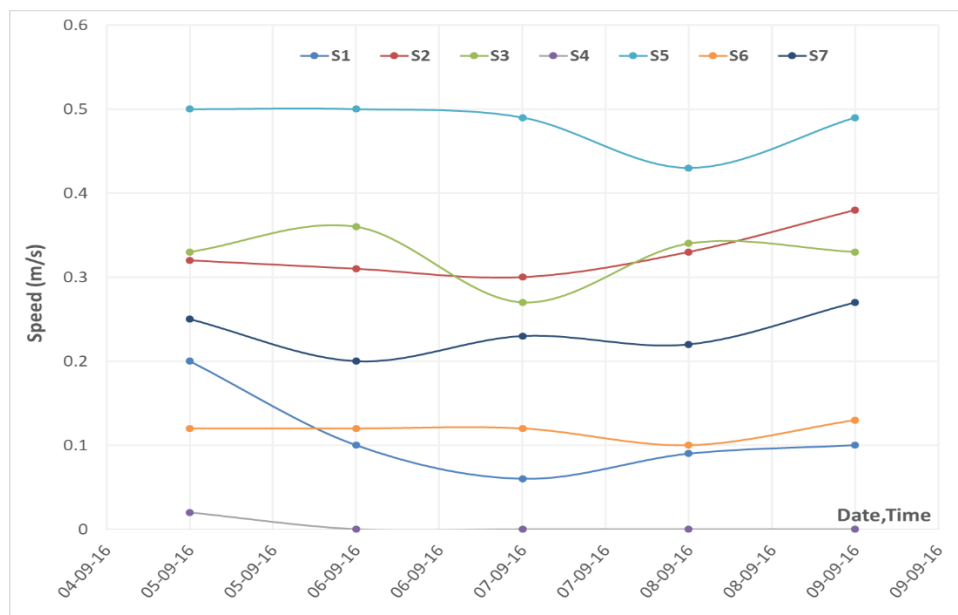


Figure 5.17 Air speed in six spots at 1.2 height over five days

Figure 5.18 illustrates the air temperatures for the seven spots at 1.2m that were mentioned above over five days. All the seven spots had the highest mean air temperatures (approximately 28°C) on 07/09/2016 compared to the other four days due to the high ambient temperature on that specific day. The air temperatures were precisely the same at all the spots all over the five days.

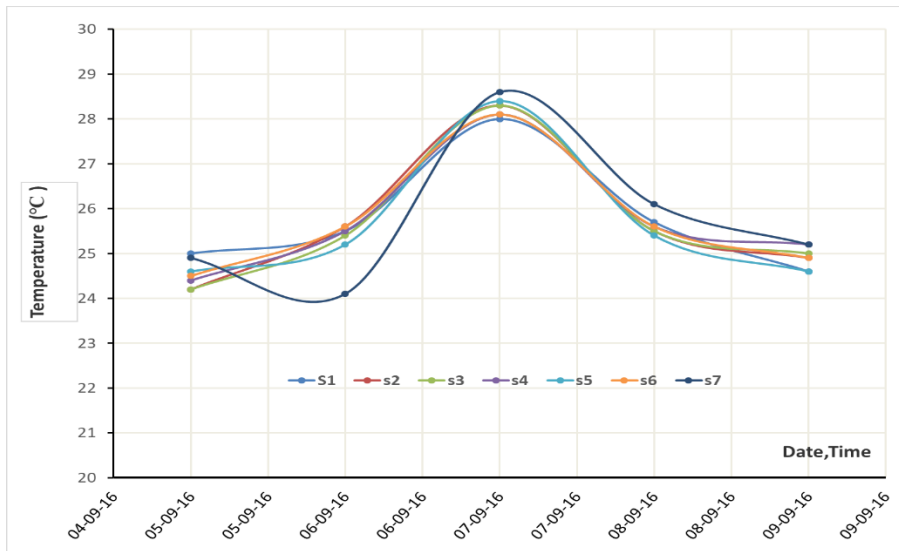


Figure 5.18 Air temperatures in seven spots over five days

Figure 5.19 shows the air speed for different spots over one day at three different times. At 13:00 the speeds at spot 5 and spot 2 were the maximum compared to the others. At spot 3 there was a steady drop in the speeds from 11:00 to 13:00 then a dramatic jump between 13:00 and 15:00.

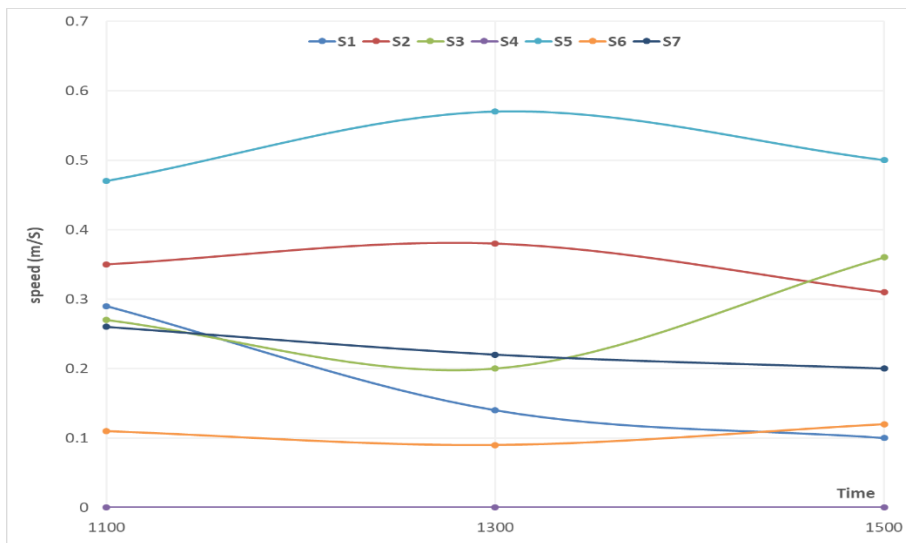


Figure 5.19 Air speed in seven spots at three different times in one day

The temperatures for the seven spots which were mentioned earlier are presented in Figure 5.20. The temperature trends for spots 1, 3 and 6 were similar from 11:00 to 15:00. However, the temperature for spot 7 reached a peak at 13:00 and hit a trough at 15:00 down to 24.1°C. There was a gradual rise in the seven spots' temperature from 11:00 to 13:00 while there was hardly any change in the temperature between 13:00 and 15:00 for that day.

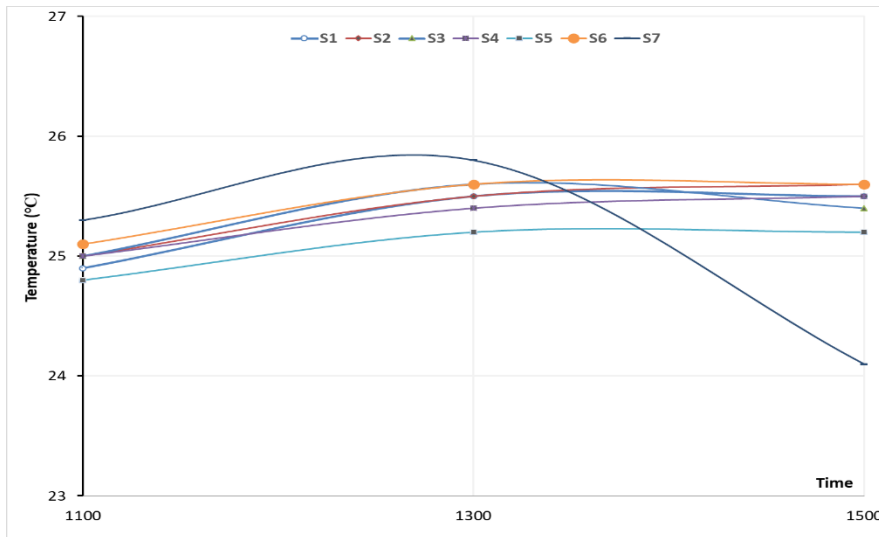


Figure 5.20 Temperature in seven spots at three different times in one day

**For summer 2017**

Table 5.2 shows the differences in air speed at the supply diffusers for two different days at 13:00 (measured as seen). Although the difference between the two days is insignificant, there is a large variation between the different diffusers due to the fact that some of the diffusers' segments were partially closed.

Table 5.2 Air speed at diffusers

Date	Air speed (m/s)							
	D1	D2	D3	D4	D5	D6	D7	D8
31/8/2017	0.03	0.03	0.3	0.3	0.6	0.6	0.9	0.9
11/9/2017	0.03	0.03	0.29	0.29	0.61	0.61	0.9	0.9

Figure 5.21 shows the measured air speed for seven different spots in the enclosure (see Figure 4.4) on 11/9/2017 at 15:00 for three heights. The air speed at spots 7 and 3 shows similar trend compared to the other spots because they have similar air flow direction. Spot 3 has the maximum air speed for both heights 1.2m and 1.8m compared to the others due to its location which had the closest distance to diffuser 8 and the air speed at that diffuser was the highest. Both spots 2 and 6 have similar air speed tendency while it was different for spot 5. In summary, the air speed at all the spots was extremely low, and sometimes they were 0 m/s at height 1.8m. The reason behind that is the speeds of the air supply diffusers were very low due to poor ventilation system performance.

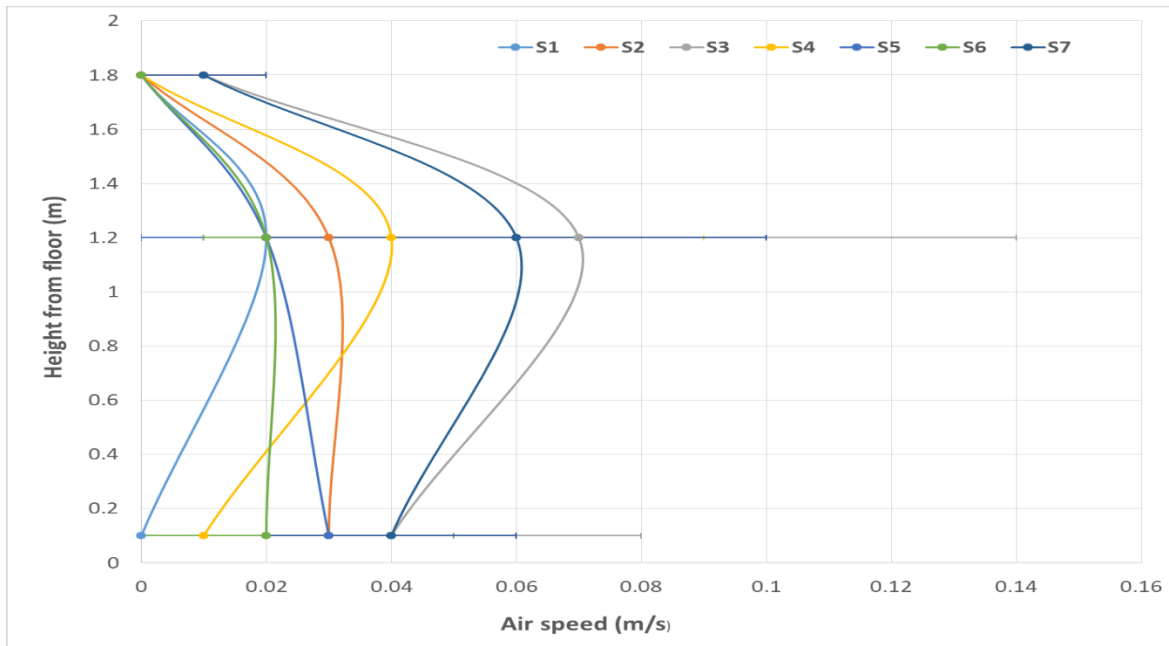


Figure 5.21 Air speed in seven spots at different heights

The measured air temperatures are presented in Figure 5.22 for seven different spots that were mentioned above for the same date and heights. The air temperatures at 1.8 m for all the spots, except spots 5 and 7, were greater than the temperatures at 0.1m due to the thermal stratification in the enclosure. The temperature at spot 4 was the highest for the three levels due to its location as it was under the main duct. The maximum temperature was 26.1°C at spot 4 while the minimum temperature was 25°C at spot 1. In general, the air temperatures were markedly high at all the spots for the three heights compared to the ambient temperature for that day which was 18.2°C.

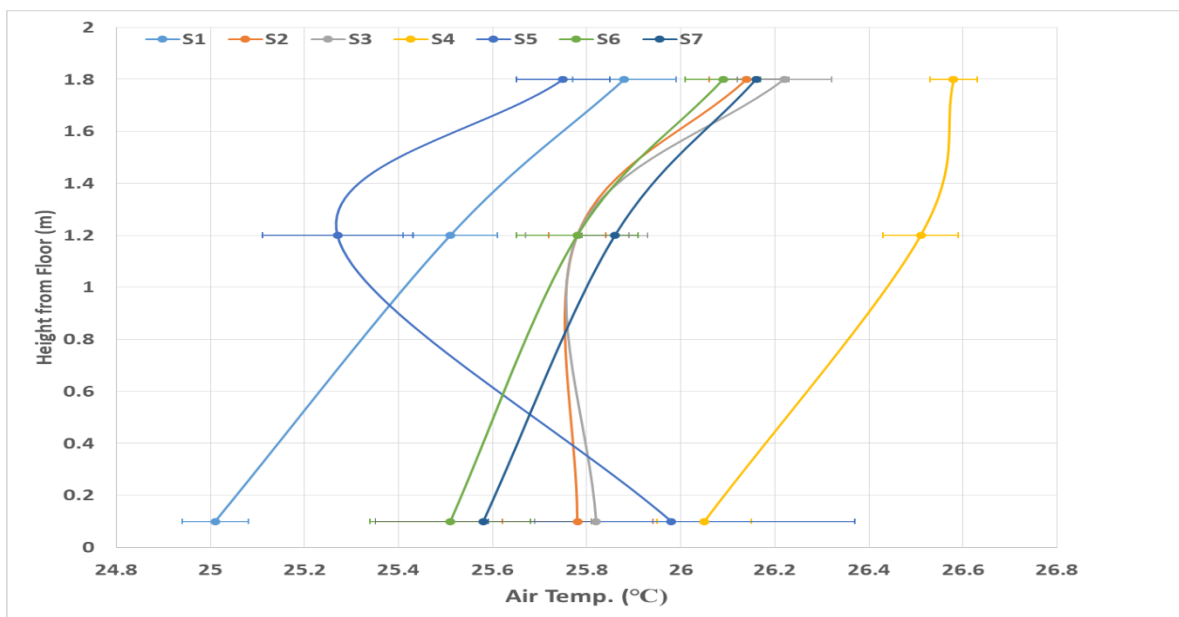


Figure 5.22 Air temperature in seven spots at different heights

### Fanger's PMV thermal comfort for summers 2016 and 2017

The acquisition of thermal-hygrometric parameters defined by BS EN ISO 7730 (BSI, 2005), BS EN ISO 10551 and ASHRAE standard 55 (2017) was the base for the measurement methodology used to evaluate comfort at specific points within the occupied zone in the large space studied using PMV and PPD indices to consider the influence of air speed and direction and relative humidity. This is because low air speed was measured in the office which has an impact on thermal comfort as will be discussed in section 5.3. The measured values of the thermal comfort parameters are tabulated in Table 5.3 for several days during summer 2016 and summer 2017.

*Table 5.3 Synthesis of measured data for several days during summer 2016 and 2017*

Date	Height (m)	Mean air temp. (°C)	Mean air speed (m/s)	RH (%)	Metabolic rate (met)	Clothing insulation (clo)	PMV	PPD (%)
5/9/2016	1.2	24.3	0.18	67.6	1.2	0.5	-0.18	6
7/9/2016	1.2	25.7	0.19	51.1	1.2	0.5	+0.07	5
9/9/2016	1.2	25.0	0.2	55.9	1.2	0.5	-0.12	5
31/8/2017	1.2	26.2	0.03	45.1	1.2	0.5	+0.46	9
5/9/2017	1.2	26.1	0.03	56.5	1.2	0.5	+0.50	11
11/9/2017	0.1	25.7	0.02	42.9	1.2	0.5	+0.3	7.0
	1.2	26.0	0.04	42.9				
	1.8	26.2	0.0	42.5				

The PMV was calculated using a spreadsheet based on the algorithm given in ISO 7730 standard (BSI, 2005). The result for the PMV values was near to zero or lower in the summer of 2016 while the values were higher than zero for all the three days in summer 2017. In fact, all of the PMV values were in the recommended internal range by ISO 7730 which is  $-0.5 + 0.5$ . Moreover, PPD which is the predicted percentage of dissatisfied and calculated in accordance with the PMV index had values in the suggested range between 0 to 15 percent (ISO 7730) for both summer 2016 and 2017 days. Also, the relative humidity in the office was generally within the comfort limits, ranging from 51% to 67% and from 42% to 44% for the summer of 2017 respectively. Furthermore, on 11/9/2017 the air temperature at height 1.8m (head level) was higher than that at 0.1m (foot level) with a mean vertical temperature difference of 0.5°C. If this difference was 3 °C or more, warm discomfort could be perceived at the head,

and cold discomfort can be felt at the feet, while the occupant is thermally neutral as a whole. In addition to that, there was no draft on any day due to the significantly low air velocities which were near to zero, particularly for the summer of 2017. Both air draft and vertical temperature difference are considered the main reasons for causing local discomfort (ASHRAE 2010)(Fathollahzadeh, Heidarinejad and Pasdarsahri, 2016).

### For summer 2018

Since CO<sub>2</sub> cannot be absorbed or filtered, it can be utilised as a good index for indoor air quality (Oke *et al.*, 2008). Figure 5.23 shows the measured CO<sub>2</sub> concentrations for seven different spots in the office (see Figure 4.4) on 25/5/2018 at 11:00 at a height of 1.2m. It can be noted that the fluctuations of the logger used to measure the CO<sub>2</sub> concentrations were minor. As shown in the figure, the CO<sub>2</sub> concentration at all the measuring spots was almost the same, which reveals that the environment within the office was uniform. It is worth mentioning that these measurements will be used to evaluate the CFD model.

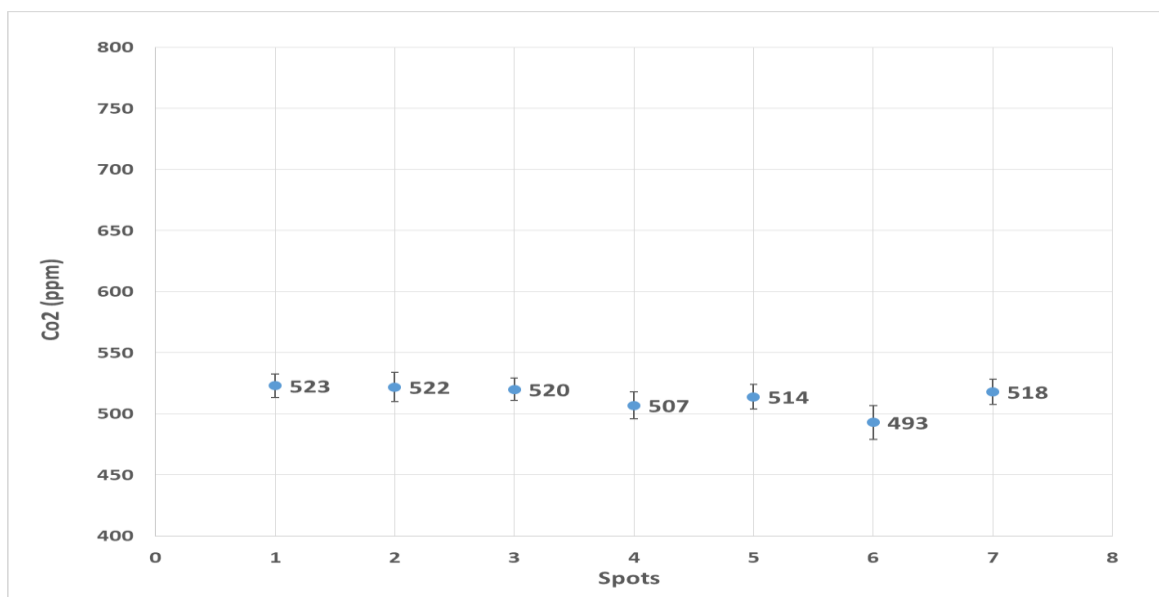


Figure 5.23 The CO<sub>2</sub> concentrations for seven different spots in the office for summer 2018

### 5.2.3 Occupants Questionnaires Results

A total of 50 questionnaires were collected during three days and processed. Table 5.4 shows the analysis of the results from the questionnaires.

Table 5.4 Questionnaires numbers, date and analysis: synthesis of main results

Date	Number of questionnaires	PMV <sub>q</sub> Actual mean vote	TDI (%) Thermal dissatisfaction	TPI (%) Thermal preference	UAMI (%) Unacceptable air movement
31/8/2017	14	0.25	28	0	50
5/9/2017	16	0.8	19	19	63
11/9/2017	20	0.25	15	5	60

For the first day of 31/8/2017 the actual mean vote PMV<sub>q</sub> was found to be slightly warm (i.e. 0.25) where about half of the people were dissatisfied with air movement. Similarly, the PMV<sub>q</sub> for day 5/9/2017 was 0.8 which appeared to be slightly warm and a very low air movement was observed which makes 63% of the office occupants uncomfortable. Consequently, the thermal dissatisfaction index was 19% on that day. In the same way, the questionnaires data for 11/9/2017 revealed a thermal sensation oriented towards warm where PMV<sub>q</sub> value was 0.25 in the office that day. About 5% TPI of people preferred to feel cooler whereas 15% TDI of them felt thermally dissatisfied. The low movement of air makes the discomfort of occupants worse where 60% UAMI of occupants were dissatisfied with the air movement. It might be concluded that the office represented a higher percentage of dissatisfied than was expected. This is possibly due to very low air velocity inside the enclosure.

Figure 5.24 shows the subjective responses to temperature for the three days. Seven of the response for days 31/8/2017 and 11/9/2017 claimed that the temperature in the office is neither hot nor cold but only three for day 5/9/2017 recorded the same. More votes for slightly warm and warm were on 5/9/2017 compared to the other two days. It is observed that no votes from any occupants in any days are within the cold and hot regions.

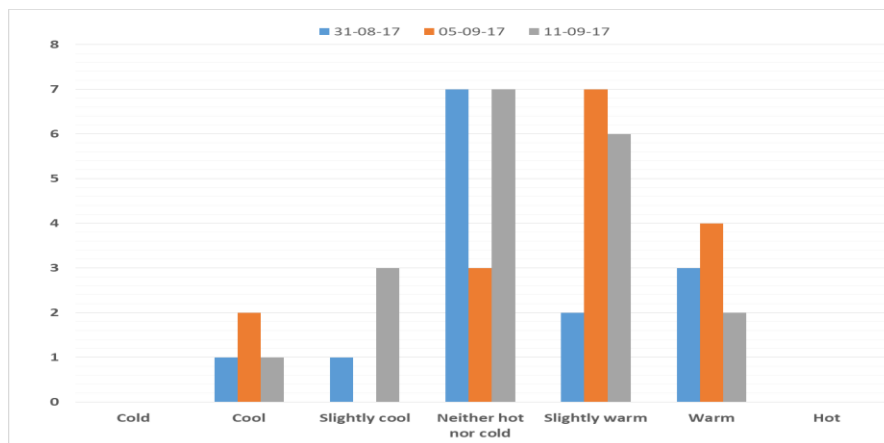


Figure 5.24 Distribution of subjective response to temperature for three days

Figure 5.25 shows that the subjective responses to humidity was biased towards a neutral category. More people in day 5/9/2017 perceived that the air was slightly humid or humid than in days 31/8/2017 and 11/9/2017. No respondent perceived the air as very humid in any of these days.

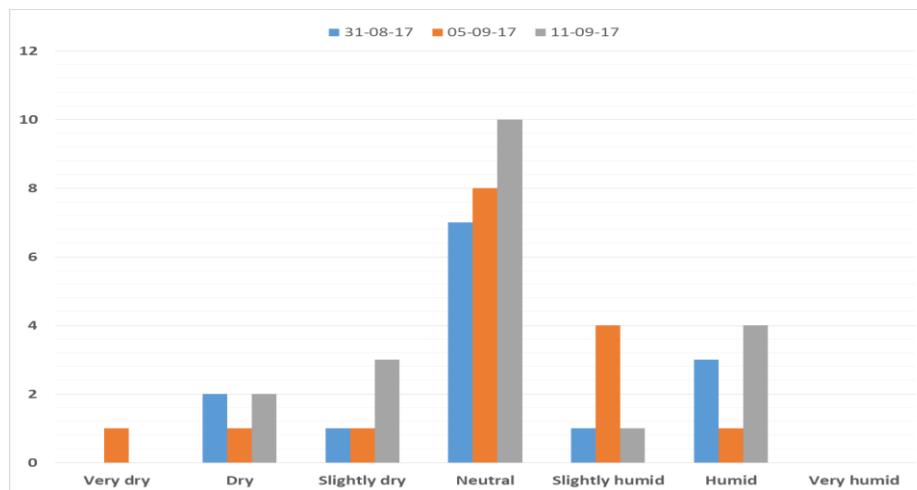


Figure 5.25 Distribution of subjective response to humidity for three days

The distribution of occupants' responses to the air movement was considerably biased towards the scale presenting the overall perception of the air being motionless, see Figure 5.26. More than half of the respondents in each day claimed that the air in the office was slightly still, still or very still. Several reported that the air movement was acceptable. It was observed that one occupant claimed that the air was somewhat draughty but no votes for draughty and very draughty responses were reported.

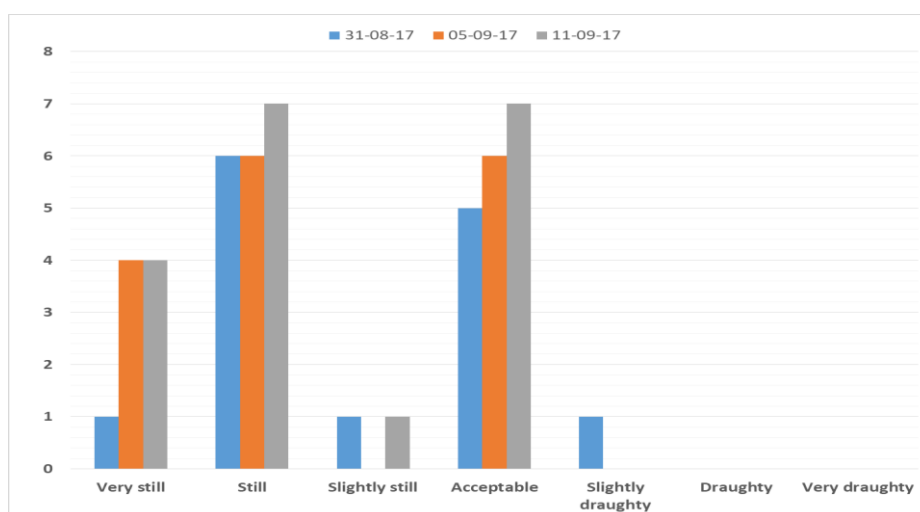


Figure 5.26 Distribution of subjective response to air movement for three days

Figure 5.27 shows the distribution of votes for the overall thermal comfort during the three days where the distribution skewed toward the comfortable and slightly comfortable regions. Only four in 31/8/2017, three in 5/9/2017 and one in 11/9/2017 voted the office was uncomfortable.

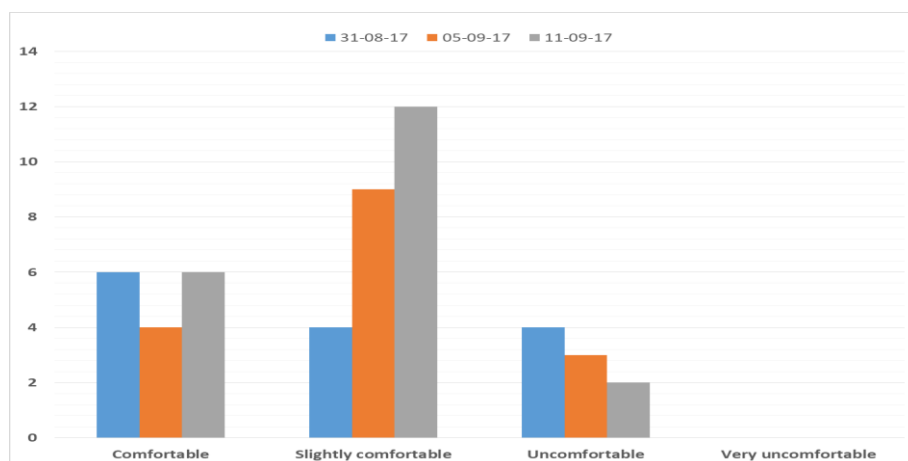


Figure 5.27. Distribution of subjective response to overall comfort for three days

### 5.3 CHAPTER SUMMARY

The data and results for the three monitoring phases; long-term, detailed spot measurements for short time period and occupant questionnaire surveys were presented in this chapter. The first measurement phase was based on data from the long-term measurements of air temperature, and the correlation of the indoor air temperature with outdoor temperature calculated for the summer of 2016 and the summer of 2017. It was observed that both results are comparable with correlations using similar analysis. Nicol (2017) points out that typically for FR buildings, the regression slope between indoor operative temperature and outdoor air temperature is in the range 0.5 to 0.6 which is similar to the regression slopes for both summers 2016 and 2017. Accordingly, the researchers' office can be treated as FR building although it has a mechanical ventilation system. CIBSE TM50 (CIBSE, 2013) table 2 suggests that the acceptable temperature range for a new or renovated free-running building is  $\pm 3K$ ; however there were nine occurrences in which the indoor air temperature exceeded the upper thermal comfort limits in summer 2017.

The second measurements phase was short term detailed measurements to include air speed at different heights in the occupied zone and some results from the CO<sub>2</sub> concentration

measurements. The comfort temperature for occupants is assumed to be most satisfied when both PMV and PPD are closed to the minimum values. Therefore, the calculated PMV and PPD values for the assigned days were within the recommended range by ISO 7730.

The last phase was a questionnaire survey in which the occupants reported that the office was generally neutral. However, a high percentage of them claimed that the air movement was not acceptable in all the assessed days during the summer of 2017. Therefore, the type of ventilation system, and in particular the configuration and position of inlets, is crucial for providing comfort without excessive heating or cooling to compensate for air movement deficiencies. Based on these results, chapter 6 and 7 will continue to investigate different air distribution systems such as impinging jet system using CFD modelling to examine their effectiveness in improving internal conditions within the occupied zone of large spaces with a minimum of energy use.

The measurements will be also used for the evaluation of the developed CFD models.

# 6 CHAPTER SIX: CFD MODELLING FOR THE CASE STUDY BUILDING

---

## 6.1 INTRODUCTION

This chapter presents the CFD modelling part of the air flow and temperature variation for the large space case-study building, CSEF. The CFD modelling and evaluation stage was carried out in three phases simultaneously for each measurement phase; the first was performed in summer 2016, the second in summer 2017 and the third in summer 2018. This chapter describes all phases of CFD modelling and evaluation as follows:

Section 6.2 describes the geometrical model

Section 6.3 presents the numerical grid

Section 6.4 describes the turbulence modelling part

Section 6.5 discusses the boundary conditions

Section 6.6 shows the grid independent study

Section 6.7 shows the CFD evaluation with the measurements

Section 6.8 presents and discusses the predictions of air temperature air velocity and CO<sub>2</sub> concentration distribution into the office building.

## 6.2 GEOMETRICAL MODEL

ANSYS workbench design modeller 17.1 with Fluent 17.1 (ANSYS Fluent, 2016) was used to simulate the large space case-study the researchers' office at CSEF building which was described in section 4.2. Some simplification of the geometrical model was made to save computing time and power while still preserving the most relevant physical aspects of the geometry. For instance, the occupants' bodies were represented as cylinders but more details are described in section 6.5.

Three CFD models were constructed to correspond with measurements which were used for the evaluation.

### **Summer 2016 model**

Since there was a steady state situation for the air temperature inside the researchers' office at CSEF building from 15:00 to 17:00 on 6/9/2016 (see Figure 5.3), the CFD simulation model was assumed to be steady-state and the simulation time used was for 15:00h with 12 occupants on that day, see Figure 6.1.

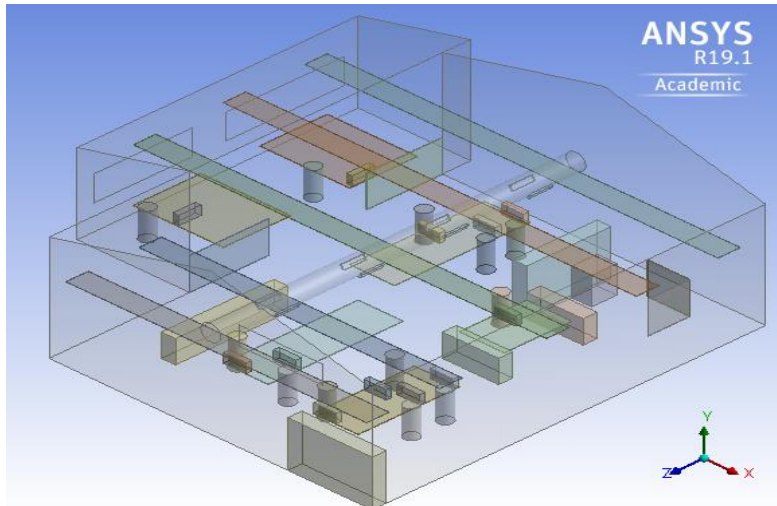


Figure 6.1 The CFD model of the researchers' office for summer 2016

### Summer 2017 and 2018 models

The same CFD modelling procedure and assumptions for the summer 2016 model were used in summer 2017 and 2018 models. The simulations time was for 15:00h on 11/09/2017 with 20 occupants and at 11:00h on 25/05/2018 with 14 occupants for summer 2017 and 2018, respectively; see Figure 6.2 and Figure 6.3.

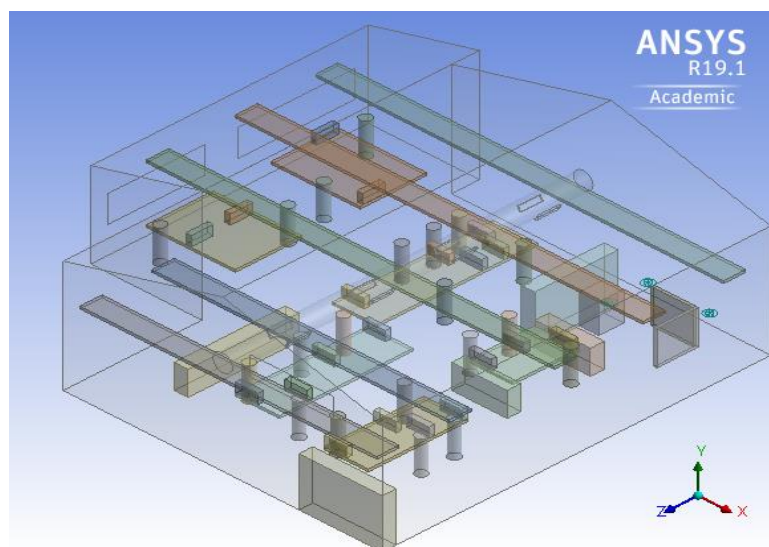


Figure 6.2 The CFD model of the researchers' office for summer 2017

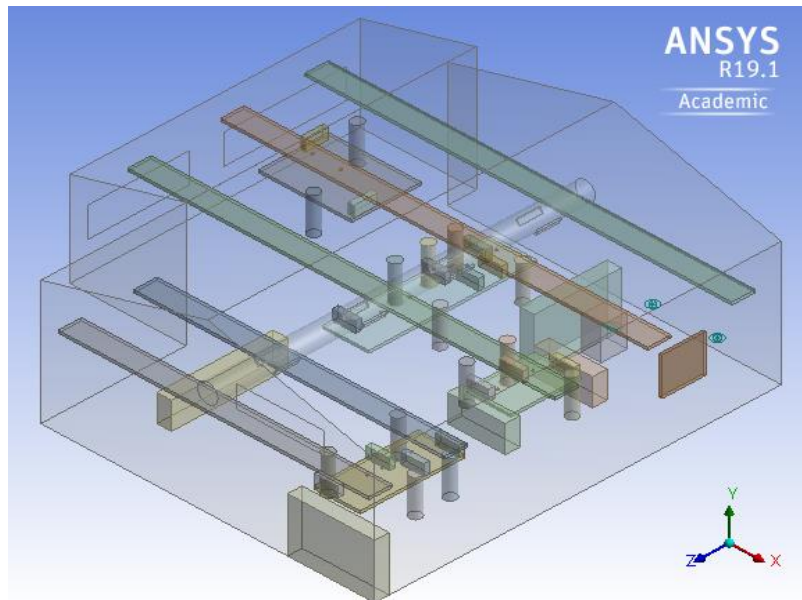


Figure 6.3 The CFD model of the researchers' office for summer 2018.

### 6.3 NUMERICAL GRID

The ANSYS code was used to construct the three-dimensional geometry and generate the mesh. Non-uniform grid strategy was utilised to cover the whole computational domain for the room. The finer grid was used close to air inlets, outlets and walls, and also the areas that were anticipated to have steep velocity gradients. A grid independency study was performed using the SST k- $\omega$  model, and three grids densities. Each of the three models were tested, see Table 6.1. The results are discussed in the grid independency study section.

Table 6.1 Grid densities for summer 2016, 2017 and 2018

Grid density	Summer 2016	Summer 2017	Summer 2018
Coarse	7,233,904	7,463,265	7,172,356
Medium	16,045,809	16,853,380	15,824,322
Fine	24,168,713	24,412,754	23,096,678

### 6.4 TURBULENCE MODELLING AND NUMERICAL ASPECTS

Several turbulence models can be used for the simulation of turbulent flow. Reynolds-averaged Navier-Stokes equation simulation using one or two-equation turbulence models such as RNG k- $\epsilon$  models, SST k- $\omega$  model and Reynolds Stress model are often used. Thai et al. (2007) made an evaluation of various turbulence models for predicting the airflow and turbulence in enclosed environments using CFD, and they recommended RNG k- $\epsilon$  model to be used in forced convection flow which is often experienced in enclosures with mechanical

ventilation systems. However, they recommended SST k- $\omega$  model for high buoyancy flow in predicting air velocity, temperature and turbulence quantities. For that reason, both the RNG k- $\epsilon$  and SST k- $\omega$  models were used in the CFD model to compare their performance by utilising the temperature and air velocity measurements. The comparison between these two turbulence models is discussed in section 6.7. For the near wall treatment Awbi (1998) pointed out that the distance of the point from the surface  $y_p$  at which the wall function is applied, i.e. the value  $y^+$  at that point. He proposed in his study that an optimum position for a heated wall is about 5 mm and about 30 mm for a heated ceiling.

The finite-volume solver Fluent 17.1 was used to simulate the flow field of the ventilated enclosure, the governing equations were solved with a segregated scheme, and the SIMPLE algorithm was used for coupling the pressure and velocity. In the discretization scheme, the non-linear and the viscous terms were calculated with second order upwind scheme while the BODY FORCE WEIGHTED scheme was used to reveal convergence when two consecutive iterations for the local variable was less than  $10^{-3}$  whereas for energy it was less than  $10^{-6}$ . Besides that, the net heat flow rate imbalance was less than 0.003% of the total flux through the system, and the net heat imbalance was less than 0.3% of the total energy flux through the system too.

## 6.5 BOUNDARY CONDITIONS

### Summer 2016 and 2017 models

The quality of the numerical solution is invariably dependent on the accuracy of the boundary conditions and how these are combined with the numerical model. In this investigation, the boundary conditions were defined based on the measurements carried out.

The body of the occupant was presented as a cylinder of height 1.4m and diameter of 0.4m giving a body surface area of approximately 1.8 m<sup>2</sup> according to (Pinkel, 1958). The clothing temperature was set to a value of 33.7°C as mentioned by Zolfaghari & Maerefat (2010). The personal computer, lighting and photocopier were presented using the actual size and dimensions. The temperature of their surfaces were set to a value of 40°C as mentioned by Lei et al. (2014). Table 6.2 summarises all the boundary conditions of the CFD models for summer 2016 and summer 2017.

Table 6.2 The Boundary conditions for CFD models for summer 2016, summer 2017.

	Details	Summer 2016	Summer 2017
<b>Date and time</b>	-	6/9/2016 at 15:00	11/9/2017 at 15:00
<b>Supply air diffusers velocity, temperature</b>	Diffuser (1)	2.7m/s , 23°C	0.03m/s , 25.8°C
	Diffuser (2)	3.2m/s , 23°C	0.03m/s , 25.8°C
	Diffuser (3)	3.0m/s , 23°C	0.29m/s , 25.6°C
	Diffuser (4)	3.1m/s , 23°C	0.29m/s , 25.6°C
	Diffuser (5)	1.0m/s , 23°C	0.61m/s , 25.6°C
	Diffuser (6)	1.0m/s , 23°C	0.61m/s , 25.8°C
	Diffuser (7)	1.0m/s , 23°C	0.90m/s , 25.6°C
	Diffuser (8)	1.0m/s , 23°C	0.90m/s , 25.8°C
<b>Ceiling surface temperature</b>		35°C	21°C
<b>Internal walls surface temperature</b>		28°C	25°C
<b>External wall surface temperature</b>		29°C	24°C
<b>Floor heat flux</b>		0 W/m <sup>2</sup>	0 W/m <sup>2</sup>
<b>Windows surface temperature</b>		39°C	21°C
<b>Number of occupants</b>		12	20
<b>Occupants clothing temperature</b> (Zolfaghari and Maerefat, 2010)		33.7°C	33.7°C
<b>Number of personal computers</b>		12	20
<b>Personal computers surface temperature</b> (Lei, Wang and Zhang, 2014)		40°C	40°C
<b>Lighting surface temperature</b> (Lei, Wang and Zhang, 2014)		40°C	40°C
<b>Number of photocopiers</b>		1	1
<b>Photocopier surface temperature</b> (Lei, Wang and Zhang, 2014)		40°C	40°C

### Summer 2018 model

Since the CO<sub>2</sub> concentration was measured for the tests in summer 2018, the CFD model for this case was developed to predict the metabolic CO<sub>2</sub> within the case-study building. As mentioned earlier in section 2.4.2, the rate of production of carbon dioxide CO<sub>2</sub> by the human's respiratory system is associated with the metabolic rate by equation 2.13.

$$G = 4 \times 10^{-5} MA$$

where  $G$  is the CO<sub>2</sub> production (L/s),  $M$  is the metabolic rate (W/m<sup>2</sup>) and  $A$  is the body surface (m<sup>2</sup>). In this study, an average sedentary adult produces around 0.005 L/s of CO<sub>2</sub> by respiratory system.

To represent the CO<sub>2</sub> production per person in the CFD model, a separate cells zone shaped as a cube (5 x 5 x 5 cm) was used for modelling species transport. One mass CO<sub>2</sub> source term was added to that cells zone. Therefore,  $G = 0.005 \text{ L/s} \approx 9.9 \times 10^{-6} \text{ kg/s}$  and as it was presented

by a cube with a volume of  $1.25 \times 10^{-4} \text{ m}^3$ , then the  $\text{CO}_2$  production per person in the CFD model is  $9.9 \times 10^{-6} \text{ kg/s}$  divided by  $1.25 \times 10^{-4} \text{ m}^3$  which leads to  $0.0792 \text{ kg/m}^3\text{s}$ . Consequently, the  $\text{CO}_2$  source term is added in the conservation of the  $\text{CO}_2$  mass fraction equation. The other boundary conditions which were used in this CFD model were similar to the boundary conditions used in summer 2016 and 2017 models and is illustrated in Table 6.3.

Table 6.3 Boundary conditions for summer 2018 CFD model

	Details	Summer 2018
<b>Date and time</b>	-	25/5/2018 at 11:00
<b>Supply air diffusers velocity, temperature and <math>\text{CO}_2</math> concentration</b>	Diffuser (1)	0.1m/s , 23°C , 400 ppm
	Diffuser (2)	0.1m/s , 23°C , 400 ppm
	Diffuser (3)	0.3m/s , 23°C , 400 ppm
	Diffuser (4)	0.3m/s , 23°C , 400 ppm
	Diffuser (5)	0.7m/s , 23°C , 400 ppm
	Diffuser (6)	0.7m/s , 23°C , 400 ppm
	Diffuser (7)	0.9m/s , 23°C , 400 ppm
	Diffuser (8)	0.9m/s , 23°C , 400 ppm
<b>Ceiling surface temperature</b>		25°C
<b>Internal walls surface temperature</b>		24°C
<b>External wall surface temperature</b>		24°C
<b>Floor heat flux</b>		0 W/m <sup>2</sup>
<b>Windows surface temperature</b>		25°C
<b>Number of occupants</b>		14
<b><math>\text{CO}_2</math> production per person (MacIntyre, 1980)</b>		$9.9 \times 10^{-6} \text{ kg/s}$
<b>Occupants clothing temperature (Zolfaghari and Maerefat, 2010)</b>		33.7°C
<b>Number of personal computers</b>		14
<b>Personal computers surface temperature (Lei, Wang and Zhang, 2014)</b>		40°C
<b>Lighting surface temperature (Lei, Wang and Zhang, 2014)</b>		40°C
<b>Number of photocopier</b>		1
<b>Photocopier surface temperature (Lei, Wang and Zhang, 2014)</b>		40°C

## 6.6 GRID INDEPENDENCY STUDY

### Summer 2016 model

The spot S2 which is shown in Figure 4.4 was selected to do this grid independency study. This location was chosen because it is not facing any supply air flow jets which provides a steadier reading during the measurement stage. The mean air velocity and temperature profiles along with the height of 0.1, 1.2, 1.8 m of the spot S2 for three mesh densities are shown in Figure 6.4 (a) and (b). It can be seen that the predicted mean temperature gradient for the three meshes mentioned in Table 6.1 are incredibly fused with less than 0.5% difference between

the two finer meshes. Also, the predicted mean velocity along three heights at the spot S2 are compared for the three tested meshes, and the finer two meshes show small difference which is about 3%. Thus, the medium grid (16,045,809) was chosen based on the close results for the two finer grids (Chen, Moshfegh and Cehlin, 2013), see Figure 6.4.

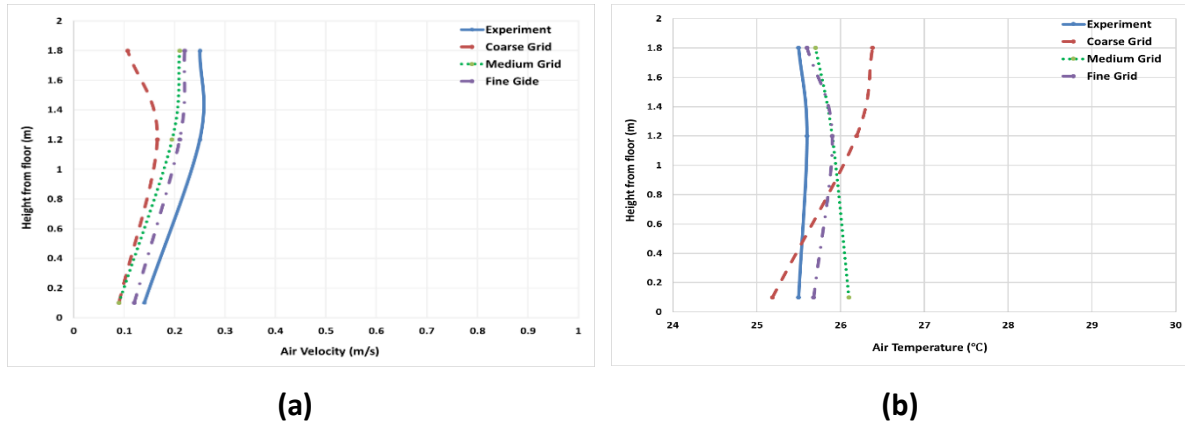


Figure 6.4 Comparisons between simulation results profiles along with the height of 0.1, 1.2, 1.8 m of the spot (S2) for three mesh densities (a) mean velocity and (b) mean temperature for summer 2016.

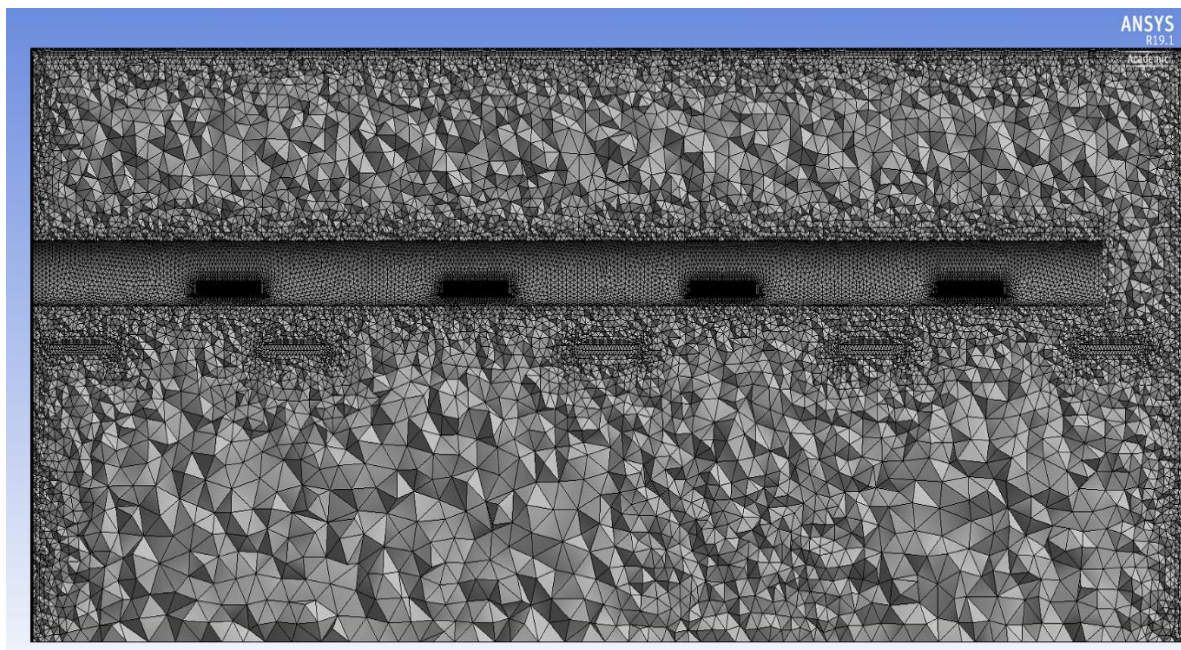


Figure 6.5 Mesh configuration in the computational domain for the summer 2016 model.

### Summer 2017 model

In the same way, the three meshes mentioned in Table 6.1 for summer 2017 were investigated for the independency of the CFD solution. Figure 6.6 (a) and (b) show the mean air velocity and temperature profiles comparison between simulation and experimental results profiles along the heights of 0.1, 1.2, 1.8m at spot S2 for three mesh densities. Based

on that, the medium grid (16,853,380) elements was chosen for summer 2017 CFD model. See Figure 6.7.

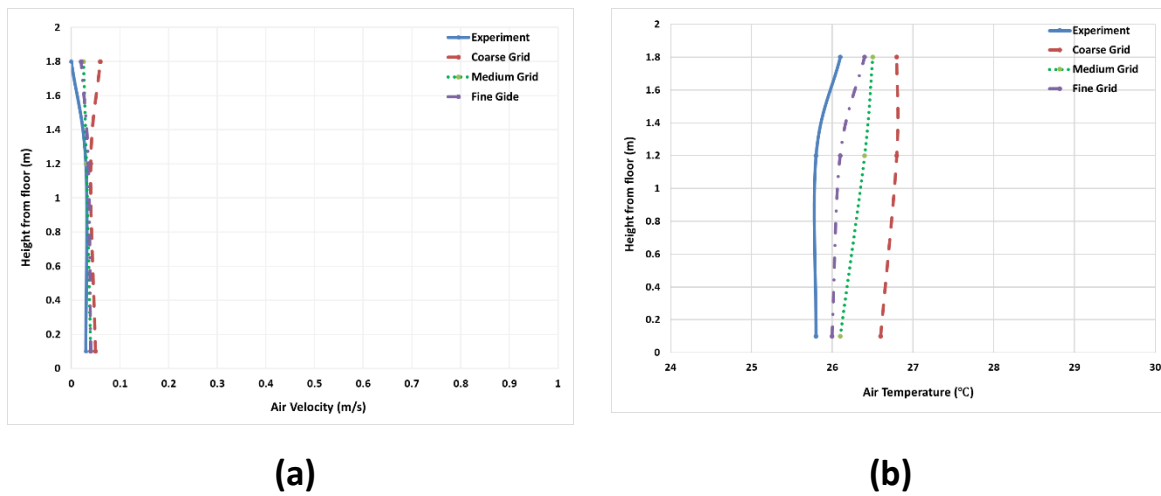


Figure 6.6 Comparison between simulation results profiles along the height of 0.1, 1.2, 1.8 m of the spot (S2) for three mesh densities (a) mean velocity and (b) mean temperature for summer 2017.

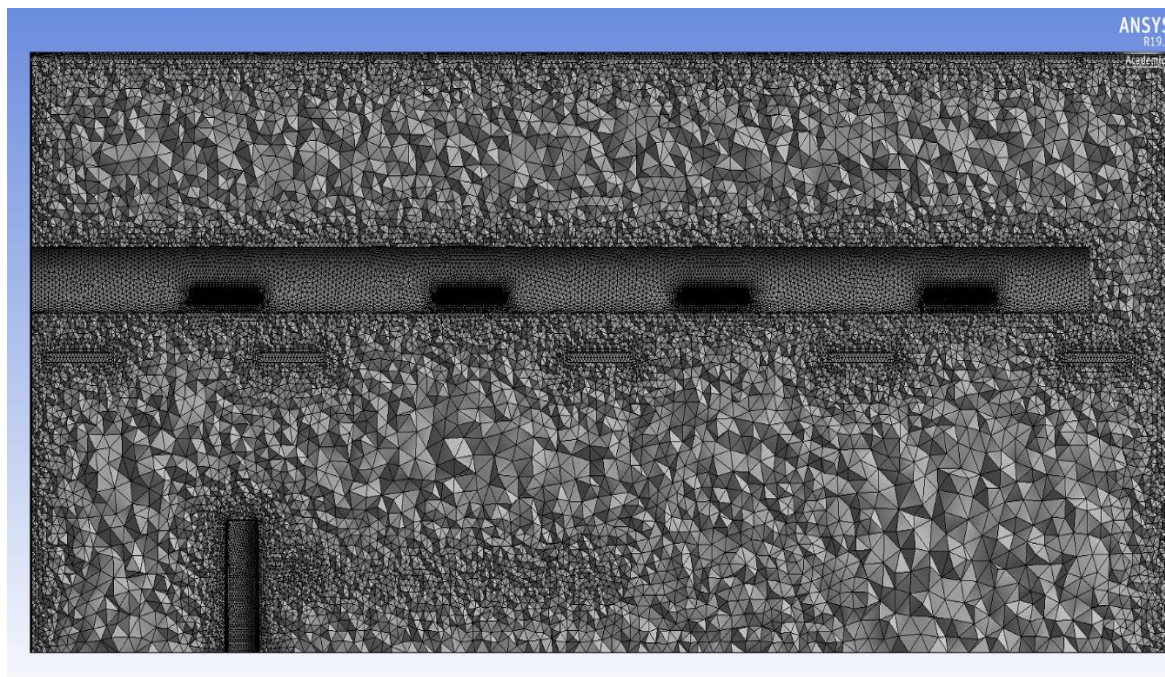


Figure 6.7 Mesh configuration in the computational domain for summer 2017 model.

### Summer 2018 model

To investigate the independency of the CFD solution for the mesh densities, the three different meshes mentioned in Table 6.1 for summer 2018 were used. Figure 6.8 shows the differences in the CO<sub>2</sub> concentration between simulation and experimental results for seven

different spots at a height of 1.2 m in the researchers' office. Based on these results, the medium grid (15,824,322) elements was chosen for 2018 CFD model, see Figure 6.9.

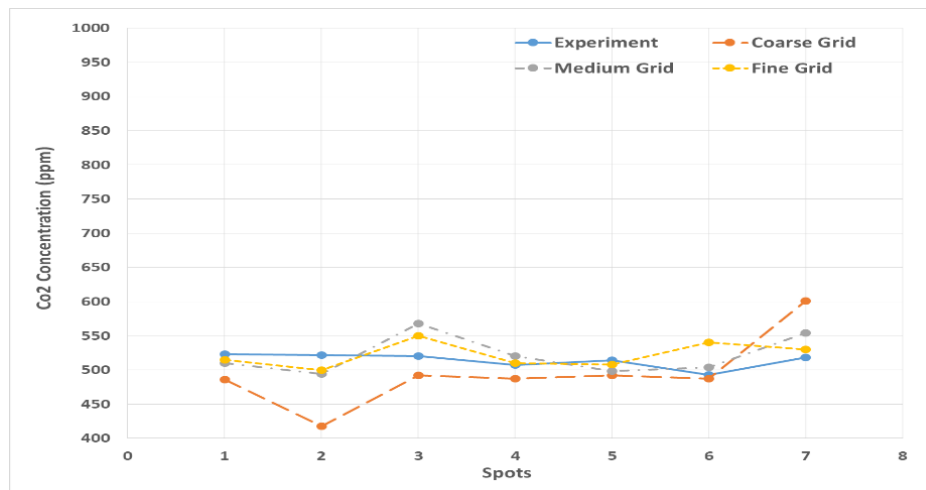


Figure 6.8 The measured and predicted CO<sub>2</sub> concentration using different numerical grids for summer 2018 model.

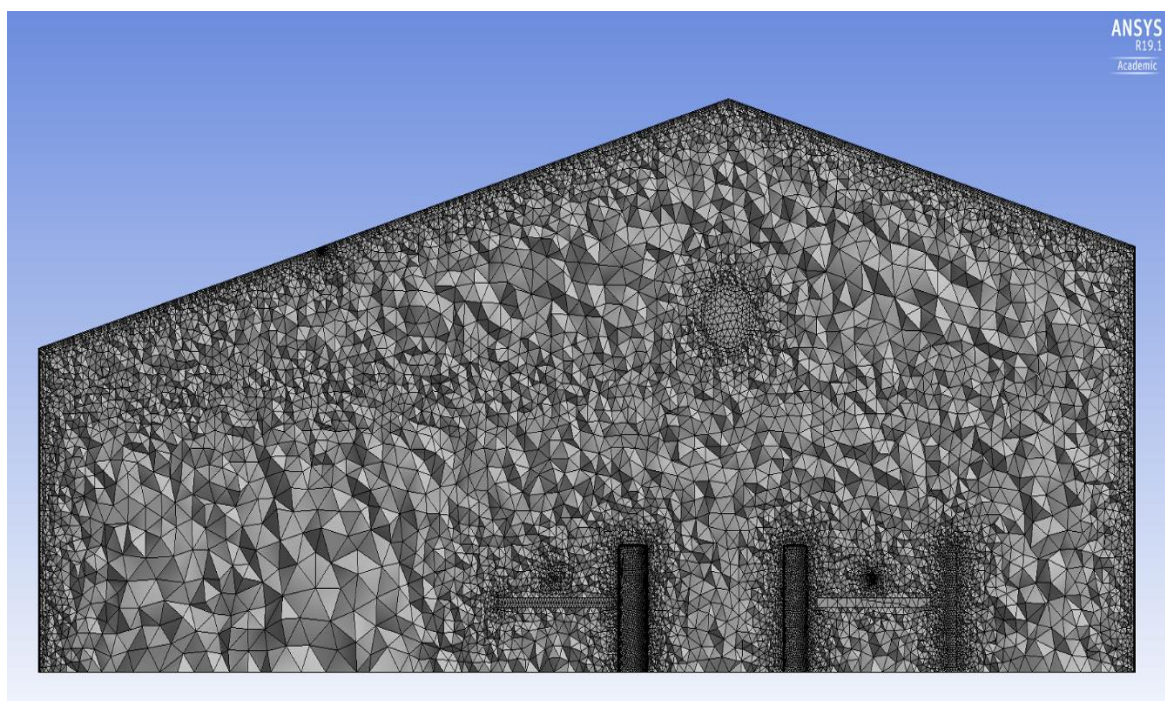


Figure 6.9 Mesh configuration in the computational domain for summer 2018 model

It is worth mentioning that the chosen grid for each summer has an element size of 0.01 m for the air inlets and outlet and 0.05 m for the other surfaces. Also, four inflation layers were employed near the walls, floor and internal heat gain surfaces, e.g. (occupants, computer and lighting) with a first element size of 5 mm and 30 mm for ceiling and a growth ratio of 1.2 to capture the effects of the boundary layer.

## 6.7 CFD EVALUATION WITH MEASUREMENTS

### For summer 2016

Four selected room locations S1, S4, S5 and S6 which are shown in Figure 4.4 were used in this analysis. Figure 6.10 (a) and (b) shows the comparisons of the mean air velocity and temperature profiles between the simulation results using the two turbulent models and experimental data at four different spots. Figure 6.10 (a) shows that both turbulence models, the RNG k- $\epsilon$ , and the SST k- $\omega$ , can predict the velocity distributing satisfactory when compared with the experimental results.

Nonetheless, the less satisfactory agreement with measurement was observed in the spot S5 at the height 1.2m. This is due to its location which is near to the one of the room doors. The predicted temperature profile is indicated in Figure 6.10 (b) in which model SST k- $\omega$  shows slightly better agreement with measurement than the RNG k- $\epsilon$  model. The high-temperature discrepancy between the prediction and measurement was up to 3.5°C in the spot S6 for RNG k- $\epsilon$  model probably due to its location near the sunny windows. Extra heat flux may be conveyed into the office and help to heat up the air around a spot S6.

The average relative percentage error between prediction and measurement across the four measured spots of the air velocity and air temperature with the RNG k- $\epsilon$  and SST k- $\omega$  models are shown in Table 6.4.

*Table 6.4 The average relative percentage error between prediction and measurement across the four measured spots of the air velocity and air temperature with the RNG k- $\epsilon$  and SST k- $\omega$  models*

	<b>Air velocity percentage error</b>	<b>Temperature percentage error</b>
<b>RNG k-<math>\epsilon</math></b>	3.5 %	4.6 %
<b>SST k-<math>\omega</math></b>	3.2 %	3.7 %

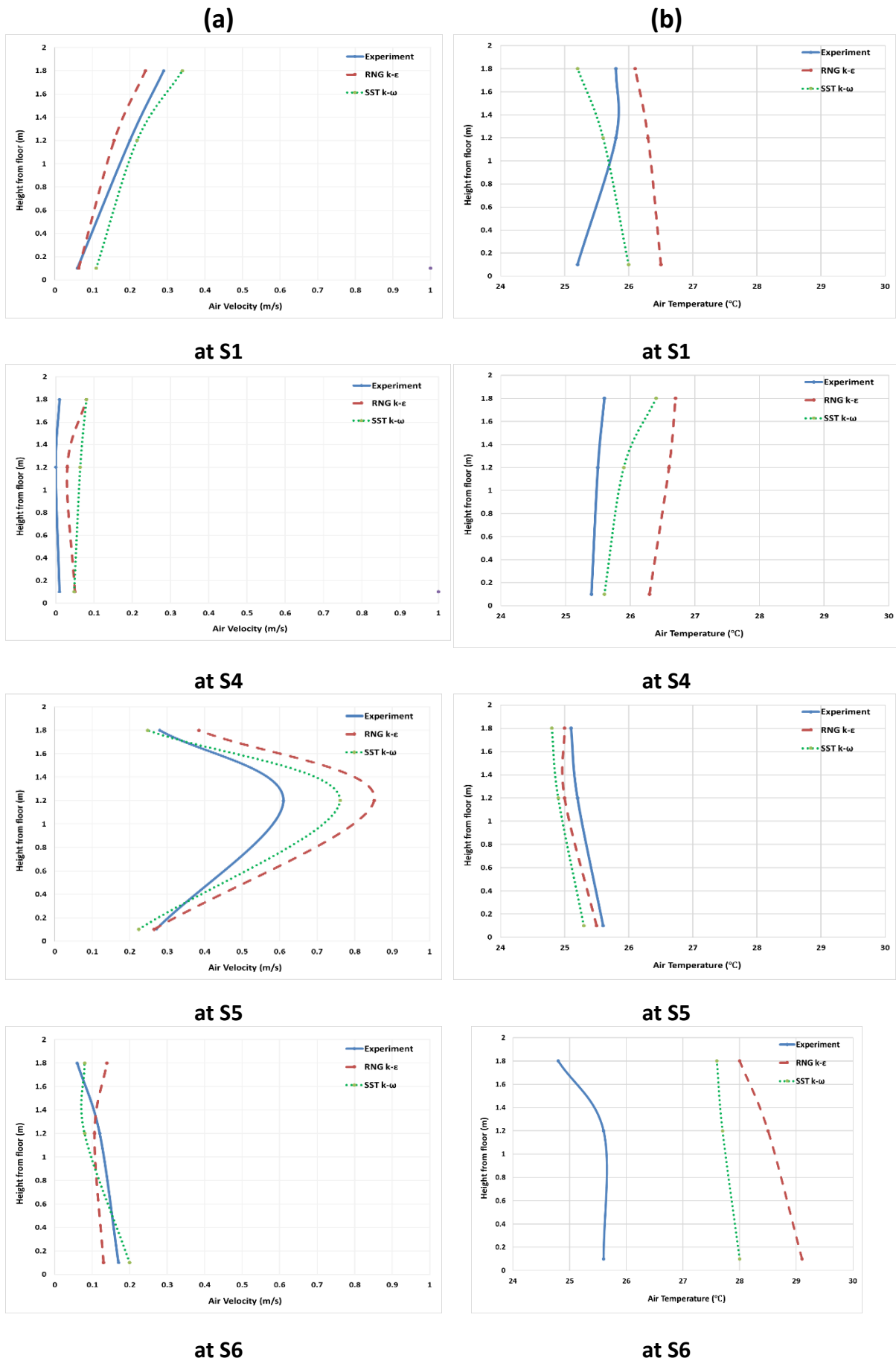


Figure 6.10 Comparisons between simulation results with measurements along three heights for spot (S1, S4, S5 and S6) (See figure 4.4): (a) mean velocity and (b) mean temperature for summer 2016.

Zhang et al. (2007) have quantified the turbulence model accuracy to four criteria; good, acceptable, marginal and poor. The relative percentage error between prediction and measurement at measured points was used in their study as a major criterion as shown in Table 6.5.

*Table 6.5 Model accuracy criteria*

<b>Model accuracy criteria</b>	<b>Error description</b>
<b>Good</b>	error < 10%
<b>Acceptable</b>	10% < error < 30%
<b>Marginal</b>	30% < error < 50%
<b>Poor</b>	error > 50%

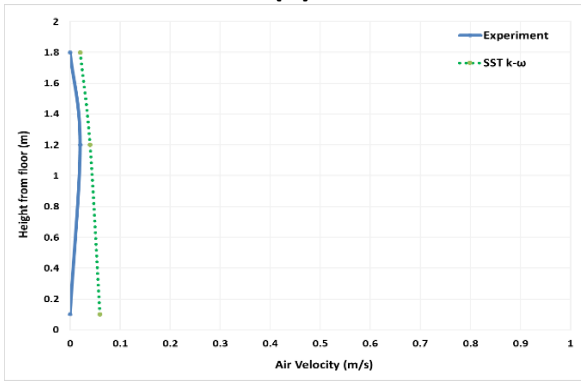
Therefore, RNG k- $\epsilon$  model was rated as good. According to the air velocity and air temperature relative percentage errors which were 3.5% and 4.6% respectively. Also, the SST k- $\omega$  model was rated as good according to the same errors which were 3.2% and 3.7% respectively.

To sum up, the prediction from SST k- $\omega$  shows better agreement with measurements in comparison with RNG k- $\epsilon$  model. Hence, the SST k- $\omega$  model was used in the present study to predict the turbulent features of air flow within the researchers' office.

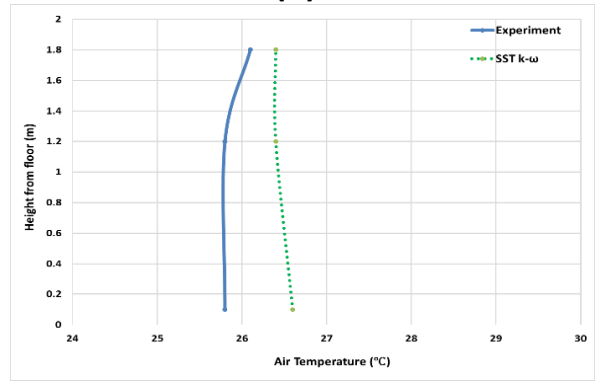
#### **For summer 2017**

As before, evaluation with the measurements was carried out using the same four selected room locations S1, S4, S5, S6 which are shown in Figure 4.4. Figure 6.11 (a) and (b) show the comparisons of the mean air velocity and temperature profiles between simulation results using the SST k- $\omega$  turbulent model and experimental data at the four different spots. Figure 6.11 (a) shows SST k- $\omega$  model is able to predict the velocity distributing satisfactory when compared with experimental results at all the four spots. Figure 6.11 (b) shows the predicted temperature profile where the high-temperature discrepancy between the prediction and measurement was up to 1.3°C in spot S5.

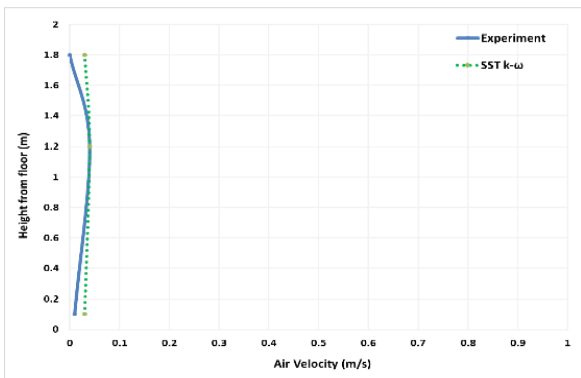
(a)



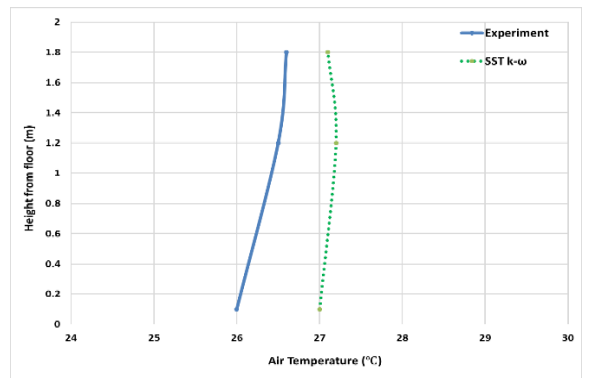
(b)



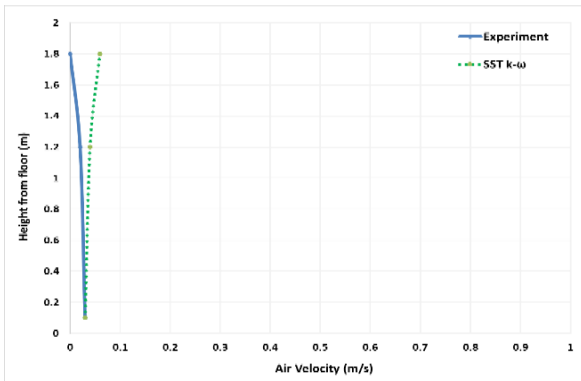
at S1



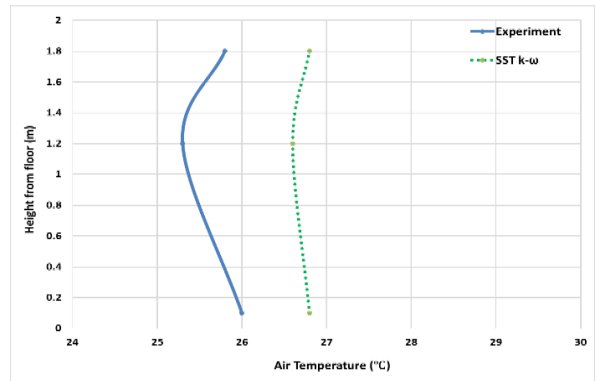
at S1



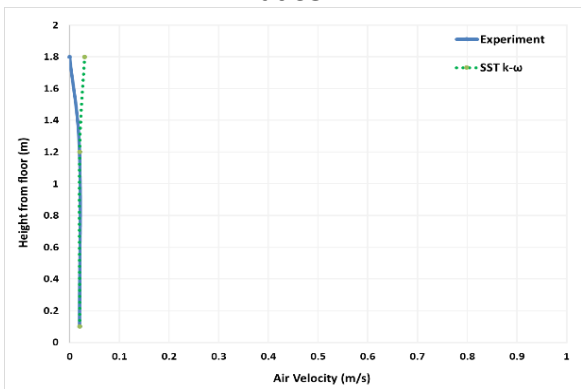
at S4



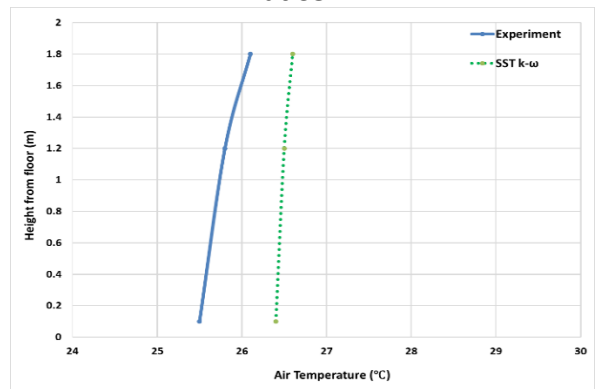
at S4



at S5



at S5



at S6

at S6

Figure 6.11 Comparison between simulation results with measurements along three heights for spots (S1, S4, S5, and S6) (See figure 4.4): (a) mean velocity and (b) mean temperature for summer 2017.

### For summer 2018

Seven selected room locations S1, S2, S3, S4, S5, S6, S7 as shown in Figure 4.4 were used to evaluate the CO<sub>2</sub> CFD results with measurements. Figure 6.12 shows a comparison between the predicted and measured CO<sub>2</sub> concentration using the SST k- $\omega$  turbulent model at the seven spots. It is seen that measured and predicted values of the CO<sub>2</sub> concentration at spots S1, S2, S4, S5 and S6 were in a very close agreement. The highest CO<sub>2</sub> concentration discrepancy was 48 ppm and 36 ppm in spots S3 and S7 respectively.

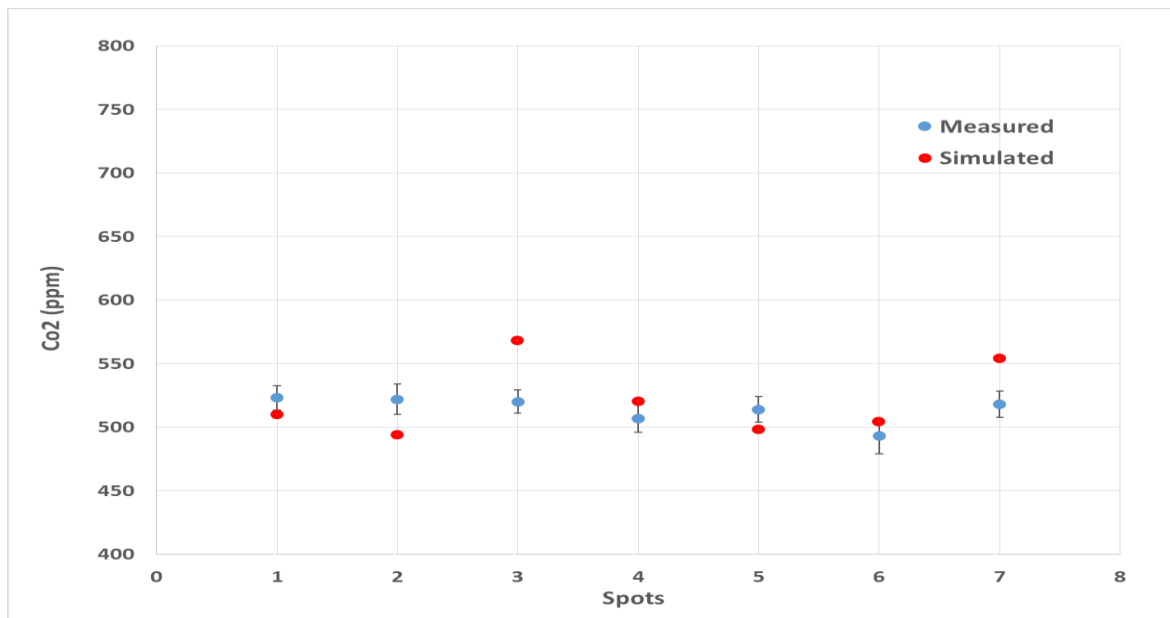


Figure 6.12 Comparison between the predicted and measured CO<sub>2</sub> concentration at the six selected room locations in the occupied zone for summer 2018

The average relative percentage errors between the prediction and the measurement of the CO<sub>2</sub> concentration across the six spots was 5.5% which confirms the suitability of the SST k- $\omega$  model (Zhang *et al.*, 2007).

It is worth mentioning that the discrepancy between the measured and predicted values which was introduced in this section could be due to the measuring equipment uncertainty and the disturbance of the air flow at these locations of the researchers' office due to the movement of some of the occupants.

## 6.8 PREDICTED RESULTS OF AIR TEMPERATURES, AIR VELOCITIES AND CO<sub>2</sub> CONCENTRATION

For summer 2016

To understand the air temperature, air velocity and distribution in the researchers' office, four planes were generated as shown in Figure 6.13. Three horizontal planes were created for heights of  $y=0.1\text{m}$  (ankle level),  $y=1.2\text{m}$  (seating head level) and  $y=1.8\text{m}$  (standing head level) while one lateral plane was located in the middle of the office at  $z=6.6\text{m}$ .

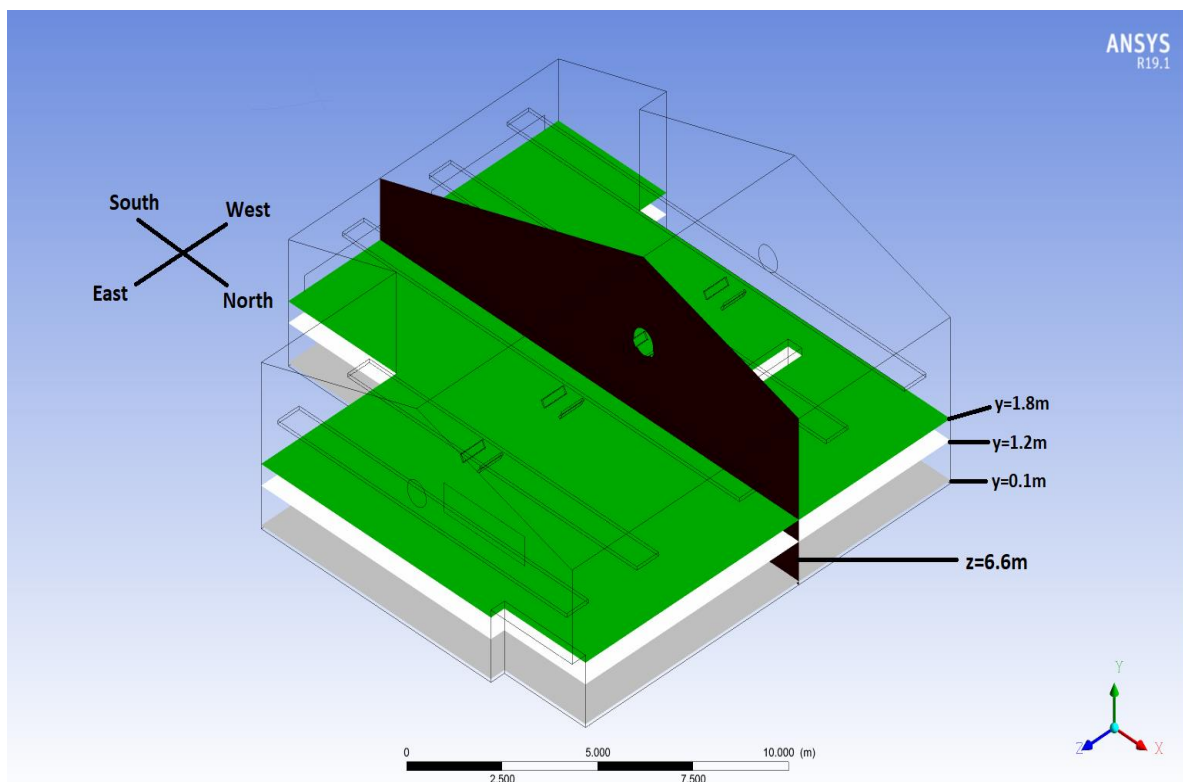


Figure 6.13 Researchers' office plans location

The qualitative numerical results indicating the temperature contours for the lateral plane at  $z=6.6\text{m}$  is shown in Figure 6.14, where an apparent temperature stratification is observed. The cold air supply gets warmer while it spreads along the office. It can be observed that the temperature tends to rise continuously along the windows wall. A convective plan is created when the air approaches the solar heated wall. It should be noted that the mean temperature at height 4m was nearly the same as the measured mean temperature ( $26^{\circ}\text{C}$ ).

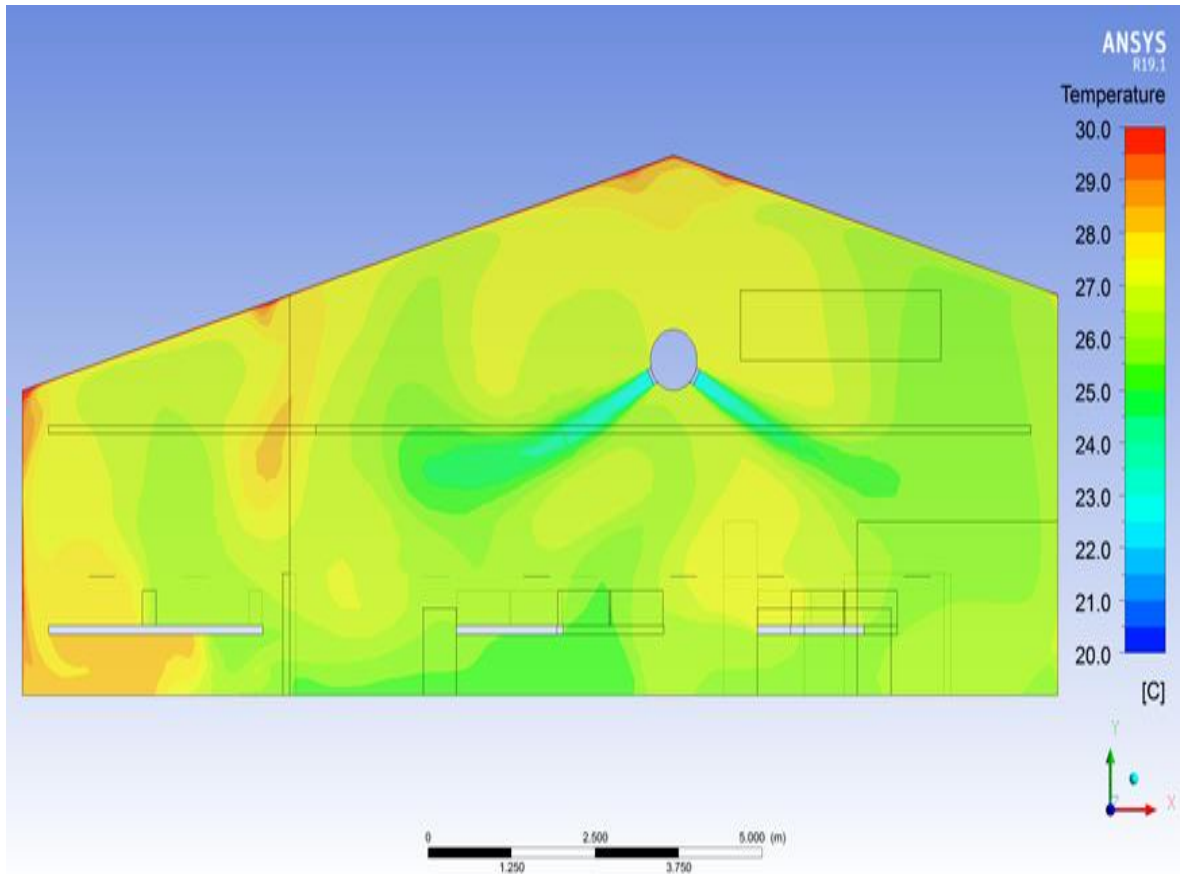
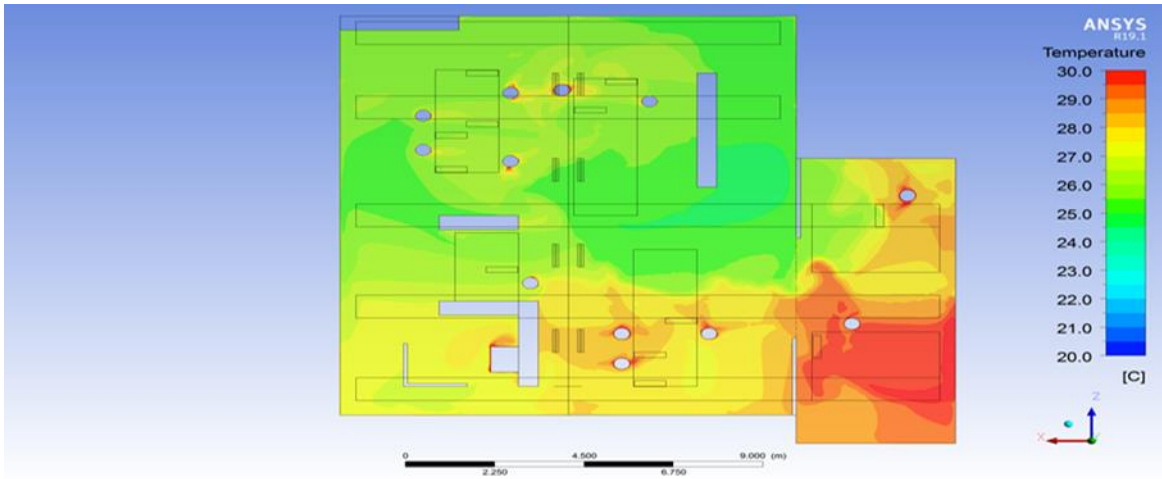


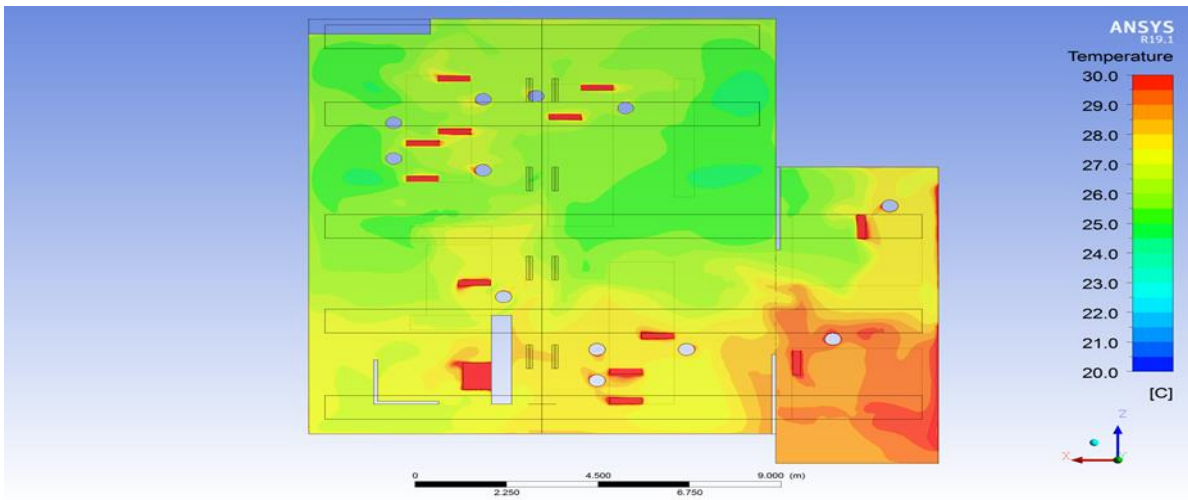
Figure 6.14 Temperature contour at the local plane ( $z=6.6\text{m}$ ) for summer 2016.

Figure 6.15 (a), (b) and (c) show the air temperature contours at three horizontal planes for heights of  $y=0.1\text{m}$ ,  $y=1.2\text{m}$  and  $y=1.8\text{m}$  respectively. It is clear that the predicted air temperatures of the south east part of the three levels is high due to its location near the solar heated window and due to the partition which may cause a bad air recirculation in that part.

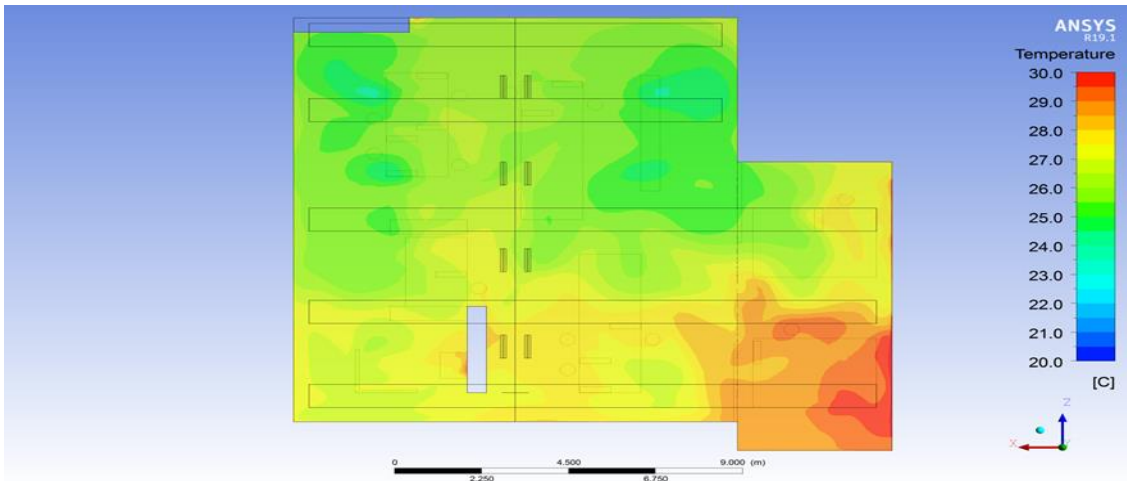
Figure 6.16 (a) and (b) display the predicted velocity vector and velocity contour for the lateral plane at  $z=6.6\text{m}$ . A cross-recirculation was created in different parts of the occupied zone of the office due to the partitions and furniture. The windows' thermal plane generated strong buoyancy force which moved the air up to the ceiling. On the other side (north side) of the office, the main flow is merged with the downward generated flows from the supply duct which increased the momentum of the air penetrating into the office.



(a) Temperature contour at the height of 0.1m from the floor

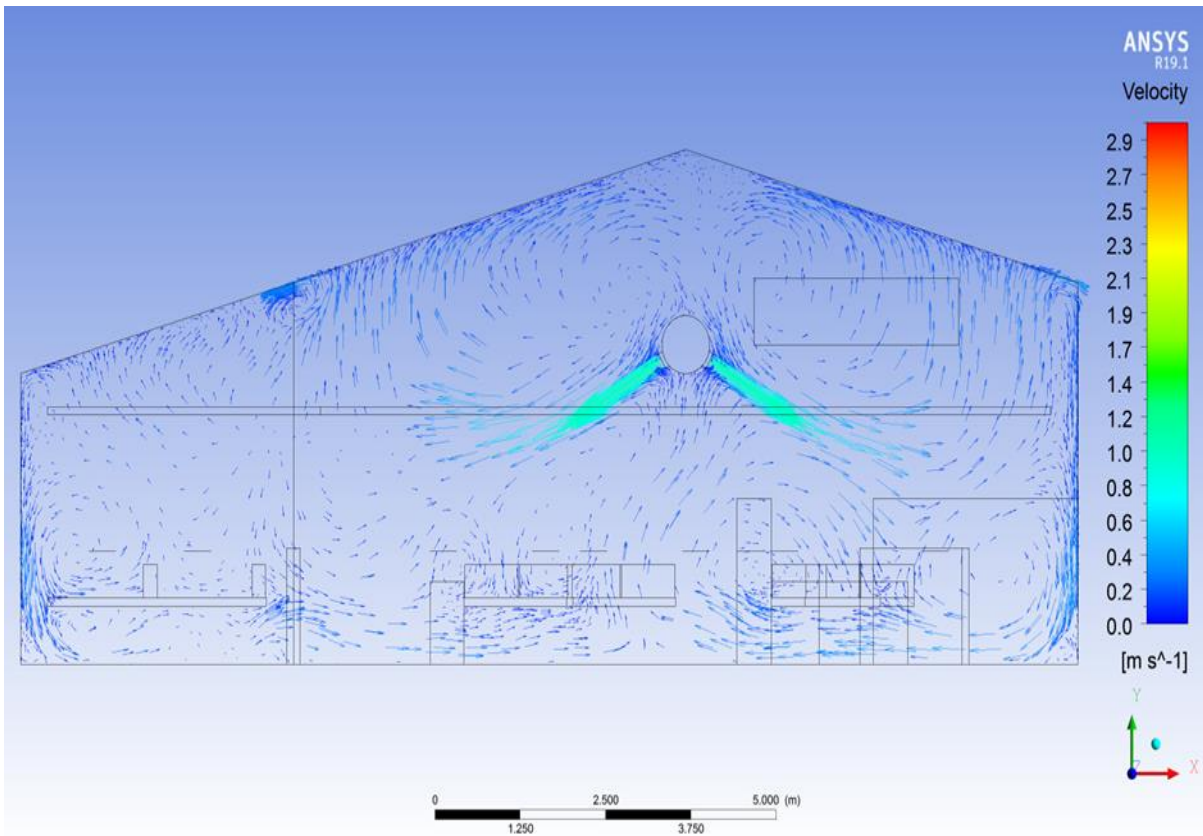


(b) Temperature contour at the height of 1.2m from the floor

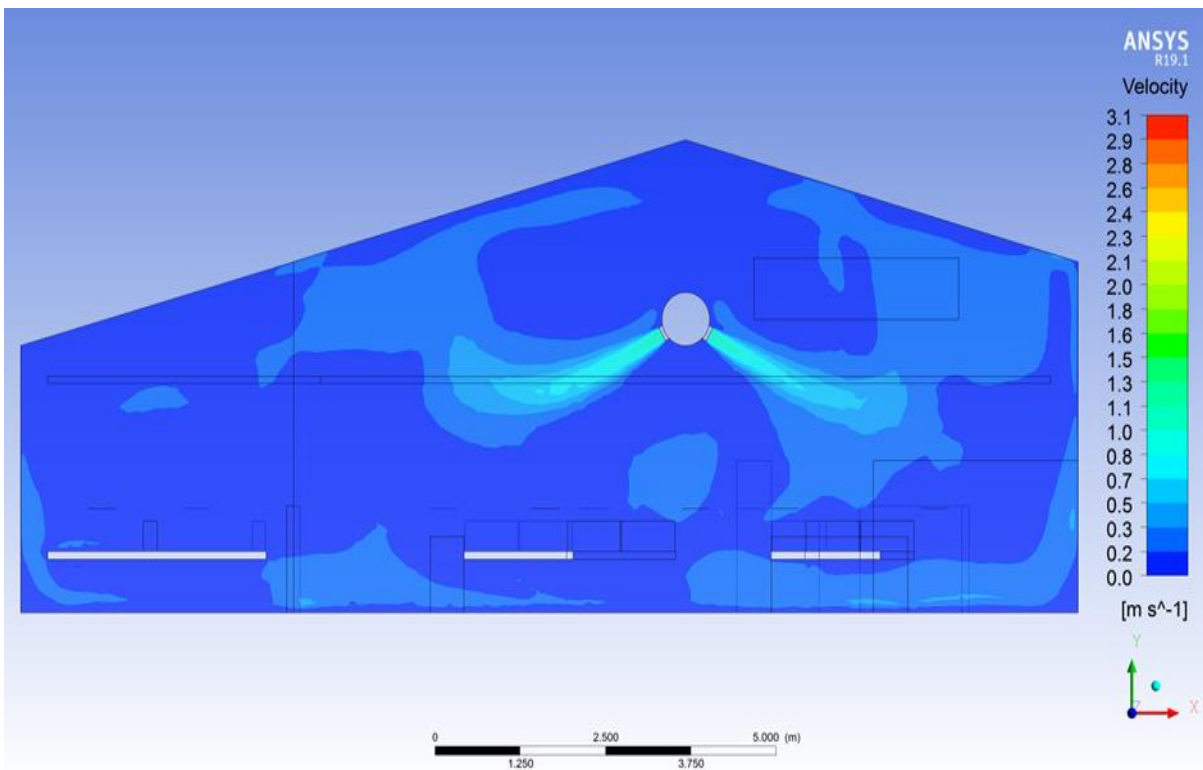


(c) Temperature contour at the height of 1.8m from the floor

Figure 6.15 Temperatures contours at different height (a)  $y=0.1m$ , (b)  $y=1.2m$  and (c)  $y=1.8m$  for summer 2016.



(a) Velocity vector on a plane located in the middle of the researchers' office for summer 2016



(b) Velocity contour on a plane located in the middle of the researchers' office for summer 2016

Figure 6.16 (a) velocity vectors (b) velocity contour on the lateral plane ( $z=6.6\text{m}$ ) for summer 2016  
**For summer 2017**

As before, three horizontal and one lateral plane were created in the simulated office to understand the variation of air temperature and air velocity as shown in Figure 6.13.

The numerical results indicating the air temperature contours on the lateral plane at  $z=6.6\text{m}$  is shown in Figure 6.17. The thermal environment created within the office was almost uniform and the highest temperatures were located around one of the computers. The air temperature contours at  $y=0.1\text{m}$ ,  $y=1.2\text{m}$  and  $y=1.8\text{m}$  planes are shown in Figure 6.18 (a), (b) and (c) respectively. It is clear that the predicted air temperatures at these levels were almost the same and were in a range of  $26.4$  to  $27.2^\circ\text{C}$ . Apart from that, high temperatures were located around the heat sources (i.e. occupants, computers and photocopier).

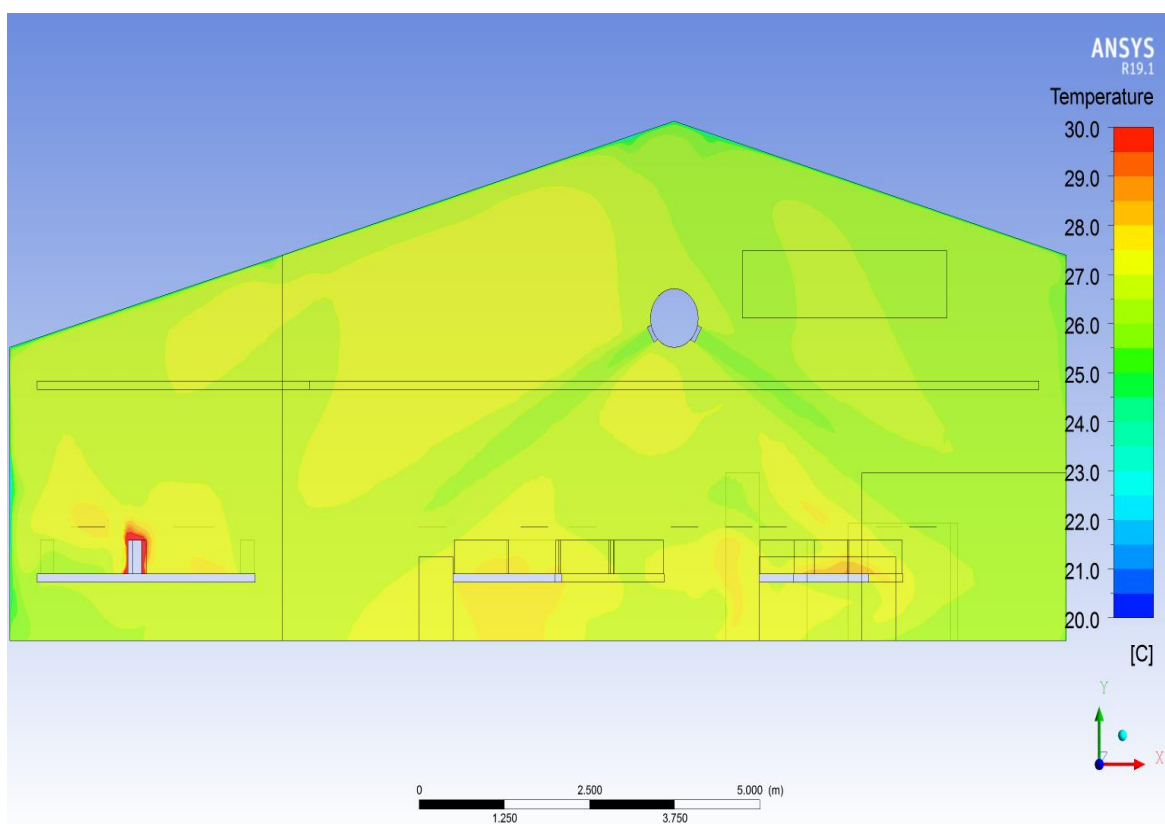
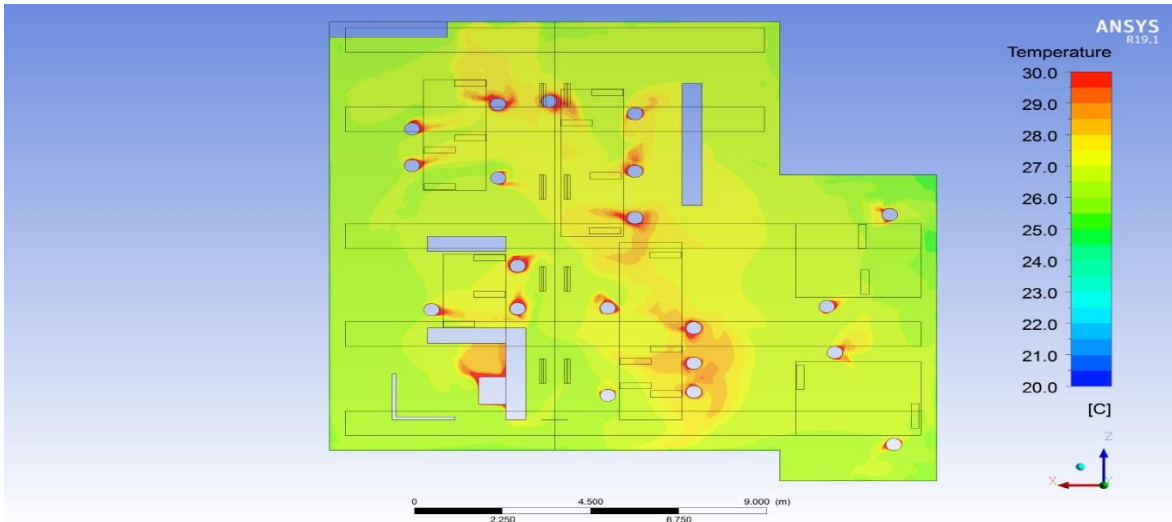
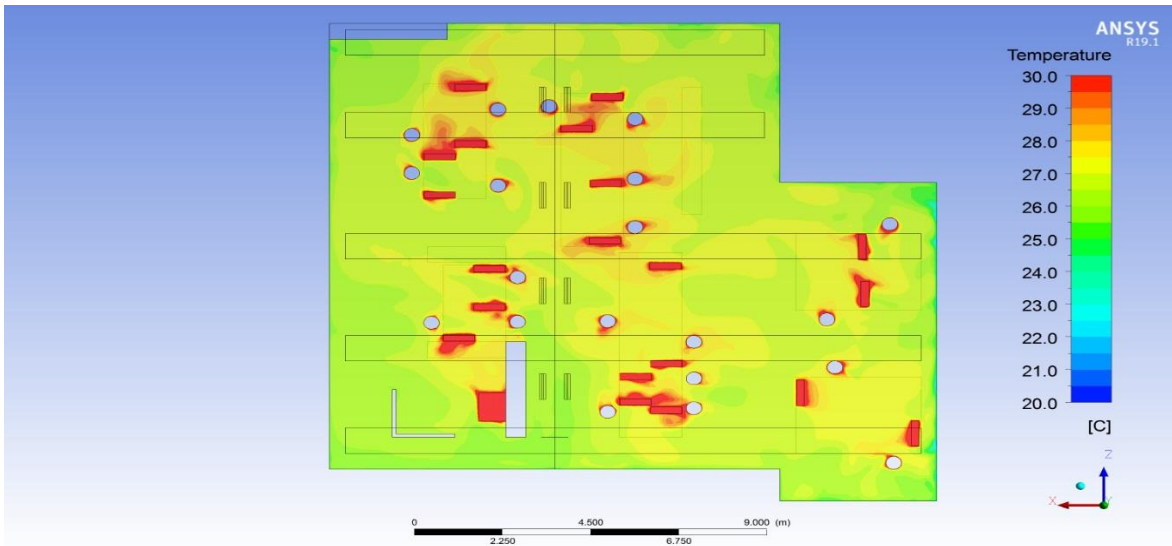


*Figure 6.17 Temperature contour at the lateral plane ( $z=6.6\text{m}$ ) for summer 2017.*

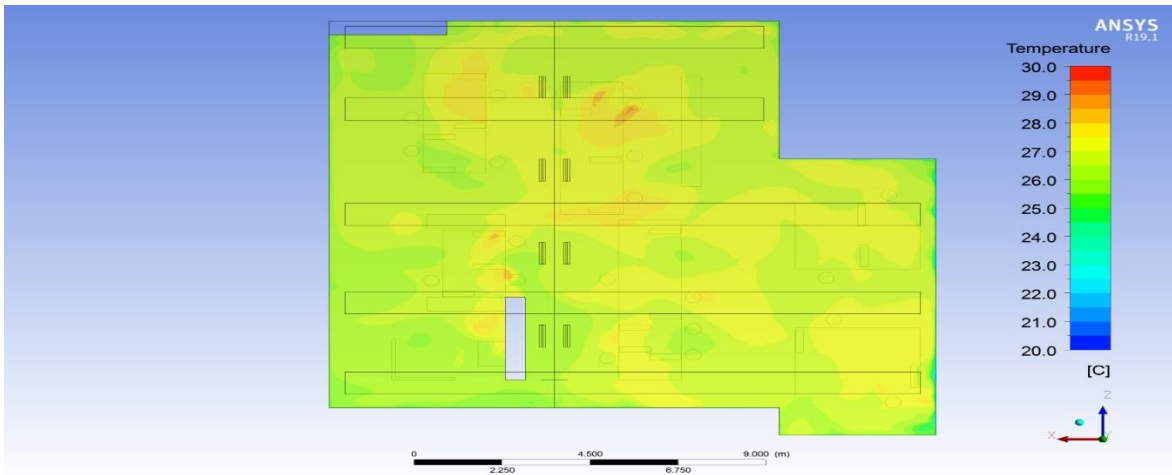
Figure 6.19 (a) and (b) display the predicted velocity vector and velocity contour for the lateral plane at  $z=6.6\text{m}$ . Very low air velocities were predicted within the occupied zone which were in the range of  $0$  to  $0.2\text{ m/s}$ .



(a) Temperature contour at the height of 0.1m from the floor

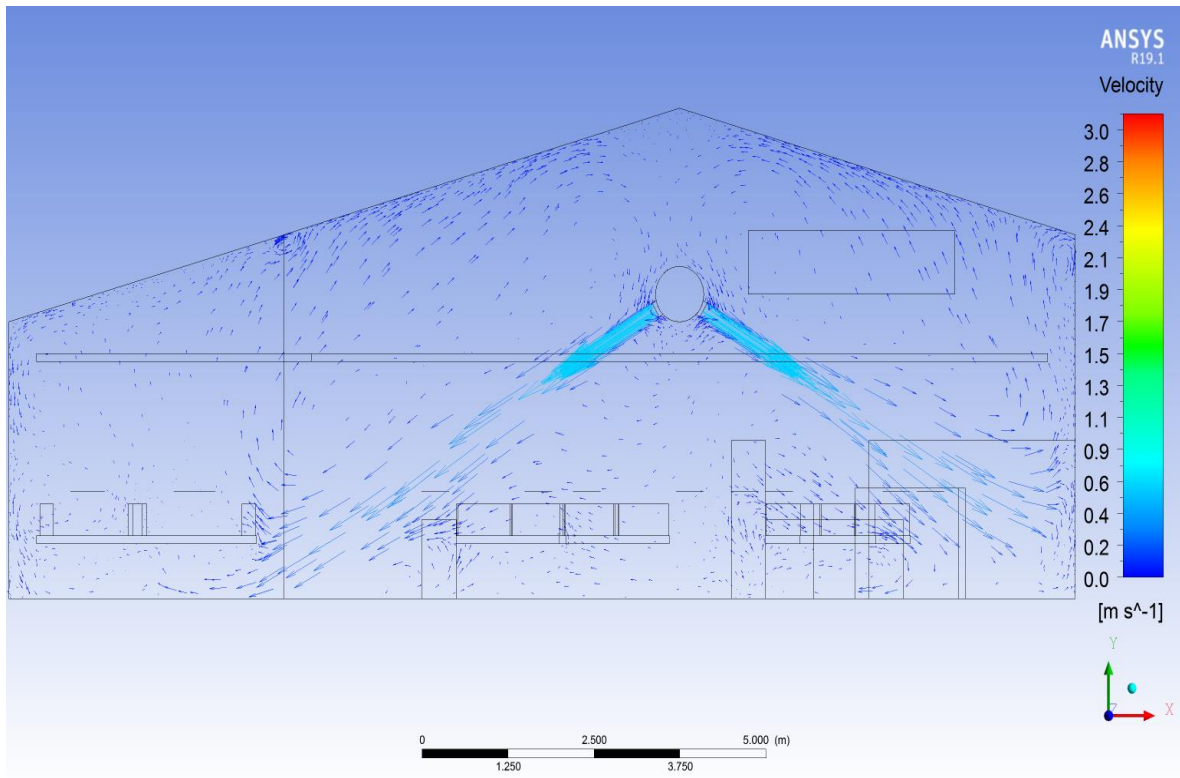


(b) Temperature contour at the height of 1.2m from the floor

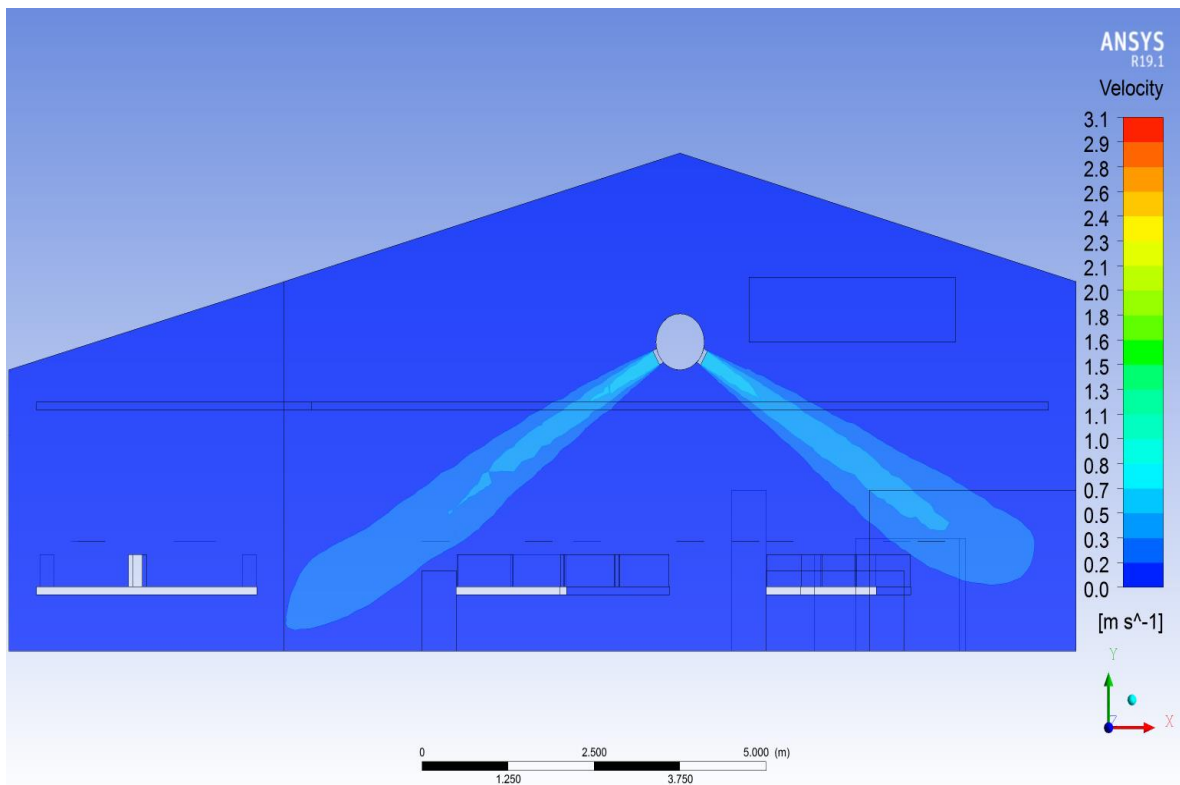


(c) Temperature contour at the height of 1.8m from the floor

Figure 6.18 Temperature contours at different height (a)  $y=0.1m$ , (b)  $y=1.2m$  and (c)  $y=1.8m$  for summer 2017.



**(a)** Velocity vector on a plane located in the middle of the researchers' office for summer 2017



**(b)** Velocity contour on a plane located in the middle of the researchers' office for summer 2017

Figure 6.19 (a) velocity vectors (b) velocity contour on the lateral plane ( $z=6.6\text{m}$ ) for summer 2017.

**For summer 2018**

One lateral plane was located in the middle of the office at  $z=6.6\text{m}$  to assess the  $\text{CO}_2$  concentration distribution in the researchers' office as shown in Figure 6.20.

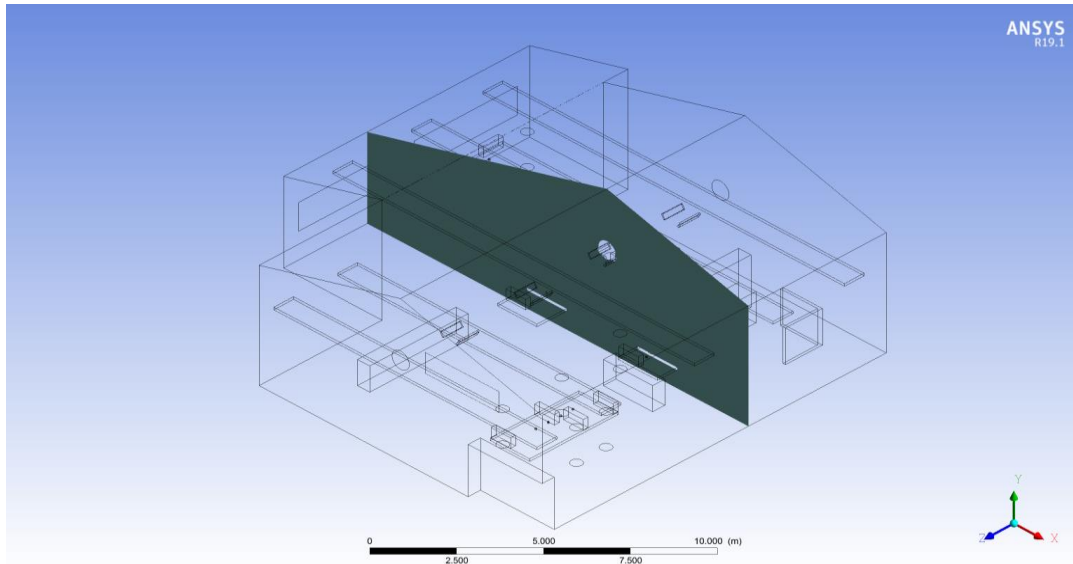


*Figure 6.20 Researchers' office plane locations for summer 2018*

Figure 6.21 shows the predicted  $\text{CO}_2$  concentrations in the lateral plane at  $z=6.6\text{m}$  where it was generally uniform between 500 to 580ppm; the maximum  $\text{CO}_2$  concentration was located near the source of generation in the occupied zone.

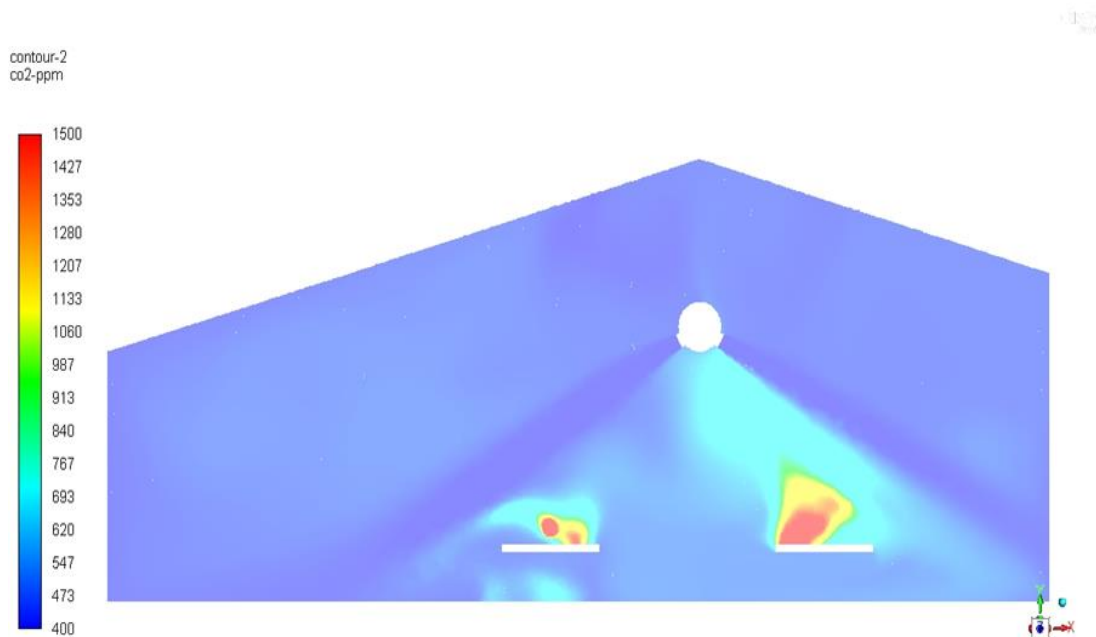


*Figure 6.21 The  $\text{CO}_2$  concentrations on the lateral plane at  $z=6.6\text{m}$*

## 6.9 CHAPTER SUMMARY

In this chapter, the CFD simulation of the air flow and temperature variation for the large space case-study building was presented. The CFD modelling and evaluation stage was carried out in these phases simultaneously for each of the measurement phases; the first was performed in summer 2016, the second in summer 2017 and the third in summer 2018. Three different numerical grids were tried for all the three models with the aim of testing for grid independency and selecting an optimum one which gave converged and accurate results. A cylinder of length 1.4 m and a diameter of 0.4 was used to represent the body of the occupant. The measured air velocity, temperature, CO<sub>2</sub> concentration of the air diffusers, surfaces temperature of walls, ceiling, personal computers and lightings were used as the boundary conditions for the CFD simulations. The predicted air temperature, air velocity and CO<sub>2</sub> concentration distribution into the office building were presented and discussed.

# 7 CHAPTER SEVEN: CFD MODELLING STUDIES OF DIFFERENT AIR DISTRIBUTION SYSTEMS

---

## 7.1 INTRODUCTION

This chapter presents the last stage of the research work which is the parametric studies with performance comparisons in the large space case-study building, CSEF. Since the developed 3-D CFD modelling tool provided good results in comparison with measurements for summers of 2016, 2017 and 2018, the models were used to carry out further CFD simulations to evaluate the performance of two different air distribution systems. These are (a) Impinging Jet Ventilation and (b) Mixing Ventilation systems. More details of the IJV and MV are included in section 2.2.

The evaluation was carried out using the Air Distribution Index (ADI) which combines several parameters such as overall ventilation effectiveness for removing pollutants and for temperature distribution, percentage of dissatisfied for air quality and predicted percentage of dissatisfied. More details of the Air Distribution Index, are given in section 2.5.

Section 7.2 presents the different test conditions which were considered for this study. Section 7.3 shows the results and discussion for these conditions.

## 7.2 TEST CONDITIONS

### 7.2.1 Test Condition Set-up

The 3-D CFD large space model for the researchers' office in the CSEF building was used in this study where different test conditions were considered for two occupancy capacity loads; full and half occupancy for summer and winter conditions. The area for the office is 201 m<sup>2</sup> and according to the Workplace Health, Safety and Welfare Regulations 1992 (Commission, 1992), 3.7 m<sup>2</sup> of a space per person should be taken as minimum in an office, where the ceiling is 3m high or higher. Thus, 5m<sup>2</sup>, was allocated as a researcher's work area, taking into the account space for filing, storage, copiers, and walking space throughout the office. Based on that, the office was modelled to have 40 and 20 researchers as a full and half occupancy loads

along with their computers respectively. The geometry of the office, lighting, photocopier, occupants and computers were kept the same as those presented in section 6.2 see Figure 7.1 and Figure 7.2.

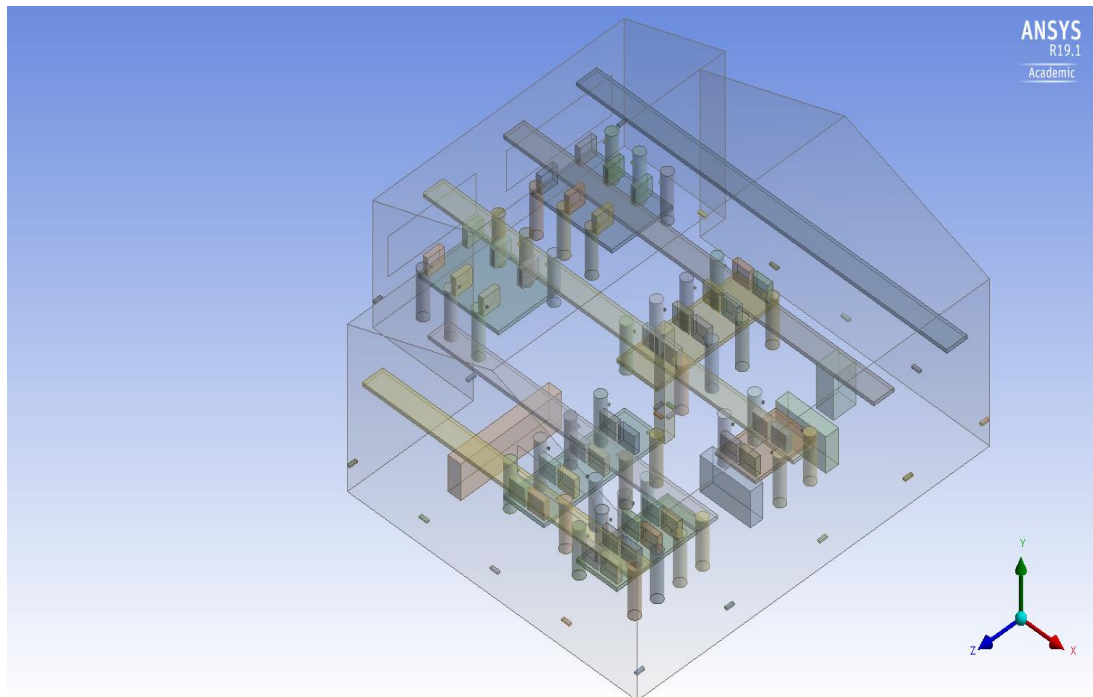


*Figure 7.1 CFD Model of the office with full occupancy*

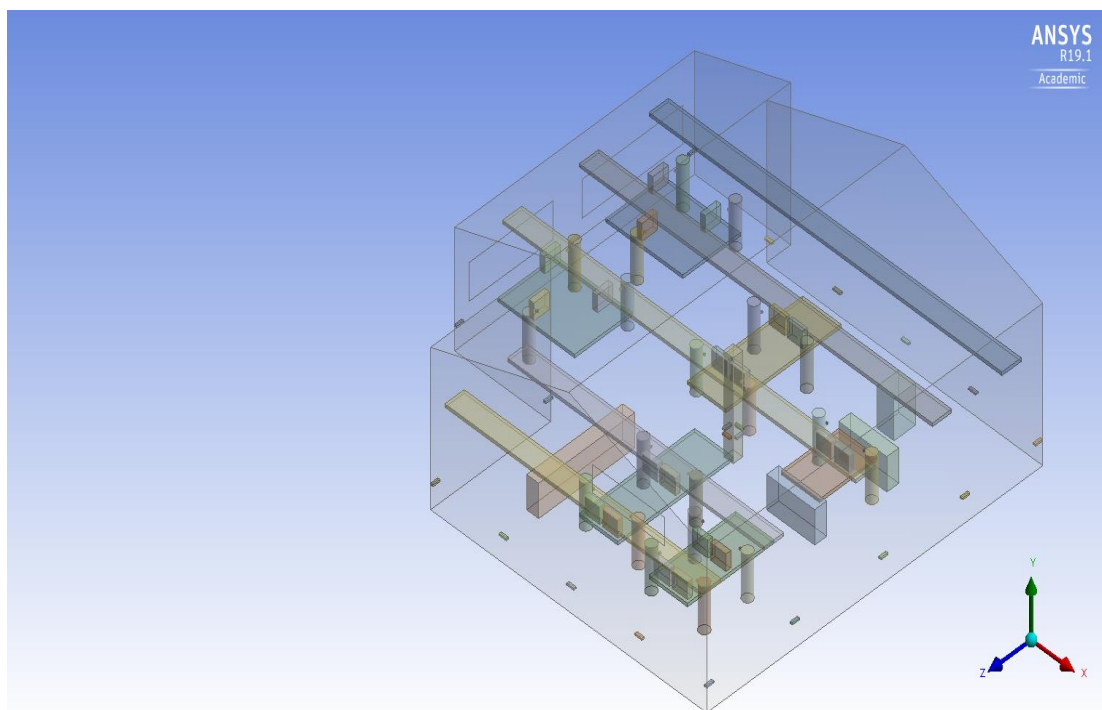


*Figure 7.2 CFD model of the office with half occupancy*

## 7.2.2 Supply Air Flow Rate

The required supply air flow rates for the modelled office of full and half occupancy were calculated from the following equation (Tymkow *et al.*, 2013; BS EN 16798-3, 2017):

$$\dot{m} = \frac{\dot{q}}{c_p(t_e - t_\infty)} \quad (7.1)$$

where  $\dot{q}$  is the thermal load (W),  $\dot{m}$  is the mass rate of air flow (kg/s),  $c_p$  is the specific heat of air (J/kg.K),  $t_e$  is the air temperature of air exhaust (°C) and  $t_\infty$  is the air temperature of air supply (°C).

To use the above equation, the  $\dot{q}$  can be calculated using HAP 4.9 which is a microcomputer program developed by Carrier Corporation (Carrier, 2010). In HAP 4.9 program, the following design assumptions were used as shown in table 7.1.

Table 7.1 Design assumptions for the calculating of the office cooling load for full and half occupancy

		Details
<b>location</b>		London-Heathrow, United Kingdom
<b>Calculation months</b>		June, July, August
<b>Load occurs</b>		16:00 , 6/7/2017
<b>Design supply temperature</b>		20°C
<b>Floor</b>		201m <sup>2</sup> , q=0 W/m <sup>2</sup>
<b>Windows</b>		8 m <sup>2</sup> , U-value=3.079 W/m <sup>2</sup> K
<b>Roof</b>		209 m <sup>2</sup> , U-value=1.613 W/m <sup>2</sup> K
<b>External wall</b>		27 m <sup>2</sup> , U-value=1.409 W/m <sup>2</sup> K
<b>Internal wall</b>		245 m <sup>2</sup> , q=0 W/m <sup>2</sup>
<b>Lighting</b>		11.2 W/m <sup>2</sup>
<b>Number occupants</b>	Full	40 ( 1.2 met, 0.5 clo, 10l/s)
	Half	20 ( 1.2 met, 0.5 clo, 10l/s)
<b>Personal computers</b>	Full	30 W/m <sup>2</sup>
	Half	15 W/m <sup>2</sup>

Therefore, from HAP the cooling loads for the modelled office were calculated to be 67.6 W/m<sup>2</sup> and 47.5 W/m<sup>2</sup> for full and half occupancy respectively. Consequently, the calculated supply air flow rates using equation 7.1 for full and half occupancy are presented in table 7.2.

Since HAP 4.9 program is used to estimate the thermal load for typical spaces and not for a large one, an initial CFD case with a full occupancy named case (A) was carried out to

determine new  $t_e$  which was substituted again in equation 7.1 to calculate the new supply air flow rate for the modelled office of full occupancy.

*Table 7.2 The calculated supply air flow rate for full and half occupancy from HAP*

Occupancy load	$c_p$ (J/kg.K)	$t_{\infty}$ (°C)	$t_e$ (°C)	$\dot{q}$ (W)	$\dot{m}$		
					(kg/s)	( $m^3$ /s)	(L/s)
Full	1.006	20.0	22.6	13591	5.20	4.33	4330
Half	1.006	20.0	22.5	9544	3.66	3.05	3050

Since no measurement was conducted for the case (A), the boundary conditions for the surface temperatures of all the office walls, ceiling, windows, occupants clothing, personal computers, lighting, and photocopier were the same as those used in the summer 2016 CFD case. However, the 8 supply air diffusers' temperature were set at 20°C and the velocity at 4.5 m/s which was calculated from the mass flow rate estimated by HAP in table 7.2. The geometry of the office, occupants, personal computers, lightning and photocopier, were kept the same as those in the summer 2016 CFD case. Also, the numerical grid used in case (A) was the same as that used previously for the CFD summer 2016 case (medium grid) as that grid gave the best results when compared with the measurements.

A similar procedure was used for another initial CFD case named case (B) which was carried out to predict the new supply air flow rate for the modelled office of half occupancy.

As a result, the predicted new supply air flow rate for the modelled office was 2.6  $m^3/s$  (65 l/s) and 1.7  $m^3/s$  (85 l/s) for full and half occupancy, respectively. For both the CFD cases (A and B) boundary conditions considered in this section are shown in Appendix II.

Therefore, for the mixing ventilation system, the number of the diffusers and their areas were kept the same as mentioned in section 6.2, i.e., 8 diffusers with 0.12 $m^2$  hence, the corresponding final supply velocities were 2.7 m/s for full occupancy and 1.8 m/s for half occupancy.

For the impinging jet ventilation system, the recommended supply velocity is in the range of 1.0—5.0 m/s towards the floor as recommended by Awbi (2003). Consequently, 21 IJV ducts each with a supply opening area of 0.03  $m^2$  and a distance of 0.7 m above the floor were uniformly distributed inside the office', as recommended by Awbi (2003). The first 17 of them were attached to the walls while the remaining 4 were attached to a column at the centre of

the office as shown in Figure 7.3. Thus, the corresponding final supply velocities were 4.1 m/s for full occupancy and 2.7 m/s for half occupancy.

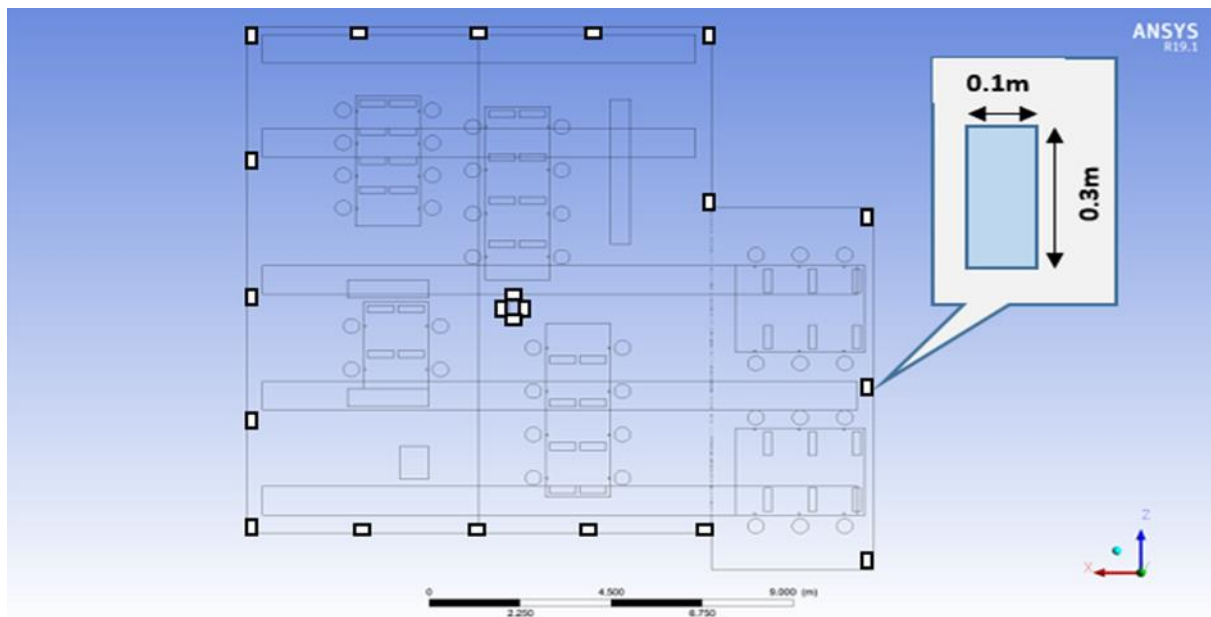


Figure 7.3 The Size and locations of the IJV inlet diffusers used in the CFD simulation

### 7.2.3 Recirculated Air

Due to the high demand of energy needed to cool and dehumidify the outdoor air, recirculating part of the conditioned air is recommended as an essential aspect of energy conservation strategies in many parts of the world (Fadeyi et al. 2009). Many HVAC designers use the recirculated air after mixing it with fresh air then supply it to space after it has been filtered and cooled. In this study, the recirculating air that was contaminated with CO<sub>2</sub> was considered on all cases presented in this section. To find the CO<sub>2</sub> concentration for recirculating air, the case (A) with the supply flow rate 2.6 m<sup>3</sup>/s was used for this study after adding CO<sub>2</sub> source terms in the model to represent the CO<sub>2</sub> production per person. More details of describing the personal CO<sub>2</sub> production in the CFD model, are given in section 6.5. At the start, only fresh air 10 L/s per person as recommended by ASHRAE standard 62.1 (American Society of Heating, 2016) with 400 ppm CO<sub>2</sub> concentration was used as a supply air flow rate. Then, the CO<sub>2</sub> concentration of the air at the exhaust was determined from the CFD output which was 808 ppm. Consequently, the CO<sub>2</sub> concentration of the new supply air which is a mixture of fresh and recirculated air was calculated to be 745 ppm as shown in Figure 7.4.

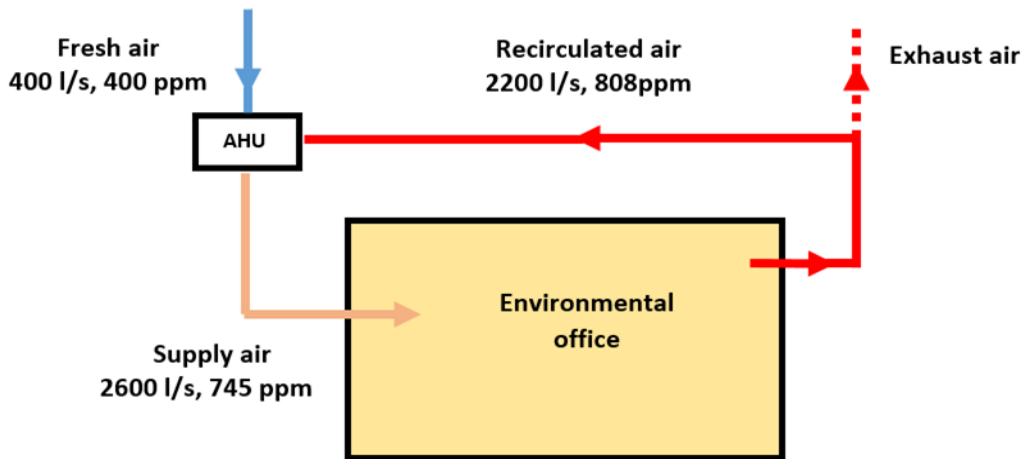


Figure 7.4 Recirculation system of the modelled office for full occupancy.

A similar procedure was used to find the CO<sub>2</sub> concentration for recirculated air for the modelled office with half occupancy. In this study, the case (B) with the supply flow rate 1.7 m<sup>3</sup>/s was used after adding the CO<sub>2</sub> source terms in the model to represent the CO<sub>2</sub> productions per person. As a result, the CO<sub>2</sub> concentration of the recirculated air was 686 ppm; whilst it was 652 ppm for the new supply air which is a mixture of fresh and recirculated air, as shown in Figure 7.5.

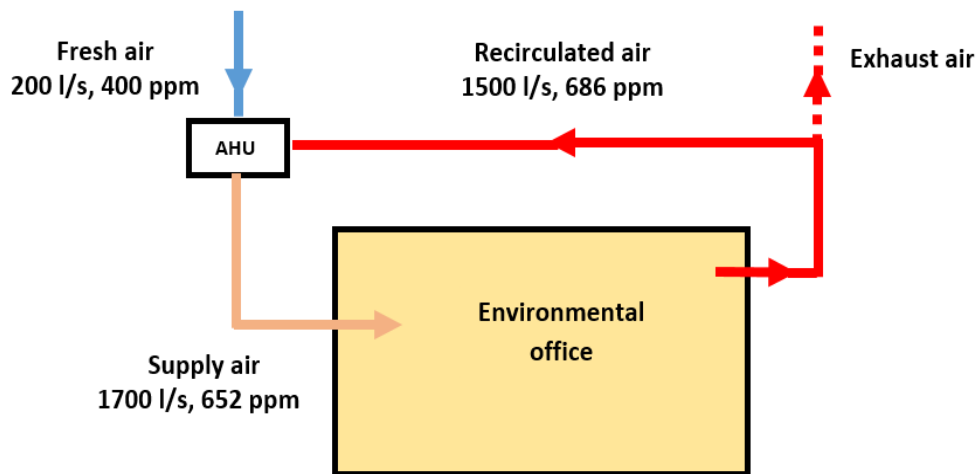


Figure 7.5 Recirculation system of the modelled office for half occupancy.

Table 7.3 summarises the CFD test conditions which were used to compare the performance of the systems MV and IJV. It is worth mentioning that according to BS EN 16798-1 (BSI, 2019), the recommended range of the mean design operative temperature for energy saving of open plan offices is 20 – 24 °C and 22 – 27 °C for heating and cooling seasons respectively. Moreover, a study by (Seppanen, Fisk and Lei, 2006) recommended that the highest

productivity in office environment is at temperature of around 22°C. Therefore, in this study the air supply temperatures presented in the table below were set by an iterative procedure to achieve a rather steady temperature condition of 22.3°C ± 0.4°C in the occupied zone of the office building for accurate comparisons.

*Table 7.3 The CFD cases used for the MV and IJV system performance comparison*

Case name		Case F-S		Case F-W		Case H-S		Case H-W	
Occupancy		Full		Full		Half		Half	
Condition		Summer		Winter		Summer		Winter	
Distribution system		MV	IJV	MV	IJV	MV	IJV	MV	IJV
Flow rate (m <sup>3</sup> /s)		2.6	2.6	2.6	2.6	1.7	1.7	1.7	1.7
Diffusers	Number	8	21	8	21	8	21	8	21
	Area (m <sup>2</sup> )	0.12	0.03	0.12	0.03	0.12	0.03	0.12	0.03
	Velocity ( m/s)	2.7	4.1	2.7	4.1	1.8	2.7	1.8	2.7
	Temperature (°C)	18	19	20	20	19	20	21	21
	CO <sub>2</sub> (ppm)	745	745	745	745	652	652	652	652

## 7.3 CFD RESULTS AND DISCUSSION

### 7.3.1 Full Occupancy Load for Summer Condition (Case F-S)

#### 7.3.1.1 Boundary Conditions

Since only CFD simulations were examined in this section and no experimental measurements were conducted, the boundary conditions for the surfaces temperature of all the office walls, ceiling, windows, occupants clothing, personal computers, lighting and photocopier were the same as those used in the CFD case for summer 2016. However, the air supply velocities and temperatures were calculated to be 2.7 m/s and 18°C for the MV system and 4.1 m/s and 19°C for the IJV system respectively as it was described in the previous section. Table 7.4 summarised the boundary conditions of Case F-S for both MV and IJV systems.

The geometry of the office, occupants, personal computers, lighting, photocopier used in this section for the MV and IJV systems are the same as those used in the summer 2016 CFD case.

However, the geometries of the supply diffusers for the IJV systems used in the Fluent case are illustrated in Figure 7.3 while for the MV system are the same as those used in the summer 2016 CFD case.

Table 7.4 Boundary conditions of Case F-S for the MV and IJV systems

	Details	Mixing System	Impinging Jet System
Supply air diffusers	Flow rate	2.6 m <sup>3</sup> /s	2.6 m <sup>3</sup> /s
	Number	8	21
	Area	0.12 m <sup>2</sup>	0.03 m <sup>2</sup>
	Velocity	2.7 m/s	4.1 m/s
	Temperature	18°C	19°C
	CO <sub>2</sub> concentration	745 ppm	745 ppm
Ceiling surface temperature		35°C	35°C
Internal walls surface temperature		28°C	28°C
External wall surface temperature		29°C	29°C
Floor heat flux		0 W/m <sup>2</sup>	0 W/m <sup>2</sup>
Windows surface temperature		39°C	39°C
Number of occupants		40	40
Occupants clothing temperature (Zolfaghari and Maerefat, 2010)		33.7°C	33.7°C
Number of personal computers		40	40
Personal computers surface temperature (Lei, Wang and Zhang, 2014)		40°C	40°C
Lighting surface temperature (Lei, Wang and Zhang, 2014)		40°C	40°C
Number of photocopiers		1	1
Photocopier surface temperature (Lei, Wang and Zhang, 2014)		40°C	40°C

### 7.3.1.2 Numerical Grids

The numerical grid utilised for MV and IJV systems were the same as those used for the summer 2016 CFD case (medium grid) as it gave the best results when compared with measurements. However, a minor modification was made to that grid to accommodate the IJV supply duct. Figure 7.6 shows the mesh configuration used in the computational domain for IJV system.

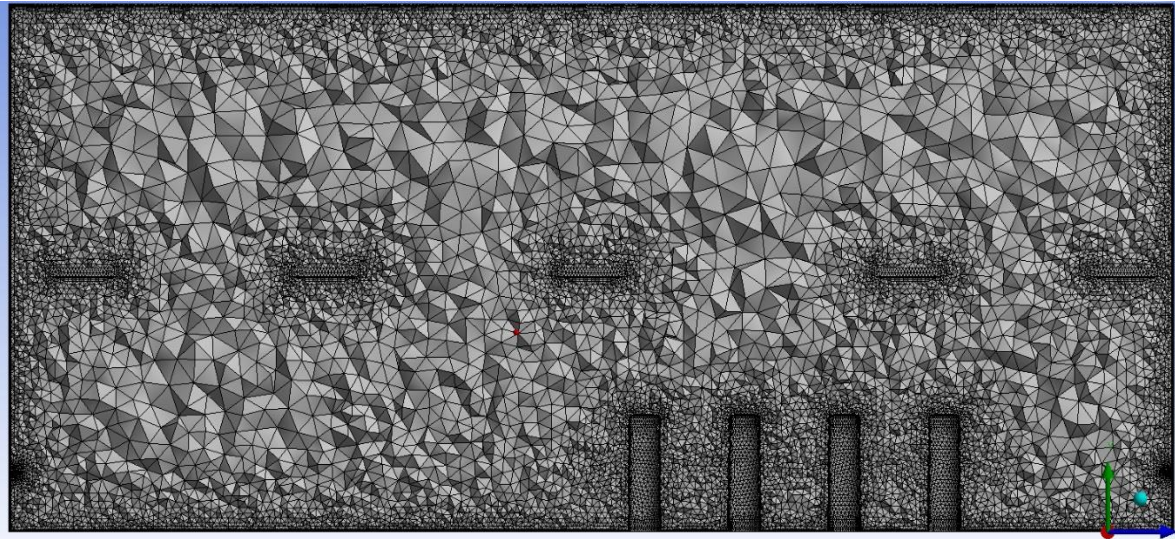


Figure 7.6 Mesh configuration in the computational domain for the IJV system of Case F-S

### 7.3.1.3 Turbulence Model

The SST k- $\omega$  turbulence model was used to predict the airflow pattern and CO<sub>2</sub> concentration distribution within the office for the MV and IJV systems cases. This is because it provided better predictions of air velocity, air temperature and CO<sub>2</sub> concentration than the RNG k- $\epsilon$  model when compared with measured values, as discussed in the previous chapter.

### 7.3.1.4 Comparison between the performance of the MV and IJV systems

The performance of both the MV and IJV systems for providing indoor air quality and thermal comfort in the occupied zone was evaluated for the case of full occupancy load for the summer condition, Case F-S as presented in Table 7.3.

Figures 7.7 through to 7.10 illustrate the air temperature contours, air velocity vectors, CO<sub>2</sub> concentration contours on a lateral plane located in the middle of the office at Z=6.6m for the MV and Z=7.2 m for the IJV systems for Case F-S.

Figure 7.7 (a) and (b) show that with the different supply air temperatures used, 18°C for the MV and 19°C for the IJV, the temperature field in both the MV and IJV systems are somewhat similar when the average temperature in the occupied area was maintained at the same level 22°C. Also, temperature stratification for the office is observed for both contours which was very significant for IJV supplies as shown in Figure 7.7 (b)

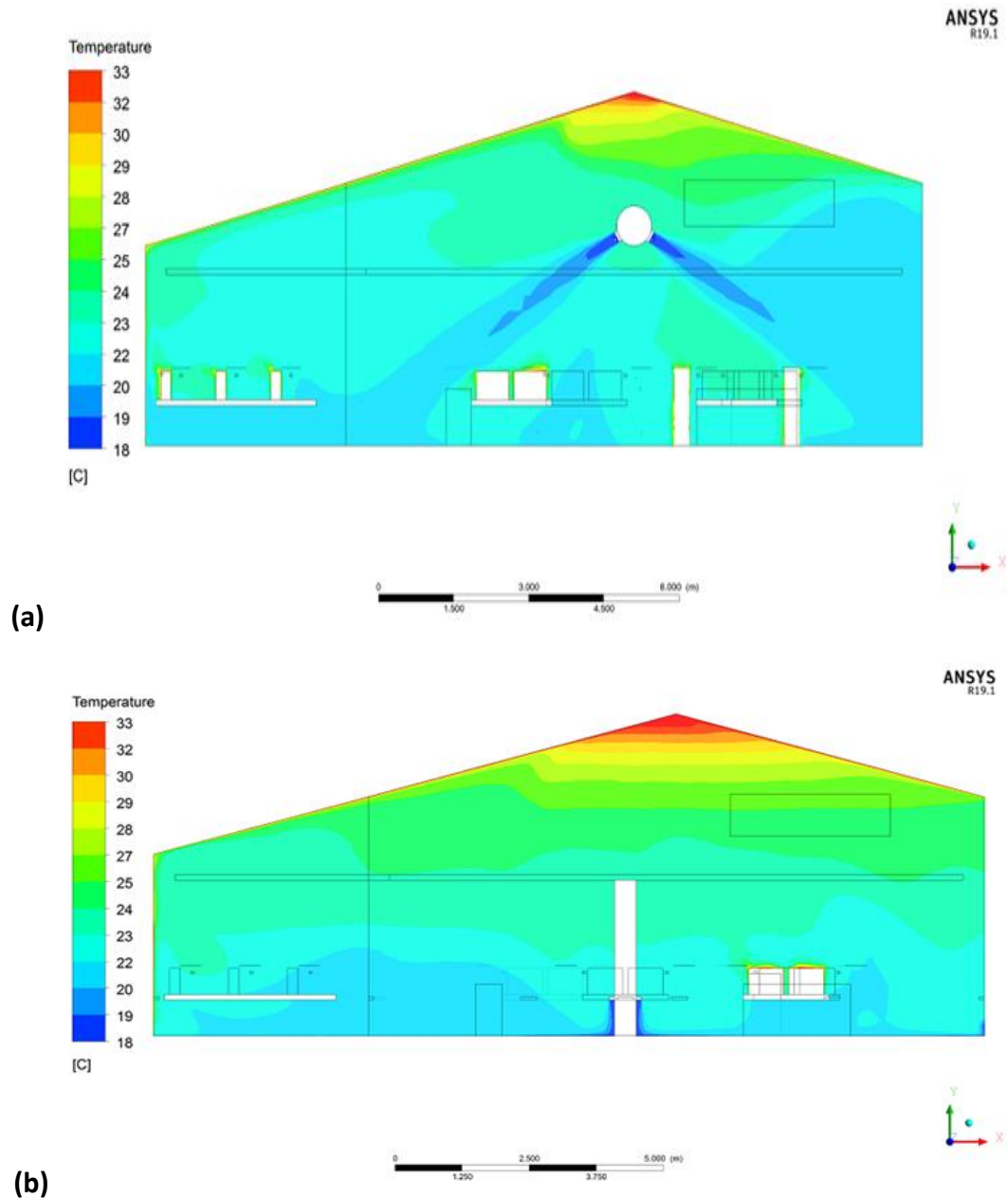


Figure 7.7 Temperature contour plots on a lateral plane located in the middle of the office for Case F-S: (a) MV system at  $Z=6.6$  m and (b) IJV system at  $Z=7.2$  m.

From Figure 7.8 (a) it can be seen that the left supply jet for the MV system is spreading over the floor towards the south (external) wall after impinging on it. In addition, the hot sources and window generate thermal plumes causing considerable buoyancy forces which move the air up to the ceiling. This large and robust air circulation produces the least stratification level by the MV system compared to the IJV system. A cross-recirculation is created in different parts of the occupied zone for both the MV and IJV systems due to partitions and furniture as shown in Figure 7.8(a) and (b). The supplied air from two IJV diffusers spreads along the floor for about 3 m and decays as it moves onto the office floor, as can be seen in Figure 7.8 (b).

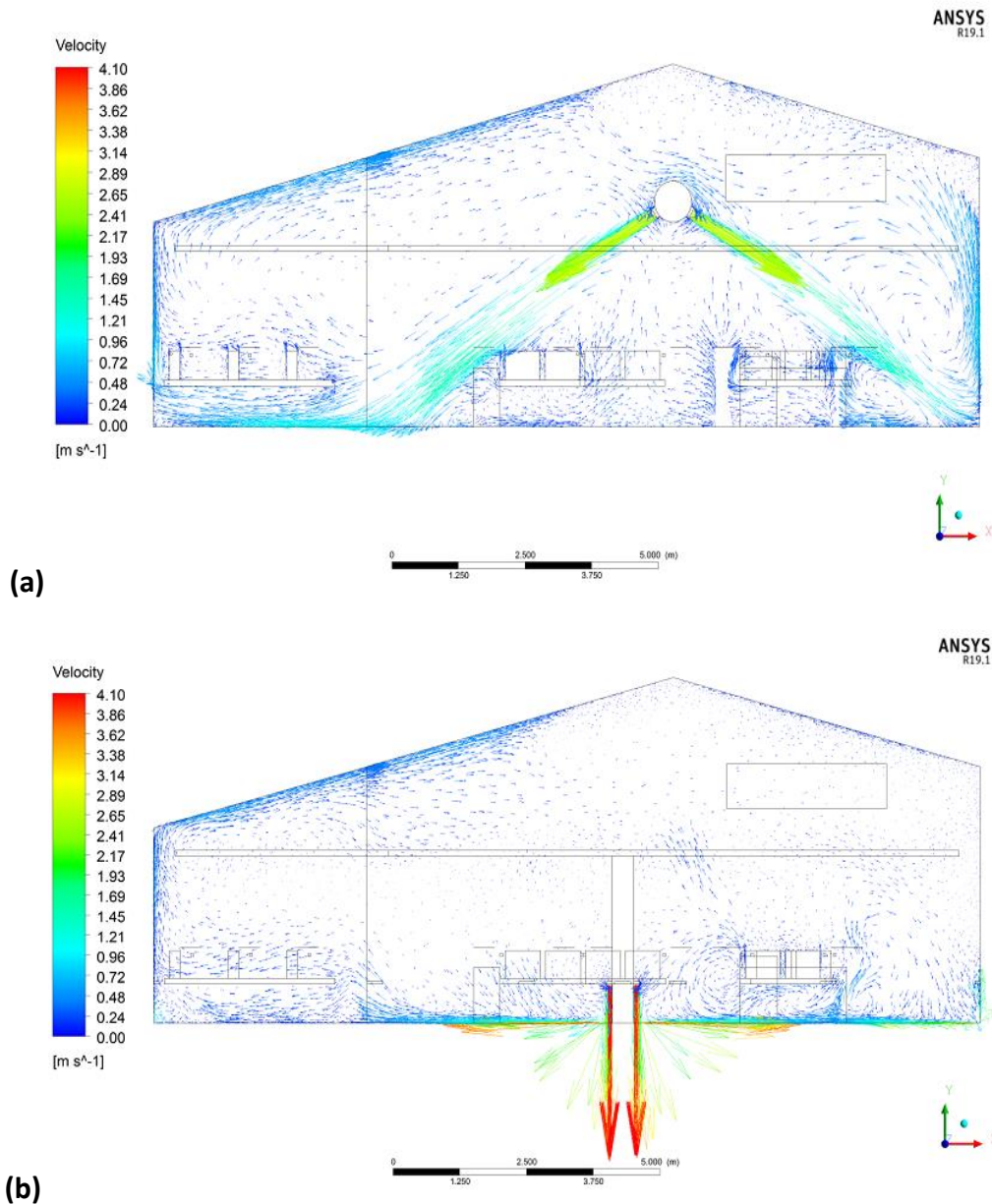


Figure 7.8 Velocity vector plots on a lateral plane located in the middle of the office for Case F-S: (a) MV system at  $Z=6.6$  m and (b) IJV system at  $Z=7.2$  m.

Figure 7.9 (a) and (b) present the velocity contours on a plane located at the height of 0.1 m from the floor level for the MV and IJV systems. The velocity distributions for the MV system are very different from those for the IJV system. In Figure 7.9 (a), there are two spots with high velocity in the south part of the office due to the impinging of two supply jets on the floor. In Figure 7.9 (b), the most noticeable high-velocity areas appear in the region near the IJV diffusers and along the walls. The region in the middle of the office has high velocity flows shaped like a Cross. Each part of this Cross was generated from a merging of the supplied air of two adjacent IJV diffusers which travel about 3m in a diagonal direction. The occupants in that direction may experience draught discomfort at foot level.

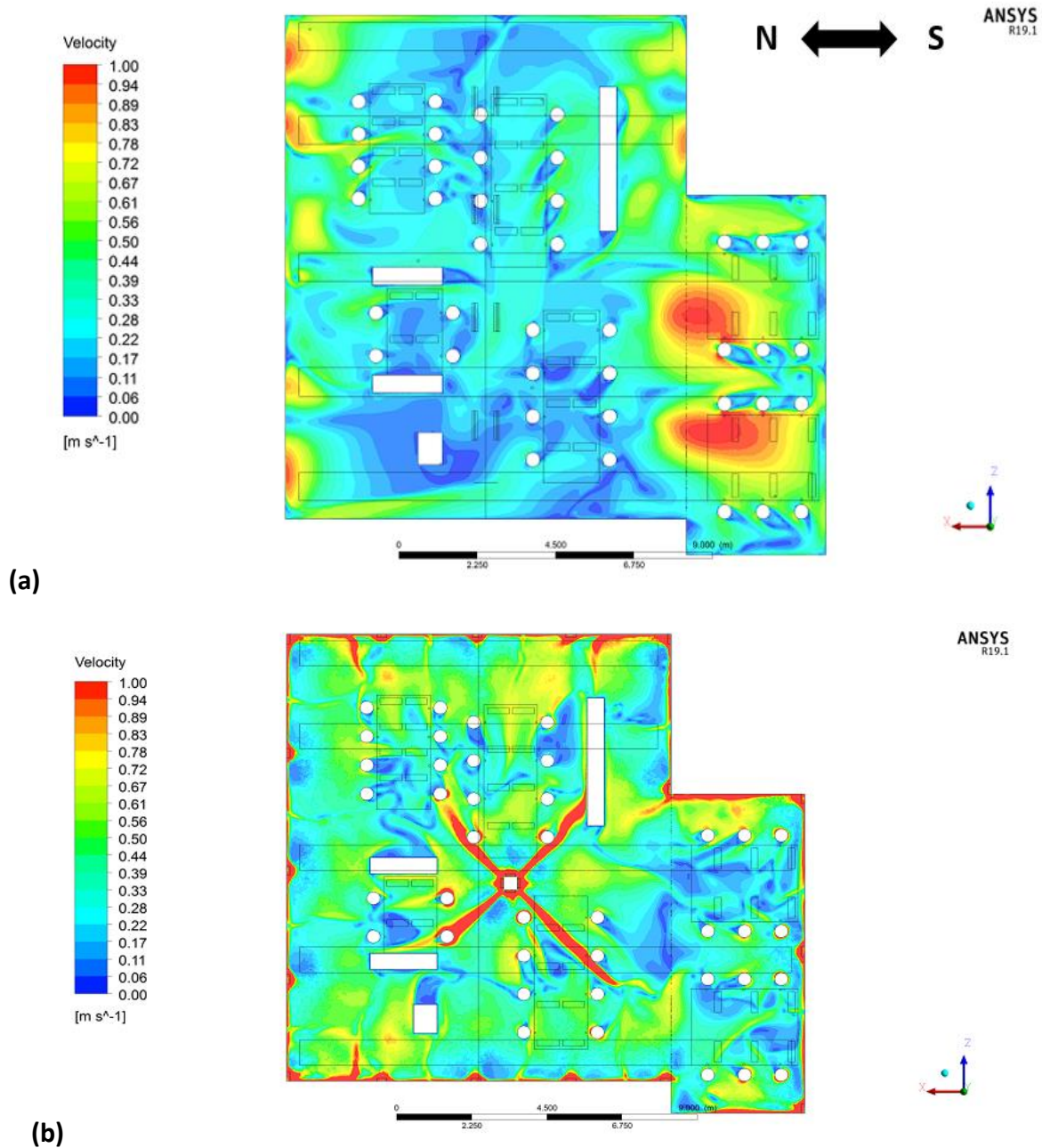
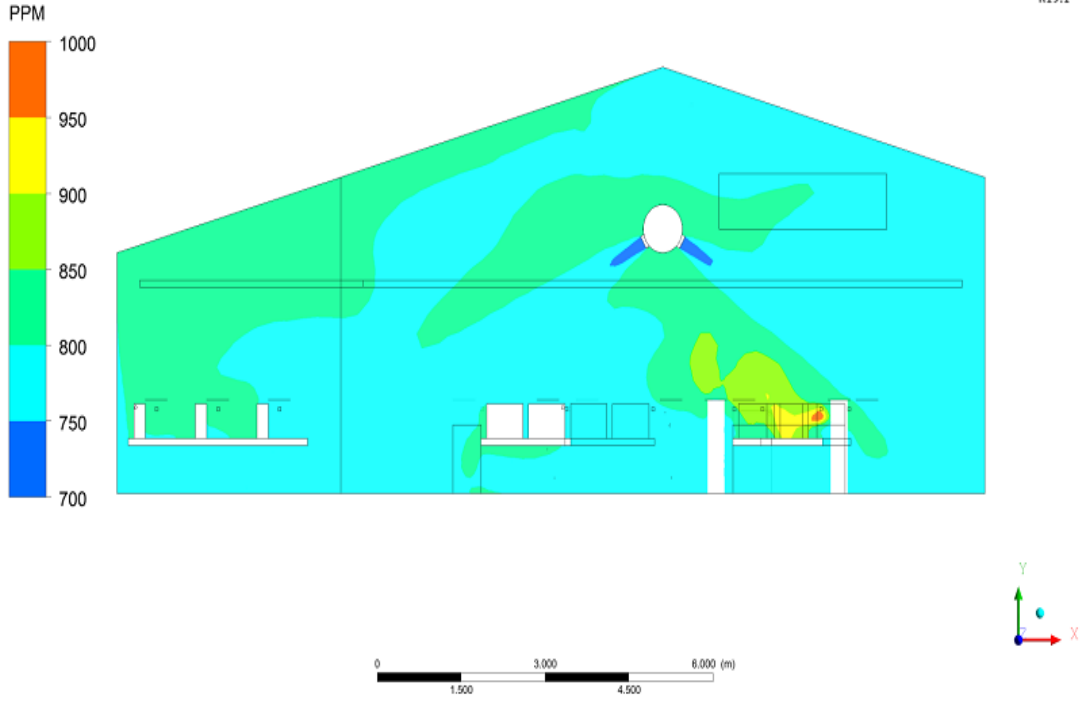
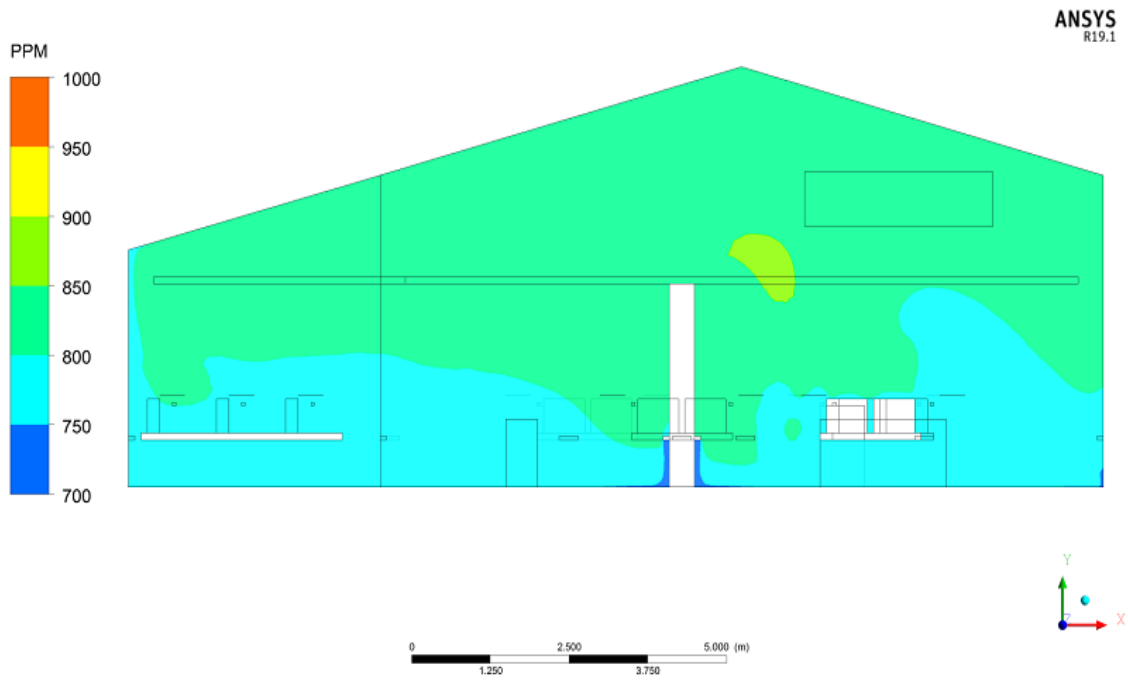


Figure 7.9 Velocity contour plots on a plane located at a height  $Y=0.1$  m for Case F-S: (a) MV system and (b) IJV system.

The predicted  $\text{CO}_2$  concentration on a vertical plane located in the middle of the office for the MV and IJV systems are shown in Figure 7.10 (a) and (b), respectively. In Figure 7.10 (a), the concentration of  $\text{CO}_2$  in a part of the occupied zone is higher than its mean value in that zone. This is because the supplied air is displaced downward and make proper mixing with the office air apart from that area due to the presence of the obstruction such as tables. However, for IJV system, the concentration of  $\text{CO}_2$  is generally uniform in the occupied zone between 750 and 800 ppm. Therefore the IJV system was more efficient in providing fresh air to the breathing zone than the MV system.



(a)



(b)

Figure 7.10 CO<sub>2</sub> concentrations contours on a lateral plane located in the middle of the office for Case F-S: (a) MV system at Z=6.6 m and (b) IJV system at Z=7.2m.

The predicted parameters were used to calculate the Air Distribution Index for this case as shown in Table 7.5. More details of the ADI are given in section 2.5.

Table 7.5 The predicted ADI for the MV and IJV systems for Case F-S

Distribution system		MV	IJV
Flow rate (m <sup>3</sup> /s)		2.6	2.6
Diffusers	Number	8	21
	Area (m <sup>2</sup> )	0.12	0.03
	Velocity ( m/s)	2.7	4.1
	Temperature (°C)	18	19
	CO <sub>2</sub> (ppm)	745	745
$\bar{\epsilon}_c$		1.17	1.78
PD (%)		15.2	15.2
$N_c$		7.7	11.7
$\bar{\epsilon}_t$		1.5	2.23
PPD (%)		40	31
$N_t$		3.75	7.2
<b>ADI</b>		5.37	9.18

As shown in table 7.5, the IJV system was able to remove contaminants and heat from the ventilated space more effectively than the MV system. Also, both air distribution numbers for air quality and for thermal comfort were higher (better) for the IJV than MV systems and consequently, it shows higher (better) ADI value. However, PPD values for both systems were too high because of dumping of cold and high velocity jet into the occupied zone.

### 7.3.2 Full Occupancy Load for Winter Condition (Case F-W)

#### 7.3.2.1 Boundary Conditions

The boundary conditions and the geometry for this case F-W were the same as those used in Case F-S except that the surfaces temperature of all the office walls, ceiling and windows were different since this case was used to simulate winter conditions. Also, the air supply temperatures for both the MV and IJV systems were set by an iterative procedure to ensure the office occupied zone in in a rather steady temperature condition of 22.3°C ± 0.4°C since the highest productivity in office environment is at temperature of around 22°C as recommended by (Seppanen, Fisk and Lei (2006)).

According to CIBSE (2008), the winter design dry bulb temperature for London (UK) is  $-4^{\circ}\text{C}$ , hence the surface temperatures of the external (South) wall, ceiling and windows were calculated using the one-dimensional heat equation (Bergman *et al.*, 2011)

$$q_x = \frac{\Delta T}{R_{tot}} \quad (7.2)$$

where  $q_x$  is the heat transfer rate (W),  $\Delta T$  is the overall temperature difference ( $^{\circ}\text{C}$ ) and  $R_{tot}$  is the total thermal resistance ( $\text{m}^2 \cdot ^{\circ}\text{C}/\text{W}$ )

Figure 7.11 shows the heat transfer through a plane wall which represents the office external wall, ceiling and window. The plane wall separates two fluids (air) at different temperatures. The heat is transferred from the hot indoor air  $T_{a,i}$  to the internal surface of the wall at  $T_{s,i}$  by convection, then by conduction through the wall and by convection from the external surface of the wall at  $T_{s,o}$  to the cold outdoor air.

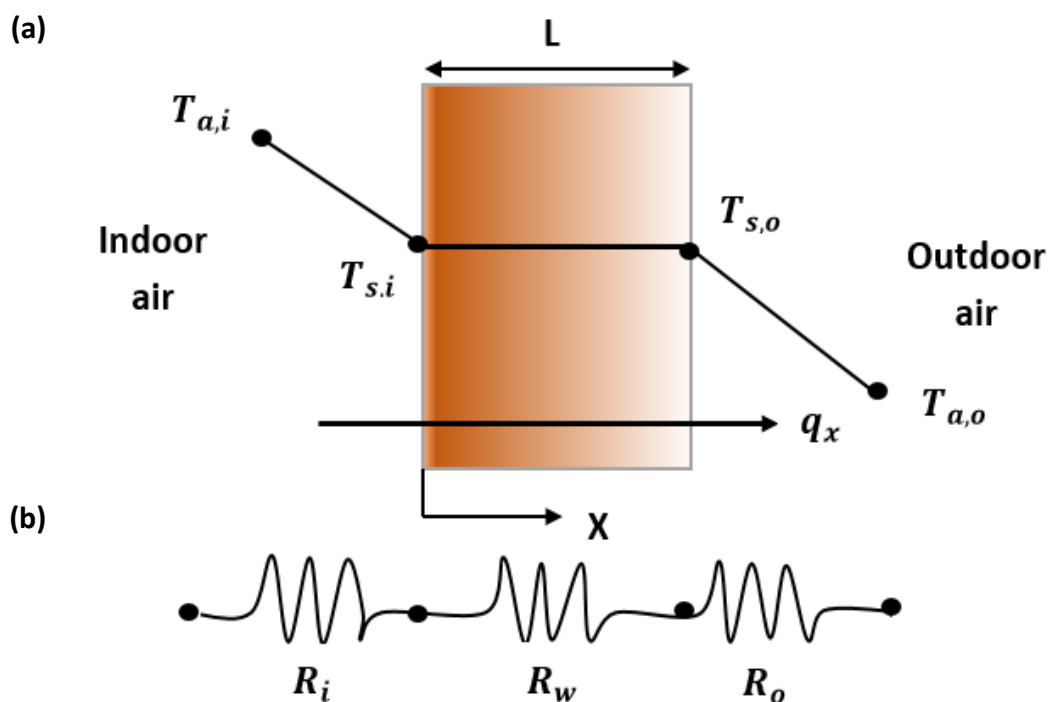


Figure 7.11 Heat transfer through a plan wall : (a) temperature distribution (b) equivalent thermal circuit.

Table 7.6 shows the calculated values of internal surface temperatures, heat transfer and the thermal resistance used in this calculation for the south wall, ceiling and window.

Table 7.6 The values of internal surface temperatures, heat transfer and the thermal resistance for the south wall, ceiling and window

	South wall	Window	Roof
$T_{a,i}$ (°C)	22	22	22
$T_{a,o}$ (°C)	- 4	- 4	- 4
$R_i$ (m <sup>2</sup> .°C/W)	0.1	0.1	0.1
$R_w$ (m <sup>2</sup> .°C/W)	0.71	0.325	0.62
$R_o$ (m <sup>2</sup> .°C/W)	0.029	0.029	0.029
$R_{tot}$ (m <sup>2</sup> .°C/W)	0.84	0.45	0.75
$\dot{q}_x$ (W/ m <sup>2</sup> )	31	57.8	34.7
$T_{s,i}$ (°C)	18.9	16.2	18.5

The internal walls were assumed to be adiabatic. Thus, table 7.7 summarises the boundary condition for Case F-W for both MV and IJV systems.

Table 7.7 Boundary conditions of Case F-W for the MV and IJV systems

	Details	Mixing System	Impinging Jet System
Supply air diffusers	Flow rate	2.6 m <sup>3</sup> /s	2.6 m <sup>3</sup> /s
	Number	8	21
	Area	0.12 m <sup>2</sup>	0.03 m <sup>2</sup>
	Velocity	2.7 m/s	4.1 m/s
	Temperature	20°C	20°C
	CO <sub>2</sub> concentration	745 ppm	745 ppm
Ceiling surface temperature		18.5°C	18.5°C
Internal walls heat flux		0 W/m <sup>2</sup>	0 W/m <sup>2</sup>
External wall surface temperature		19°C	19°C
Floor heat flux		0 W/m <sup>2</sup>	0 W/m <sup>2</sup>
Windows surface temperature		16°C	16°C
Number of occupants		40	40
Occupants clothing temperature (Zolfaghari and Maerefat, 2010)		33.7°C	33.7°C
Number of personal computers		40	40
Personal computers surface temperature (Lei, Wang and Zhang, 2014)		40°C	40°C
Lighting surface temperature (Lei, Wang and Zhang, 2014)		40°C	40°C
Number of photocopiers		1	1
Photocopier surface temperature (Lei, Wang and Zhang, 2014)		40°C	40°C

### 7.3.2.2 Numerical grids and turbulence model

The numerical grid and the turbulence model used for this case were the same as those used for Case F-S.

### 7.3.2.3 Comparison between the performance of the MV and IJV systems

The case of full occupancy load at winter, Case F-W in table 7.3, was used to investigate the performance of the MV and IJV systems in providing indoor air quality and thermal comfort in the occupied zone.

To place the office's occupied zone in a rather steady temperature condition of  $22.3^{\circ}\text{C} \pm 0.4^{\circ}\text{C}$ , the air supply temperatures were set by iterative trial to be  $20^{\circ}\text{C}$  for both MV and IJV systems respectively for the winter condition. Consequently, the case F-W became a cooling condition rather than heating. This was due to the internal heat loads generated in the office from occupants, personal computers, lightning and photocopier were higher than the external heat loss. Thus, the air supply temperatures were lower than the mean office temperature which were  $22.7^{\circ}\text{C}$  for MV and  $22.5^{\circ}\text{C}$  for IJV systems respectively.

A comparison of the predicted air temperature, air velocity and  $\text{CO}_2$  concentration are shown in Figure 7.12 to 7.15 on a lateral plane located in the middle of the office at  $Z=6.6$  m for the MV system and  $Z=7.2$  m for the IJV system for Case F-W.

As can be seen from Figure 7.12 (b), the air temperature in the office is higher in the unoccupied zone and lower in the occupied area for the IJV system which is unlike the air temperature profile for the MV system as in Figure 7.12 (a). This led to an increase in the overall heat removal effectiveness value from 1.1 for the MV system to 1.4 for the IJV system (see table 7.8). Also, there was no considerable observation of temperature stratification for both systems due to the cold ceiling  $T=18.5^{\circ}\text{C}$ .

As shown in Figure 7.13 (a) large air circulation can be observed in the south part of the office which was generated by both air jets supply momentum force and buoyancy force from heat sources. However, the air near the cold window formed a descending turbulent plume which entrains the air in part en-route towards the floor. This led to creating a small counterclockwise recirculation in that region of the office.

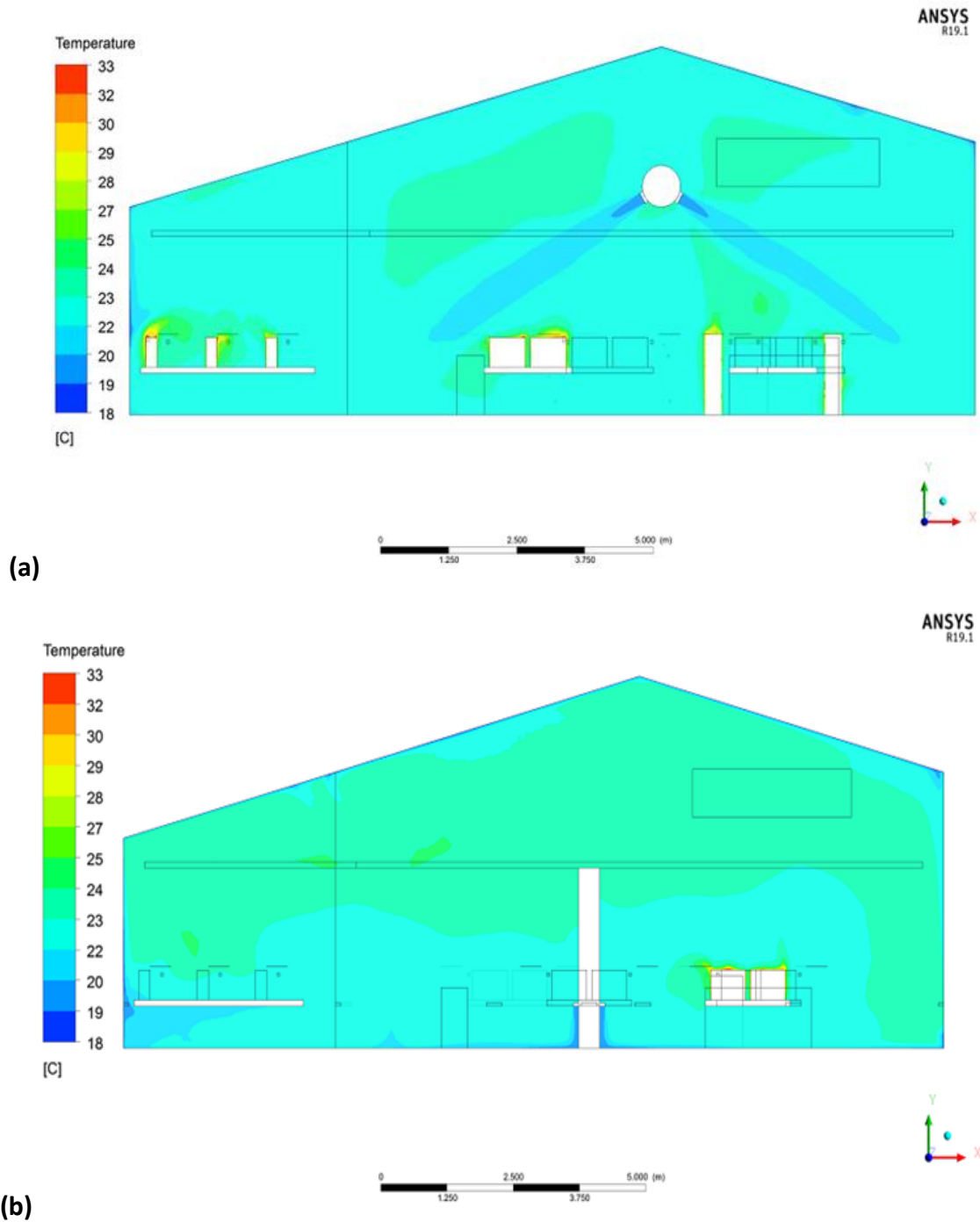


Figure 7.12 Temperature contour plots on a lateral plane located in the middle of the office for Case F-W: (a) MV systems at Z=6.6 m and (b) IJV system at Z=7.2 m

In Figure 7.13 (b), two similar counterclockwise recirculations were formed near the cold window and ceiling in the south side of the office for the IJV system for the same reasons mentioned in the MV system case. That cold air layer prevents the thermal stratification from being generated due to the buoyancy effects for both systems. The mean velocities in the occupied zone for the IJV was 0.23 m/s which is within the recommended limit of less than 0.25 m/s by ISO standard 7730 (BSI, 2005) while it was 0.28 m/s for the MV system.

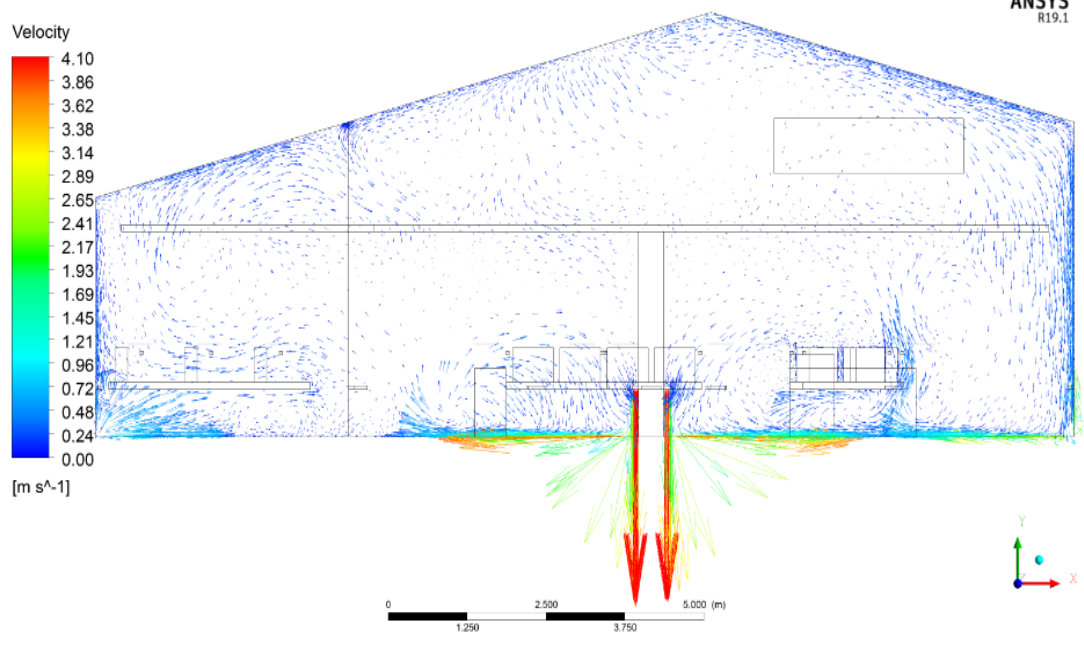
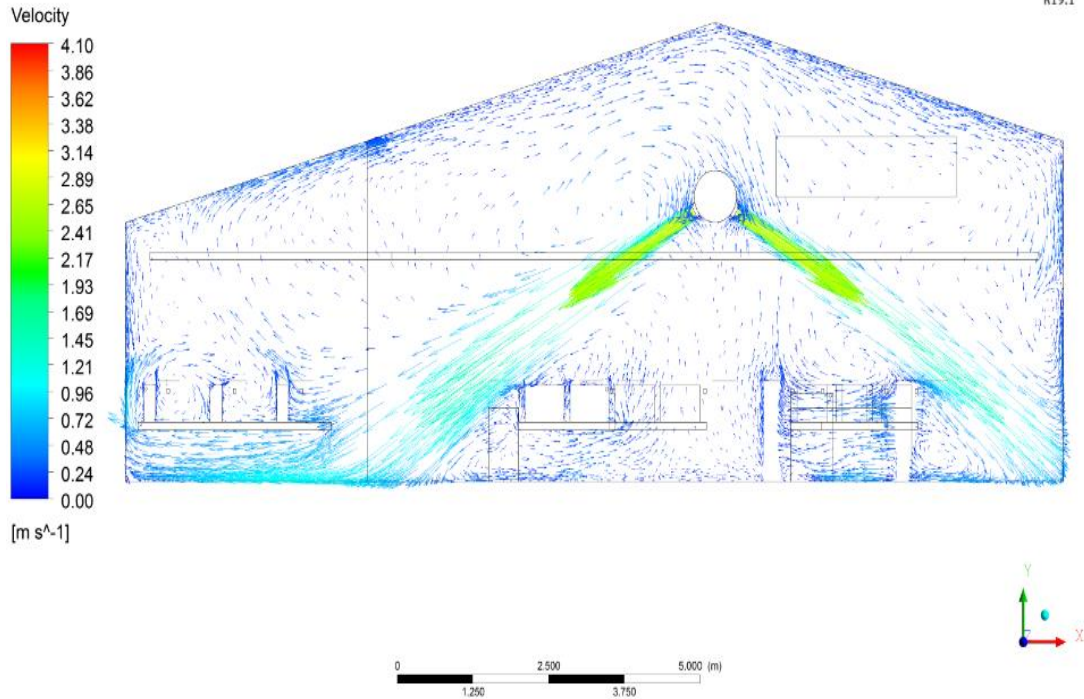


Figure 7.13 Velocity vector plots on a lateral plane located in the middle of the office for Case F-W: (a) MV system at  $Z=6.6$  m and (b) IJV system at  $Z=7.2$  m.

The spread of the impinging Jets over the floor produced a velocity distribution which was different from that for the MV system. Figure 7.14 (a) and (b) show the velocity contours on a horizontal plane at a height  $y=0.1$  m for the MV and IJV systems.

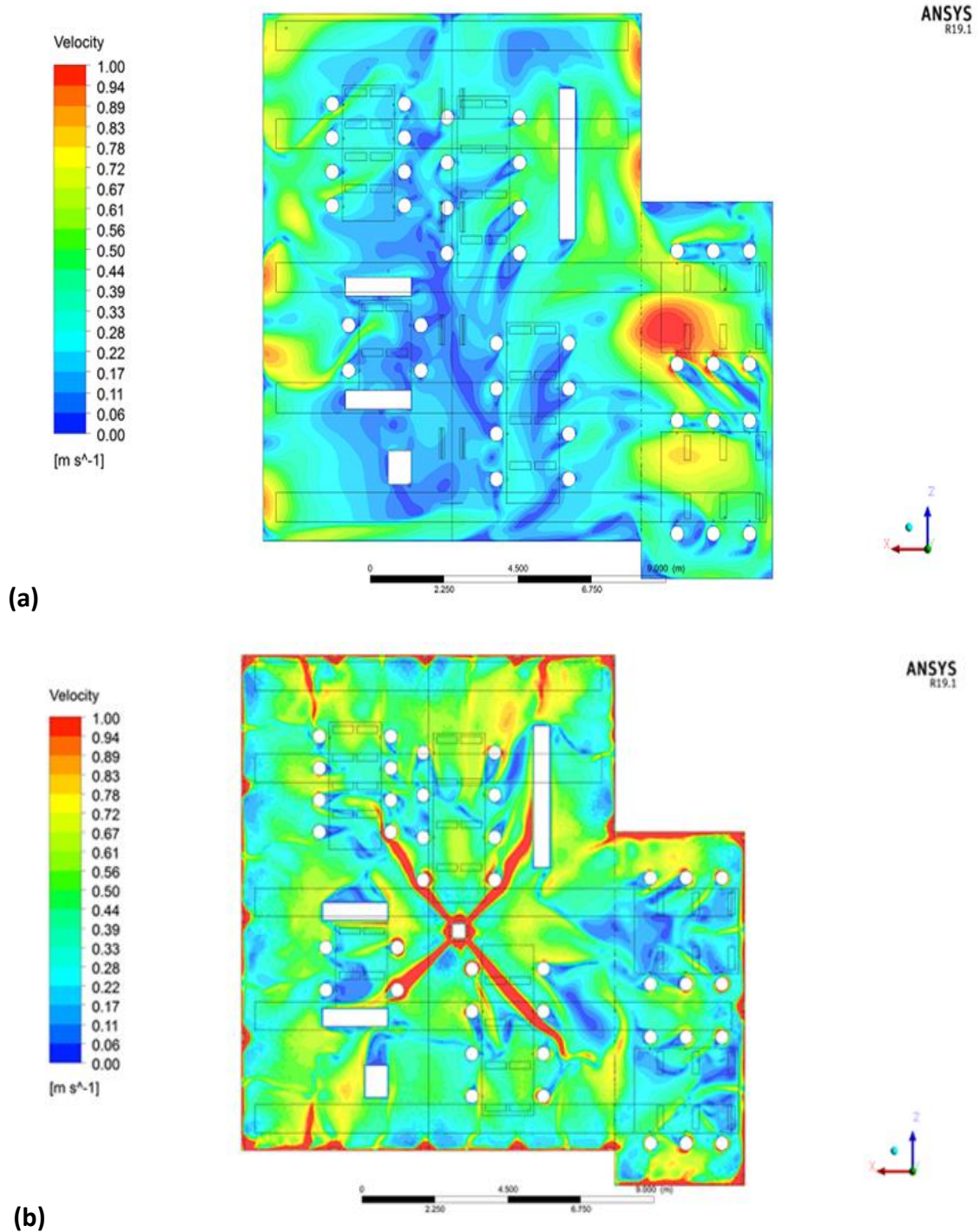


Figure 7.14 Velocity contour plots on a plane at a height  $y=0.1$  m for case F-W: (a) MV system and (b) IJV system.

Figure 7.15 (a) and (b) shows planes of the CO<sub>2</sub> stratification for both systems. Figure 7.15 (a) shows that there was a good air mixing in the office and there is a lower stratification of CO<sub>2</sub> for the MV system compared to the IJV system as shown in Figure 7.15 (b). This was due to the “dumping” effect of the air supplies in the case of MV system. However, the value of the

overall ventilation effectiveness for the removal of pollutants for the IJV systems was higher than its value for the MV system (see Table 7.8).

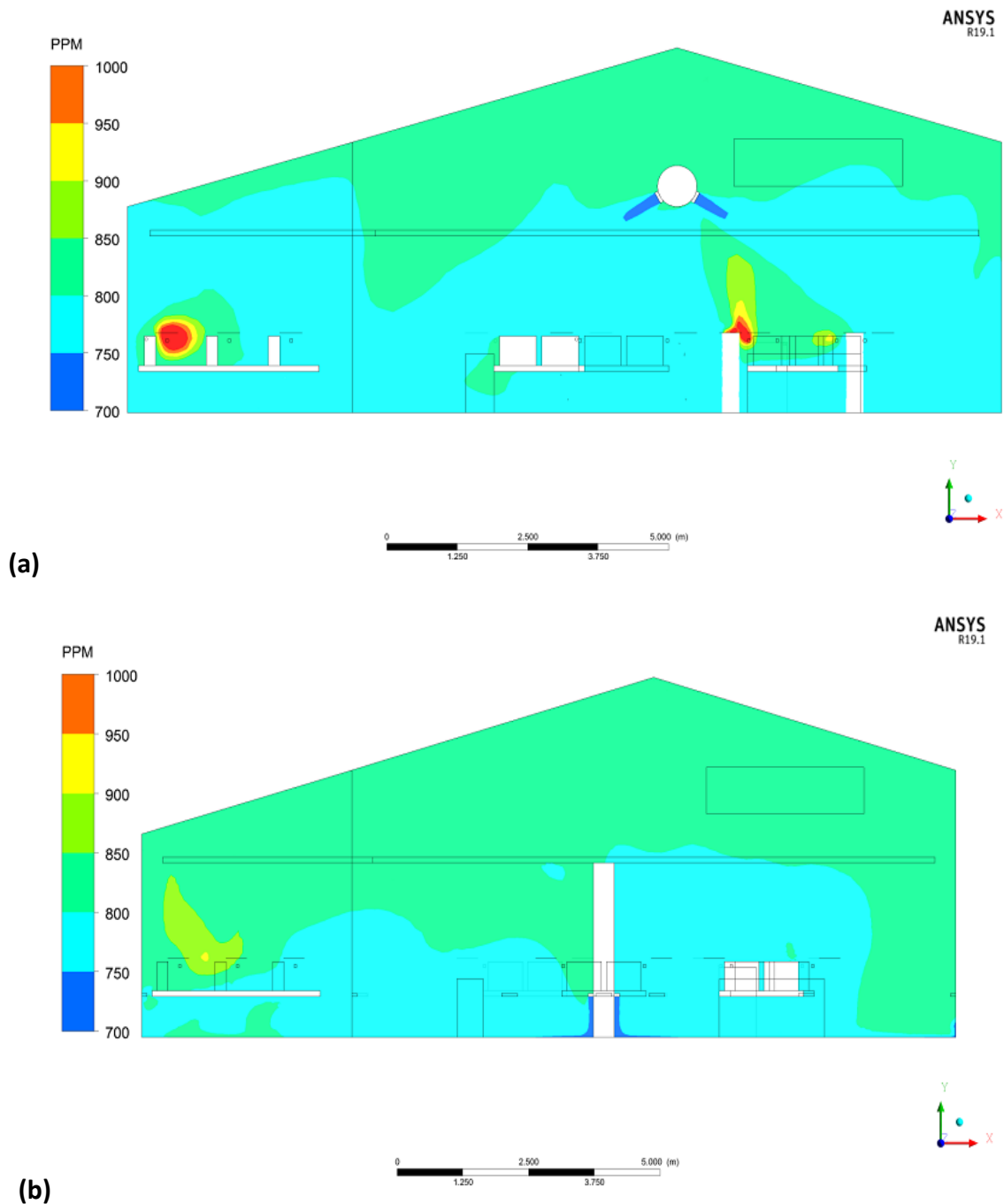


Figure 7.15 CO<sub>2</sub> concentration contours on a lateral plane located in the middle of the office for Case F-W: (a) MV system at Z=6.6 m and (b) IJV system at Z=7.2 m.

The ADI was calculated for the Case F-W from the predicted parameters as shown in Table 7.8. It can be seen that the MV and IJV systems have the same values of PPD, although the air distribution number for thermal comfort was higher for the IJV than MV systems. The results reveal that the highest values of  $\bar{\epsilon}_c$ ,  $\bar{\epsilon}_t$ ,  $N_c$ ,  $N_t$  and ADI were produced by IJV.

Table 7.8 The predicted ADI for the Case F-W

Distribution system		MV	IJV
Flow rate (m <sup>3</sup> /s)		2.6	2.6
Diffusers	Number	8	21
	Area (m <sup>2</sup> )	0.12	0.03
	Velocity ( m/s)	2.7	4.1
	Temperature (°C)	20	20
	CO <sub>2</sub> (ppm)	745	745
$\bar{\epsilon}_c$		1.1	1.4
PD (%)		15.2	15.2
$N_c$		7.2	9.3
$\bar{\epsilon}_t$		1.1	1.36
PPD (%)		5	5
$N_t$		22	27.2
ADI		12.6	15.9

### 7.3.3 Half Occupancy Load for Summer Condition (Case H-S)

#### 7.3.3.1 Boundary Conditions

Since no experimental measurements were conducted, the boundary condition for the temperature of surfaces of all the office walls, ceiling, windows, occupants clothing, personal computers, lighting and photocopier were the same as those used in Case F-S. However, as described in section 7.2, the calculated air flow rate for half occupancy was 1.7 m<sup>3</sup>/s and the average temperature in the occupied zone was maintained at the level of 22°C ± 0.2°C for both MV and IJV systems.

Hence, the supply velocities and temperatures were 1.8 m/s and 19°C for the MV system and 2.7 m/s and 20°C for the IJV system. Table 7.9 summarised the boundary conditions of Case H-S for both MV and IJV systems.

Table 7.9 Boundary conditions of Case H-S for the MV and IJV systems

	Details	Mixing System	Impinging Jet System
Supply air diffusers	Flow rate	1.7 m <sup>3</sup> /s	1.7 m <sup>3</sup> /s
	Number	8	21
	Area	0.12 m <sup>2</sup>	0.03 m <sup>2</sup>
	Velocity	1.8 m/s	2.7 m/s
	Temperature	19°C	20°C
	CO <sub>2</sub> concentration	652 ppm	652 ppm
Ceiling surface temperature		35°C	35°C
Internal walls surface temperature		28°C	28°C
External wall surface temperature		29°C	29°C
Floor heat flux		0 W/m <sup>2</sup>	0 W/m <sup>2</sup>
Windows surface temperature		39°C	39°C
Number of occupants		20	20
Occupants clothing temperature (Zolfaghari and Maerefat, 2010)		33.7°C	33.7°C
Number of personal computers		20	20
Personal computers surface temperature (Lei, Wang and Zhang, 2014)		40°C	40°C
Lighting surface temperature (Lei, Wang and Zhang, 2014)		40°C	40°C
Number of photocopiers		1	1
Photocopier surface temperature (Lei, Wang and Zhang, 2014)		40°C	40°C

### 7.3.3.2 Numerical grid

The numerical grid utilised for the MV and IJV systems were similar to those used for Case F-S. However, the mesh elements numbers were less since the number of occupants, and their computers were half those for Case F-S. Figure 7.16 shows the mesh configuration in the computational domain for the IJV system.

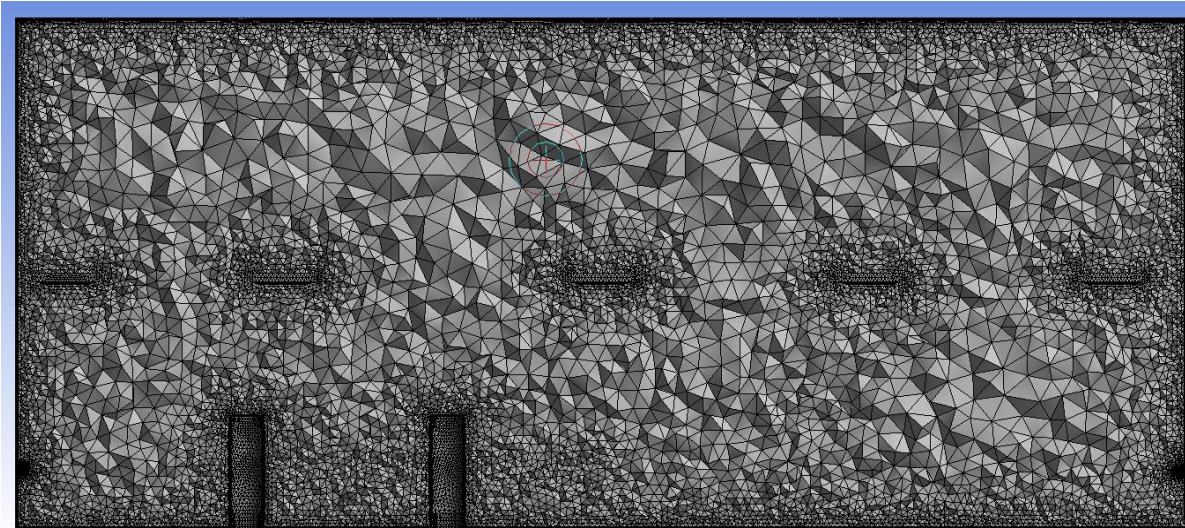


Figure 7.16 Mesh configuration in the computational domain for the IJV system for the Case H-S.

### 7.3.3.3 Turbulence model

The SST k- $\omega$  turbulence model was used to predict the air flow pattern and CO<sub>2</sub> concentration distribution within the office for the MV and IJV systems. This is because this model provided better predictions for air velocity, air temperature and CO<sub>2</sub> concentration than the RNG k- $\epsilon$  model when compared with measured values.

### 7.3.3.4 Comparisons between the performance of the MV and IJV systems

The performance of both MV and IJV systems in providing indoor air quality and thermal comfort in the occupied zone was evaluated for the case of half occupancy load for summer, Case H-S in Table 7.3.

Figure 7.17 through to 7.120 show the air temperature contours, air velocity vectors, CO<sub>2</sub> concentration contours on a lateral plane located in the middle of the office at Z=6.6 m for the MV system and Z=7.2 m for the IJV system for case H-S.

Figure 7.17 (a) and (b) shows the temperature contours in the middle of the office and the temperature stratification in the case of MV and IJV systems. The mean air temperature in the occupied zone for the MV system is higher than that for the IJV system. This is because in the IJV system, the cold jet over the floor has sufficient momentum to continue along the floor despite the heat sources due to the occupants. As for the MV system case, the cold jet momentum was not strong enough to produce good air mixing inside the office. Thus,  $\bar{\epsilon}_t$  value was 1.75 for the MV system compared to 3.5 for IJV system (see table 7.10).

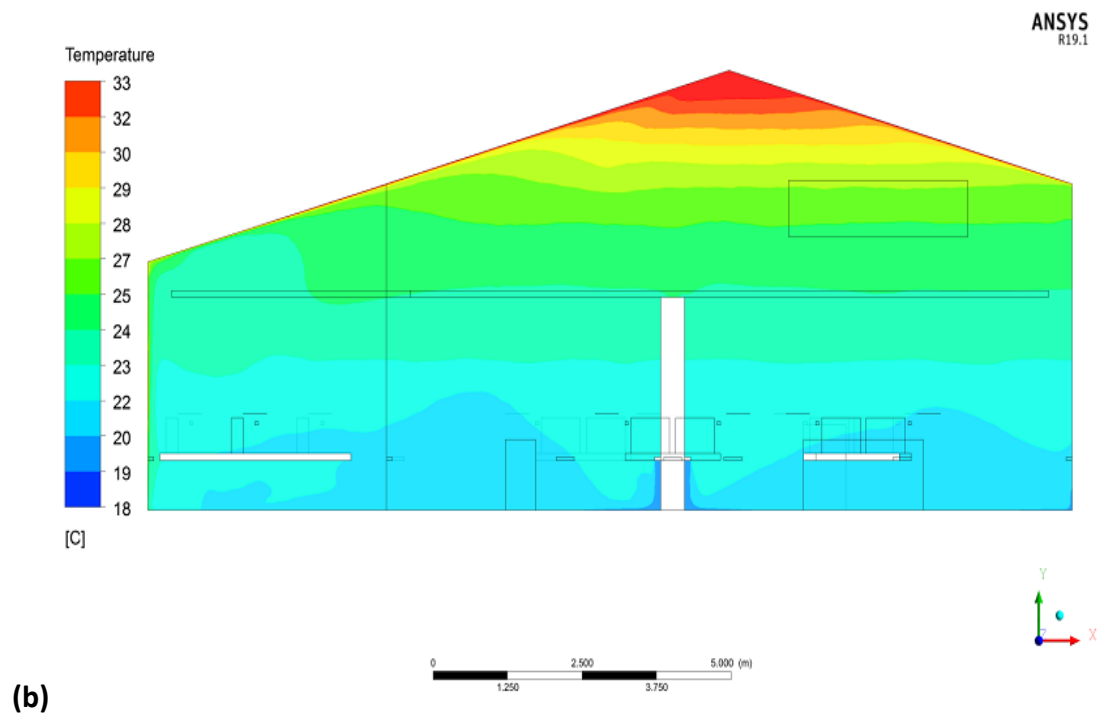
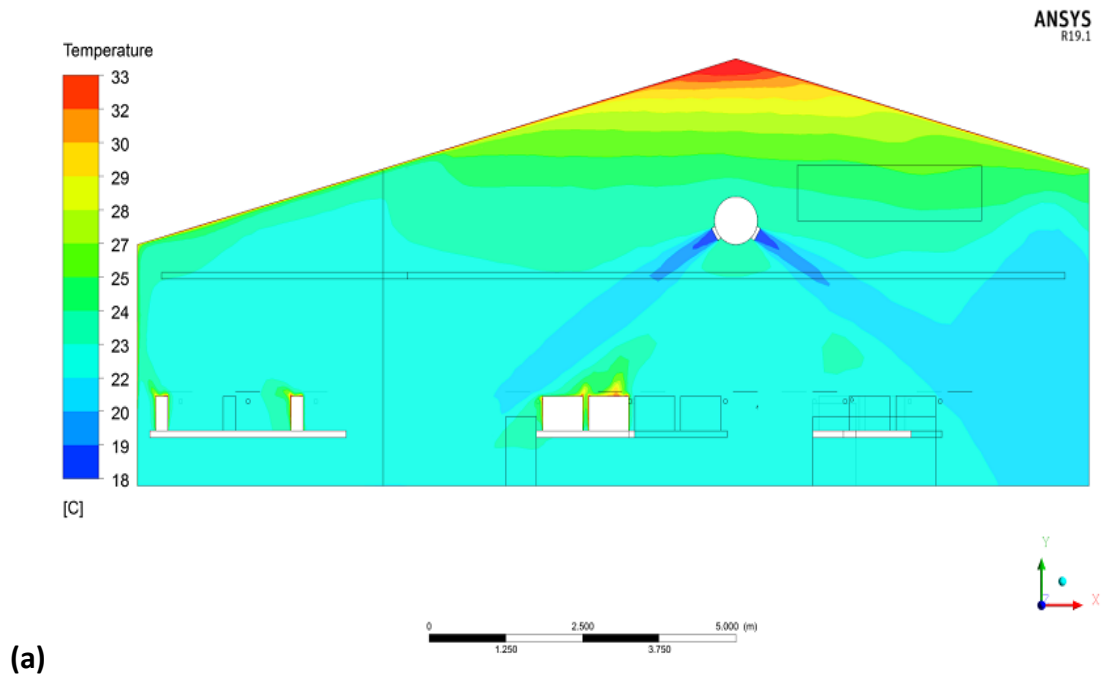


Figure 7.17 Temperature contour plots on a lateral plane located in the middle of the office for Case H-S: (a) MV system at  $Z=6.6$  m and (b) IJV system at  $Z=7.2$  m.

As can be seen from Figure 7.18 (a), a large clockwise air circulation is present on the left side of the office. The stable thermal stratification near the ceiling tends to slow down this circulation. Also, on the right side of the office, another extensive air recirculation was created with counterclockwise direction. In Figure 7.18 (b) for the IJV case, the window and the left part of the ceiling thermal plume created a strong buoyancy force which pushes the air up to the highest part of the office.

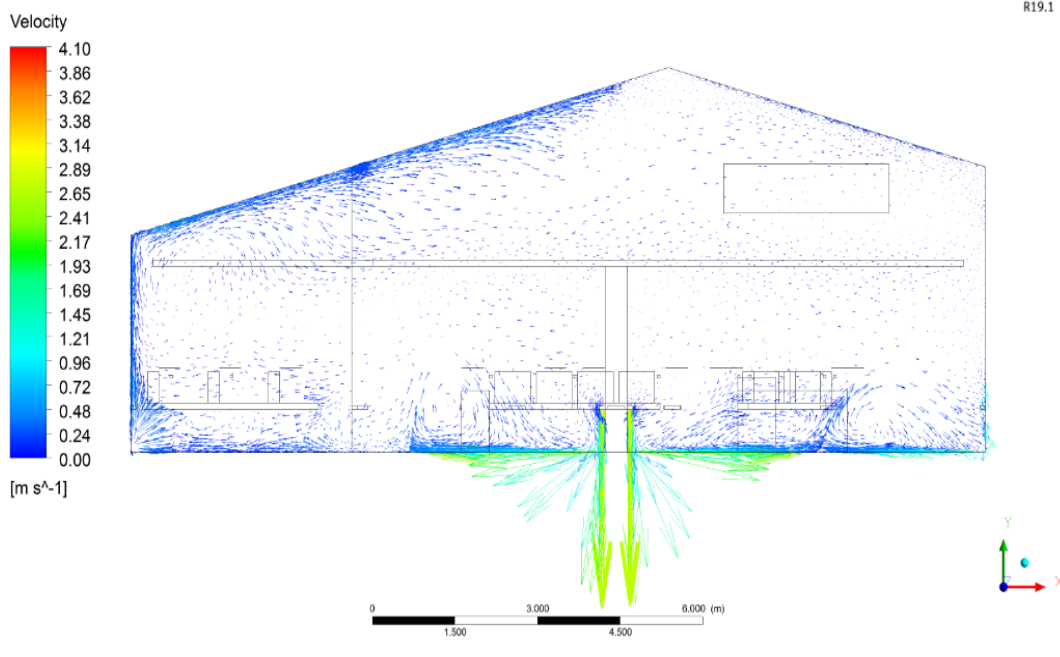
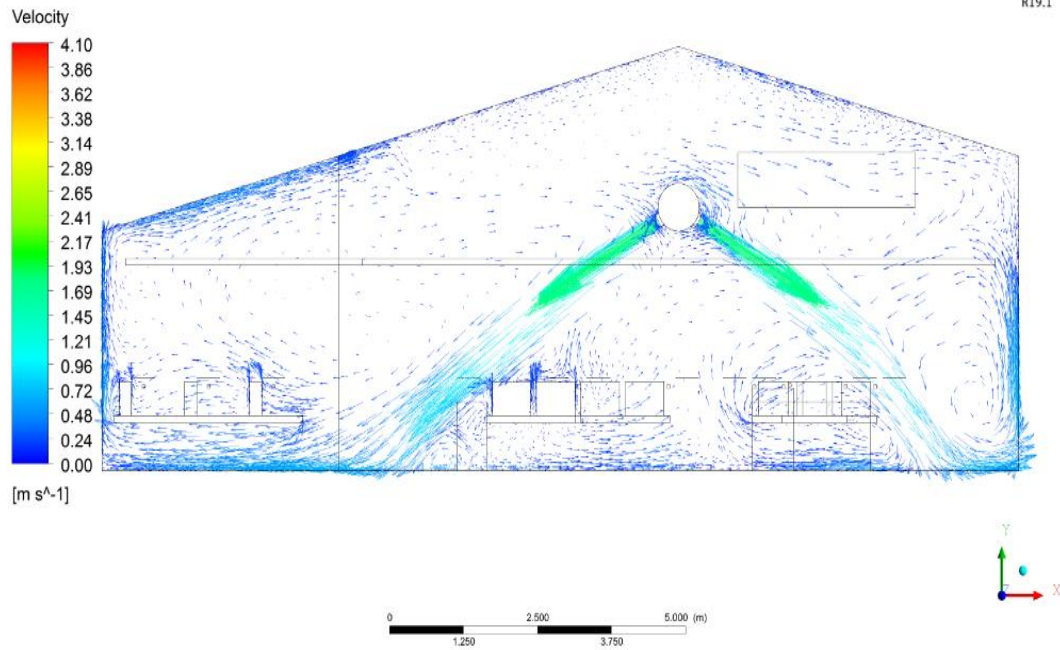


Figure 7.18. Velocity vectors on a lateral plane located in the middle of the office for Case H-S: (a) MV system at  $Z=6.6$  m and (b) IJV system at  $Z=7.2$  m.

In Figure 7.19 (a), relatively high velocities can be seen in several regions at the height of 0.1 m above the floor. This is due to the supplied air impingement over the floor in these regions which then spreads radially along the floor. For the IJV system in Figure 7.19 (b), more uniform velocity distribution at this level is observed apart of four regions which have a high air movement caused by merging two adjacent jets. These merging jets penetrate the office for

a relatively long distance causing draught discomfort for the occupants seated in their direction.

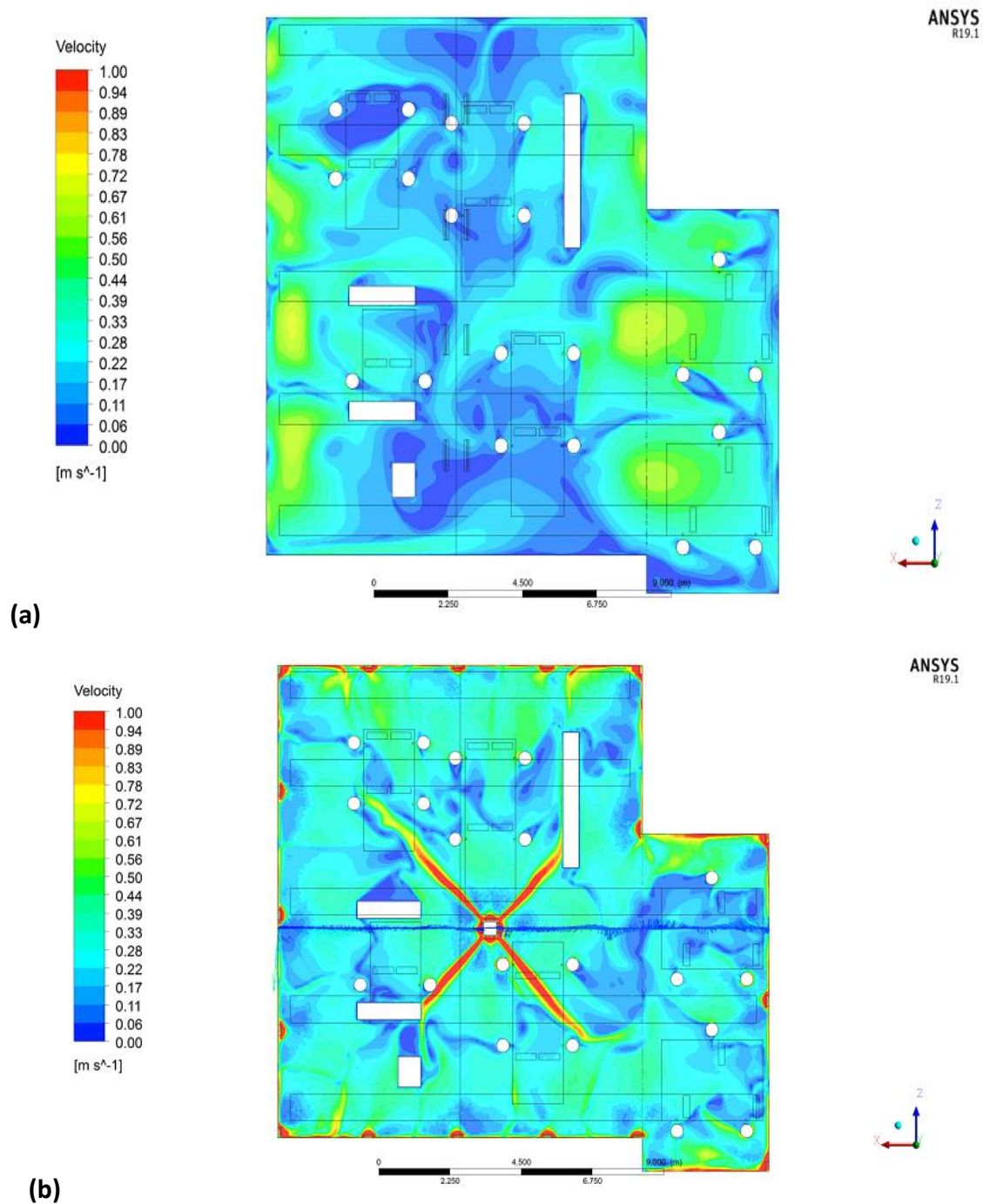


Figure 7.19 Velocity contour plots on a plane located at a height  $Y=0.1$  m for Case H-S: (a) MV system and (b) IJV system

It is noticed that the occupied zone has a low and uniform  $CO_2$  concentration for IJV system compared to that for the MV system as shown in Figure 7.20 (a) and (b). As evidence of that, the overall ventilation effectiveness for contaminant removal value is 1.16 for the MV system compared to 2.35 for the IJV system (see table 7.10).

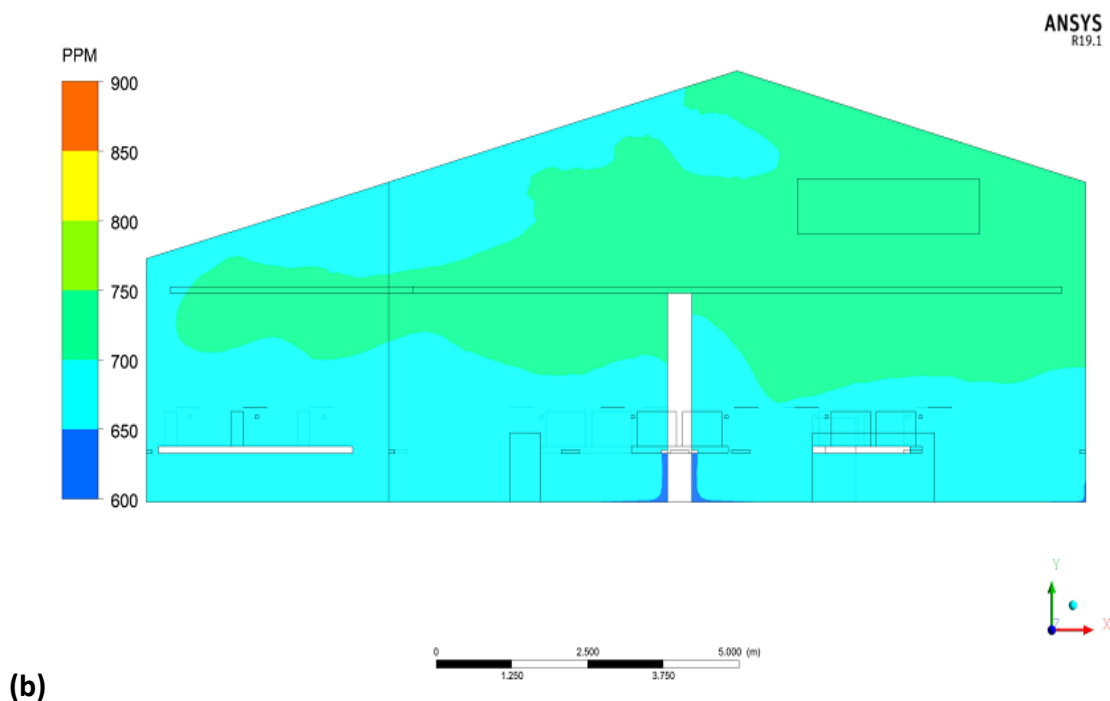
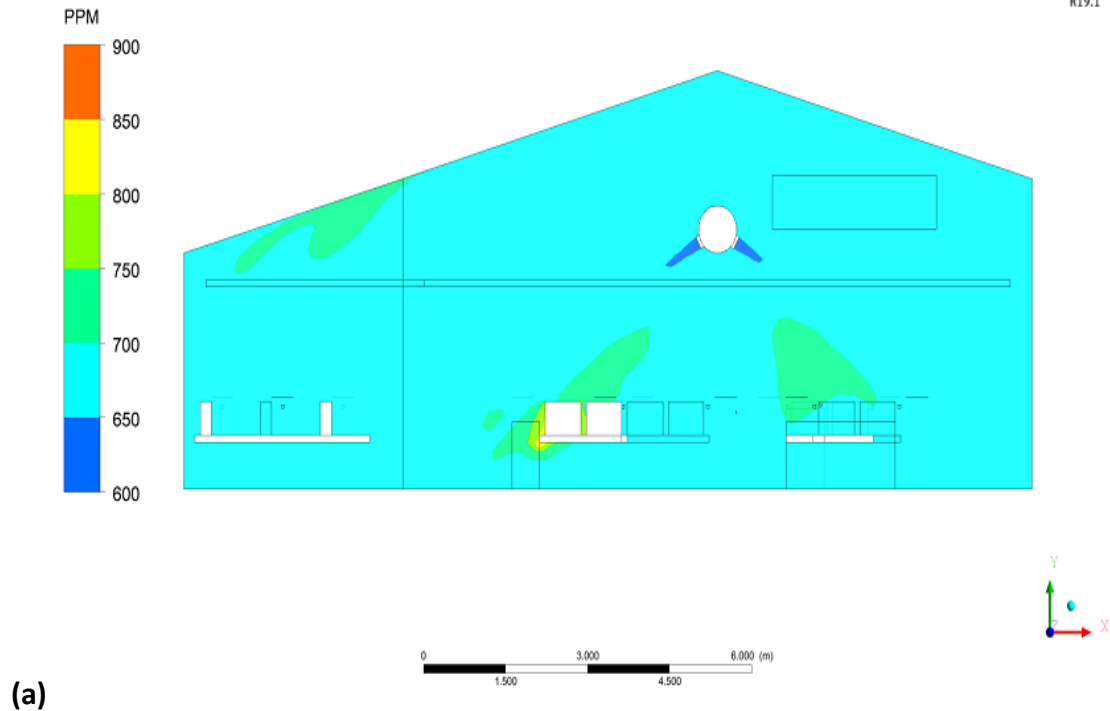


Figure 7.20 CO<sub>2</sub> concentrations contour on a lateral plane located in the middle of the office for Case H-S: (a) MV system at Z=6.6 m and (b) IJV system at Z=7.2 m.

Table 7.10 shows the predicted ADI parameters for this case for the MV and IJV systems. From that table it can be seen that the air distribution numbers for air quality and thermal comfort for the MV system were 7.63 and 6.73 respectively while they were double these values for the IJV system. Hence, the results reveal that the highest value of ADI was produced by the IJV system which was 15.

Table 7.10 The predicted ADI for the MV and IJV systems for Case (H-S).

Distribution system		MV	IJV
Flow rate (m <sup>3</sup> /s)		1.7	1.7
Diffusers	Number	8	21
	Area (m <sup>2</sup> )	0.12	0.03
	Velocity ( m/s)	1.8	2.7
	Temperature (°C)	19	20
	CO <sub>2</sub> (ppm)	652	652
$\bar{\epsilon}_c$		1.16	2.35
PD (%)		15.2	15.2
$N_c$		7.63	15.4
$\bar{\epsilon}_t$		1.75	3.5
PPD (%)		26	24
$N_t$		6.73	14.6
ADI		7.17	15.0

### 7.3.4 Half Occupancy Load for Winter Condition (Case H-W)

#### 7.3.4.1 Boundary conditions

The boundary conditions for surfaces temperature of all the office walls, ceiling, windows, occupants clothing, personal computers, lightning and photocopier were the same as those used in Case H-W. The calculated air flow rate for half occupancy was 1.7 m<sup>3</sup>/s, as described in section 7.2, and the average temperature in the occupancy zone was maintained at the level of 22°C ± 0.2°C for both MV and IJV systems. Therefore, the supply velocities and temperatures were 1.8 m/s and 20°C for the MV system while they were 2.7 m/s and 20°C for the IJV system. Table 7.9 summarised the boundary conditions of Case H-W for both MV and IJV systems.

Table 7.11 Boundary conditions for Case H-W for MV and IJV systems

	Details	Mixing System	Impinging Jet System
Supply air diffusers	Flow rate	1.7 m <sup>3</sup> /s	1.7 m <sup>3</sup> /s
	Number	8	21
	Area	0.12 m <sup>2</sup>	0.03 m <sup>2</sup>
	Velocity	1.8 m/s	2.7 m/s
	Temperature	21°C	21°C
	CO <sub>2</sub> concentration	652 ppm	652 ppm
Ceiling surface temperature		18.5°C	18.5°C
Internal walls surface temperature		0 W/m <sup>2</sup>	0 W/m <sup>2</sup>
External wall surface temperature		19°C	19°C
Floor heat flux		0 W/m <sup>2</sup>	0 W/m <sup>2</sup>
Windows surface temperature		16°C	16°C
Number of occupants		20	20
Occupants clothing temperature (Zolfaghari and Maerefat, 2010)		33.7°C	33.7°C
Number of personal computers		20	20
Personal computers surface temperature (Lei, Wang and Zhang, 2014)		40°C	40°C
Lighting surface temperature (Lei, Wang and Zhang, 2014)		40°C	40°C
Number of photocopiers		1	1
Photocopier surface temperature (Lei, Wang and Zhang, 2014)		40°C	40°C

#### 7.3.4.2 Numerical Grid and Turbulence Model

The numerical grid and the turbulence model used for this case were the same as those used for case H-S.

#### 7.3.4.3 Comparison between the performance of the MV and IJV systems for winter.

The performance of both MV and IJV systems in providing indoor air quality and thermal comfort in the occupied zone was evaluated for the case of half occupancy in winter, Case H-W in Table 7.3.

Figures 7.21 through 7.24 shows the air temperature contours, air velocity vectors and CO<sub>2</sub> concentration contours on a lateral plane located in the middle of the office at Z= 6.6 m for the MV system and Z= 7.2 m for the IJV system for case H-W.

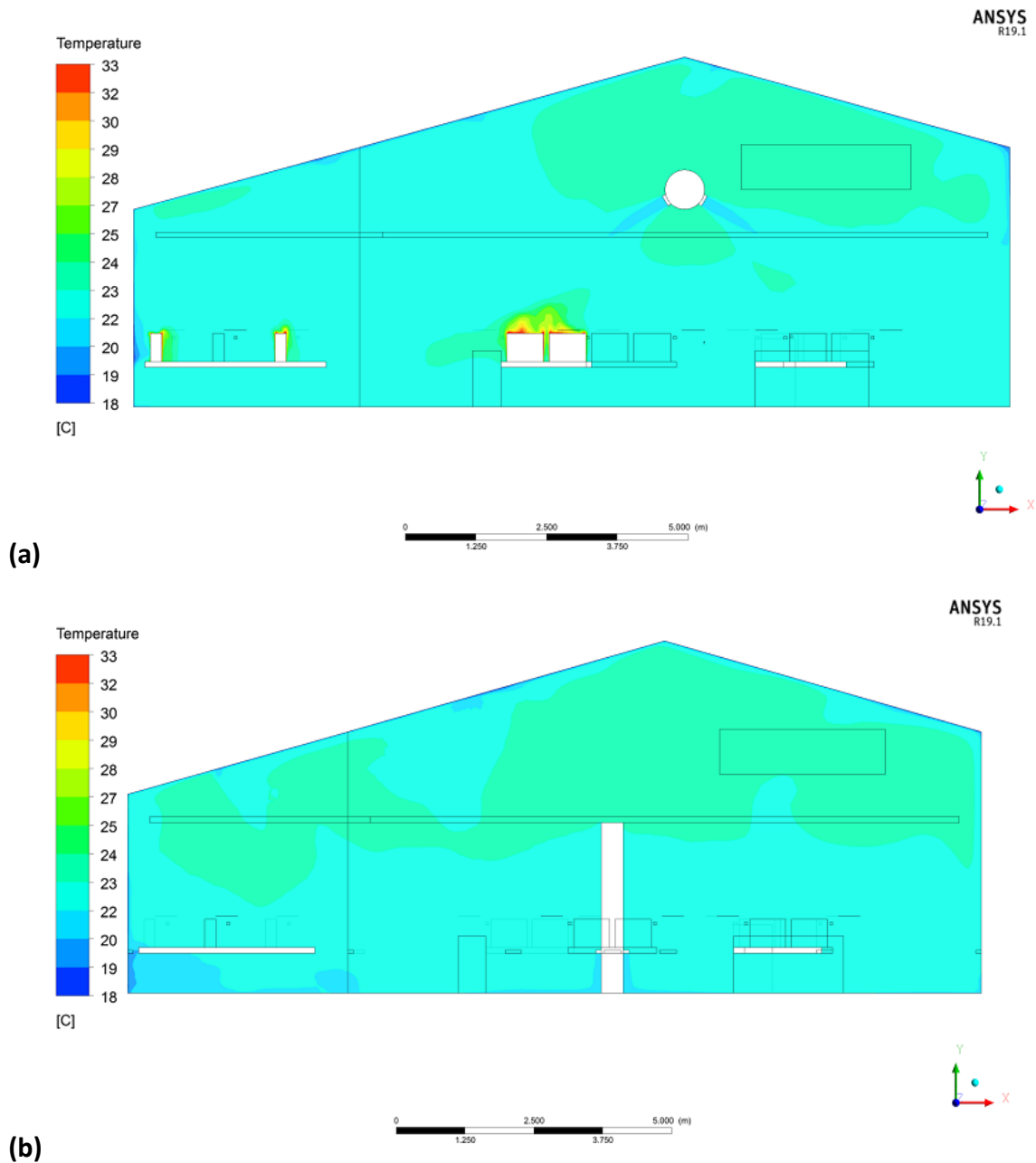


Figure 7.21 Temperature contour plots on a lateral plane located in the middle of the office for Case H-W: (a) MV system at  $Z=6.6\text{m}$  and (b) IJV system at  $Z=7.2\text{m}$ .

In a plane located in the middle of the office, the temperature distribution for the MV and IJV systems are illustrated in Figure 7.21 (a) and (b), respectively. A down draught caused by the cold ceiling and window occurs along the south wall creating a thermal discomfort near that wall as seen in both plots. Thermal plumes above the computers are observed as in Figure 7.21 (a). A higher temperature in the upper zone than in the lower zone is observed for the IJV system's profile compared with MV system's profile. This explains why the value of the overall ventilation for heat removal for the IJV system 1.83 was higher than for the MV system 1.18.

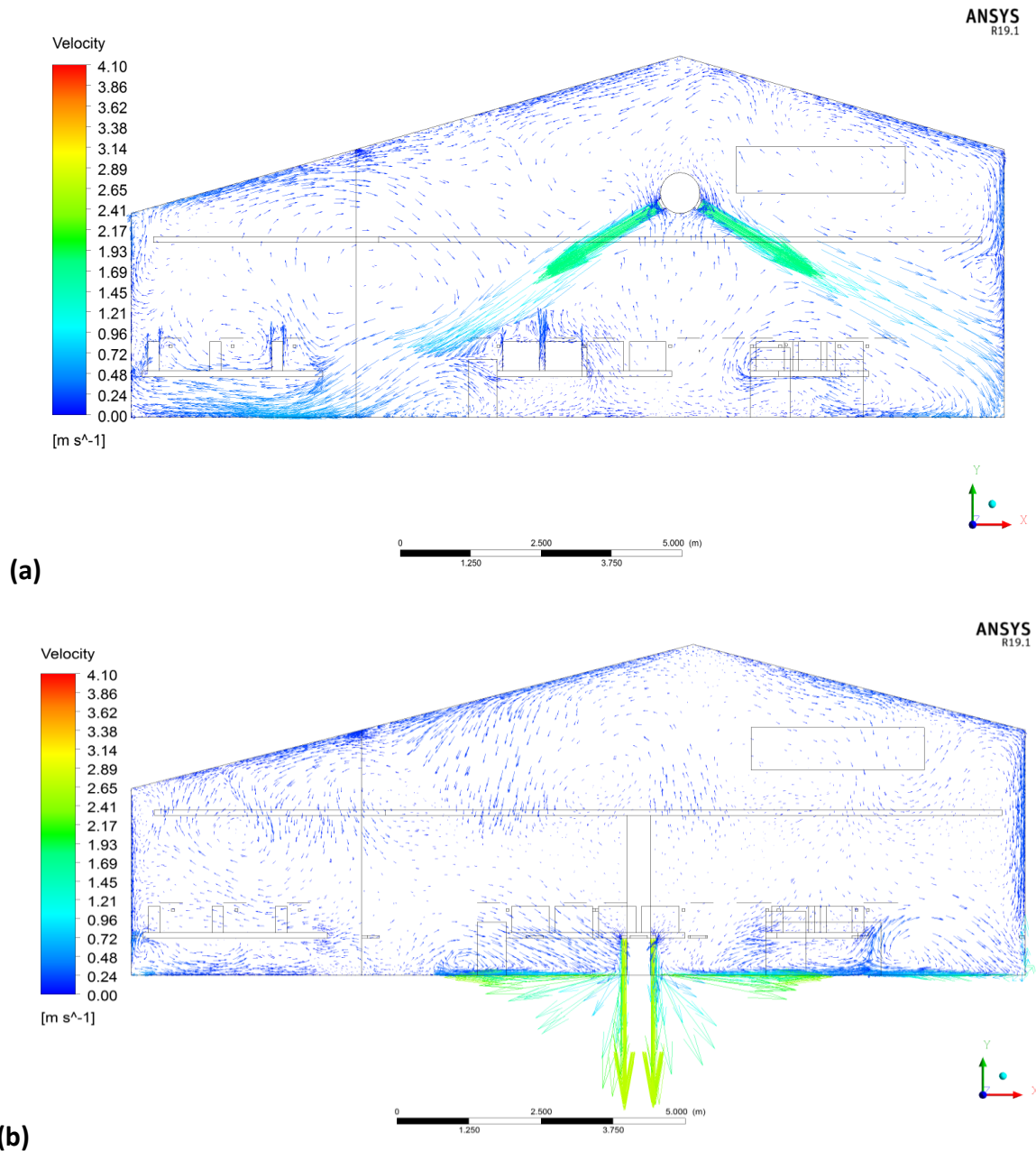
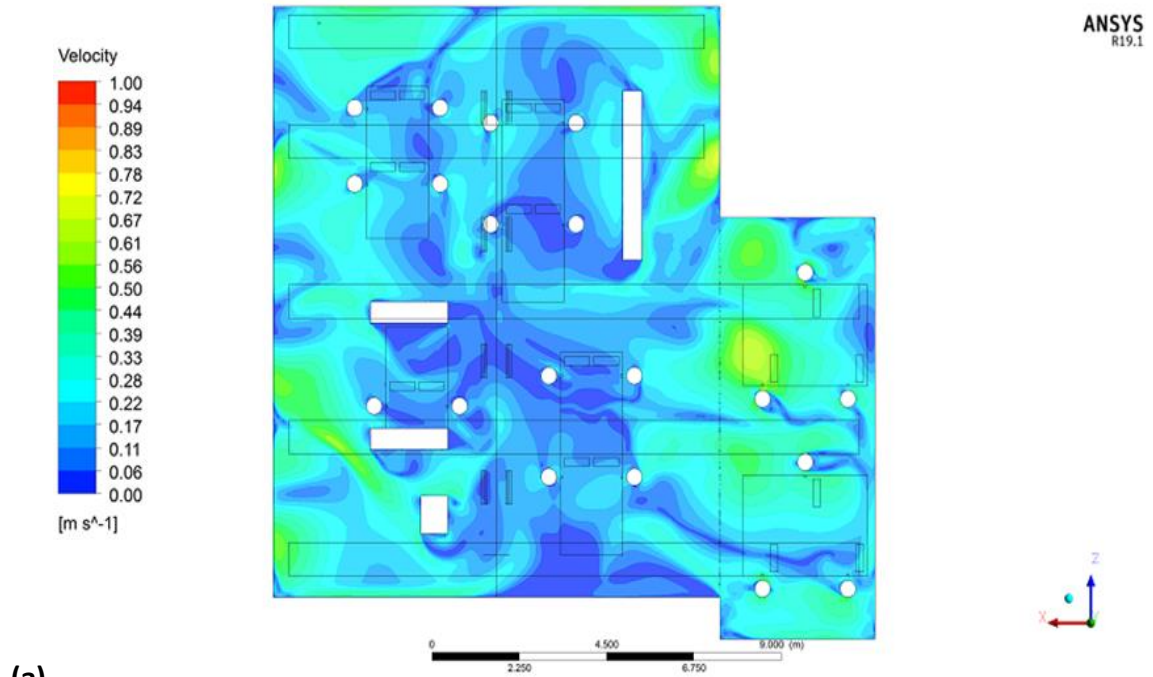
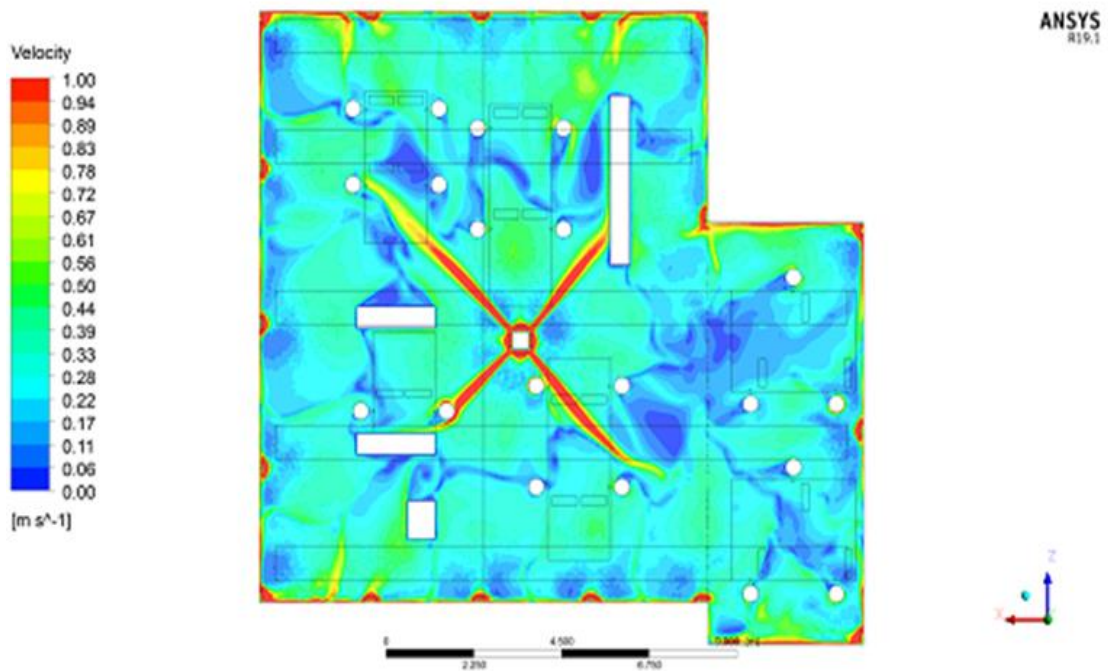


Figure 7.22 Velocity vector plots on a lateral plane located in the middle of the office for Case H-W: (a) MV system at  $Z=6.6$  m and (b) IJV system at  $Z=7.2$  m.

As can be seen in Figure 7.22 (a), an intense mixing occurs between the supplied air and the surrounding air in the whole ventilated office resulting in a uniform air temperature distribution along the height of the office for the MV system. On the other hand, in the IJV system, the supplied air is impinged onto the floor with high momentum and it spreads along the floor resulting in a uniform air temperature distribution in the occupied zone, and this is a significant advantage of the IJV system. The mean air velocity in the occupied area for the MV system is slightly higher than that for the IJV system. This is because of the relatively high supply velocities for the MV system that reaches some parts of the occupied zone.



(a)



(b)

Figure 7.23 Velocity contour plots on a plane at a high  $Y=0.1$  m for Case H-W: (a) MV system and (b) IJV system.

Figure 7.23 (a) and (b) show the velocity contour on a horizontal plane at a height  $Y=0.1$  m for the MV and IJV system, respectively. Several regions have relatively high air velocity since the supplied air reaches these regions as shown for the MV system. For a single IJV diffuser, which is shown in Figure 7.23 (b), the supplied air impinges on the floor and spreads in the radial direction along the floor then decays as it enters inside the office.

Furthermore, some air is more likely to move along the wall which merges with the air coming from the adjacent IJV diffuser. The merged air moves in a direction along the wall towards the office's occupied zone. Moreover, the generated new jet formed from two adjacent IJV diffusers has significantly stronger momentum which is causing a higher velocity and more extended penetration into the office.

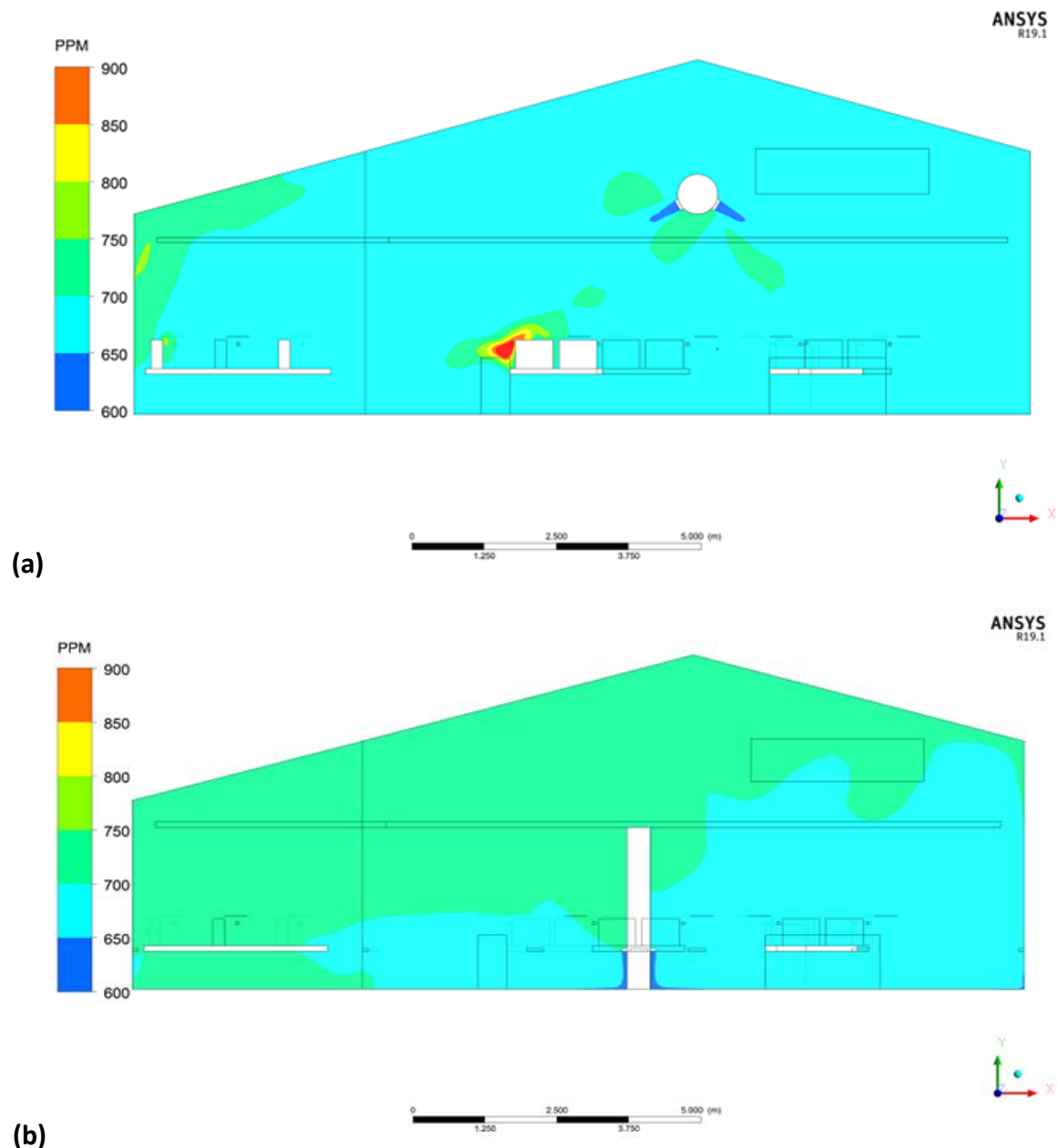


Figure 7.24 CO<sub>2</sub> concentration contours on a lateral plane located in the middle of the office for Case H-W: (a) MV system at Z= 6.6 m and (b) IJV system at Z= 7.2 m

Figure 7.24 (a) and (b) show the CO<sub>2</sub> concentration contours on a vertical plane located in the middle of the office for half occupancy in winter. A uniform CO<sub>2</sub> concentration can be seen in Figure 7.24 (a) for the MV system due to a good air mixing in the office. The CO<sub>2</sub> concentration

in the region near the window is relatively high. This is due to the downward acceleration of the high CO<sub>2</sub> concentration air in the upper zone by the downdraught when passing along cold ceiling and window. Though, the value for  $\bar{\varepsilon}_c$  for the MV and IJV systems are relatively similar (see Table 7.12).

Table 7.12 shows the predicted ADI parameters for the MV and IJV systems for case H-W.

Table 7.12 The predicted ADI for case H-W

Distribution system		MV	IJV
Flow rate (m <sup>3</sup> /s)		1.7	1.7
Diffusers	Number	8	21
	Area (m <sup>2</sup> )	0.12	0.03
	Velocity ( m/s)	1.8	2.7
	Temperature (°C)	21	21
	CO <sub>2</sub> (ppm)	652	652
$\bar{\varepsilon}_c$		1.22	1.4
PD (%)		15.2	15.2
$N_c$		8.0	9.2
$\bar{\varepsilon}_t$		1.18	1.83
PPD (%)		6	5
$N_t$		20.0	36.6
<b>ADI</b>		12.6	18.3

The predicted average PPD values for both systems are quite low up to 6%, though the value of  $\bar{\varepsilon}_t$  for the IJV system was slightly higher than that for the MV systems as shown in the table. Thus, the air distribution number for thermal comfort is higher for the IJV system by 1.8 times than that for the MV system. Hence, the highest value of the ADI was obtained from the IJV system (see table 7.12).

### 7.3.5 Discussion of Results

The findings were consistent with those of similar studies found in the literature which were conducted in typical spaces.

A study was carried out by Karimipanah, Sandberg and Awbi (2000) to compare the performance of four air distribution systems including MV and IJV in a full-size class room. The results implied that the IJV system has a higher ventilation effectiveness value than the

MV system. Cho, Awbi and Karimipannah (2002) conducted a study to test experimentally and numerically the performance of four different ventilation systems; MV, IJV, DV (wall displacement) and DF (floor displacement). The experiments were carried out in the environmental chamber of the University of Reading with two heat loads 36 W/m<sup>2</sup> and 60 W/m<sup>2</sup>. The results revealed that the IJV system has higher ventilation effectiveness for both contaminant removal and heat removal than the MV system for both heat loads. Also,  $N_t$  and  $N_c$  for the IJV system for both heat loads were higher than those for the MV system. Another study by Karimipannah, Awbi and Moshfegh (2008) was carried out to evaluate the thermal and air quality effectiveness in a room for four different ventilation systems, including the MV and the IJV. They found that the highest value of the effectiveness  $\epsilon_t$  and  $\epsilon_c$  were generated by the IJV compared to MV. Also, they found higher air flow rate was required for the MV than that for the IJV system for achieving the same ADI value. Thus, the MV system is more energy intensive than the IJV since the flow rate is related to the fan power consumption and the energy required to condition the supply air.

## 7.4 CHAPTER SUMMARY

Four different CFD conditions were used to compare the performance of the systems MV and IJV. The first case was full occupancy load for summer named Case F-S and the second was for winter, which was named Case F-W. The third and fourth cases were half occupancy load for summer and winter and named Case H-S and Case H-W respectively. The ventilation performance of these systems were examined by applying the Air Distribution Index for the first time in large spaces. Based on the results obtained, the IJV system performed better than the MV system for all the test conditions considered as it provided higher ADI values. Also, it was observed that as the internal heat load decreases, the ventilation performance generally improved except for the MV system in winter which stayed the same; ADI value was 12.6 for both winter cases F-W and H-W. The IJV system performed better in the summer than in the winter (knowing that it was a cooling condition not heating) for both full and half occupancy loads. Since the occupied zone temperature was maintained at 22°C, the IJV system performed better than the MV system where the air supply temperature for the IJV system was higher by 1 °C than that for the MV system for both summer cases, and it was the same for winter cases. Thus, the IJV system uses less power than the MV system while still perform better.

# 8 CHAPTER EIGHT: CONCLUSIONS AND RECOMMENDATIONS FOR FUTURE WORK

---

## 8.1 INTRODUCTION

The thesis aimed to study, experimentally and computationally, the air distribution in large spaces and apply the Air Distribution Index for assessing the performance of ventilation systems used in such spaces. The ADI is an important index combining the level of thermal comfort, indoor air quality and consequently the energy performance provided by an air distribution system. This index has been applied to typical occupied spaces but not so extensively to large spaces. A second aim of the research was to examine the performance of a novel ventilation system, which is the impinging jet ventilation, in large spaces numerically and compare its performance with the typical mixing ventilation system, which is widely used.

The research was carried out in three stages, which were: measurements, simulations and parametric studies with performance comparisons.

The objectives stated at the start of this thesis were fulfilled as follows:

### Objective 1- Case Study:

An existing large space building ventilated with a mixing system was monitored, and the results were presented in chapters 4 and 5 to understand the airflow pattern, temperature distribution, thermal comfort and indoor air quality.

### Objective 2 – Thermal Comfort Models:

The capabilities of different thermal comfort models in predicting human responses in large space for different seasons were investigated in chapter 5.

### Objective 3 – CFD Simulations:

A 3-D CFD model for the large space used in this research was developed and evaluated (chapter 6) to investigate its capability for the prediction air temperature, air velocity and CO<sub>2</sub> concentration.

#### Objective 4 – Air Distribution:

Various airflow distribution strategies used in large spaces for providing thermal comfort, indoor air quality and energy consumption were investigated. However, the most suitable one, which is the IJV system, was selected for this research.

#### Objective 5 – Ventilation Performance:

The performance of two different ventilation systems (Impinging jet and mixing) in providing acceptable indoor environment was compared numerically for a large space (chapter 7). The effects of two different occupancy capacity loads for summer and winter conditions were used for this comparison.

## 8.2 CONCLUSIONS

This research was performed in three stages, which were: measurements, simulations and parametric studies with performance comparisons. The measurements' stage focused on understanding the airflow pattern, temperature variation and thermal comfort in the large space case-study building, CSEF. This stage was performed in three different phases; long-term measurements during the summer of 2016 and 2017, spot detailed measurements during the slot time periods in summer 2016, 2017 and 2018 and occupant questionnaire surveys only in summer 2017. The long-term measurements phase included measuring the air temperature and relative humidity at different heights in a number of locations in the occupied zone, as well as in the area above the occupied zone for one month in summer 2016 and three months in summer 2017. The spot detailed measurement phase involved measurements of air temperature, air speed and relative humidity for seven different spots which were chosen to represent typical positions of occupants for five days in summer 2016 and three days in summer 2017. At each spot, the measurements were taken at heights of 0.1m (foot level), 1.2m (head of a seated individual) and 1.8m (head of a standing individual) above the floor. For summer 2018, similar measurements for air temperature and air speed

was carried out as well as CO<sub>2</sub> concentration for use in evaluating the CFD model. The occupant questionnaire surveys phase included a collection of data for three days in summer 2017 using questionnaires provided in ISO 10551 and guided by recent literature. The questionnaire was developed to assess the thermal environment based on the occupants' thermal sensation votes, thermal preference votes, air movement in the office as well as the freshness of air which was used to assess the air quality inside the office.

Data gathered from measurements enabled the development and evaluation of CFD models to perform simulations of air flow and temperature variations in the case-study building for summer 2016, summer 2017 and for CO<sub>2</sub> concentration as well for summer 2018 using ANSYS Fluent software. Non-uniform grid strategy was used to cover the whole computational domain for the office. A grid independency study was performed using three densities for each of the three models. Two recommended turbulence models, RNG k- $\epsilon$  and SST k- $\omega$ , were used in the CFD model to compare their performance using the temperature and air velocity measurements. Also, the measurements were used to define the boundary conditions needed to produce an accurate numerical solution. To evaluate the CFD models for summer 2016 and summer 2017, comparisons of the mean air velocity and temperature profiles were performed between the simulation results and experimental data at different selected office locations. For the summer 2018 CFD model, similar spots were used to evaluate the CO<sub>2</sub> concentration results with measurements.

The last stage of the research work was the parametric study with performance comparisons using the simulation tool (CFD models) since it was found to be faster and more economical compared to experimental measurements which are also quite expensive and time-consuming. Therefore, these CFD models were further implemented to assess the performance of two different air distribution systems, i.e. mixing and impinging jet. The performance of these two ventilation systems was examined under two occupancy capacity loads, full and half occupancy for summer and winter conditions. Four different cases were generated; Case F-S (full load occupancy for summer), Case F-W (full load occupancy for winter), Case W-S (half load occupancy for summer) and Case H-W (half load occupancy for winter).

The air distribution index which combines several parameters such as overall ventilation effectiveness for removing pollutants and for temperature distribution, percentage of dissatisfied for air quality and predicted percentage of dissatisfied was used to evaluate the performance of these two ventilation systems.

The conclusions drawn from the measurements' stage can be summarised as follows:

- a. The data from the long-term measurements phase which was used to evaluate the indoor thermal comfort showed that the regression slopes between the indoor operative temperature and outdoor air temperature for the case-study building for both summer 2016 and 2017 were similar to the regression slope of published results for free-running buildings. Hence, the case-study building can be treated as FR building, although it has a mechanical ventilation system. This is in agreement with literature which suggests that the thermal performance of mechanically ventilated buildings could be assessed using the adaptive thermal comfort model.
- b. The questionnaire surveys' results showed that the occupants were generally neutral in their assessment of the space. This is in agreement with the spot measurements which indicated conditions within the thermal comfort range as recommended by ISO 7730. However, a high percentage of occupants claimed that the air movement was not acceptable in all the assessed days during the summer of 2017.
- c. In general, the existing ventilation system in this case-study building was able to meet the requirement for thermal comfort for most of the time in terms of temperature and humidity. However, with regards to the air movement, this did not achieve the recommended and desired levels, and this has also been indicated by the occupants during the survey.

The results of the simulations indicated the following conclusions:

- a. Both RNG k- $\epsilon$  and SST k- $\omega$  turbulence models were capable of capturing the main flow features when results were compared with the experimental findings. However, the prediction from SST k- $\omega$  model were slightly better for the mean velocity values.
- b. Very close agreement was achieved between the predicted and measured values during evaluation.

Based on the results acquired from all the modelling test conditions, the conclusions that can be drawn are as follows:

- a. The IJV system showed better air quality and thermal comfort when compared with those for the MV system and thus produced higher ADI values. Table 8.1 presents the summary of the calculations for the four cases.

Table 8.1 The predicted ADI for the four cases

Cases		Case F-S		Case F-W		Case H-S		Case H-W	
<b>Distribution system</b>		MV	IJV	MV	IJV	MV	IJV	MV	IJV
<b>Flow rate (m<sup>3</sup>/s)</b>		2.6	2.6	2.6	2.6	1.7	1.7	1.7	1.7
<b>Diffusers</b>	Number	8	21	8	21	8	21	8	21
	Area (m <sup>2</sup> )	0.12	0.03	0.12	0.03	0.12	0.03	0.12	0.03
	Velocity ( m/s)	2.7	4.1	2.7	4.1	1.8	2.7	1.8	2.7
	Temperature (°C)	18	19	20	20	19	20	21	21
	CO <sub>2</sub> (ppm)	745	745	745	745	652	652	652	652
$\bar{\epsilon}_c$		1.17	1.78	1.1	1.4	1.16	2.35	1.22	1.4
<b>PD (%)</b>		15.2	15.2	15.2	15.2	15.2	15.2	15.2	15.2
$N_c$		7.7	11.7	7.2	9.3	7.63	15.4	8.0	9.2
$\bar{\epsilon}_t$		1.5	2.23	1.1	1.36	1.75	3.5	1.18	1.83
<b>PPD (%)</b>		40	31	5	5	26	24	6	5
$N_t$		3.75	7.2	22	27.2	6.73	14.6	20.0	36.6
<b>ADI</b>		5.37	9.18	12.6	15.9	7.17	15.0	12.6	18.3

- b. It was noticed that generally, the performance of the two ventilation systems was enhanced when the internal heat load decreased, excluding the MV system in winter which stayed the same; ADI value was 12.6 for both winter Cases F-W and Case H-W.
- c. For the winter condition, since the generated internal heat loads were higher than the external heat loss, both winter Cases F-W and H-W became cooling conditions rather than heating.
- d. For the full and half occupancy capacity loads, the best performance for both ventilation systems was found in the winter rather than the summer.
- e. The IJV system performed better than the MV system in terms of the energy consumption since the air supply temperature for the IJV system was higher by 1°C than that for the MV system for both summer cases.

- f. In general, the ADI concept presented in this work could be a beneficial tool for evaluating a ventilation system performance in large spaces as it provides assessments for both air quality and thermal comfort.

This study was conducted for a large space in the moderate climate of the UK. However, more extreme conditions could be considered to assess the performance of such air distribution systems.

### 8.3 RECOMMENDATIONS FOR FUTURE WORK

The recommendations for future work can be summaries as follow:

- a. The ADI investigation in this work was only carried out for two types of ventilation systems in large enclosures which were mixing and impinging jet. However, other types of air distribution systems such as confluent jet ventilation CJV system should be considered and tested in large spaces for its performance using the ADI index.
- b. Examination of the two systems, i.e. mixing and impinging jet, in different kinds of large space buildings such as exhibition hall, shopping mall and airport terminals with different occupancy patterns.
- c. The effect of different return grille locations on the performance of different ventilation system should be considered in such large enclosures. For example, two different return grille heights should be considered. One grille could be located at the end of the occupant zone, i.e. 1.8m, where air at that level could be used as a recirculated air. The second grille could be located at a height near the ceiling to discharge the accumulated stagnant air in that area.

## References

- Al-ajmi, F. F. (2010) 'Thermal comfort in air-conditioned mosques in the dry desert climate', *Building and Environment*. 45(11), pp. 2407–2413. doi: 10.1016/j.buildenv.2010.05.003.
- Almesri, I. F. and Awbi, H. B. (2011) 'Predictions of thermal comfort in stratified room environment', *Building Simulation*, 4(2), pp. 169–180. doi: 10.1007/s12273-011-0036-5.
- American Society of Heating, R. and A.-C. E. (2016) *Standard 62.1 User's Manual: Based on ANSI/ASHRAE Standard 62.1-2016, Ventilation for Acceptable Indoor Air Quality*. ASHRAE.
- Anderson, D. A., Tannehill, J. C. and Pletcher, R. H. (1997) *Computational fluid mechanics and heat transfer*. Taylor & Francis.
- Anderson, J. D. (1995) *Computational fluid dynamics :the basics with applications*, McGraw-Hill. doi: 10.1017/CBO9780511780066.
- ANSYS Fluent (2016) 'Thory guide'. ANSYS Inc.,.
- Ashrae (2010) 'ANSI/ASHRAE 55-2010 : Thermal Environmental Conditions for Human Occupancy', *ASHRAE*, p. 30. doi: 10.1007/s11926-011-0203-9.
- Astronautics, A. I. of A. and (1998) *AIAA guide for the verification and validation of computational fluid dynamics simulations*. American Institute of aeronautics and astronautics.
- Awbi, H. (2003) *Ventilation of buildings*. doi: 10.1080/02786820490519234.
- Awbi, H. B. (1989) 'Application of computational fluid dynamics in room ventilation', *Building and environment*. 24(1), pp. 73–84.
- Awbi, Hazim B. (1998) 'Calculation of convective heat transfer coefficients of room surfaces for natural convection', *Energy and Buildings*, 28(2), pp. 219–227. doi: 10.1016/S0378-7788(98)00022-X.
- Awbi, H B (1998) 'Energy efficient room air distribution', *Renewable Energy*. 15(1), pp. 293–299.
- Awbi, H. B. (2008) 'Assessing the performance of room air distribution systems', in *Proceedings of Conference on Efficient Building*. Faro, Portugal, pp. 1–8.
- Awbi, H. B. and Gan, G. (1993) 'Evaluation of the overall performance of room air distribution', in *Proceedings of the 6th International Conference on Indoor Air Quality and*

*Climate, Helsinki*, pp. 283–288.

Baldwin, B. and Barth, T. (1990) 'A one-equation turbulence transport model for high Reynolds number wall-bounded flows', in. doi: 10.2514/6.1991-610.

Bergman, T. L. *et al.* (2011) *Fundamentals of heat and mass transfer*. John Wiley & Sons.

BS EN 15251 (2007) 'Indoor environmental input parameters for design and assessment of energy performance of buildings- addressing indoor air quality , thermal environment , lighting and acoustics Contents', 3(BS EN 15251), pp. 1–50.

BS EN 16798-1 (2019) *Energy performance of buildings — Ventilation for buildings Part 1: Indoor environmental input parameters for design and assessment of energy performance of buildings addressing indoor air quality, thermal environment, lighting and acoustics - Module M1-6*.

BS EN 16798-3 (2017) *Energy performance of buildings — Ventilation for buildings Part 3: For non-residential buildings - Performance requirements for ventilation and room-conditioning systems (Modules M5-1, M5-4)*.

BS EN ISO-16000-26 (2012) *Indoor air- Part 26 :Sampling strategy for carbon dioxide (CO2)*. doi: 10.1017/cbo9780511844652.021.

BSI (2005) 'BS EN ISO 7730: 2005: Ergonomics of the thermal environment Analytical determination and interpretation of thermal comfort using calculation of the PMV and PPD indices and local thermal comfort criteria', *Management*, 3, pp. 605–615. doi: 10.1016/j.soildyn.2004.11.005.

BSI (2019) 'BS EN 16798-1: 2019: Energy performance of buildings - Ventilation for buildings- Part 1:Indoor environmental input parameters for design and assessment of energy performance of buildings addressing indoor air quality, thermal environment, lighting and acoustics', (BS EN 16798-1).

Buratti, C. and Ricciardi, P. (2009) 'Adaptive analysis of thermal comfort in university classrooms: Correlation between experimental data and mathematical models', *Building and Environment*. 44(4), pp. 674–687. doi: 10.1016/j.buildenv.2008.06.001.

Calay, R. K., Borresen, B. A. and Holdø, A. E. (2000) 'Selective ventilation in large enclosures', *Energy and Buildings*, pp. 281–289. doi: 10.1016/S0378-7788(00)00054-2.

Carrier (2010) 'hourly analysis program and system design load program'. NY: Syracuse.

- Chen, H. J., Moshfegh, B. and Cehlin, M. (2012) 'Numerical investigation of the flow behavior of an isothermal impinging jet in a room', *Building and Environment*, 49(1), pp. 154–166. doi: 10.1016/j.buildenv.2011.09.027.
- Chen, H.J., Moshfegh, B. and Cehlin, M. (2012) 'Numerical investigation of the flow behavior of an isothermal impinging jet in a room', *Building and Environment*, 49, pp. 154–166. doi: 10.1016/j.buildenv.2011.09.027.
- Chen, H. J., Moshfegh, B. and Cehlin, M. (2013) 'Investigation on the flow and thermal behavior of impinging jet ventilation systems in an office with different heat loads', *Building and Environment*, 59, pp. 127–144. doi: 10.1016/j.buildenv.2012.08.014.
- Chen, Q. and Srebric, J. (2011) 'A Procedure for Verification, Validation, and Reporting of Indoor Environment CFD Analyses', *HVAC&R Research*, 8(2), pp. 201–216. doi: 10.1080/10789669.2002.10391437.
- Chen, Q. and Xu, W. (1998) 'A zero-equation turbulence model for indoor airflow simulation', *Energy and buildings*, 28(2), pp. 137–144.
- Cheong, K. W. D. *et al.* (2003) 'Thermal comfort study of an air-conditioned lecture theatre in the tropics', *Building and Environment*, 38(1), pp. 63–73. doi: 10.1016/S0360-1323(02)00020-3.
- Cheong, K. W. D. and Lau, H. Y. T. (2003) 'Development and application of an indoor air quality audit to an air-conditioned tertiary institutional building in the tropics', *Building and Environment*, 38(4), pp. 605–616. doi: 10.1016/S0360-1323(02)00183-X.
- Cho, Y., Awbi, H. B. and Karimipanah, T. (2002) 'A comparison between four different ventilation systems', in *Proceeding of Roomvent 2002*. Copenhagen, Denmark, pp. 181–184. doi: 10.2307/3405502.
- CIBSE (2008) 'Current and Future CIBSE TRY/DSY Hourly Weather Data Set–14 sites [CD-ROM]'. The Chartered Institution of Building Services Engineers London.
- CIBSE (2013) 'The limits of thermal comfort : avoiding overheating in European buildings', *CIBSE Tm52*, pp. 1–25. doi: 10.1017/CBO9781107415324.004.
- CIBSE (2015) *CIBSE Guide A: Environmental Design*, CIBSE Publications. doi: 10.1016/0360-1323(94)00059-2.
- Commission, E. (2018) *Energy Performance of Buildings*. doi:

10.1108/ss.2005.11023aab.001.

Commission, H. and safety (1992) *Workplace Health, Safety and Welfare. Workplace (Health, Safety and Welfare) Regulations 1992. Approved Code of Practice and Guidance.* HM Stationery Office.

D'Agostino, D. and Congedo, P. M. (2014) 'CFD modeling and moisture dynamics implications of ventilation scenarios in historical buildings', *Building and Environment*. 79, pp. 181–193. doi: 10.1016/j.buildenv.2014.05.007.

Davidson, L. and Nielsen, P. V (1996) 'Large eddy simulations of the flow in a three-dimensional ventilated room'. Institutet for Bygningsteknik, Aalborg Universitet.

Denman, A. R., Crockett, R. G. M. and Groves-Kirkby, C. J. (2018) 'An assessment of the effectiveness of UK building regulations for new homes in Radon Affected Areas', *Journal of environmental radioactivity*. 192, pp. 166–171.

Fadeyi, M. O., Weschler, C. J. and Tham, K. W. (2009) 'The impact of recirculation, ventilation and filters on secondary organic aerosols generated by indoor chemistry', *Atmospheric Environment*. 43(22–23), pp. 3538–3547.

Fanger, P. O. (1967) 'Calculation of thermal comfort-introduction of a basic comfort equation', *ASHRAE Transactions*, 73.

Fanger, P. O. (1970) *Thermal comfort: Analysis and applications in environmental engineering.*, *Thermal comfort. Analysis and applications in environmental engineering.*

Available at:

<http://www.cabdirect.org/abstracts/19722700268.html%5Cnpapers2://publication/uuid/5CE163C3-F9AC-4937-A143-1238F1D806C5>.

Fanger, P. O. (1972) 'Thermal comfort, analysis and application in environmental engineering', *New York, McGraw-Hill*.

Fanger, P. O. (1988) 'Introduction of the olf and the decipol units to quantify air pollution perceived by humans indoors and outdoors', *Energy and Buildings*, 12(1), pp. 1–6. doi: 10.1016/0378-7788(88)90051-5.

Fanger, P. O. (2000) 'Provide good air quality for people and improve their productivity', *Air Distribution in Rooms, (ROOMVENT 2000, Editor: HB Awbi)*, 1, pp. 1–5.

Fathollahzadeh, M. H., Heidarinejad, G. and Pasdarsahri, H. (2016) 'Producing a better

performance for the under floor air distribution system in a dense occupancy space', *Energy and Buildings*. 126, pp. 230–238. doi: 10.1016/j.enbuild.2016.05.008.

Ferziger, J. H. and Peric, M. (2012) *Computational methods for fluid dynamics*.

Fiala, D. (1998) 'Dynamic simulation of human heat transfer and thermal comfort.', *Thesis*, (January 1998). Available at: <https://www.dora.dmu.ac.uk/xmlui/handle/2086/4129>.

Gagge, A. P., Fobelets, A. P. and Berglund, L. G. (1986) 'STANDARD PREDICTIVE INDEX OF HUMAN RESPONSE TO THE THERMAL ENVIRONMENT.', in *ASHRAE Transactions*, pp. 709–731.

Geng, Y. *et al.* (2017) 'The impact of thermal environment on occupant IEQ perception and productivity', *Building and Environment*. 121, pp. 158–167.

Gładyszewska-Fiedoruk, K. (2011) 'Analysis of stack ventilation system effectiveness in an average kindergarten in north-eastern Poland', *Energy and Buildings*. 43(9), pp. 2488–2493.

Hackley, B., Feinstein, A. and Dixon, J. (2007) 'Air pollution: impact on maternal and perinatal health', *Journal of midwifery & women's health*. 52(5), pp. 435–443.

Hangan, H. *et al.* (2001) 'Case study: Numerical simulations for comfort assessment and optimization of the ventilation design for complex atriums', *Journal of Wind Engineering and Industrial Aerodynamics*, 89(11), pp. 1031–1045. doi: 10.1016/S0167-6105(01)00097-6.

Heiselberg, P., Murakami, S. and Roulet, C. (1998) 'Ventilation of large spaces in buildings', *Final Report IEA Annex*. Available at: <http://citeseerx.ist.psu.edu/viewdoc/download?doi=10.1.1.121.2480&rep=rep1&type=pdf>.

HOBO (no date) *Onset HOBO and InTemp Data Loggers*. Available at: <http://www.onsetcomp.com/> (Accessed: 16 May 2017).

Al horr, Y. *et al.* (2016) 'Impact of indoor environmental quality on occupant well-being and comfort: A review of the literature', *International Journal of Sustainable Built Environment*. doi: 10.1016/j.ijbsbe.2016.03.006.

Huizenga, C. *et al.* (2006) 'Air quality and thermal comfort in office buildings: results of a large indoor environmental quality survey'.

Huizenga, C., Hui, Z. and Arens, E. (2001) 'A model of human physiology and comfort for assessing complex thermal environments', *Building and Environment*, 36(6), pp. 691–699. doi: 10.1016/S0360-1323(00)00061-5.

Humphreys, M. A., Rijal, H. B. and Nicol, J. F. (2013) 'Updating the adaptive relation between climate and comfort indoors; new insights and an extended database', *Building and Environment*. 63, pp. 40–55. doi: 10.1016/j.buildenv.2013.01.024.

Ingersoll, J. G. *et al.* (1992) *Automobile passenger compartment thermal comfort model-Part II: Human thermal comfort calculation*. SAE Technical Paper.

International Energy Agency (IEA) (1998) 'IEA Annex 26: Energy Efficient Ventilation of Large Enclosures - Technical Synthesis Report'.

International Energy Agency (IEA) (2018) *Energy Efficiency: Buildings*. Available at: <https://www.iea.org/topics/energyefficiency/buildings/> (Accessed: 9 July 2019).

Jurelionis, A. and Seduikyte, L. (2008) 'Thermal comfort conditions and air distribution in educational buildings', in *The 11th International Conference on Indoor Air Quality and Climate*. Copenhagen, Denmark, p. Paper ID:319.

Karimipannah, Taghi. and Awbi, H. B. (2002) 'Theoretical and experimental investigation of impinging jet ventilation and comparison with wall displacement ventilation', *Building and Environment*, 37, pp. 1329–1342. doi: 10.1016/S0360-1323(01)00117-2.

Karimipannah, Taghi, Awbi, H. B. and Moshfegh, B. (2008) 'The air distribution index as an indicator for energy consumption and performance of ventilation systems', *Journal of the Human-Environment System*. Japanese Society of Human-Environment System, 11(2), pp. 77–84.

Karimipannah, T., Awbi, H. B. and Moshfegh, B. (2008) 'The Air Distribution Index as an Indicator for Energy Consumption and Performance of Ventilation Systems', *Journal of the Human-Environment System*, 11(2), pp. 77–84. doi: 10.1618/jhes.11.77.

Karimipannah, T., Sandberg, M. and Awbi, H. B. (2000) 'A comparative study of different air distribution systems in a classroom', in *Proceedings of the Roomvent*, pp. 1013–1018.

Kavgic, M. *et al.* (2008) 'Analysis of thermal comfort and indoor air quality in a mechanically ventilated theatre', *Energy and Buildings*, 40(7), pp. 1334–1343. doi: 10.1016/j.enbuild.2007.12.002.

Kukadia, V. and Upton, S. (2019) 'Ensuring good indoor air quality in buildings', *BRE Trust*.

Launder, B. E. and Spalding, D. B. (1972) *Mathematical models of turbulence*. Academic press.

- Lei, L., Wang, S. and Zhang, T. (2014) 'Inverse determination of wall boundary convective heat fluxes in indoor environments based on CFD', *Energy and Buildings*. 73, pp. 130–136. doi: 10.1016/j.enbuild.2013.12.056.
- Li, Q. *et al.* (2009) 'CFD study of the thermal environment in an air-conditioned train station building', *Building and Environment*. 44(7), pp. 1452–1465. doi: 10.1016/j.buildenv.2008.08.010.
- Liz, W. (2018) *ENERGY CONSUMPTION IN THE UK*. Available at: [https://assets.publishing.service.gov.uk/government/uploads/system/uploads/attachment\\_data/file/729317/Energy\\_Consumption\\_in\\_the\\_UK\\_\\_ECUK\\_\\_2018.pdf](https://assets.publishing.service.gov.uk/government/uploads/system/uploads/attachment_data/file/729317/Energy_Consumption_in_the_UK__ECUK__2018.pdf) (Accessed: 9 July 2019).
- MacIntyre, F. (1980) 'The absorption of fossil-fuel CO<sub>2</sub> by the ocean', *Oceanologica Acta*, 3, pp. 505–516.
- Mahyuddin, N. and Awbi, H. (2010) 'The spatial distribution of carbon dioxide in an environmental test chamber', *Building and Environment*. Elsevier, 45(9), pp. 1993–2001.
- Mateus, N. M. and Carrilho da Graça, G. (2017) 'Simulated and measured performance of displacement ventilation systems in large rooms', *Building and Environment*. Elsevier Ltd, 114, pp. 470–482. doi: 10.1016/j.buildenv.2017.01.002.
- McQuiston, F. C. and Parker, J. D. (1982) 'Heating, ventilating, and air conditioning: analysis and design'.
- Menter, F. R. (1994) 'Two-equation eddy-viscosity turbulence models for engineering applications', *AIAA journal*, 32(8), pp. 1598–1605.
- Muhielddeen, M. W., Adam, N. M. and Salman, B. H. (2015) 'Experimental and numerical studies of reducing cooling load of lecture hall', *Energy and Buildings*. 89, pp. 163–169. doi: 10.1016/j.enbuild.2014.12.026.
- Nicol, F. (2017) 'Temperature and adaptive comfort in heated, cooled and free-running dwellings', *Building Research and Information*. 45(7), pp. 730–744. doi: 10.1080/09613218.2017.1283922.
- Nielsen, P. V. (1998) 'Selection of turbulence models for prediction of room airflow', in *ASHRAE Transactions*.
- Nielsen, P. V *et al.* (2007) 'REHVA Guidebook No 10: Computational fluid dynamics in

ventilation design', *REHVA, Forssa, Finland*.

Oke, S. A. *et al.* (2008) 'A mathematical modelling of the intensity of contaminants (CO<sub>2</sub>) on occupancy level of a space in continuous use'. Inderscience Enterprises Limited.

Organization, W. H. (2010) 'WHO guidelines for indoor air quality: selected pollutants'. World Health Organization. Regional Office for Europe.

Patankar, S. (1980) *Numerical heat transfer and fluid flow*.

Patankar, S. V and Spalding, D. B. (1983) 'A calculation procedure for heat, mass and momentum transfer in three-dimensional parabolic flows', in *Numerical Prediction of Flow, Heat Transfer, Turbulence and Combustion*. pp. 54–73.

Pinkel, D. (1958) 'The use of body surface area as a criterion of drug dosage in cancer chemotherapy.', *Cancer research*, 18(3), pp. 853–856.

Ricciardi, P. and Buratti, C. (2015) 'Thermal comfort in the Frascini theatre (Pavia, Italy): Correlation between data from questionnaires, measurements, and mathematical model', *Energy and Buildings*. 99, pp. 243–252. doi: 10.1016/j.enbuild.2015.03.055.

Ricciardi, P., Ziletti, A. and Buratti, C. (2016) 'Evaluation of thermal comfort in an historical Italian opera theatre by the calculation of the neutral comfort temperature', *Building and Environment*. 102, pp. 116–127. doi: 10.1016/j.buildenv.2016.03.011.

Sandberg, M. (1981) 'What is ventilation efficiency?', *Building and environment*. 16(2), pp. 123–135.

Santamouris, M. *et al.* (2008) 'Experimental investigation of the air flow and indoor carbon dioxide concentration in classrooms with intermittent natural ventilation', *Energy and Buildings*. 40(10), pp. 1833–1843.

Seppanen, O., Fisk, W. J. and Lei, Q. H. (2006) *Effect of temperature on task performance in office environment*. Ernest Orlando Lawrence Berkeley National Laboratory, Berkeley, CA (US).

Shah, S. and Dufva, K. (2017) 'CFD modeling of airflow in a kitchen environment: Towards improving energy efficiency in buildings'. Kaakkois-Suomen ammattikorkeakoulu.

Shih, T.-H. *et al.* (1995) 'A new k- $\epsilon$  eddy viscosity model for high Reynolds number turbulent flows', *Computers & Fluids*. 24(3), pp. 227–238.

- Skistad, H. *et al.* (2002) *Displacement ventilation in non-industrial premises. REHVA Guidebook no. 1.* ISBN 82-594-239-3.
- Standard, A. (2017) 'Standard 55–2017 Thermal Environmental Conditions for Human Occupancy', *Ashrae: Atlanta, GA, USA.*
- Taylor, J. (1997) *Introduction to error analysis, the study of uncertainties in physical measurements.*
- Thai, Z. Q. *et al.* (2007) 'Evaluation of various turbulence models in predicting airflow and turbulence in enclosed environments by CFD: part 1 - Summary of prevalent turbulence models' 13(6), pp. 853–870. doi: 10.1080/10789669.2007.10391459.
- Tymkow, P. *et al.* (2013) *Building services design for energy efficient buildings.* Routledge.
- Ürge-Vorsatz, D. *et al.* (2015) 'Heating and cooling energy trends and drivers in buildings', *Renewable and Sustainable Energy Reviews.* 41, pp. 85–98.
- Wargocki, P. *et al.* (2002) 'Air quality in a simulated office environment as a result of reducing pollution sources and increasing ventilation', in *Energy and Buildings.* doi: 10.1016/S0378-7788(02)00096-8.
- Wesseling, P. (2009) *Principles of computational fluid dynamics.*
- Wilcox, D. C. (1988) 'Reassessment of the scale-determining equation for advanced turbulence models', *AIAA journal*, 26(11), pp. 1299–1310.
- Wyon, D. P. *et al.* (1989) 'Standard procedures for assessing vehicle climate with a thermal manikin', *SAE transactions*, 98(6), pp. 46–56. doi: 10.4271/890049.
- Yakhot, V. and Orszag, S. A. (1986) 'Renormalization group analysis of turbulence. I. Basic theory', *Journal of Scientific Computing*, 1(1), pp. 3–51. doi: 10.1007/BF01061452.
- Ye, X. *et al.* (2016) 'Heating energy consumption of impinging jet ventilation and mixing ventilation in large-height spaces: A comparison study', *Energy and Buildings.* 130, pp. 697–708. doi: 10.1016/j.enbuild.2016.08.055.
- Ye, X. *et al.* (2019) 'Comparison study of contaminant distribution and indoor air quality in large-height spaces between impinging jet and mixing ventilation systems in heating mode', *Building and Environment.* p. 106159.
- Zhai, Z. J. *et al.* (2007) 'Evaluation of various turbulence models in predicting airflow and

turbulence in enclosed environments by CFD: Part 1—Summary of prevalent turbulence models’, *Hvac&R Research*. 13(6), pp. 853–870.

Zhang, W. and Chen, Q. (2000) ‘Large Eddy Simulation of Natural and Mixed Convection Airflow Indoors with Two Simple Filtered Dynamic Subgrid Scale Models’, *Numerical Heat Transfer; Part A: Applications*. 37(5), pp. 447–463. doi: 10.1080/104077800274154.

Zhang, Z. *et al.* (2007) ‘Evaluation of various turbulence models in predicting airflow and turbulence in enclosed environments by CFD: Part 2—Comparison with experimental data from literature’, *Hvac&R Research*. 13(6), pp. 871–886.

Zhao, X., Yu, W. and Tan, D. (2017) ‘Thermal Comfort Study Based on Questionnaire Survey among Occupants in Different Climate Zones in China’, *International Journal of Environmental Science and Development*, 8(6), pp. 430–434. doi: 10.18178/ijesd.2017.8.6.992.

Zolfaghari, A. and Maerefat, M. (2010) ‘A new simplified thermoregulatory bioheat model for evaluating thermal response of the human body to transient environments’, *Building and Environment*, 45(10), pp. 2068–2076. doi: 10.1016/j.buildenv.2010.03.002.

# Appendix I: Thermal Comfort and Indoor Air Quality Questionnaire



College of Engineering, Design and Physical Sciences Research Ethics Committee  
Brunel University London  
Kingston Lane  
Uxbridge  
UB8 3PH  
United Kingdom  
www.brunel.ac.uk

24 July 2017

## LETTER OF APPROVAL

Applicant: Mr Ali Alzaid  
Project Title: THERMAL COMFORT AND INDOOR AIR QUALITY QUESTIONNAIRE  
Reference: 7234-LR-Jul/2017- 7915-1

Dear Mr Ali Alzaid

The Research Ethics Committee has considered the above application recently submitted by you.

The Chair, acting under delegated authority has agreed that there is no objection on ethical grounds to the proposed study. Approval is given on the understanding that the conditions of approval set out below are followed:

- The agreed protocol must be followed. Any changes to the protocol will require prior approval from the Committee by way of an application for an amendment.
- The Committee recommends that you complete the Ethics Training module via Blackboard Learn prior to commencing your research project. Please click on the link below and complete the course online.  
[https://blackboard.brunel.ac.uk/webapps/blackboard/content/listContent.jsp?course\\_id= 8579\\_1&content\\_id= 322757\\_1](https://blackboard.brunel.ac.uk/webapps/blackboard/content/listContent.jsp?course_id= 8579_1&content_id= 322757_1)

### Please note that:

- Research Participant Information Sheets and (where relevant) flyers, posters, and consent forms should include a clear statement that research ethics approval has been obtained from the relevant Research Ethics Committee.
- The Research Participant Information Sheets should include a clear statement that queries should be directed, in the first instance, to the Supervisor (where relevant), or the researcher. Complaints, on the other hand, should be directed, in the first instance, to the Chair of the relevant Research Ethics Committee.
- Approval to proceed with the study is granted subject to receipt by the Committee of satisfactory responses to any conditions that may appear above, in addition to any subsequent changes to the protocol.
- The Research Ethics Committee reserves the right to sample and review documentation, including raw data, relevant to the study
- You may not undertake any research activity if you are not a registered student of Brunel University or if you cease to become registered, including abeyance or temporary withdrawal. As a deregistered student you would not be insured to undertake research activity. Research activity includes the recruitment of participants, undertaking consent procedures and collection of data. Breach of this requirement constitutes research misconduct and is a disciplinary offence.

Professor Hua Zhao

Chair

College of Engineering, Design and Physical Sciences Research Ethics Committee  
Brunel University London

## PARTICIPANT INFORMATION SHEET

**Study title:** THERMAL COMFORT AND INDOOR AIR QUALITY QUESTIONNAIRE FOR AN OPEN PLAN OFFICE

### **Invitation Paragraph**

You are being invited to take part in a research study (Questionnaire). Before you decide, it is important for you to understand why the research is being done and what it will involve. Please take the time to read the following information carefully and ask me if there is anything that is not clear or if you would like more information. Take time to decide whether or not you wish to take part.

Thank you for reading this.

### **What is the purpose of the study?**

Thermal sensation and comfort feedback is one of the indices which are used to evaluate the performance of a ventilation system. Consequently, this survey is a part of a study to evaluate the thermal comfort and indoor air quality (IAQ) of this open plan office at CSEF building.

### **Why have been invited to participate?**

Because I feel that you might provide valuable input into the process of evaluating the thermal comfort and IAQ in this office that your views are valuable.

### **Do I have to take part?**

As participation is entirely voluntary, it is up to you to decide whether or not to take part. If you do decide to take part you will be given this information sheet to keep and you are still free to withdraw at any time and without giving a reason.'

### **What will happen to me if I take part?**

You will evaluate thermal comfort and indoor air quality (IAQ) using the questionnaire techniques. You will be involved in this evaluation several times this summer 2017 for just a period of ten minutes.

### **What do I have to do?**

Just answering the questionnaire.

**What are the possible disadvantages and risks of taking part?**

There are no disadvantages or risks in taking part other than a small amount of your time and effort.

**What if something goes wrong?**

The ethical guidelines and procedures put in place will ensure that a) there is very little that can go wrong and if it did would have no impact on any participant.

**Will my taking part in this study be kept confidential?** The data will be anonymized – so that no individual is attributed to any particular view. The data will be aggregated and so it will be impossible to distinguish between participants.

**What will happen to the results of the research study?** Your response will be transferred anonymised to a spreadsheet and the original questionnaire will be destroyed.

**Who is organising and funding the research?** Brunel University.

**What are the indemnity arrangements?** Brunel University provides appropriate insurance cover for research which has received ethical approval.

**Who has reviewed the study?** Brunel University Research Ethics Committee.

- **Passage on Research Integrity**

Brunel University is committed to compliance with the Universities UK Research Integrity Concordat. You are entitled to expect the highest level of integrity from our researchers during the course of their research.'

**Contact for further information:**

College of Engineering, Design and Physical Sciences: [cedps-research@brunel.ac.uk](mailto:cedps-research@brunel.ac.uk)

**Note:** Research ethics approval for this questionnaire has been obtained from the relevant Research Ethics Committee.

Thank you for taking part in this study

# THERMAL COMFORT AND INDOOR AIR QUALITY QUESTIONNAIRE

## FOR AN OPEN PLAN OFFICE

*This survey is part of a study to evaluate the thermal comfort and indoor air quality of the open plan office at CSEF building.*

*Your participation in this survey is much appreciated.*

1.

Gender:  Male  Female

2. How would you feel about the temperature in this moment?

**Head Level**

- Cold
- Cool
- Slightly cool
- Neither hot nor cold
- Slightly warm
- Warm
- Hot

**Foot Level**

- Cold
- Cool
- Slightly cool
- Neither hot nor cold
- Slightly warm
- Warm
- Hot

**Overall**

- Cold
- Cool
- Slightly cool
- Neither hot nor cold
- Slightly warm
- Warm
- Hot

3. How would you like to feel about temperature?

**Head Level**

- Much cooler
- Cooler
- Slightly cooler
- Without change
- Slightly warmer
- Warmer
- Much warmer

**Foot Level**

- Much cooler
- Cooler
- Slightly cooler
- Without change
- Slightly warmer
- Warmer
- Much warmer

**Overall**

- Much cooler
- Cooler
- Slightly cooler
- Without change
- Slightly warmer
- Warmer
- Much warmer

4. How would you describe the air movement at this precise moment?

**Head Level**

- Very still
- Still
- Slightly still
- Acceptable
- Slightly draughty
- Draughty
- Very draughty

**Foot Level**

- Very still
- Still
- Slightly still
- Acceptable
- Slightly draughty
- Draughty
- Very draughty

**Overall**

- Very still
- Still
- Slightly still
- Acceptable
- Slightly draughty
- Draughty
- Very draughty

5. How would you prefer the air movement to be now?

**Head Level**

- Much more air movement
- More air movement
- Slightly more air movement
- Without change
- Slightly less air movement
- Less air movement
- Much less air movement

**Foot Level**

- Much more air movement
- More air movement
- Slightly more air movement
- Without change
- Slightly less air movement
- Less air movement
- Much less air movement

**Overall**

- Much more air movement
- More air movement
- Slightly more air movement
- Without change
- Slightly less air movement
- Less air movement
- Much less air movement



## Appendix II: Boundary Conditions for Case A and Case B

Table 1 Boundary conditions of Case A for the MV system

	Details	Mixing System
Supply air diffusers	Flow rate	4.33 m <sup>3</sup> /s
	Number	8
	Area	0.12 m <sup>2</sup>
	Velocity	4.5 m/s
	Temperature	20°C
	CO <sub>2</sub> concentration	400 ppm
	Ceiling surface temperature	
Internal walls surface temperature		28°C
External wall surface temperature		29°C
Floor heat flux		0 W/m <sup>2</sup>
Windows surface temperature		39°C
Number of occupants		40
Occupants clothing temperature (Zolfaghari and Maerefat, 2010)		33.7°C
Number of personal computers		40
Personal computers surface temperature (Lei, Wang and Zhang, 2014)		40°C
Lighting surface temperature (Lei, Wang and Zhang, 2014)		40°C
Number of photocopiers		1
Photocopier surface temperature (Lei, Wang and Zhang, 2014)		40°C

Table 2 Boundary conditions of Case B for the MV system

	Details	Mixing System
Supply air diffusers	Flow rate	3.05 m <sup>3</sup> /s
	Number	8
	Area	0.12 m <sup>2</sup>
	Velocity	3.17 m/s
	Temperature	20°C
	CO <sub>2</sub> concentration	400 ppm
Ceiling surface temperature		35°C
Internal walls surface temperature		28°C
External wall surface temperature		29°C
Floor heat flux		0 W/m <sup>2</sup>
Windows surface temperature		39°C
Number of occupants		20
Occupants clothing temperature (Zolfaghari and Maerefat, 2010)		33.7°C
Number of personal computers		20
Personal computers surface temperature (Lei, Wang and Zhang, 2014)		40°C
Lighting surface temperature (Lei, Wang and Zhang, 2014)		40°C
Number of photocopiers		1
Photocopier surface temperature (Lei, Wang and Zhang, 2014)		40°C